



The University of
Nottingham

UNITED KINGDOM • CHINA • MALAYSIA

INVESTIGATING THE POSSIBLE ROLE OF FATTY ACID BINDING PROTEINS (FABPs) IN NOCICEPTIVE PAIN PROCESSING



Louis Alex Brailsford BSc (Hons) Biochemistry

Thesis submitted to the University of Nottingham for the
degree of Doctor of Philosophy

August 2017

Contents

Abstract.....	9
Publications.....	11
Declaration.....	12
Acknowledgements.....	13
List of common/key abbreviations.....	14
Chapter 1: General Introduction.....	16
1.0 Background.....	16
1.1 Neurobiology of pain – the concept of the nociceptor and an overview of nociceptor function.....	16
1.2 Distinctions between different types of nociceptors.....	21
1.2.1 Anatomical and physiological overview.....	21
1.2.2 Neurochemical differences between nociceptors.....	23
1.2.3 Projections of the central terminals of nociceptors into the dorsal horn and an overview of the processing of noxious input in the central nervous system.....	25
1.2.4 The processing and transmission of nociceptive information to the higher brain centres.....	27
1.3 Classification of pain syndromes.....	27
1.3.1 Types of pain: Nociceptive, inflammatory and neuropathic pain.....	27
1.3.2 Nociceptive pain processing (acute trauma).....	28
1.3.3 Inflammatory pain.....	28
1.4 TRP channels and pain.....	29
1.4.1 An introduction to TRP channels and TRPV1.....	29
1.4.2 Structure and function of TRPV1.....	30
1.5 Regulation of TRPV1 activity.....	34
1.5.1 Inflammatory hyperalgesia and TRPV1.....	34
1.5.2 Nerve growth factor.....	34
1.5.3. The effects of bradykinin and lipid mediators.....	35
1.5.4 Endogenous lipid activators of TRPV1, the 'endovanilloids.'.....	39
1.6 PPARs and pain.....	44
1.6.1 PPAR and their molecular mechanism of action.....	44
1.6.2 The role of PPAR α in pain.....	45
1.7 Fatty acid binding proteins (FABPs).....	48
1.7.1 An introduction to FABPs.....	48
1.7.2. Structure of the FABPs.....	49
1.7.3 FABPs as modulators of lipid signalling pathways. Implications for TRPV1 and PPARs in nociception.....	51

1.8 Aims of thesis	53
Chapter 2: Materials and Methods	55
Materials	55
2.0 Bacterial and mammalian cell culture media.....	55
2.0.1 Bacterial cell culture media.....	55
2.0.2 Mammalian cell culture media and transfection reagents.....	55
2.1 Antibiotics and drugs.....	56
2.2 Buffers and solutions.....	57
2.2.1 Protein expression and purification buffers	57
2.2.2 Buffers for agarose gel electrophoresis	57
2.2.3 Buffers for sodium dodecyl polyacrylamide gel electrophoresis, coomassie blue staining, and immunoblotting.....	58
2.2.4 Buffers for histology and immunofluorescence.....	60
2.3 Live cell calcium (Ca ²⁺) imaging solutions	60
Methods	62
2.4 Bacterial cell culture methods.....	62
2.4.1 Preparation of chemically competent E.coli cells	62
2.4.2 Transformation of chemically competent E.coli with plasmid DNA	62
2.4.3 Small and large-scale propagation of bacteria	63
2.5 Nucleic acid methods.....	63
2.5.1 Isolation of plasmid DNA from bacterial cell cultures	63
2.5.2 Isolation of total RNA from cell cultures.....	64
2.5.3 Determination of DNA and RNA concentration	64
2.5.4 Digestion of DNA with restriction endonuclease enzymes	65
2.5.5 Analysis of DNA by agarose gel electrophoresis	65
2.5.6 Extraction and subsequent purification of DNA fragments from agarose gels for molecular cloning	66
2.5.7 Reverse transcription (RT) of isolated RNA to complementary DNA (cDNA)	66
2.5.8 Polymerase Chain Reaction (PCR).....	66
2.5.9 Molecular cloning	67
2.6 Protein techniques.....	69
2.6.1 Protein isolation using radio-immunoprecipitation (RIPA) buffer	69
2.6.2 Sodium Dodecyl Sulphate Polyacrylamide Gel Electrophoresis (SDS-PAGE)	70
2.6.3 Protein transfer and immunoblotting (IB).....	70
2.6.4 Coomassie blue staining	71
2.6.5 Concentrating protein by trichloroacetic acid (TCA) precipitation.....	72

2.7 Expression and purification of recombinant histidine tagged human FABPs.....	72
2.7.1 Inducing the expression of recombinant Hexa-histidine tagged FABPs in bacterial cell cultures	72
2.7.2 Confirmation of recombinant protein expression by SDS-PAGE.....	73
2.7.3 Preparation of native cell lysates for protein purification.....	73
2.7.4 Purification of Hexa-histidine tagged FABPs by immobilized metal (Ni ²⁺) affinity chromatography (IMAC)	74
2.7.5 De-lipidating purified recombinant FABPs using Lipidex-1000	75
2.7.6 Concentrating dilute de-lipidated purified FABPs by ultrafiltration.....	75
2.7.7 Determination of protein concentration using the Beer-Lambert law	76
2.8 In vitro fluorescent displacement assays	77
2.8.1 Generating an FABP – 12 NBD stearate saturation curve	77
2.8.2 Displacement of bound 12-NBD stearate with AEA and 13 (S) HODE	77
2.9 Primary cell culture methods	78
2.9.1 Preparation of sterile 10cm coated cell culture dishes	78
2.9.2 Primary cell culture: Isolation of rat dorsal root ganglia cell bodies.....	78
2.9.3 Isolating DRG neuronal cell bodies from non-neuronal cells	79
2.10 Cell line cell culture and transfection of cell lines	80
2.10.1 Cell Lines.....	80
2.10.2 Resuscitation of cryopreserved cell lines	80
2.10.3 Maintenance and sub culturing of cell lines	80
2.10.4 Cell Counting using Cedex-XS cell counting system	81
2.10.5 Transiently transfecting adherent cell lines.....	81
2.11 Histology and immunofluorescence.....	82
2.11.1 Preparation of DRG tissue sections (performed Dr. J J Burston).....	82
2.11.2 Cresyl violet staining.....	82
2.11.3 Immunohistochemistry (IHC).....	83
2.11.4 Immunocytochemistry (ICC)	84
2.12 Live cell calcium (Ca ²⁺) imaging assays	85
2.12.1 Preparation of drugs and compounds.....	85
2.12.2 Preparation of cells for transfection.....	85
2.12.3 Preparing and loading cells with Fura-2AM	85
2.12.4 Measuring intracellular Ca ²⁺ concentration [Ca ²⁺] _i ; Ratiometric imaging	86
2.12.5 Measuring changes in [Ca ²⁺] _i in response to drug.....	86
2.12.6 Ca ²⁺ reconstitution experiment after stimulation with carbachol.....	87
2.13 Quantitative TaqMan® gene expression assays.....	88

2.13.1 Primer – probe design for TaqMan® gene expression assays.....	88
2.13.2 Performing TaqMan® gene expression assays	88
Chapter 3: The identification of FABP and PPAR isotypes in rat dorsal root ganglia cell cultures	92
3.0 Introduction: In vitro rat DRG cell culture model.....	92
3.1 Aim of study.....	93
3.1.1 Summary of specific experimental objectives.....	93
3.2 Results	94
3.2.1 Detecting PPAR, FABP and TRPV1 mRNA transcripts in freshly isolated rat DRG cell bodies and the associated cells by RT-PCR	94
3.2.2 Comparing FABP, PPAR and TRPV1 expression levels in fresh rat DRG isolations vs. 24-hour static rat DRG cell cultures by QRT-PCR.....	97
3.2.3 Isolation of DRG cell bodies from non-neuronal cells in heterogeneous cell culture preparation	102
3.2.4 Comparing the gene expression profile of the isolated DRG cell bodies and non-neuronal cells.....	104
3.2.5 Immunostaining for FABP5 and FABP7 in DRG tissue sections.....	109
3.3 Summary of key findings and results.....	118
3.4 Discussion.....	119
Chapter 4: Expression and purification of recombinant FABPs for use in fluorescence displacement assays	123
4.0 Introduction.....	123
4.1 Methods in brief, calculations, and statistics	127
4.2 Summary of experimental objectives for chapter 4.....	129
4.3 Results	130
4.3.1 A fraction of FABP5 and FABP8 is soluble when expressed at 37°C, but FABP7 is not soluble	130
4.3.2 Re-expressing FABP7 at lower temperature gives a fraction of soluble protein ..	132
4.3.3 Purification of FABPs by immobilized Ni ²⁺ - metal affinity chromatography (IMAC)	133
4.3.4 12-NBD stearate binds to purified FABPs 5, 7 & 8	134
4.3.5 Determining the dissociation constants (K _d) of 12-NBD stearate for FABPs 5, 7 & 8	138
4.3.6 Determining the binding affinity and specificity of AEA and 13 (S) HODE for FABPs 5, 7 & 8	140
4.4 Summary of key findings and results.....	146
4.5 Discussion – FABPs as intracellular shuttles for TRPV1 ligands.....	147
Chapter 5: The development of an in vitro mammalian cell culture system to probe for TRPV1/PPAR – FABP protein-protein interactions	150

5.0 Introduction.....	150
5.0.1 Background: Establishing a physical interaction between TRPV1 and FABP isotypes.....	150
5.1 Bimolecular fluorescence complementation (BiFC)	151
5.1.1 The principle of the BiFC assay	151
5.1.2 The structure and function of Yellow Fluorescent Protein and its variants	151
5.1.3 Preparing YFP fragments for BiFC.....	153
5.1.4 Summary and justification for the use of BiFC in this thesis	156
5.2 A summary of the experimental aims for chapter 5.....	156
5.3 Results	157
5.3.1 Generating an expression vector encoding for YFP-C tagged TRPV1: an overview of the cloning strategy	157
5.3.2 Analysis of PCR amplicons by gel electrophoresis.....	158
5.3.3 Agarose gel analysis of recovered plasmid DNA constructs digested with restriction endonucleases	160
5.3.4 Immunoblot analysis of transfected COS-7 cells.....	162
5.3.5 Immunostaining and immunolocalization of chimeric proteins in transfected COS- 7 cells	165
5.3.6 Does TRPV1 retain its functionality as a tagged protein when expressed in COS-7 cells?	170
5.3.7 Validation of the BiFC method with positive controls.....	174
5.3.8 BiFC: Establishing a functional PPAR – RXR α dimerization in COS-7 cells	177
5.3.9 BiFC: Probing for a physical association between YFP-N FABPs and TRPV1 linker YFP-C.....	181
5.4 Discussion.....	190
Chapter 6: Developing Fura-2AM based fluorescent Ca ²⁺ imaging assays to demonstrate a functional association between TRPV1 and FABPs.....	193
6.0 Introduction.....	193
6.1 Methods in brief	198
6.2 A summary of the experimental aims for chapter 6.....	200
6.3 Approach I – Confirmation of TRPV1 functionality in transfected COS-7 cells.....	201
6.4 Approach I – Does co-expressing FABP7 or FABP8 enhance the effect of AEA at TRPV1 receptors.....	204
6.5 Approach II - Characterization of HeLa cell lines I: Detection of FABP and NAPE – PLD mRNA transcripts by RT-PCR, TaqMan® gene expression assays and immunoblotting	206
6.6 WT HeLa cells express functional muscarinic receptors that are responsive to stimulation with carbachol (CCH)	214

6.7 TRPV1 expressing HeLa cells reconstituted in CaCl ₂ allow Ca ²⁺ re-entry into the cytosol independent of CCH stimulation.....	217
6.8 Summary of key findings and results.....	223
6.9 Discussion.....	224
Chapter 7: General discussion.....	228
7.1 An alternative approach to TRPV1 antagonism.....	228
7.2 Proof of concept: Identifying distinct FABP isoforms as intracellular endovanilloid carriers	229
7.3 Proof of concept: Characterisation of the identified FABPs as intracellular AEA and 13(S)HODE carriers.....	230
7.4 Future work.....	232
7.4.1 In situ hybridization (ISH)	232
7.4.2 Developing alternative approaches to investigating TRPV1/PPAR-FABP interactions in cultured cells	232
7.4.3 Investigating the role of PPAR signalling in the DRGs and their possible interactions with the FABPs.....	234
Chapter 8: References	237
Chapter 9: Appendices.....	251
9.1 PCR cloning primers and the corresponding plasmid DNA vectors constructed.	251
Primer pairs used for cloning into pBluescript SK- to give pBluescript vectors.....	251
• Primer Sequences are reported 5' > 3'	251
• Gene – vector generated listed	251
• cDNA template used in PCR is listed.....	251
• 'cDNA template used to amplify...' refers to the nucleotide sequence used from NCBI nucleotide when designing PCR primer pairs.....	251
Primer pairs for cloning to give pcDNA3.1/Zeo (+) Expression vectors for BiFC.....	251
• Sequences are reported 5' > 3'	251
• Kozak consensus sequence in Red	251
• Gene – vector generated listed	251
Primer pairs for cloning into full length human TRPV1 and FABP7 into pcDNA3.1 Zeo (+) to give pcDNA3.1/Zeo (+) Expression vectors	253
• Sequences are reported 5' > 3'	253
• Restriction sites underlined.....	253
• Kozak consensus sequence in Red	253
• Gene – vector generated listed	253
9.2 Sequence verified Plasmid DNA constructs supplied by others	254

Table 9.1 Sequence verified Plasmid DNA vectors sourced or constructed by fellow academic colleagues. Each plasmid encodes for the full length cDNA of each gene.....	254
9.3 PCR primers pairs used in RT-PCR	255
Table 9.2: Primers used in RT-PCR on cDNA from rat DRGs and tissues	255
9.4 Primers and Probes used in TaqMan®/QRT-PCR gene expression assays	257
9.5 Primary and secondary antibodies used in this thesis.....	259

Abstract

The transient receptor potential vanilloid 1 (TRPV1) channel protein is activated by lipid metabolites synthesized in the cytosol of nociceptors in response to noxious stimulation. Lipid species include the endocannabinoid anandamide (AEA) and the linoleic acid metabolite 13 (S) hydroxyoctadecadienoic acid (HODE) which act as endogenous TRPV1 ligands (endovanilloids) by evoking TRPV1 mediated Ca^{2+} entry. Members of the fatty acid binding protein (FABP) family have been widely reported to act as intracellular lipid binding proteins for hydrophobic lipid species in aqueous cytosolic environments. The aim of this thesis was to identify which FABP isoforms could solubilize then shuttle AEA and 13(S)HODE to TRPV1 during nociception. Inhibiting FABP mediated transportation of endovanilloids could represent an alternative approach to analgesia by indirectly antagonizing TRPV1 activity during nociception while avoiding the widely reported negative side effects of direct antagonism.

For the first time, it was found that FABP isoforms 5, 7 and 8 were expressed in rat dorsal root ganglia cell preparations. Furthermore, subsequent cell free competitive binding assays confirmed that FABP5, 7 and 8 could all physically bind to AEA and 13(S)HODE albeit with variable affinities. The ability of FABP 5, 7 and 8 to physically associate with TRPV1 and therefore deliver AEA was then assessed in live mammalian cell lines transfected with plasmid DNA constructs expressing recombinant TRPV1 and FABPs. Physical interactions between TRPV1 and FABP5, 7 and 8 were observed in COS-7 cells examined by fluorescence microscopy. However, when increases in intracellular Ca^{2+} levels were measured in COS-7 cells co-expressing TRPV1 and FABP, in response to treatment with $1\mu\text{M}$ AEA, the magnitude of AEA evoked Ca^{2+} influxes were not significantly different to those observed in COS-7 cells not co-expressing the FABPs. This suggested that the FABPs did not functionally associate with TRPV1

and did not deliver AEA to TRPV1 receptors. In conclusion, data in thesis showed that the FABP isoforms expressed in DRG cell preparations could physically associate with lipid species reported to activate TRPV1 during nociception.

Publications

Burston, J. J., D. R. Sagar, P. Shao, M. Bai, E. King, **L. Brailsford**, J. M. Turner, G. J. Hathway, A. J. Bennett, D. A. Walsh, D. A. Kendall, A. Lichtman, and V. Chapman, 2013, Cannabinoid CB2 Receptors Regulate Central Sensitization and Pain Responses Associated with Osteoarthritis of the Knee Joint: Plos One, v. 8.

Declaration

I carried out all the experiments and analyses in this thesis except for the rat DRG isolations performed by Paul Millns and Dr. James J Burston. Isolated DRGs were then cultured by myself. DRG tissue sections were prepared by Dr. James J Burston.

Louis Alex Brailsford

August 2017

Acknowledgements

I would like to say a huge thank you to Dr. Andrew Bennett and Professor Vicky Chapman for their supervision and guidance. I enjoyed the many conversations and debates about FABP, PPAR and TRPV1 function, that we had since my time as 3rd year as an undergraduate! I am extremely proud of my association with FRAME, and the ARUK pain centre. I would also like to say a huge thank you to James Burston and Paul Millns for their support. James, you were an absolute rock, a fantastic mentor, and a true gentleman. If there was ever a blue print for a dedicated post-doc, it is you! I do miss our discussions of scientific ideas/theories and your support during tough times. I am also hugely grateful to Paul for his patience, answering my endless questions and teaching me so much about Ca²⁺ imaging.

On a personal level, I would like to thank so many people who supported me during my time as a Ph.D. student. Elke for her encouragement, kindness and for being a fantastic human being. Helen G, Dave H, and Liaque, for being fantastic 'work parents', keeping me sane, and for their endless kindness and moral support. Fatiha, Fatema, Salima, Alex W, Rachel, Mazen, Suvik, Rich, Michael G, Dave Kendall, Steve Alex, Jane Arnold, Deb Merrick and Jerusalem for their unwavering support, patience and kindness. I'd also like to say a big thank you to all Monika and Nikki for their endless technical support during my five years at the FAL. My final big thank you goes to Tara, she is someone I really do miss seeing/annoying every day.

List of common/key abbreviations

AEA	Anandamide
BiFC	Bimolecular Fluorescence Complementation
CCH	Carbachol
COX	Cyclo-oxygenase
DRG	Dorsal root ganglia
EC	Endocannabinoid
FAAH	Fatty acid amide hydrolase
FABP	Fatty acid binding protein
IL-1 β	Interleukin 1 β
LOX	Lipoxygenase
mACh- R	Metabotropic Musacrinic receptor
NAE	N-acylethanolamines
NAPE- PLD	N-acylethanolphosphatidylethanolamine – specific phospholipase D
NGF	Nerve Growth Factor
OEA	Oleoylethanolamine
PEA	Palmitoylethanolamine
PPAR	Peroxisome Proliferator Activated Receptor
PK	Protein Kinase
RXR α	Retinoid X Receptor
SGC	Satellite Glial Cell
TRP	Transient receptor potential Transient receptor potential Vanilloid Subfamily
TRPV1	1
TG	Trigeminal Ganglia
TNF α	Tumour Necrosis Factor α

Chapter 1: General Introduction

Chapter 1: General Introduction

1.0 Background

Almost 20 years ago, the discovery of the transient receptor vanilloid subfamily 1 (TRPV1) ion channel in the seminal paper by Caterina et al. (1), revolutionized the field of pain biology. Since then, TRPV1 has been shown to be one of the key receptors responsible for the detection of painful stimuli at the peripheral terminals of sensory neurons (2, 3).

TRPV1 soon became an attractive pharmacological target for analgesics to combat pain. However, direct antagonism of TRPV1 with various synthetic compounds has been met with mixed success (4). The emphasis of this thesis is to start the process of seeking new ways to 'tame' the TRPV1 receptor in a neuronal specific manner as opposed to direct systemic antagonism, which unintentionally affects TRPV1 receptors expressed in non-neuronal tissues (5-8).

In sensory neurons, endogenous lipid species are synthesized on demand in response to painful stimuli. These lipid species activate or modulate TRPV1 activity during nociception. Therefore, disrupting the synthesis or the possible delivery of such lipid species to TRPV1 becomes an alternative approach to analgesia. This chapter will discuss the main molecular players that are and could be implicated in this strategy.

1.1 Neurobiology of pain – the concept of the nociceptor and an overview of nociceptor function

As per the International Association for the Study of Pain (IASP), pain can be defined as *“an unpleasant sensory and emotional experience associated with actual or potential tissue damage, or described in terms of such damage.”* Pain is necessary to alert us to the presence of injury or potential injury.

Therefore, acute pain is considered to play a protective role and serve as an alarm system to danger by bringing about nocifensive behaviour, for example jumping or withdrawing from the area of the body affected/exposed to danger (11-13).

The detection of painful or noxious stimuli (nociception) is encoded then processed by a specialized subpopulation of primary sensory neurons. The term coined for such sensory neurons is the nociceptors (9, 14). A more accurate definition of a nociceptor is a primary sensory neuron with a high threshold level of activation. This means that high-intensity stimuli of specific and distinct sensory modality (noxious stimuli) are required to activate nociceptive sensory neurons (14, 15).

The nociceptors innervate various visceral-peripheral regions of the body and are derived from the cell bodies or 'soma' of dorsal root and trigeminal ganglia (13-15). Dorsal root ganglia (DRG) and trigeminal ganglia (TG) are described as anatomical structures which anchor the soma-cell bodies of nociceptive afferent nerve fibres (11, 13, 15). Nociceptive cell bodies-soma sprout two projecting axons, one of which extends and innervates the periphery such as skin, brain, and internal organs. It is then the peripheral nerve terminal of this axon, that is responsible for the transduction of noxious chemical, thermal or mechanical stimuli from the viscera (14). The other axon travels in the opposite direction where the central nerve terminals synapse with neurons in the spinal cord, that transmit the noxious input to supraspinal sites and higher brain centres (Figure 1.1).

The ability of nociceptors to transduce noxious stimuli can be attributed to the expression of a repertoire of nocisensors at the peripheral nerve terminals. Nocisensors are receptors, more specifically high-threshold ion channels, which detect then transduce noxious stimuli. Specific examples of such ion channels include acid sensing ion channels (ASIC), transient receptor potential vanilloid

receptors (TRPV) and ionotropic purinoreceptors, of which the latter is gated by adenosine triphosphate (ATP) when released from damaged tissues (12, 14, 17).

The activation of such ion channels by noxious stimuli evokes a change in the membrane potential (receptor potential) of the peripheral nerve terminals due to influxes of ions. This is concomitant with the depolarization of the peripheral nerve terminals and the activation of voltage gated sodium channels (15). This results in the propagation and transmission of action potentials along the axons of the nociceptive sensory neurons and the release of neurotransmitters, such as glutamate, from the central terminals into the dorsal horn of the spinal cord (14) (Figure 1.2).

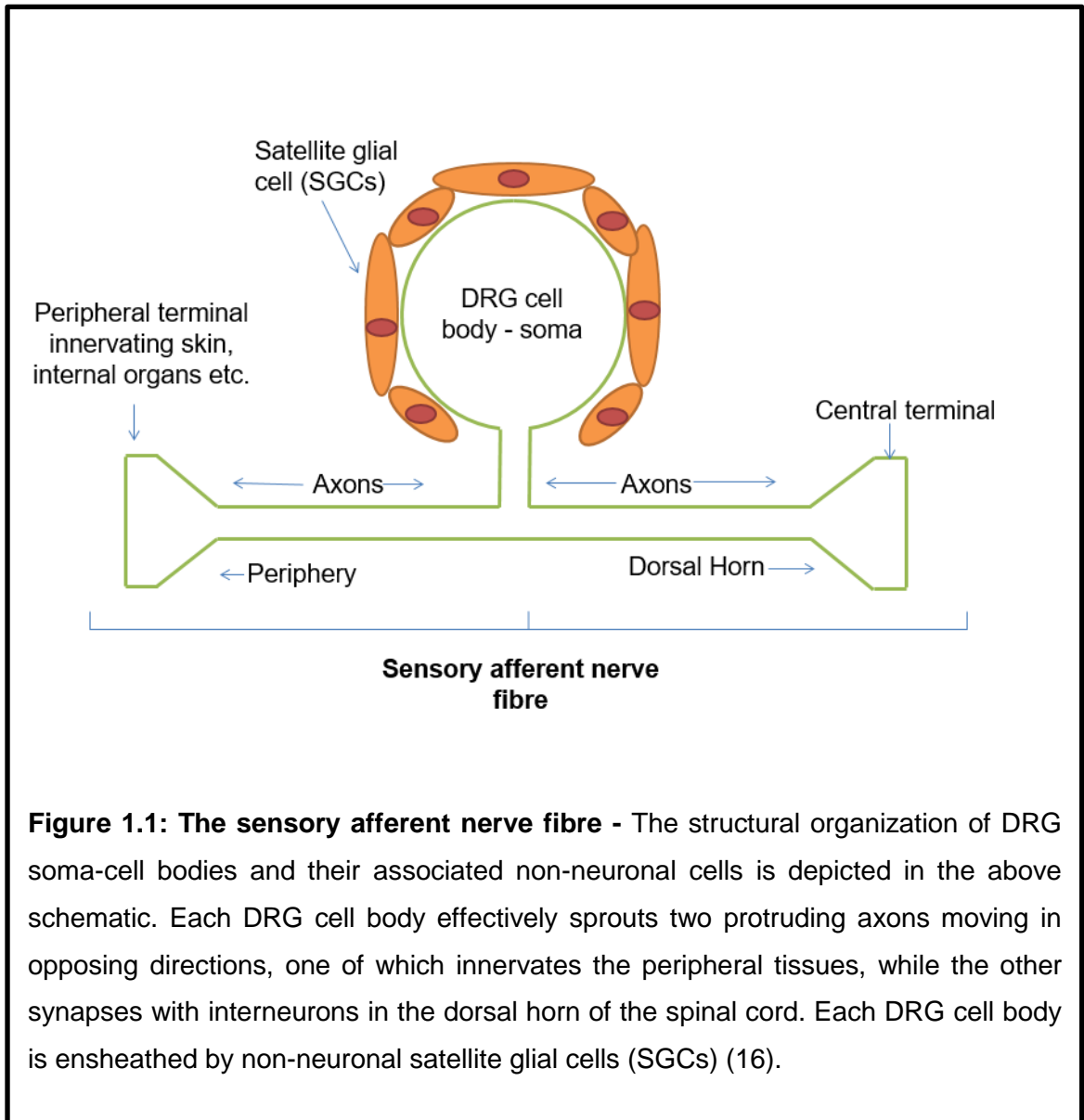


Figure 1.1: The sensory afferent nerve fibre - The structural organization of DRG soma-cell bodies and their associated non-neuronal cells is depicted in the above schematic. Each DRG cell body effectively sprouts two protruding axons moving in opposing directions, one of which innervates the peripheral tissues, while the other synapses with interneurons in the dorsal horn of the spinal cord. Each DRG cell body is ensheathed by non-neuronal satellite glial cells (SGCs) (16).

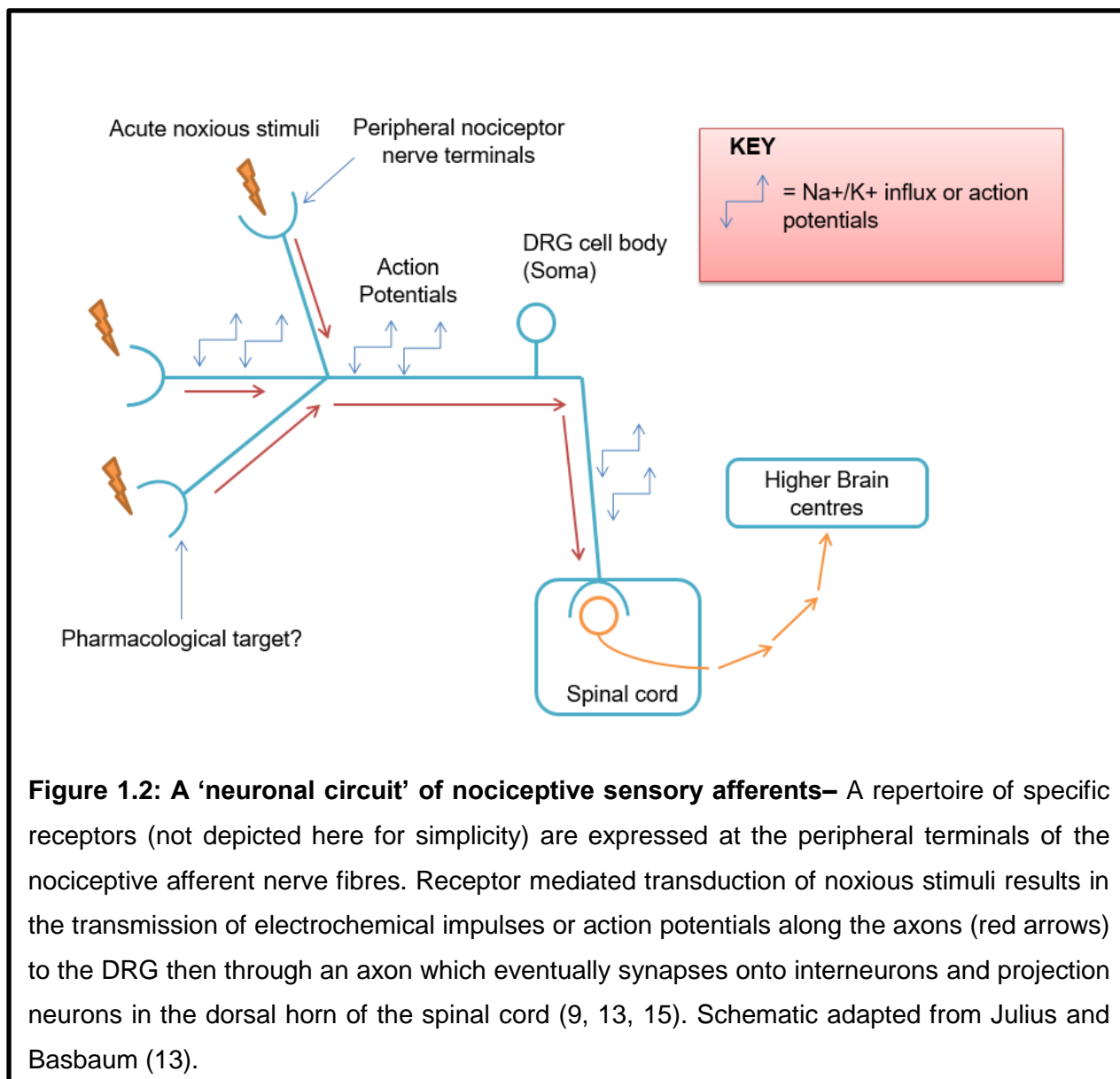


Figure 1.2: A 'neuronal circuit' of nociceptive sensory afferents– A repertoire of specific receptors (not depicted here for simplicity) are expressed at the peripheral terminals of the nociceptive afferent nerve fibres. Receptor mediated transduction of noxious stimuli results in the transmission of electrochemical impulses or action potentials along the axons (red arrows) to the DRG then through an axon which eventually synapses onto interneurons and projection neurons in the dorsal horn of the spinal cord (9, 13, 15). Schematic adapted from Julius and Basbaum (13).

1.2 Distinctions between different types of nociceptors

1.2.1 Anatomical and physiological overview

Primary sensory neurons/afferent nerve fibres can be categorized into distinct groups and differentiated from each other, based on specific anatomical, physiological and neurochemical differences. Specific examples of anatomical features include axonal diameter and the absence or presence, or extent of myelination (myelination status). These anatomical features determine what is known as the conduction velocity of the primary sensory neurons. Conduction velocity is the speed at which action potentials (electrical signals) move and propagate along the axons/processes of neurons. It has been widely reported that the difference in conduction velocity of nociceptive afferents and non-nociceptive sensory afferents, is related to and governed by axonal diameter and myelination status (13, 15, 18).

Three categories of primary sensory neurons exist and include $A\alpha/\beta$, $A\delta$, and Chemosensitive (C)-fibres. Differences in conduction velocity, myelination status and the role of nociception will be discussed for each category of a primary sensory neuron. The axons of $A\alpha/\beta$ fibres are extensively myelinated and exhibit a large axonal diameter and consequently rapidly transmit electrical impulses, which is reflected in their reportedly high conduction velocities (13, 18). The primary role of $A\alpha/\beta$ afferent nerve fibres is in the detection of innocuous sensory (mechanical) stimuli such as light touch, this being an example of so called proprioception. Interestingly, there is experimental data that suggest a proportion of $A\alpha/\beta$ afferent nerve fibres are also responsive to noxious sensory input and therefore could be considered as nociceptors (15, 18).

Examples of well-established nociceptive afferents exhibiting marked differences in conduction velocities include the A δ and C fibres. A δ fibres are of a medium diameter and are lightly myelinated. Consequently, the axons of A δ fibres present faster conduction velocities (5- 30 metres/sec) to that of the small diameter and unmyelinated axons of C-fibres (0.4-1.4 meters/sec) (Figure 1.3). Therefore, A δ nociceptors can mediate the sensation of acute fast/sharp pain, so called 'first' pain in contrast to the axons of the C-fibres which are responsible for conveying dull and diffuse pain sensations, so called 'second pain' (11, 13, 18).

Subsequent studies have provided a body of electrophysiological evidence and data that have facilitated further classification and characterisation of the different types of A δ and C fibres, present in nociceptive afferents. Such evidence has provided greater detail and insight into the exact role A δ and C fibres play in mediating the detection of different types of noxious stimuli.

A δ fibres: Three types of A δ fibre have been defined. Type 1 and 2 A δ fibres are both polymodal nociceptors responsible for the detection of noxious chemical, mechanical and thermal stimuli (11). Type 3/High-Threshold Mechanical nociceptors (HTM) are responsible for the detection of both mechanical and chemical noxious stimuli but are reported not to respond to noxious thermal stimulation (11, 13, 18).

C-fibres: Most of the C-fibres are polymodal nociceptors, and this encompasses those afferent fibres that are both responsive to chemical and mechanical noxious stimulation. However, some C-fibres that respond to noxious thermal stimulation are mechanically insensitive. Interestingly, these mechanically insensitive C-fibre afferents are more sensitive to stimulation with noxious chemicals. This plays a major role in instances of tissue injury and inflammation when there is an array of pro-inflammatory chemicals/mediators released from infiltrating immune cells,

particularly when these mediators can increase the excitability of such C-fibres. Finally, it is interesting to note that not all C-fibres are receptive to nociceptive sensory input. Indeed, some low threshold C-fibres, convey innocuous sensory input such as stroking and cooling (11, 13, 18).

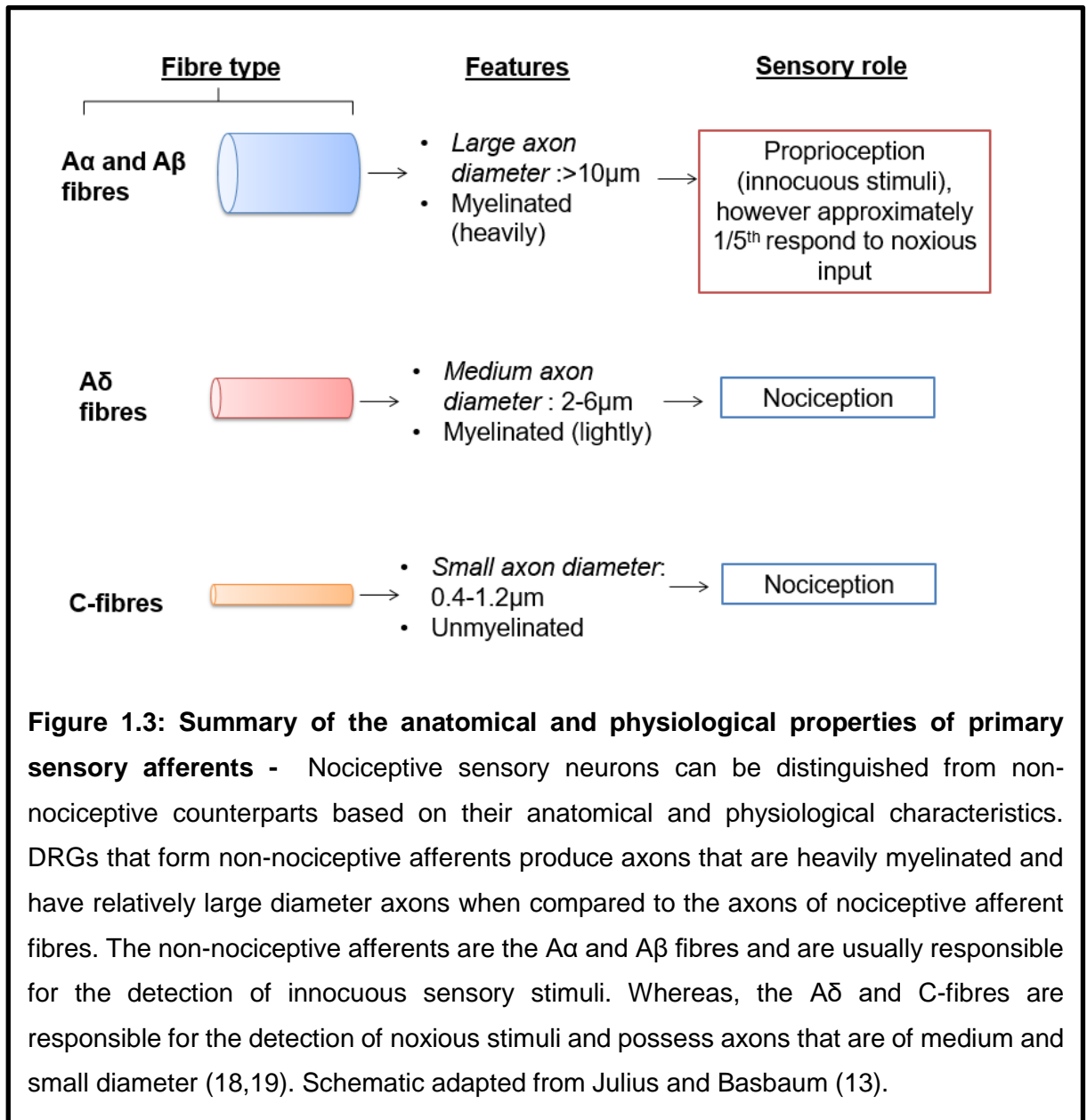
1.2.2 Neurochemical differences between nociceptors

Further characterization of nociceptive sensory afferents, has demonstrated that fundamental differences in neurochemistry exist between different populations of nociceptors; however, the functional consequences of these differences remain elusive. A myriad of cell markers has been used in the classification of nociceptive afferents, which include cell surface receptors and molecules/proteins which are expressed then secreted from the nociceptive terminals i.e. neuropeptides (11, 13, 18).

These neurochemical differences, which were observed when comparing the cell bodies of nociceptive sensory afferents, led to the categorization of nociceptors as either peptidergic or non-peptidergic (11,13). The peptidergic subset of nociceptors, which accounts for 50% of C-fibres and 20% A δ fibres and encompasses approximately 40% of all DRG cells in rats, express and release the neuropeptides; substance P (SP), calcitonin gene related peptide (CGRP) and somatostatin (STT). The non-peptidergic population of nociceptors, i.e. the non-peptidergic C-fibres, do not express such neuropeptides, but are distinguishable from other peptidergic cell bodies, due to their ability to bind plant isolectin B4 (IB4) and their expression of the enzyme, fluoride resistant acid phosphatase (FRAP) (13, 18, 19).

Collectively the neurotrophins and their cognate receptors, constitute two families of proteins, that are both responsible for the growth and development of neuronal cells (20).

The early development of nociceptive neurons is dependent on the neurotrophin, nerve growth factor (NGF), and its engagement with tropomyosin-related tyrosine kinase A (TrkA) receptor. However, it is only the peptidergic and not the IB4 positive/non-peptidergic neurons during adulthood, that expresses TrkA.



1.2.3 Projections of the central terminals of nociceptors into the dorsal horn and an overview of the processing of noxious input in the central nervous system

The first site in the central nervous system, responsible for the processing and coding of noxious input from the periphery, is the spinal cord. The spinal cord consists of two anatomical regions known the dorsal and ventral horns. The dorsal horn of the spinal cord is organized into regions known as laminae. The axons of nociceptive afferents project into the dorsal horn of the spinal cord where their central terminals, synapse with dorsal horn neurons. Dorsal horn neurons include the nociceptive interneurons and projection neurons, both of which are found in distinct and specific laminae of the dorsal horn. This is sometimes referred to as a nociceptive circuit (21).

The central terminals of both peptidergic C-fibres and A δ fibres terminate the most superficially within the dorsal horn. More specifically, the central terminals of C-fibres and A δ fibres synapse with pain projection neurons in lamina I and with interneurons in the outer most region of lamina II respectively. While the non-peptidergic C-fibres project onto interneurons in the inner part of lamina II. Therefore, spinal cord neurons in both lamina I and II are responsible for processing noxious sensory input from the C-fibres and A δ fibres. However, deeper projections of A δ fibres into the dorsal horn have also been observed. Indeed, A δ nociceptors along with A β fibres, have both been shown to project onto pain projection neurons in lamina V (Figure 1.4). Consequently, both noxious and innocuous stimuli converge on projection neurons in lamina V (11, 13, 18).

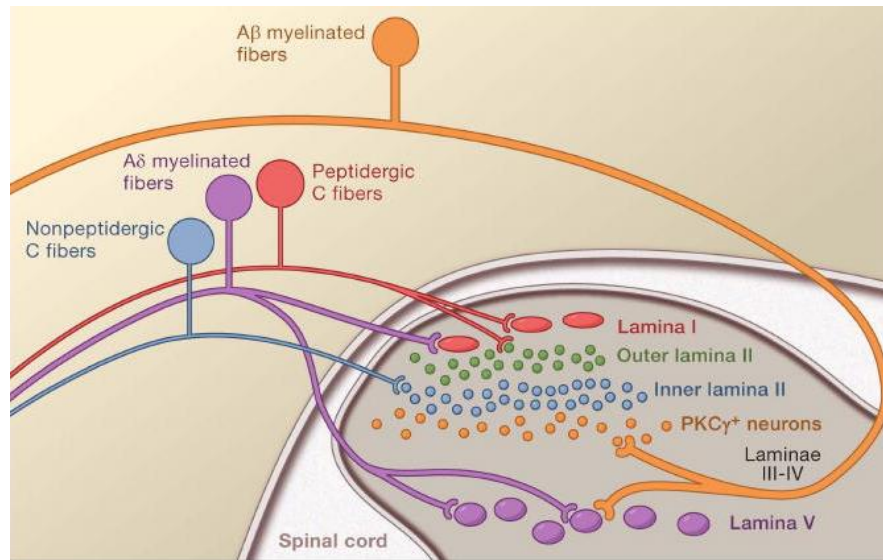


Figure 1.4: Schematic is depicting how the different afferent nerve fibres project and terminate in distinct lamina in the dorsal horn of the spinal cord.

Adapted from Basbaum et al. (11)

1.2.4 The processing and transmission of nociceptive information to the higher brain centres

The projection neurons are responsible for the transmission of nociceptive information from the dorsal horn. The ascending axons of the projection neurons travel in the spinothalamic and spinoreticulothalamic tracts, where they eventually synapse with neurons located in specific regions of the brain, including the thalamus and brainstem. From the thalamus, further projections allow for the further transmission of nociceptive information to the somatosensory cortex, where the location and intensity of pain can be processed and deciphered. This is the ascending pathway (15).

1.3 Classification of pain syndromes

1.3.1 Types of pain: Nociceptive, inflammatory and neuropathic pain

Encompassed within the general definition of pain, are three broad classifications of different types of pain syndrome. These include nociceptive, inflammatory and neuropathic pain, all of which can be distinguished from each other based on the following; 1) the nature/type of initiating stimulus 2) the type of sensory neuron involved i.e. if there is involvement of nociceptive and/or non-nociceptive afferent fibres in mediating the detection of sensory input and 3) the role of the peripheral and/or central nervous system and the function/role of the pain type i.e. is it protective or responsible for healing and repair. Nociceptive and inflammatory pain are the two types of pain syndrome of interest in this chapter and thesis.

1.3.2 Nociceptive pain processing (acute trauma)

Nociceptive pain has a protective role; it serves as an alarm system to danger and occurs in instances of acute trauma. For example, exposure to noxious chemicals or heat will activate high threshold nociceptive afferents in the peripheral nervous system. More specifically the detection of noxious environmental stimuli by nociceptive sensory afferents is mediated by nociceptors at the peripheral nerve terminals. Receptor stimulation is then converted or transduced via the activation of a plethora of voltage gated Na^+ and K^+ channels (15, 22). The resulting electrical impulses convey nociceptive sensory input by propagating action potentials along the axons of afferent nerve fibres via the DRG to dorsal horn neurons in the spinal cord, as discussed previously.

1.3.3 Inflammatory pain

Inflammatory pain occurs in instances of tissue injury and damage. This is due to the recruitment and infiltration of non-neuronal cells such as mast cells, macrophages, platelets, neutrophils, basophils, keratinocytes, and fibroblasts, all of which release an array of lipid and protein pro-algesic mediators. The result is an inflammatory soup of various lipophilic and protein pro-algesics (2, 14, 23). These pro-nociceptive mediators directly interact with their cognate receptors at the peripheral terminals of innervating nociceptive sensory afferents. The engaged receptors then signal via a myriad of intracellular pathways that converge and positively modulate the activity of nociceptive ion channels or increase the expression and number of nociceptive ion channels in the membrane (14, 23).

Normally, a stimulus that exceeds the high nociceptive threshold of nociceptors will evoke the sensation of pain. Indeed, a linear relationship is observed between stimulus intensity and the pain experienced i.e. when the intensity of the painful stimulus applied is gradually increased. However, the effect of pro-algesic

mediators released during tissue damage on nociceptive afferents leads to a reduction in their threshold level of activation and is concomitant with increased responsiveness of the neurons; this is a phenomenon known as peripheral sensitization. These changes to nociceptor threshold levels of activation manifest itself in two forms. The first being pain hypersensitivity or inflammatory hyperalgesia i.e. exaggerated responses to painful stimuli.

The second manifestation is allodynia i.e. the interpretation of normally innocuous stimuli as painful (11, 14, 15). Later in this chapter, inflammatory pain and hyperalgesia will be discussed in significantly more detail in the context of TRPV1.

1.4 TRP channels and pain

1.4.1 An introduction to TRP channels and TRPV1

The transient receptor potential (TRP) channel family has 27 members that serve a range of different physiological roles and respond to many transient stimuli, including; light, temperature, mechanical, osmolarity and taste (7, 12, 24). In short TRP channels are key players in the detection of several sensory stimuli. Exposure to any of the stimuli leads to influxes of monovalent (Na^+) and divalent (Ca^{2+}) cations down their electrochemical gradient. This leads to increases in intracellular ion concentration and cellular depolarization (12, 25). Additionally, increases in ion concentrations have many functional consequences i.e. elevations in intracellular Ca^{2+} concentration will influence a range of cellular signalling events that may control or govern cell activity (26). TRP channels have been divided into several distinct classes or subfamilies. These include the following; canonical (TRPC), vanilloid (TRPV), melastatin (TRPM), ankyrin (TRPA), mucolipin (TRPM) and polycystin (TRPP) subfamilies (4,12). Mutated forms of the TRP channels are implicated in various diseases. Therefore, an understanding of their biochemical

and physiological activity is crucial. Vanilloid subfamily member 1 commonly referred as to the transient receptor potential vanilloid subfamily 1 (TRPV1) is the key channel protein of interest in this thesis.

1.4.2 Structure and function of TRPV1

The TRPV1 protein is a non-selective cation channel that is expressed in many distinct tissues and cell types and therefore plays a critical role in a range of biochemical and physiological processes (27, 28). These range from the detection of noxious stimuli to modulating cellular differentiation (29-35). One of the most well-understood processes that TRPV1 has a role in is the detection of painful noxious stimuli by the nociceptors. The molecular mechanism by which this occurs and is regulated is the focus of this thesis.

The structure and topology of TRPV1 channel consist of 6 transmembrane spanning alpha (α) helices with a pore forming region or loop between 5th and 6th TM helices (Figure 1.5). This constitutes one TRPV1 subunit and consistent with other TRP channels, TRPV1 forms homo-tetramers (24, 36).

Akin to other TRP channels, TRPV1 is activated by a range of stimuli including pungent compounds like capsaicin, noxious heat ($\geq 42^{\circ}\text{C}$) and acidity ($\text{pH} < 6$) all of which can cause a subsequent Ca^{2+} influx leading to the generation of action potentials to the dorsal horn of the spinal cord followed by signalling onto the higher brain centres where pain is perceived (2, 13, 38). Therefore, multiple stimuli can converge on TRPV1 receptors (2, 39). Given its reactivity to different thermal and mechanical stimuli, the term polymodal was applied when describing TRPV1. Each of these highlighted stimuli will now be considered.

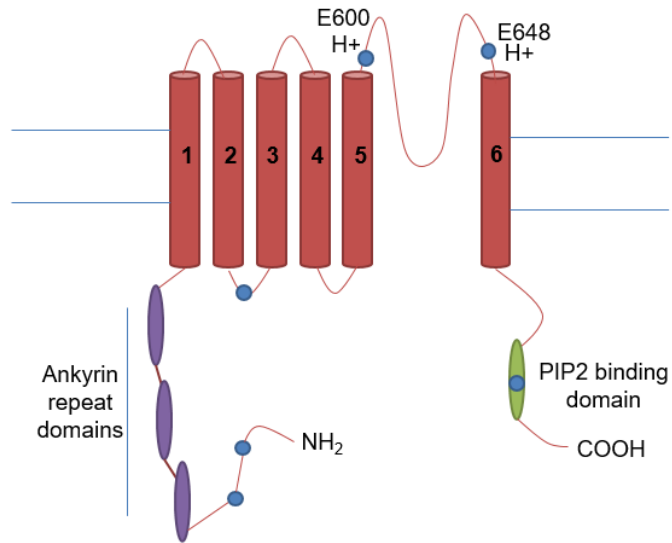


Figure 1.5: Structure-topology of TRPV1 - TRPV1 is composed of 6 transmembrane spanning domains or α helices. Two glutamate residues E600 and E648 are responsible for binding protons. The PIP2 binding domain, as the name implies, binds to phosphoinositide phosphatidyl-4,5-bisphosphate (PIP₂). The cytosolic ankyrin repeat domains (ARDs) are hypothesized to regulate channel function and activity; however, the exact nature of their role is still emerging (12). Schematic adapted from Szallasi et al. (39)

One of the most well-known and defining characteristics of TRPV1 is its responsiveness to the vanilloid capsaicin (Figure 1.6). Capsaicin is the piquant active ingredient of chili pepper and is TRPV1 specific concerning the receptors it targets (1, 37, 39). It was this defining feature of TRPV1 that led to its discovery and subsequent cloning and isolation. Furthermore, sensitivity to capsaicin can be used as a means of identifying key subpopulations of nociceptive sensory afferents, of which the majority are C-fibres and the minority being A δ fibres (1, 13, 37).

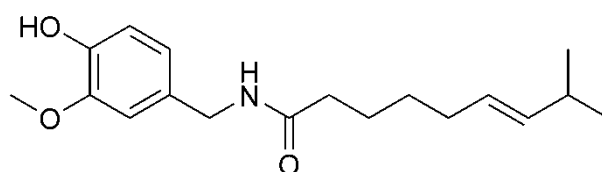


Figure 1.6: The chemical structure of capsaicin.

Stimulation of TRPV1 positive nociceptive sensory afferents with capsaicin has many downstream effects. One consequence is the secretion of neurotransmitters from the afferent and central nerve terminals of TRPV1 expressing nociceptors. Neuro-modulatory molecules released include both nonpeptide and peptide transmitters. Glutamate is one example of a neurotransmitter released at the central terminals, while neuropeptides substance P and calcitonin gene related peptide (CGRP), are both released in response to TRPV1 activation (14, 40).

TRPV1 is a thermo-sensitive receptor and can act as an endogenous transducer in response to changes in body temperature (10). As already partly alluded to, TRPV1 has been long characterized as an intrinsically heat sensitive channel and gives functional responses to stimulation to what are considered as noxious temperatures i.e. those that are more than $\geq 42^{\circ}\text{C}$ (2, 10, 39). The importance of TRPV1 as a thermo-sensing receptor is critical, as exemplified in TRPV1 knock out studies in mice, where heat sensitivity was lost (10, 39).

In vivo, decreases in pH can result from tissue injury-damage due to the recruitment of infiltrating inflammatory cells. The result is referred to as pro-algesic tissue acidosis (23, 42, 43). The resulting acidic microenvironment contributes directly to the sensitivity of TRPV1. Acidic pH will enhance the effects of other noxious stimuli and agonists at TRPV1, evoking TRPV1 mediated $\text{Ca}^{2+}/\text{Na}^{+}$ entry (3, 17, 41).

For example, the temperature threshold level of activation for TRPV1 is decreased in instances of tissue injury where the pH of surrounding microenvironment is < 5.9 . The result is that TRPV1 is activated at ambient or non-noxious temperatures. This modulation of TRPV1 sensitivity is a common feature that will be discussed later. As with capsaicin stimulation, acidity has also been shown to increase levels

of CGRP expression and release due to the activation of TRPV1 (Figure 1.7) (14, 40).

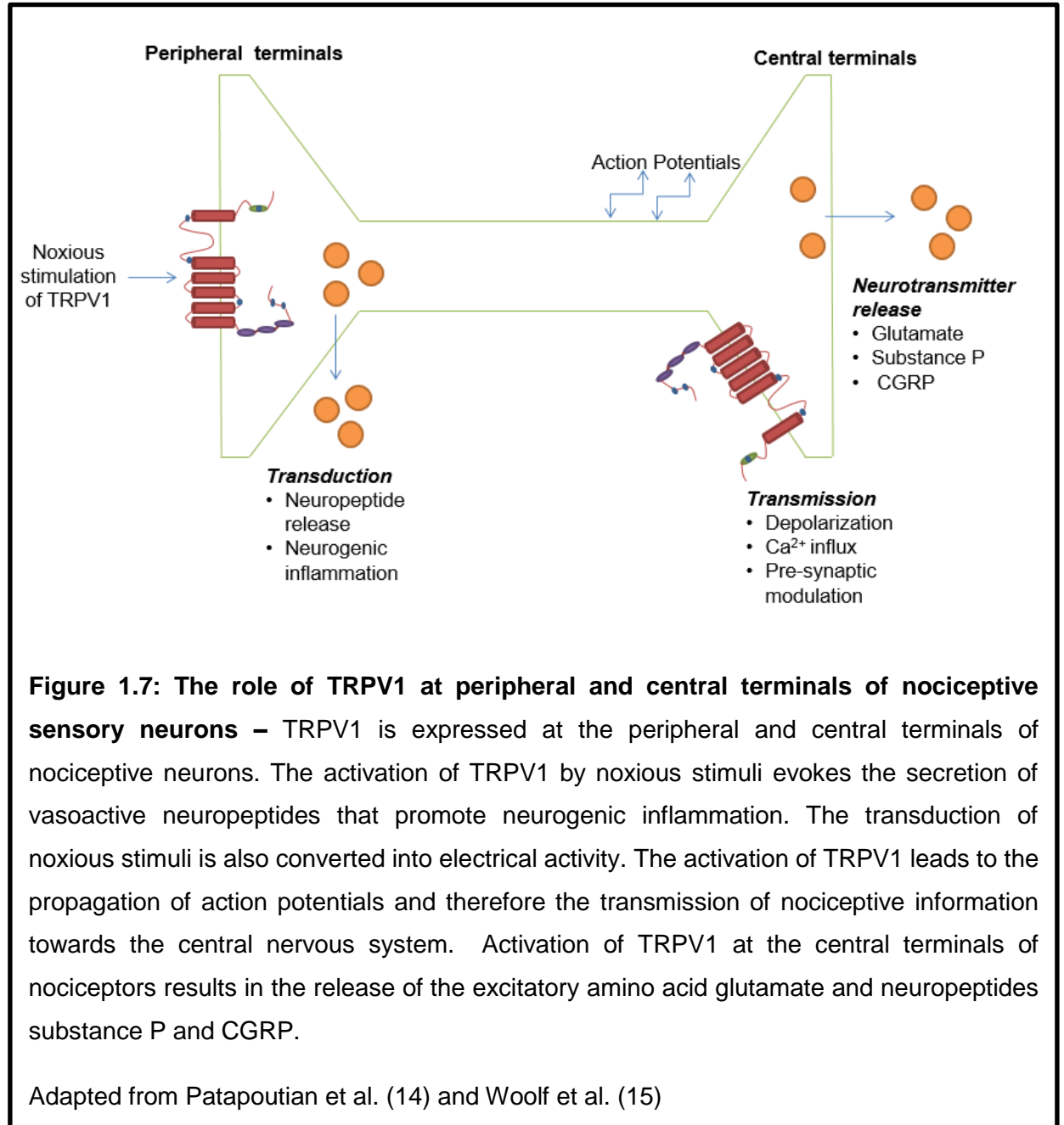


Figure 1.7: The role of TRPV1 at peripheral and central terminals of nociceptive sensory neurons – TRPV1 is expressed at the peripheral and central terminals of nociceptive neurons. The activation of TRPV1 by noxious stimuli evokes the secretion of vasoactive neuropeptides that promote neurogenic inflammation. The transduction of noxious stimuli is also converted into electrical activity. The activation of TRPV1 leads to the propagation of action potentials and therefore the transmission of nociceptive information towards the central nervous system. Activation of TRPV1 at the central terminals of nociceptors results in the release of the excitatory amino acid glutamate and neuropeptides substance P and CGRP.

Adapted from Patapoutian et al. (14) and Woolf et al. (15)

1.5 Regulation of TRPV1 activity

1.5.1 Inflammatory hyperalgesia and TRPV1

As discussed previously components of the inflammatory soup have been shown to influence the sensitivity state of nociceptive sensory afferents and TRPV1. Indeed, inflammation is accompanied by hypersensitivity to heat, which is absent in rodent models of inflammatory hyperalgesia, where the TRPV1 gene had been deleted. This strongly suggests that TRPV1 is a critical player in the development of thermal hyperalgesia (3, 17, 23). Examples of such pro-algesic mediators that influence TRPV1 include neurotrophins, prostaglandins, bradykinin, chemokines, prokinecticins, tumour necrosis factor α (TNF α), ATP and glutamate, some of which will be examined in detail concerning TRPV1 (45-47, 55).

1.5.2 Nerve growth factor

The neurotrophin, nerve growth factor (NGF) is typically associated with its role in neuronal development and survival, however, during adulthood, NGF is a critical component of the inflammatory soup and can exert a potent pro-nociceptive effect on nociceptive sensory neurons (46, 48). NGF, therefore, plays an essential role in the development of inflammatory hyperalgesia. NGF can do so, by acting directly at peptidergic C-fibres, which express its cognate receptor, tyrosine receptor kinase A (TrkA). NGF signalling via TrkA results in the activation of downstream signalling cascades; this includes the activation of phosphoinositide 3 kinase (PI3K), followed by the immediate downstream activation of the cytosolic non-receptor tyrosine kinase, Src kinase (48, 50). TRPV1 can be stored in intracellular-cytosolic vesicles in sensory afferents and transported in an anterograde manner to the membrane from the soma of the nociceptor (14, 49, 50).

This occurs in response to Src kinase mediated phosphorylation of a specific tyrosine residue (Y200) in human TRPV1 (48, 50). Thus, TRPV1 is effectively inserted into the membrane of peripheral nociceptive nerve terminals 'on demand.' NGF can also act independently of TrkA, and still increase levels of TRPV1 at the peripheral nerve terminals of C-fibres (50). The mechanism requires NGF to be transported in a retrograde manner to the soma of nociceptive afferents, where there is activation of the mitogen activated protein kinase (MAPK) p38 and subsequent increases in TRPV1 expression and its trafficking from the soma to the peripheral nerve terminals (17, 50). In summary, NGF elevates numbers of available TRPV1 channels, resulting in increased Ca²⁺ influxes at the peripheral terminals, which in turn increases the excitability and sensitivity of the nociceptive sensory neurons. (Figure 1.8) Furthermore, NGF can be considered to have brought about a phenotypic change in the nociceptive afferent by increasing TRPV1 levels (14, 48).

1.5.3. The effects of bradykinin and lipid mediators

Bradykinin: The nonapeptide bradykinin (BK), is an example of potent pro-algesic mediator, that is released in instances of tissue injury. BK plays a critical role in the development of inflammatory hyperalgesia, and previous studies have widely reported that BK can directly excite and evoke currents in nociceptive sensory afferents, but can also sensitize nociceptors to other stimuli such as heat (17, 23, 51). Of interest, is the effect of BK on TRPV1 activity; indeed, BK has been shown to both sensitize TRPV1 and induce the de novo synthesis of endogenous lipid species that directly bind to and activate TRPV1 in nociceptive sensory neurons (51, 53). The latter will be discussed later in this chapter.

The underlying mechanisms that underpin BK mediated sensitization of TRPV1 start with the engagement of BK at its cognate receptors in the peripheral nerve terminal of the nociceptors. BK can exert its biological effects on TRPV1 via

engaging and signalling through its G-protein coupled receptors (GPCRs), B1 and B2 (17, 53, 54).

Immediately downstream of BK signalling at the B2 receptor, is the activation of many intracellular signal transduction networks, one of which includes the lipid metabolizing enzyme phospholipase C- β (PLC- β). The activation of the PLC- β enzyme results in the metabolism (hydrolysis) of its membranous lipid substrate, phosphatidylinositol 4,5-bisphosphate (PIP₂) to inositol 1,4,5-trisphosphate (IP₃) and diacylglycerol (DAG). Free IP₃ is then able to diffuse through the cytosol and mobilize Ca²⁺ from intracellular/internal ER Ca²⁺ stores, via the activation and gating of IP₃ receptors (IP₃R). The consequence of which is increased cytosolic concentrations of Ca²⁺ (17, 54).

The products of PIP₂ hydrolysis have important effects and consequence on both TRPV1 activity and sensitivity (17, 54). PIP₂ exerts what is described as a tonic inhibitory effect on TRPV1 by interacting with the PIP₂ binding domain at the C-termini of TRPV1 channels. This inhibition is overcome by the breakdown of PIP₂ in response to cleavage by PLC- β , the consequence of which is the sensitization of TRPV1 to other noxious stimuli (17).

Protein kinase C (PKC), more specifically the epsilon (ϵ) isoform of PKC, translocates to the membrane, where it is activated by the second product of PIP₂ breakdown, DAG. Activated PKC ϵ then, in turn, mediates the phosphorylation of TRPV1 at two specific serine residues; S502 and S800 (17, 54, 56). Taken together, the hydrolysis of PIP₂ and subsequent phosphorylation of TRPV1 can potentiate TRPV1 activity by increasing its sensitivity to other noxious stimuli such as heat, acid and the vanilloid capsaicin (56).

Lipid mediators: Prostaglandins (PGs) are a family of pro-algesic lipid mediators derived from the unsaturated free fatty acid arachidonic acid (AA). In brief, AA is liberated from the plasma membrane by phospholipases, for subsequent metabolism by cyclooxygenase isozymes, generating PGs (51, 55).

Two PGs are of interest; these include Prostaglandin E₂ (PGE₂) and Prostaglandin I₂ (PGI₂). These two PGs are generated in response to tissue injury and play a critical role in the development inflammatory hyperalgesia by influencing the activity and sensitivity of TRPV1 (51).

Both PGE₂ and PGI₂, released from the infiltrating and residual non-neuronal/immune cells can signal in a paracrine manner by interacting with their cognate receptors at the peripheral nerve terminal of nociceptors in a manner comparable to other pro-algesic mediators such as BK. PGE₂ and PGI₂ interact and signal through prostanoid receptors, EP and IP respectively. Once EP and IP receptors are activated they can signal downstream to two specific intracellular signalling cascades, the first of which results in the activation of PKC and the other being the cAMP/Protein Kinase A (PKA) cascade, both of which lead to the phosphorylation of TRPV1, modulating its sensitivity to other noxious stimuli. For example, there is a considerable body of evidence showing that PGE₂ can potentiate capsaicin evoked responses in nociceptive afferents (17, 51, 55). This is mediated by the cAMP/PKA pathway (56).

TISSUE INJURY - INFLAMMATION

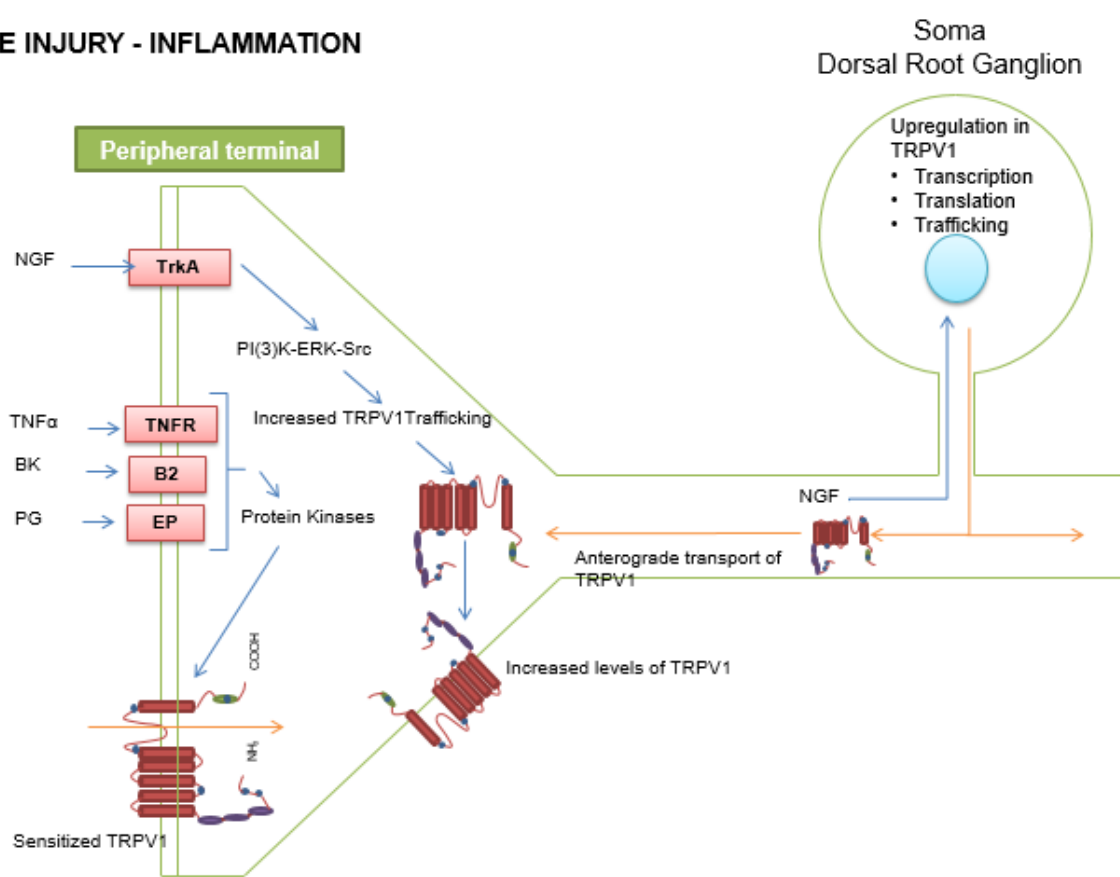


Figure 1.8: The implications of peripheral sensitization on TRPV1 activity in nociceptive neurons – During tissue injury and peripheral inflammation there is an array of pro-inflammatory and pro-algesic lipid mediators that act synergistically to increase the sensitivity and induce a state of hypersensitivity nociceptive nerve terminals, in which TRPV1 is affected. Pro-algesic mediators include; nerve growth factor (NGF), tumour necrosis factor α (TNF α), bradykinin (BK) and prostaglandins (PG), which engage with their respective receptors TrkA, TNFR, B2 and EP expressed on nociceptive nerve terminals. NGF is transported to the dorsal root ganglion of a nociceptive afferent in a retrograde manner, to upregulate the expression of TRPV1, while NGF signalling at the TrkA receptor leads to the insertion of a greater number of TRPV1 receptors into the membrane of nociceptive nerve terminals. TNF α , BK, and PGs acting at their cognate receptors activate various intracellular signalling cascades that modulate the activity of TRPV1 receptors by reducing their threshold for activation, and potentially their binding kinetics to other endogenously generated pro-nociceptive lipid derived ligands. The net effect of all these factors combined is a reduction in pain threshold. TrkA, tyrosine kinase A; TNFR, TNF α receptor; B2, Bradykinin receptor; EP, Prostaglandin receptor. Adapted from Patapoutian et al. (14).

1.5.4 Endogenous lipid activators of TRPV1, the 'endovanilloids.'

An increasing number of endogenous lipid metabolites, derived from long chain fatty acids, have been identified in recent years as modulators of TRPV1 activity. Such endogenous species have been shown to act as TRPV1 agonists or partial agonists, with some endogenous agonists exhibiting potencies comparable to that of capsaicin (57-59). These are collectively referred to as the endovanilloids and are generated via various metabolic pathways (60, 61). Increasing numbers of endovanilloids have been and are being identified; therefore, the ones discussed in this chapter are a selection of the main endovanilloids of interest. The endovanilloids of interest will be grouped into two categories which include N-acylethanolamines (NAEs) and the oxidation products of both linoleic and arachidonic acid (61, 62).

Examples of NAEs include anandamide (AEA) and N-arachidonoyldopamine (NADA). While arachidonic and linoleic can be oxidized by lipoxygenases, cyclooxygenases and cytochrome P450 enzymes to produce pro-nociceptive oxidized lipid metabolites (57, 68, 70). These include hydroxyoctadecadienoic (HODEs) and hydroxyeicosetraenoic acid (HETEs) (Figure 1.9) (53, 65, 67). Unlike most neurotransmitters, the endovanilloids are not synthesized, stored, then released from vesicles; instead they are synthesized rapidly *de novo* / on demand.

Anandamide (AEA): A considerable body of research over the last 10-15 years has provided substantive evidence to legitimize a collection of neutral neuro-modulatory lipids, collectively described as N-acylethanolamines (NAEs), as endogenous activators or modulators of TRPV1 activity (58, 67). One of the most widely investigated NAEs responsible for activating TRPV1, is arachidonylethanolamine (AEA) or 'anandamide.' AEA was discovered in the early 1990s from porcine brain and was originally identified as an endocannabinoid

i.e. an endogenous agonist which activates anti-nociceptive Cannabinoid receptors (CB) 1 and 2 (62, 63, 67). Interestingly, it has been shown to activate-regulate nociceptive TRPV1 channel activity. AEA biosynthesis is catalyzed in a Ca^{2+} dependent manner by the enzyme N-acylethanolphosphatidylethanolamine-specific phospholipase D (NAPE-PLD) (65). Conversely, the inactivation AEA is brought into effect by its hydrolysis into arachidonic acid and ethanolamine (Figure 1.10). This is mediated by intracellular lipid binding proteins (iLBPs) that sequester then shuttle AEA for degradation and turnover to the amide hydrolysing enzyme fatty acid amide hydrolase (FAAH) (76, 77, 116).

Despite sharing similar affinities, the potency of AEA at TRPV1 receptors is comparably lower than that of capsaicin. It, therefore, has been questioned whether AEA serves as an endogenous 'full' agonist or does it act as an endogenous modulatory lipid or partial agonist. Previous studies have shown that AEA behaves as a full agonist at recombinant TRPV1 receptors that are highly expressed in cell lines, but its efficacy-potency is still comparably low to that of capsaicin.

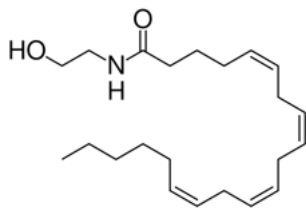
Oxidative metabolites of LA and AA: The oxidation of linoleic acid (LA) produces specific oxidized linoleic acid metabolites (OLAMs) that activate TRPV1 (68, 72). These oxidative metabolites include 9 or 13 hydroxyoctadecadienoic acid (9 or 13-HODE) and were shown to be synthesized on demand in response to noxious stimulation (68). Both OLAMs were shown to activate TRPV1 in native cultured trigeminal ganglia cells and transfected CHO cell lines expressing high levels of recombinant TRPV1 (68, 69). The enzyme implicated in the generation of these specific OLAMs was originally thought to be 15-Lipoxygenase (15-LOX) (68, 69, 74). However, the research group who originally identified 9/13-HODE as TRPV1 activators have now demonstrated that cytochrome P450 enzymes (CYPs-450),

in native TG cells, are most likely responsible for the oxidation of LA to TRPV1 specific OLAMs (Figure 1.10) (71-73).

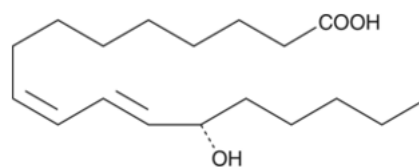
However, the role of 9 and 13 HODE as bone fide endogenous TRPV1 activators at present, remains controversial. When directly comparing the activity of AEA and HODE at TRPV1 receptors expressed in cell lines, it was found that the HODEs were markedly less potent as endovanilloids than AEA. Indeed both 9 and 13 HODE were reported as being almost inactive at TRPV1 receptors expressed in cultured cells (75).

The last endovanilloids to be discussed are the HETEs. The inflammatory mediator, bradykinin (BK) can excite nociceptive sensory neurons and evoke the sensation of pain by activating TRPV1. BK signalling at its receptor at the peripheral terminal of nociceptors was shown to mobilize arachidonic acid (AA) from the membrane by activating the enzyme phospholipase A2 (PLA₂). Free AA is a substrate for the enzyme, 12-lipoxygenase (12-LOX). 12-LOX mediated oxidation of AA was shown to produce the lipid metabolite, 12-hydroperoxyeicosatetraenoic acid (12-HPETE), which then, in turn, activates TRPV1 (Figure 1.10). Furthermore, C-fibres treated with 12-LOX antagonist or TRPV1 receptor antagonist capsazepine were unable to fire the same number of action potentials to those C-fibres exposed to BK but not treated with either antagonist (53). This confirms the involvement of TRPV1, but also demonstrates that 12-HPETE, the product of 12-LOX metabolism (which is rapidly reduced to 12-HETE) activates TRPV1 because of BK stimulation. While, 15-LOX oxidizes AA to produce 15-(S)-hydroperoxyeicosatetraenoic (15 S HpETE) and 15-(S)-hydroxyeicosatetraenoic acids (15 S HETE), both of which are reported to activate TRPV1 (62).

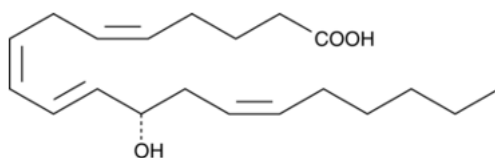
A) AEA



B) 13(S)HODE



C) 12-HETE



D) 15-HETE

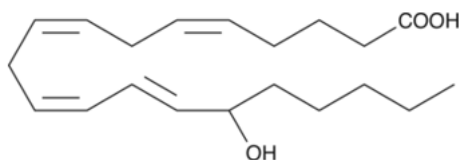


Figure 1.9: Chemical structure of endogenously synthesized TRPV1 ligands or endovanilloids – The skeletal structures represent the four different endovanilloids discussed in the main body of text. They are; **A)** the uncharged n-acylethanolamines (NAE) anandamide (AEA) **B)** 13(S) HODE **C)** 12-HETE and **D)** 15-HETE.

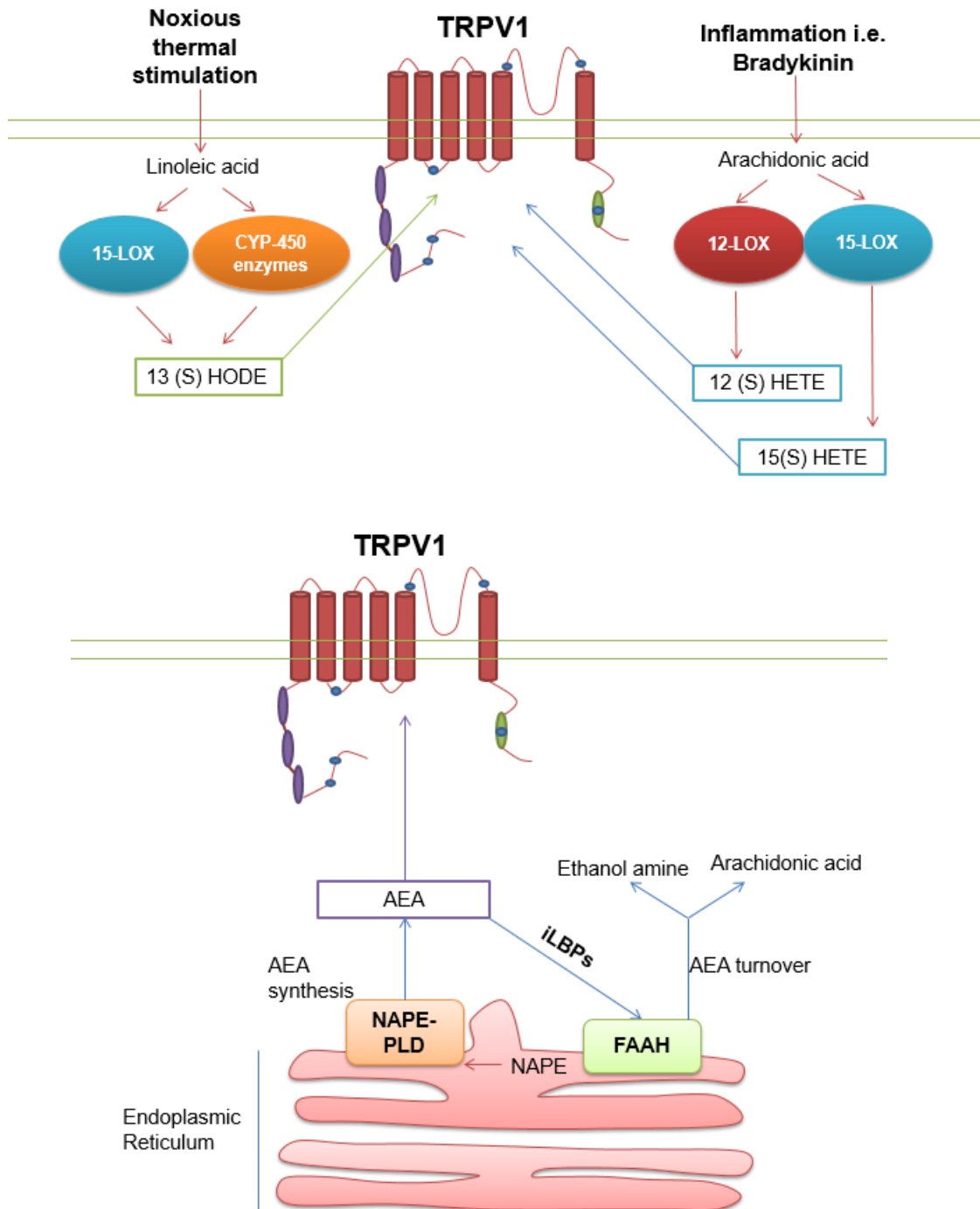


Figure 1.10: Endogenously synthesized lipids are activators of TRPV1 – In response to noxious stimuli or inflammatory mediators, there is a rapid synthesis of lipid derived species which activate TRPV1. In response to noxious heat, linoleic acid is oxidized by 15-LOX and CYP450 enzymes to 13(S) HODE, which activates TRPV1 and causes inward Ca^{2+} currents in nociceptors. Bradykinin has been shown to induce the endogenous synthesis of 12, and 15(S) HETE from 12/15-LOX mediated oxidation of arachidonic acid. AEA is synthesized by NAPE-PLD from its precursor NAPE in a Ca^{2+} dependent manner. AEA has also been reported to activate TRPV1 receptors and amplify Ca^{2+} influx. The effects of AEA can be terminated by FAAH mediated catabolism – hydrolysis to ethanolamine and arachidonic acid.

1.6 PPARs and pain

1.6.1 PPAR and their molecular mechanism of action

The peroxisome proliferator activated nuclear receptors (PPARs) are members of the nuclear receptor family of ligand dependent transcription factors. Three PPAR isoforms are known and are referred to as PPAR α , PPAR β , and PPAR γ with each isoform being encoded by a distinct gene (80). PPARs are known to play an instrumental role in the regulation of a variety of biochemical and physiological processes, these range from the metabolism of nutrients such as lipids and carbohydrates to the control of inflammatory gene expression (80). PPARs exert their effect by regulating the expression of genes, which are implicated in the aforementioned biological processes, in a ligand dependent manner (81, 88, 89).

PPARs form obligate heterodimers with the retinoid X receptor (RXR), and as a dimeric protein complex, they are thought to constitutively associate with DNA PPAR response elements (PPREs) of target genes (80, 84). In this situation, the 3D structure or conformation of PPARs favours the recruitment of co-repressor proteins. The result is a PPAR protein complex that under these conditions actively silences the expression of target genes (83, 84). Intracellular and extracellular lipid metabolism generates a variety of different lipophilic species which can activate PPARs in a ligand dependent manner (82, 86, 91).

Additionally, PPARs can also be activated by a range of synthetic compounds. Upon the binding of a specific agonist, there is a conformational change in the 3D structure of the PPAR, which results in the recruitment of coactivator proteins that play a role in the upregulation of PPAR responsive genes (80, 85, 88). This is referred to as ligand dependent transactivation. Conversely, activation of PPARs can downregulate the expression of target genes, which is achieved via

antagonizing the actions of associated transcription factors. This referred to ligand dependent PPAR mediated transrepression (85).

1.6.2 The role of PPAR α in pain

In addition to their roles in controlling energy homeostasis, PPARs have also been implicated in the regulation of nociception, more specifically pain syndromes including inflammatory hyperalgesia and neuropathic pain processing (90,93). Evidence from experimental models of inflammatory pain and neuropathic pain show that the stimulation of PPAR receptors with PPAR ligands sees a concomitant decrease in proinflammatory gene expression levels, which is attributed to the molecular mechanism of ligand dependent-trans-repression (Section 1.6.1).

PPAR α was found to be expressed in DRGs, and over the last decade or more it has emerged as a critical player in the processing of noxious sensory input (94). PPAR α appears to exert a constitutively homeostatic role in nociceptive primary sensory neurons by preventing ectopic neuronal firing, in part by maintaining the resting potentials of unstimulated nociceptive afferents (92, 97, 98).

It is thought that two distinct molecular mechanisms underpinning the anti-nociceptive and anti-hyperalgesic activity of PPAR α may exist. In various rodent models of inflammatory hyperalgesia, the administration of PPAR α specific synthetic and natural agonists (PEA) has been shown to rapidly reduce and reverse pain-related behaviors (95, 96). Importantly in models of inflammatory hyperalgesia, where the PPAR α gene was ablated, rodents were unresponsive to the anti-nociceptive properties of PPAR α specific agonists and exhibited an exaggerated sensitivity to pro-algesic mediators (95, 96).

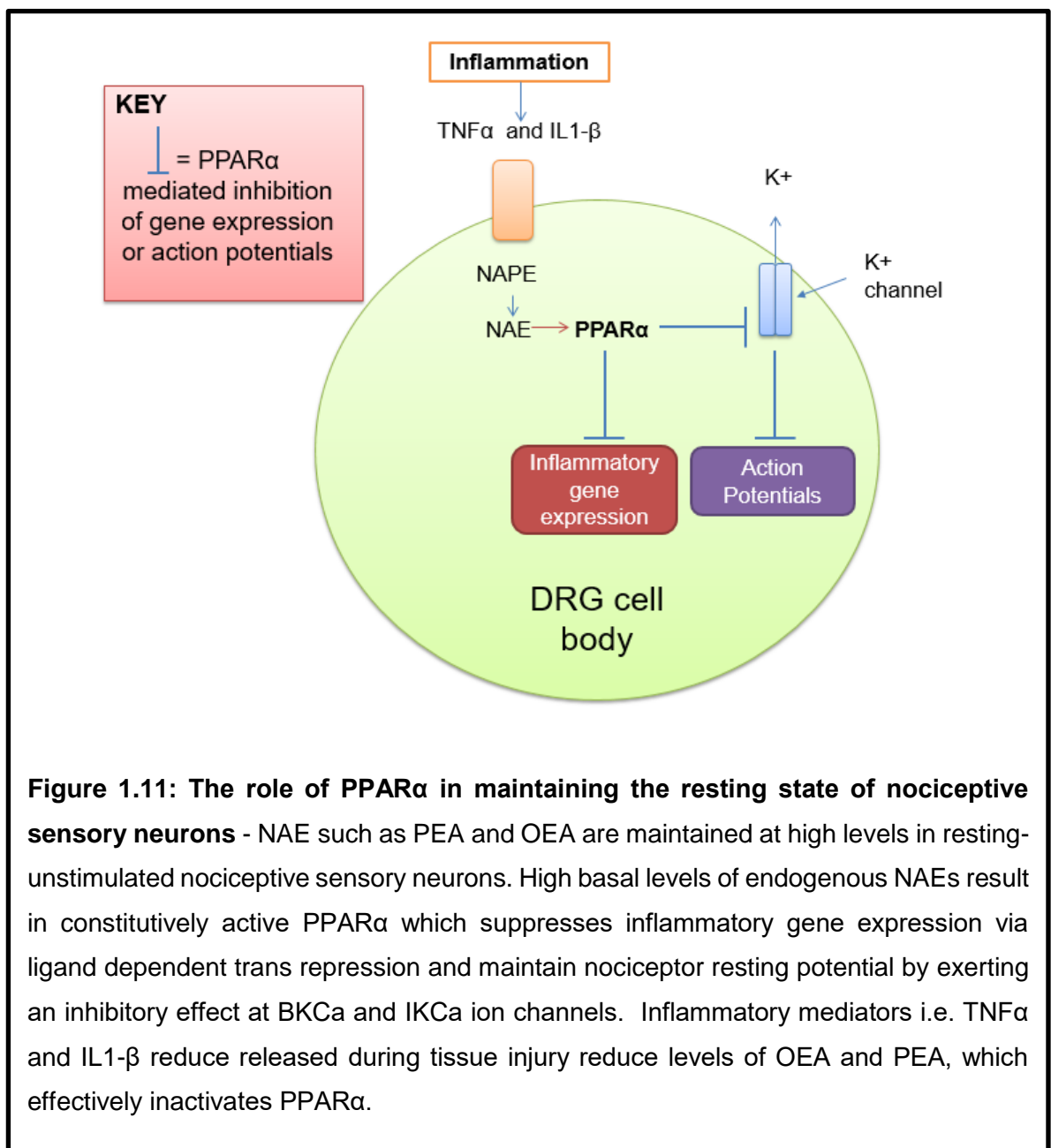
The rapid nature of the anti-nociceptive effect exerted by stimulated PPAR α is incompatible with PPAR α mediated regulation of gene expression and is indicative

of a non-transcriptional-related mechanism (94, 95). Previous experimental evidence has shown that activated PPAR α mediates its effect at different types of Ca²⁺ activated K⁺ channels, which include large (BK_{Ca}) and intermediate (IK_{Ca}) conductance channels (95). It is already established that these channels influence and control the excitability of sensory afferents. Unfortunately, the exact nature of the molecular mechanism that underpins how activated PPAR α controls channel gating remains elusive (Figure 1.11).

However, D'Agostino et al. (95) demonstrated that the canonical mechanisms of PPAR α action are still relevant in inflammatory hyperalgesia. Stimulation of PPAR α with PEA was shown to reduce the expression of pro-algesic mediator synthesizing enzymes Cyclo-oxygenase-2 (COX-2) and inducible nitric oxide synthase (iNOS) in DRGs.

In summary, PPAR α is expressed in DRGs and has been implicated in counteracting the effects of inflammatory hyperalgesia on neuronal cell excitability (98). In the absence of tissue injury and inflammation, the DRG cells abundantly synthesize uncharged neuromodulatory lipids, N-acylethanolamines (NAEs) from the shared precursor N-acylphosphatidylethanolamine. NAEs include palmitoylethanolamine (PEA) and oleoylethanolamine (OEA) and are thought to play a major role regarding influencing and exhibiting a tonic inhibitory control over the neuronal excitability of nociceptive sensory afferents. PEA and OEA mediate their effects in a PPAR α dependent manner by two distinct mechanisms, one of which actively suppresses inflammatory gene expression and the other inhibits ion channel activity, both of which can influence nociceptor sensitivity and excitability respectively. In this sense, NAEs can be considered to play a homeostatic role in actively maintaining a state of nociceptive quiescence.

In instances of tissue injury and inflammation this inactivity is lost. The presence of bacterial endotoxin Lipopolysaccharide (LPS) and the array of pro-inflammatory cytokines released from infiltrating immune cells suppress the biosynthesis of the OEA and PEA. The result is the cessation of NAE signalling at PPAR α and concomitant loss of tonic inhibition of transcription and non-transcriptional pro-nociceptive signalling pathways.



1.7 Fatty acid binding proteins (FABPs)

1.7.1 An introduction to FABPs

The hydrophobic nature of extra/intracellular lipid species such as endovanilloids and PPAR ligands renders them incompatible with the aqueous environment of the cytosol. The basic immiscibility of de novo synthesized endogenous lipids such as AEA, PEA and 13 (S) HODE in the aqueous cytosol, dictates that some form of suitable transient storage and trafficking be required. Furthermore, such lipophilic species have a transient life span and are prone to enzymatic mediated degradation. Therefore, intracellular lipid binding proteins (iLBPs) mediate the shuttling of lipid ligands to their required destination to exert their biochemical/physiological effect (99).

The 14-15 kDa fatty acid binding proteins (FABPs) is a group of highly conserved cytosolic proteins which are examples of iLBPs that can solubilize then shuttle lipophilic species. FABPs are expressed in a plethora of different tissues and play key roles in modulating a range of metabolic and cellular signalling processes (100-102). FABPs can sequester a range of lipophilic species reversibly, and this includes short or long chain saturated and unsaturated fatty acids but also encompasses a range of other lipid derived species including prostaglandins and endocannabinoids (103). Ten separate genes encoding nine different FABPs arose by successive gene duplication, and each FABP was allocated a name based upon the tissue in which it was found to be expressed (104, 105). However, note that this nomenclature can pose difficulties, as over many years it has been found that FABP expression is not as tissue specific as some naming systems imply. For this thesis, FABPs will be referred to numerically (Table 1.1).

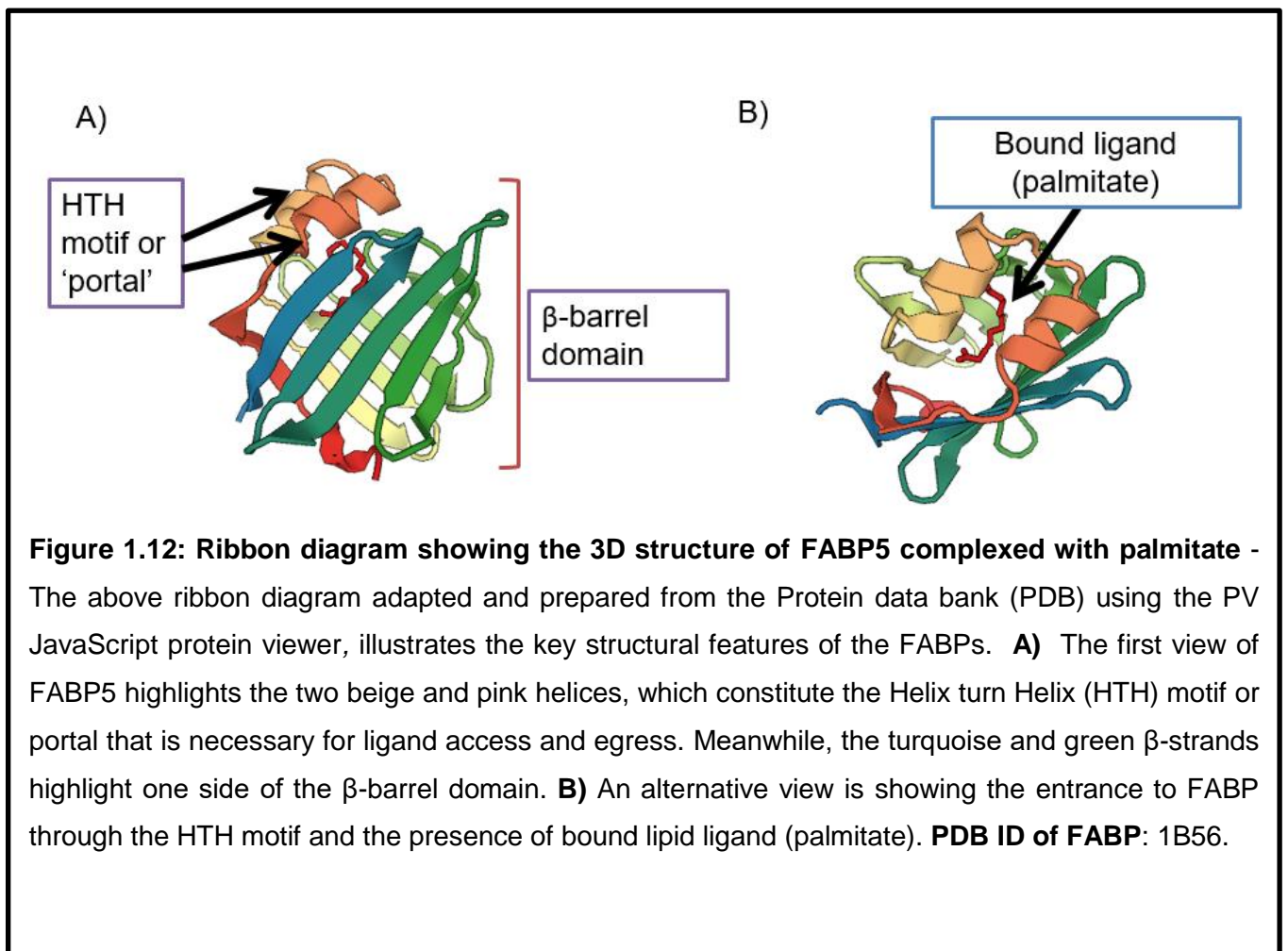
Table 1.1: A summary of the various FABPs, some of their synonyms and sites of expression

FABP	'Synonyms' also indicating its site of expression	Other sites(s) of expression
1	Liver (L)- FABP	Kidney, Intestine, Pancreas, Lung, Stomach
2	Intestinal (I)- FABP	Liver
3	Heart (H)-FABP	Aorta, brown adipose tissue, brain, placenta, skeletal muscle, mammary gland, testis, adrenal gland
4	Adipocyte (A)-FABP	<i>Macrophage</i> , dendritic cell, and adipocyte
5	Keratinocyte (K)-FABP	<i>Macrophage</i> , Tongue, dendritic cell, retina, spleen, mammary gland, Liver, Heart, lung, Lens, adipocyte, Skeletal muscle, intestine.
6	Ileal (II)-FABP	Adrenal gland, Stomach, and ovary
7	Brain (B)-FABP	Retina, mammary gland, glial cell
8	Myelin (M)-FABP	-
9	Testis (T)-FABP	Salivary gland and mammary gland
12	Testis (T)-FABP	Testes, Retina

1.7.2. Structure of the FABPs

The FABPs are all remarkably similar in the overall 3D structure and fold that they adopt. This is despite the poor and inconsistent amino acid sequence homologies (which range from 20-70%) observed when directly comparing the primary amino acids sequence of the different FABP isotypes (103). Biophysical techniques which include X-ray crystallography and nuclear magnetic resonance spectroscopy, have allowed for the determination of the 3D structure of isolated recombinant FABPs. They have revealed that all FABPs consist of the following 3-dimensional structural framework; a β barrel composed of 10 antiparallel β strands which are split or organized into two β sheets which are roughly perpendicular concerning each other, with the barrel containing the ligand binding pocket (Figure 1.12) (104). The binding cavity or pocket for lipophilic species of the FABPs is markedly larger compared to

ligand it accommodates. Within the binding cavity, the positively charged side chain of the amino acid residue, Arginine, interacts with the negatively charged carboxylate group of fatty acid ligands. Framing the barrel is a Helix turn Helix motif (HTH), a structural feature that has been argued to act as a 'gateway' to permit entry - exit of lipophilic ligand (103,105).



1.7.3 FABPs as modulators of lipid signalling pathways. Implications for TRPV1 and PPARs in nociception.

As the name implies the principle role of each FABP isotype is to act as an intracellular lipid shuttle that sequesters and protects hydrophobic ligand species from the aqueous environment of the cytosol and in some cases from degradation. Functionally FABPs mediate the transportation of their lipid cargo to various cellular destinations that influence metabolic, transcriptional and non-transcriptional networks that govern cell activity and fate (106, 111, 114).

For example, previous experimental evidence has argued FABP3 play a fundamental role in delivery of palmitate to mitochondria for β -oxidation in skeletal muscle tissue (103). Genetic ablation of FABP3 was shown to reduce oxidative metabolism of the fatty acid, palmitate, which suggests that to sustain mitochondrial - β - oxidation FABP3-mediated shuttling of palmitate is necessary (104, 105).

It has been widely reported that FABPs influence transcriptional signalling networks that control cell survival and differentiation by regulating and modulating the activity of transcription factors i.e. ligand dependent nuclear receptors. This is achieved by controlling the delivery of stimulatory lipophilic ligands (110,111, 113).

Cell survival can be influenced at the level of gene expression by FABP5. The consequence of high FABP5 expression results in partitioning retinoic acid away from the retinoic acid receptor (RAR) and towards the nuclear receptor PPAR β/δ , which upregulates the expression of pro-cell survival genes and indirectly downregulates the expression of pro-apoptotic genes (102, 109).

FABP5 has also been shown to influence cellular differentiation. FABP5 is expressed in keratinocytes and mediates the uptake of linoleic acid for conversion of 13(S) HODE. 13(S) HODE signals to activate the transcription factor NF κ B, which upregulates the expression of specific genes required for keratinocyte differentiation.

A phenomenon which is counteracted in keratinocytes where there is genetic ablation of FABP5 (111).

As alluded to above FABPs act as intracellular carriers of lipophilic activating ligands for PPARs, for example, FABP4 is shuttled continuously between the cytosol and nucleus to mediate the delivery of activating ligands for PPAR γ (113). Whereas FABP5 has been shown to transport and enhance the effect of uncharged neuro-modulatory lipid oleoylethanolamide (OEA) at PPAR α (112).

Interestingly, specific ligands can influence the subcellular localization of FABP7 and therefore its associating protein partners. FABP7 has been implicated as a diagnostic marker in malignant gliomas (MG). Arachidonic acid and DocosaHexaenoic Acid (DHA) both bind to FABP7 but produce distinct and differential-modulatory effects on MG cell line activity. When it is bound to AA, FABP7 will interact with Cyclo-oxygenase-2 (COX-2) to provide AA substrate for enzymatic conversion to prostaglandins, which are implicated in signalling processes that promote cell migration. Whereas DHA has anti-migratory effect as it causes FABP7 to localize to the nucleus and activate PPAR γ (114, 115).

Cell culture based studies have also provided evidence for FABP mediated trafficking of NAEs such as AEA and OEA to PPARs and hydrolysing enzymes. Examples include FABP5 mediated trafficking of OEA to PPAR α in cultured HeLa cells. While previous studies have shown FABP5 and 7 to deliver AEA for inactivation by fatty acid amide hydrolase (FAAH), an enzyme which catalyzes the catabolism of AEA to arachidonic acid and ethanolamine (116). In summary, the FABPs serve as integral molecular components to modulate a key range of physiological processes.

1.8 Aims of thesis

The central objective of this thesis is to establish whether members of the FABP family shuttle pro-nociceptive endovanilloids to activate TRPV1. A secondary aim is to determine the expression of PPAR isotypes in DRGs. This was for future investigations, which will examine the interplay between PPARs FABPs in DRGs. The family of endovanilloids include AEA and OLAMs such as 13(S) HODE and have been reported to activate or exert a modulatory effect on TRPV1 activity during acute nociceptive pain processing and inflammatory hyperalgesia. Direct antagonism of TRPV1 with synthetic compounds has been shown to produce many unwanted side-effects. Therefore, alternative approaches are required to reduce or dampen TRPV1 activity, as opposed full inhibition.

Based on previous experimental evidence reviewed in this introduction, this thesis hypothesizes that FABPs transport newly synthesized endovanilloids to activate TRPV1. Inhibition of FABP mediated delivery of such endovanilloids with pharmacological agents, would ablate this signalling axis and efficiently indirectly inhibit TRPV1 activity. Work undertaken in this thesis sought to establish the interaction between FABPs and TRPV1.

The specific aims and objective are summarized below

1. Firstly, establish which FABP isotypes and PPAR isoforms are expressed in the cells – soma of the rat DRG.
2. Establish that the FABPs expressed in DRGs could physically bind to two of the best characterized endovanilloids AEA and 13 (S) HODE.
3. Illustrate that the FABPs bound to pro-nociceptive lipid cargo; AEA or 13(S) HODE, could physically associate with recombinant TRPV1 expressed in a non-native cell culture system.

Chapter 2: Materials and Methods

Chapter 2: Materials and Methods

Materials

All chemicals and reagents were purchased from Sigma or BDH unless otherwise stated.

2.0 Bacterial and mammalian cell culture media

2.0.1 Bacterial cell culture media

Luria Bertani (LB) Broth pH7.4: 1 litre of LB Broth bacterial growth medium was prepared by dissolving 10g tryptone, 5g yeast extract and 5g of NaCl in 900ml HPLC grade H₂O then adjusting the pH to 7.4 with 1M NaOH. The volume was then adjusted to 1 litre with HPLC grade water. LB Broth was sterilized by autoclaving at 120°C for 20 minutes.

LB Agar: LB Agar was prepared by adding agar to LB Broth at a final concentration of 1.5% [w/v] followed by autoclaving as above.

2.0.2 Mammalian cell culture media and transfection reagents

Neurobasal® Medium (NBM) Gibco™ Life Technologies (Thermo-Fisher): NBM containing 4500mg.L⁻¹ glucose and 25mg.L⁻¹ sodium pyruvate was supplemented with 10% [w/v] horse serum, nerve growth factor (NGF) 25ng.ml⁻¹, glial-cell line derived neurotrophic growth factor (GDNF) 50ng.ml⁻¹, 5mM L-glutamine, 200U.ml⁻¹ penicillin and 200µg.ml⁻¹ streptomycin.

Dulbecco's Modified Eagles Medium (DMEM) (Sigma): DMEM containing 4500mg.L⁻¹ glucose and 100mg.L⁻¹ sodium pyruvate was supplemented with 10% (v/v) foetal bovine serum (FBS), 2mM L-glutamine, 100U.ml⁻¹ penicillin and 100µg.ml⁻¹ streptomycin sulphate.

Sterile Phosphate Buffered Saline (PBS): 1 PBS tablet was dissolved in 100ml of HPLC grade water, followed by autoclaving as described previously.

Transfection Reagents: X-treme™ Gene HP (Roche, Cat. No.06366546001) or Lipofectamine® 2000 (Invitrogen™, Life Technologies, Cat. No 11668-019) were used for transient transfections.

2.1 Antibiotics and drugs

Ampicillin (Sigma): Ampicillin was prepared as 100mg.ml⁻¹ stock solution in sterile HPLC grade H₂O then passed through a 0.2µm Sartorius sterile filter unit and stored at -20°C. Ampicillin stock was then diluted to a final working concentration of 100µg.ml⁻¹ in cooled LB Broth or LB Agar.

Kanamycin (Sigma): Kanamycin was prepared as 30 mg.ml⁻¹ stock solutions in sterile HPLC grade H₂O, sterile filtered and stored at -20°C as above. When required, kanamycin stock was diluted with LB Broth or LB Agar to a final working concentration of 30µg.ml⁻¹.

Arachidonic acid (Sigma): Arachidonic acid was reconstituted in DMSO to give a 60mM stock.

Anandamide (TOCRIS, Cat No. 1339): Anandamide was supplied in absolute ethanol at a concentration of 5mg.ml⁻¹ which equated to 14.4mM. Anandamide was then diluted with absolute ethanol to give a 10mM working stock.

13 (S) Hydroxyoctadecadienoic acid (HODE) (Cayman Chemicals 38610): 1ml of 13(S) HODE in absolute ethanol was supplied at a concentration 1mg.ml⁻¹ which equated to a concentration of 3.4mM. The concentration of 13(S) HODE was increased to 10mM by reducing the volume of the solvent to 337µL. This was achieved by gentle evaporation by blowing the original stock of 13(S)HODE with inert nitrogen gas, at low pressure.

12-N-methyl-(7-nitrobenz-2-oxa-1,3-diazo) amino stearic acid (12-NBD stearate) (Avanti Polar Lipids, 810110P): 2mg of 12-NBD stearate powder was dissolved in DMSO to give a 10mM stock. The 10mM stock was aliquoted and stored in tinted glass vials at -20°C. The 10mM working stock was then diluted as and when required with DMSO or an aqueous buffer.

Isopropyl β -D-1 galactopyranoside (IPTG): A 1M stock of IPTG was prepared in HPLC grade H₂O then sterile filtered as above. The 1M stock was then diluted a 1000-fold into liquid bacterial cultures to a final concentration of 1mM.

2.2 Buffers and solutions

2.2.1 Protein expression and purification buffers

Potassium phosphate buffer pH7.4: 300mM KCl and 50mM KH₂PO₄.

Native lysis buffer pH7.4: 5mM Imidazole, 300mM KCl and 50mM KH₂PO₄, 1% [w/v] sodium deoxycholate and 1% [w/v] Triton X-100.

Native wash buffer 1 pH7.4: 5mM Imidazole, 300mM KCl, and 50mM KH₂PO₄.

Native wash buffer 2 pH7.4: 10mM Imidazole, 300mM KCl, and 50mM KH₂PO₄.

Native elution buffer pH7.4: 250mM Imidazole, 300mM KCl and 50mM KH₂PO₄.

2.2.2 Buffers for agarose gel electrophoresis

50 x Tris Acetate-EDTA (TAE): 2M Tris, 2M acetic acid and 50mM EDTA pH 7.6. 50x TAE was routinely diluted to 1x TAE with HPLC grade water for electrophoresis.

2.2.3 Buffers for sodium dodecyl polyacrylamide gel electrophoresis, coomassie blue staining, and immunoblotting

Radio-Immunoprecipitation Lysis Buffer: 150mM NaCl, 25mM Tris-HCl, 1% [w/v] Triton X-100, 1% [w/v] sodium deoxycholate, 0.1% [w/v] SDS and 1 × Roche complete cocktail protease inhibitor.

2 × Laemmli loading buffer: 4% [w/v] SDS, 20% [v/v] glycerol, 120mM Tris-HCl pH6.8 0.02% [w/v] bromophenol blue and 200mM DTT in HPLC grade water. Loading buffer was then stored at -20°C. 2x Laemmli loading buffer was routinely diluted to a 1x working concentration.

4 × Resolving Gel Buffer: pH8.8 1.5M Tris Base, 0.4% [w/v] SDS

4 × Stacking Gel Buffer pH6.8: 0.5M Tris Base, 0.4% [w/v] SDS.

8-15% Resolving gels: 10ml of resolving gel was prepared by diluting 2.7ml – 5ml of 30% (w/v) acrylamide (Sigma) with 2.5ml of 4 × resolving gel buffer and then the addition of 4.6 – 2.3ml of HPLC grade water. To polymerise the acrylamide, 0.02µL of tetramethylethylenediamine (TEMED) was followed by 200 µL of 10% [w/v] Ammonium Persulphate (APS). The gel was then immediately poured.

Stacking gel: 10ml of stacking gel was prepared by adding 1ml of 30% [w/v] acrylamide to 6.5ml HPLC grade water and 2.5ml of 4 × stacking buffer. Acrylamide was polymerized by addition of 10 µL of TEMED then 100 µL of 10% [w/v] APS.

10 × Running buffer: 30g of Tris Base, 144g of glycine and 10g of SDS was dissolved in 900ml of HPLC grade H₂O. The final volume was then adjusted to 1000ml with HPLC grade H₂O. For electrophoresis, 1x running buffer was prepared by diluting 100ml of 10 × running buffer with 900ml of HPLC grade H₂O.

10 × Transfer Buffer (TB): 1 litre of 10 × TB was prepared by initially dissolving 30g of Tris-Base and 144g of glycine in 900ml of HPLC grade H₂O. The final volume was then adjusted to 1000ml with HPLC grade H₂O.

1 × TB: 1 litre of 1× TB was prepared by diluting 80ml of 10 × TB with 160ml of methanol and HPLC grade water to a final volume of 1000ml.

Coomassie blue stain: Coomassie Blue stain contained 0.25% [w/v] coomassie brilliant blue R-250, 7.5% [v/v] acetic acid and 45% [v/v] isopropanol in HPLC grade H₂O.

De-staining solution: 7.5% [v/v] Acetic acid and 25% [v/v] isopropanol in HPLC grade H₂O.

10 × Tris Buffered Saline (TBS) pH7.6: 24.2g of Tris Base and 80.1g of NaCl was dissolved 800ml of HPLC grade water. The pH was adjusted to 7.6, and the final volume was made up to 1000ml with HPLC grade water to give a 10×TBS stock.

1 × Tris Buffered Saline Tween- 20 (TBST): .1ml of Tween-20 was added to 100ml of 10×TBS followed by dilution with 900ml of HPLC grade water to give TBST (1× TBS, 0.1% [v/v] Tween-20)

Blocking solution: Non-fat dry milk powder was dissolved to 5% [w/v] with 1×TBST

2.2.4 Buffers for histology and immunofluorescence

Paraformaldehyde (PFA): A 100ml stock of 4% [w/v] PFA was prepared by gradually dissolving 20g of PFA in 70ml of PBS by heating at 70 - 90°C and gentle stirring until a colourless solution was formed. The solution was then allowed to cool, and the final volume was then adjusted to 100ml with PBS. 4% PFA was then filtered using 3mm Whatman Filter paper.

Cresyl violet: 0.1% [w/v] Cresyl violet acetate in 0.25% [v/v] acetic acid. Acetic acid was diluted to final concentration of 0.25% [v/v] with HPLC grade water. 0.1g of cresyl violet acetate was dissolved in 100ml of 0.25% [v/v] acetic acid solution.

Differentiate solution: 95% [v/v] ethanol containing 2 drops of glacial acetic acid from a plastic Pasteur pipette.

Triton Tris Buffered Saline (TTBS) pH7.4: For 1 litre of TTBS, 8.7g of NaCl was initially dissolved in 50ml of Tris-HCl (Sigma T2663), followed by the addition of 3ml of Triton-X 100 then 800ml of HPLC grade water. The pH was adjusted to 7.4, and the final volume was adjusted 1000ml.

PBS – Tween 20 (PBST): Tween-20 was added to PBS at a final concentration of 0.25%

PBST – BSA 1% [w/v]: BSA was added to PBST to a final concentration 1%.

Blocking Solution: PBST containing 3% serum.

2.3 Live cell calcium (Ca²⁺) imaging solutions

Regular Ca²⁺ imaging buffer pH7.4: 145mM NaCl, 5mM KCl, 2mM CaCl₂, 1mM MgSO₄·7H₂O, 10mM HEPES, 10mM(D)-glucose and 2.5mM probenecid.

Ca²⁺ free imaging buffer pH7.4: 145mM NaCl, 5mM KCl, 1mM MgSO₄·7H₂O, 10mM HEPES, 10mM(D)-glucose and 2.5mM probenecid.

(+) Ca²⁺ reconstitution imaging buffer: 145mM NaCl, 5mM KCl, 2.5mM CaCl₂, 1mM MgSO₄.7H₂O, 10mM HEPES, 10mM(D)-glucose and 2.5mM probenecid.

Methods

2.4 Bacterial cell culture methods

2.4.1 Preparation of chemically competent *E.coli* cells

From a freshly streaked LB Agar plate, a single colony of DH5 α or SoluBL21™ *E.coli* cells was inoculated in 5ml of LB Broth and grown for 18 hours at 250rpm in an orbital shaker at 37°C. The overnight culture was then diluted 1:100 into 50ml of LB Broth contained in a sterile 250ml Pyrex® Flask and grown at 250rpm in an orbital shaker at 37°C until cell density reached a value of 0.2-0.3 when absorbance was measured at a wavelength of 600nm (OD₆₀₀). Cells were then harvested by centrifugation at 3,500 × *g* at 4°C for 10 minutes using an Allegra® X-22R refrigerated centrifuge. Pelleted cells were then resuspended in sterile 100mM CaCl₂ and chilled on ice for 30 minutes. The cell suspension was then recentrifuged as described previously. The resulting cell pellet was resuspended in 1.25ml of 20% (v/v) glycerol – 80mM CaCl₂ solution. Resuspended cells were then aliquoted into pre-chilled Eppendorf tubes and stored at -80 °C.

2.4.2 Transformation of chemically competent *E.coli* with plasmid DNA

A 100ng of plasmid DNA was added to a 50 μ l aliquot of chemically competent DH5 α or SoluBL21™ *E.coli* cells. Cells were then incubated on ice for 30 minutes followed by heat shock for 30 seconds at 42°C. Cells were incubated back on the ice for a further 2 minutes. 950 μ l of LB Broth was then added to the cells, which were then grown at 37°C at 250rpm in an orbital shaker for 45 minutes. 100 μ l of transformed cells were then spread onto freshly prepared LB Agar containing the appropriate antibiotic compatible with the plasmid used in the transformation. Plates were then incubated overnight at 37°C. Single colonies were then inoculated into 5ml of LB Broth using a sterile plastic loop.

2.4.3 Small and large-scale propagation of bacteria

A single bacterial colony from an LB Agar-antibiotic selection plate was inoculated into 5ml of LB Broth containing the appropriate antibiotic. Bacteria were then propagated at 37°C in an orbital shaker at 250rpm for 18-24 hours. The overnight culture was then used in a small-scale plasmid DNA isolation or used to inoculate a larger scale bacterial culture and to prepare a 50% bacterial glycerol stock, by diluting 1ml of the overnight 5ml culture with an equal volume sterile 100% glycerol. The bacterial glycerol stock was then stored at -80°C. The remainder of the small-scale culture was diluted 1:500 into 100ml of LB Broth containing appropriate antibiotic and then grown as described previously.

2.5 Nucleic acid methods

2.5.1 Isolation of plasmid DNA from bacterial cell cultures

DH5α *E.coli* cells were harvested by centrifugation of 2ml aliquots of overnight culture at 13,000× *g* for 5 minutes at room temperature. Plasmid DNA was isolated from the pelleted bacterial cells using QIAPrep Spin Mini Prep Kit (QIAGEN) according to the manufacturer's instructions. DNA was eluted from the column using 50µl of autoclaved HPLC grade H₂O. To obtain an increased yield of plasmid DNA, a larger 100ml bacterial culture was grown overnight. Plasmid DNA was isolated from this larger scale culture using a NucleoBond® PC 100 plasmid DNA purification kit (Macherey-Nagel) following the manufacturer's guidelines.

2.5.2 Isolation of total RNA from cell cultures

Total RNA was extracted from cell cultures using 500µl of TriReagent by scraping. Tri-Reagent extracts were then decanted into RNase free 1.5ml Eppendorf tubes followed by the addition of 100µl of 1-Bromo-3-chloropropane (BCP). Samples were then vortexed briefly and allowed to incubate at ambient temperature for 5 minutes followed by centrifugation at 12,000 × *g* at 4°C using a refrigerated bench top microcentrifuge. The resulting top aqueous phases were decanted into fresh RNase free microfuge tubes followed by the addition of the following by mixing; 175µl of 3M sodium acetate, 350µl of isopropanol and 1µl of 20µg.ml⁻¹ molecular biology grade glycogen (Roche). Samples were then stored at -20°C for 18 hours to aid RNA precipitation. RNA pellets were then recovered by centrifugation for 15 minutes at 12,000 × *g* at 4°C. The resulting RNA pellets were then washed twice with 75% [v/v] ethanol, with each wash being followed by centrifugation for 10 minutes at 12,000 × *g* at 4°C. The final RNA pellets were allowed to air dry briefly and then reconstituted in 50µl of RNase free – DEPC treated HPLC grade H₂O. RNA extractions were then incubated at 65°C for 5 minutes. Samples were then briefly centrifuged and stored at - 80°C.

2.5.3 Determination of DNA and RNA concentration

DNA and RNA concentration was determined using an FLUOstar® Omega plate reader (BMGLABTECH). The pedestals of the LVis plate (BMGLABTECH) were cleaned with 100% ethanol and with autoclaved HPLC grade H₂O. The LVis plate was then read by FLUOstar® Omega plate reader to confirm the cleanliness of each micro-drop well and the upper pedestal. Each micro-drop well was blanked with 2µL of autoclaved HPLC grade H₂O then cleaned. 2µL of DNA/RNA was analysed per micro-drop well, and the concentration of DNA/RNA was determined by measuring absorbance at 260nm. The purity of DNA and RNA was determined by measuring the ratio of the absorbance at 260 and 280nm. A ratio of 1.8 for DNA

was considered as pure where as a ratio of 1.8 - 2.0 for RNA was considered as pure.

2.5.4 Digestion of DNA with restriction endonuclease enzymes

DNA was digested with restriction endonuclease High-Fidelity® (HF) enzymes (New England Bio Labs) in a 50µl reaction at 37°C for 60 minutes. A typical 50µL reaction contained: 1µg DNA, 10 units of each restriction endonuclease enzyme required, 1 × NEBuffer CutSmart, and HPLC grade water up to a final volume of 50µl.

2.5.5 Analysis of DNA by agarose gel electrophoresis

An agarose gel was prepared by melting 0.7 – 1.5g per 100ml of autoclaved 1 × TAE. The amount of agarose melted was dependent on the size of the DNA fragment to be resolved by electrophoresis. Once the gel had cooled to an appropriate temperature, ethidium bromide was added at a final concentration of 0.2 – 0.5µg.ml⁻¹. The gel was then poured into a cast, and the comb was placed at the top of the gel. Once the gel had solidified, it was submerged in a multi-sub choice horizontal gene flow electrophoresis tank (G9-0014) containing 500ml of 1×TAE buffer. Aliquots of 0.1kb (N3231), 1kb (N3232) NEB molecular weight ladders and DNA samples were diluted to a final volume of 25µl with HPLC grade water followed by the addition of 5µl 6 × DNA loading dye (B7021S). DNA samples were then loaded onto the agarose gel and resolved by electrophoresis at 100V. After electrophoresis, DNA bands were visualized using a UV transilluminator. Gel images were acquired using GeneSnap software (Syngene) or DNA bands were excised from the agarose gel for further processing.

2.5.6 Extraction and subsequent purification of DNA fragments from agarose gels for molecular cloning

DNA bands were visualized under UV light using a UV trans-illuminator and excised from an agarose gel using a clean, sterile scalpel. The weight of the gel slice was recorded in a tared 15ml Falcon tube. DNA was purified from the gel slices using a GenElute™ gel extraction kit (Sigma-Aldrich) according to manufacturer's guidelines.

2.5.7 Reverse transcription (RT) of isolated RNA to complementary DNA (cDNA)

Isolated RNA was reverse transcribed to cDNA using AffinityScript™ multi-temperature reverse transcriptase (Agilent Technologies): 250-500ng of RNA was added to an RNase free microcentrifuge tube, followed by the addition of 300ng of random primer (Promega) and RNase free HPLC grade water up to a final volume 14.2µL. The reaction was mixed by repeat pipetting, then incubated at 65°C for 5 minutes and then allowed to cool 10 minutes at room temperature. The reaction mixture was then centrifuged at maximum speed in a bench top microcentrifuge after which the following was added by mixing; 2µL 10 × AffinityScript™ transcription buffer, 2µL of 100mM DTT, 1µL 25mM dNTP, 1µL AffinityScript™ multi-temperature reverse transcriptase and 1µL of RNase block giving the reaction mixture a final volume of 21.2µL. The reverse transcription mixture was incubated at the following temperatures: 25°C for 10 minutes, 50°C for 60 minutes and then 70°C for 15 minutes. The resulting cDNA was then stored at -20°C.

2.5.8 Polymerase Chain Reaction (PCR)

Amplifying target DNA sequences was carried out using a Bio-Rad T100™ thermal cycler and Phusion® High Fidelity (HF) DNA polymerase (New England Bio Labs, M0530S). A typical 50µL PCR reaction contained 1 × HF Buffer, 200µM dNTP, 0.5µM forward primer, 0.5µM reverse primer, 1 - 5µL cDNA template, 3% [v/v]

DMSO, 1.0-unit Phusion® HF DNA polymerase and HPLC grade water up to a final volume of 50µL. Where plasmid DNA served as template DNA, 50ng of the template was used in the PCR. Once assembled, the reaction mixture was mixed by repeat pipetting then centrifuged briefly at maximum speed. The reaction was then subject to the thermocycling parameters summarized in Table 2.1. Aliquots of the amplicons were then analysed by agarose electrophoresis as 2.5.5. If required for down-stream sub-cloning, PCR products were purified using a GenElute™ PCR clean up kit. The annealing temperature used for each primer pair in a PCR reaction is listed in the appendix. PCR primer sequences are listed in the appendix.

Table 2.1 Thermo-cycling parameters used in the amplification of all target genes by PCR

Step/Stage	Temperature (°C)	Duration (minutes)	Cycles
1. Initial denaturation	98	5:00	1
2. Denaturation	98	0:30	35
3. Annealing	58-72	0:30	
4. Extension	72	0:30	
5. <u>Final</u> extension	72	7:00	1

2.5.9 Molecular cloning

DNA digestion: Target genes were amplified by PCR as described previously, using primer pairs each containing restriction sites at their 5'ends. PCR amplicons were purified using a GenElute™ PCR Clean-Up Kit (Sigma-Aldrich) according to manufacturer's instructions. Plasmid DNA and purified PCR amplicons were

digested with 10.0 units of each of the appropriate restriction endonuclease enzymes (New England Bio-Labs) as in 2.5.4. Linearized plasmid DNA and cut PCR product were resolved and isolated by agarose gel electrophoresis as previously 2.5.6. In the case of blunt ended ligations, plasmid DNA was dephosphorylated with Calf Intestinal Alkaline Phosphatase (CIP) (New England Bio-Labs, M0201S) for 30 minutes at 37°C.

A typical 20µl de-phosphorylation reaction contained the following: 10.0 units of CIP, 1µg EcoRV- HF® cut-linearized plasmid DNA, 1 × restriction digestion buffer 3 (New England Bio-Labs) and HPLC grade water up to a final volume of 20µl.

Target genes were amplified by PCR as described in 2.5.8. PCR products were purified using a GenElute™ PCR clean-up Kit (Sigma-Aldrich) according to manufacturer's instructions. Purified PCR product was then phosphorylated at the 5' and 3' ends of the amplicon, using T4 polynucleotide kinase for 1 hour at 37°C in a 50µL reaction containing the following: 1× T4 DNA ligase buffer, 10.0 units of T4 DNA polynucleotide kinase (New England Bio-Labs, M0201S), 2.4% [w/v] PEG 6000 (Fermentas), 1µg purified PCR product and HPLC grade water up to a final volume of 50µl.

Ligation: PCR amplicon was ligated into linearized plasmid DNA using T4 DNA ligase (New England Bio-Labs,) at 15°C for 18 hours in a 20µl reaction containing the following: 50ng of plasmid DNA, 50ng PCR amplicon, 10.0 units of T4 DNA ligase, 1× T4 DNA ligase buffer and HPLC grade water up to 20µl.

Recovery of ligation reactions: 1µl of the overnight ligation reaction was transformed into chemically competent DH5α *E.coli* as in 2.4.2 A single colony of transformed DH5α *E.coli* was inoculated into 5ml of LB Broth containing plasmid selective antibiotic and propagated overnight at 37°C as previously. Plasmid DNA was isolated from the overnight culture using a QIAPrep spin miniprep kit

(QIAGEN) according to the manufacturer's instructions. The concentration of the recovered plasmid DNA was determined as in 2.5.3. Plasmid DNA was diluted to a final concentration of $100\text{ng}\cdot\mu\text{l}^{-1}$ with HPLC grade.

Diluted plasmid DNA was subjected to DNA sequencing (Source Biosciences, Nottingham, UK) to confirm DNA construct integrity. The plasmids constructed and the restriction enzymes used are detailed in the appendix.

2.6 Protein techniques

2.6.1 Protein isolation using radio-immunoprecipitation (RIPA) buffer

Protein was isolated from overnight cell cultures or tissues using an appropriate volume of radio-immunoprecipitation (RIPA) buffer. Cells were briefly rinsed with PBS which was then aspirated away and replaced with RIPA buffer for cell lysis. Cell lysates were scraped into a pre-chilled 1.5ml Eppendorf tube and subjected to sonication on ice for 10 seconds using a Misonix micro tip ultrasonicator at amplitude 1. There was a total of 3×10 -second sonications, with a 30-second interval between pulses. Tissue samples were homogenized in RIPA using a tissue homogenizer until a cloudy suspension devoid any obvious particulate matter, was seen. Tissue and cell lysates were subject to end over end rotation for 45 minutes at 4°C . Both tissue and cell lysates were clarified by centrifugation at $13,000 \times g$ for 15 minutes at 4°C in a bench top microcentrifuge. The resulting supernatants were decanted into a fresh microcentrifuge tube. The protein concentration of each supernatant was determined in triplicate using the Pierce® BCA assay kit and Bovine Serum Albumin (BSA) as a standard. The assay was performed in a 96 well plate according to the manufacturer's instructions (Thermo-Fisher Scientific).

2.6.2 Sodium Dodecyl Sulphate Polyacrylamide Gel Electrophoresis (SDS-PAGE)

15µl aliquots of protein samples or supernatants were added to an equal volume of 2 × Laemmli loading buffer and boiled at 99°C for 5 minutes. Samples were briefly centrifuged at maximum speed then loaded onto SDS polyacrylamide (8-15%) gel pre-assembled in a mini protean (Bio-Rad) electrophoresis tank. 10µl of precision plus protein™ kaleidoscope™ pre-stained protein standard molecular weight ladder (Bio-Rad) was also loaded per gel. Proteins were separated by electrophoresis at 100V until the visible molecular weight ladder had suitably resolved. After the electrophoresis, the gel was disassembled and prepared for immunoblotting or Coomassie blue staining.

2.6.3 Protein transfer and immunoblotting (IB)

The gel was transferred on top of the Amersham™Hybond™-ECL nitrocellulose membrane (GE Healthcare) saturated with transfer buffer stacked on top of a piece of Whatman No.3 filter paper and sponge also saturated with transfer buffer in an open plastic cassette. The gel and membrane were then 'sandwiched' by placing another piece of transfer buffer soaked Whatman No.3 filter paper and sponge on top of the gel. The plastic cassette was then closed and secured with a plastic clamp. The plastic cassette containing the membrane gel sandwich was then placed in a mini trans-blot cell tank (Bio-Rad) containing transfer buffer and an ice pack. Proteins were transferred by running the tank for 110V for 1 hour. Successful transfer was confirmed by staining the membrane with Ponceau red stain (Sigma) for 2 minutes with mild agitation. The membrane was then washed repeatedly with HPLC grade water with mild agitation until the majority of the stain had been removed.

The membrane was then blocked with blocking solution (1 × TBST containing 5% [w/v] non-fat dry milk) for 1 hour at room temperature with mild agitation. Primary antibodies were diluted to the appropriate final concentration with blocking solution. The membrane was then probed with diluted primary antibody/antibodies for 16 hours at 4°C with agitation. The following day, the membrane was washed three times with 1 × TBST for 15 minutes at ambient temperature with agitation. Anti- IgG- IRDYE LI-COR® secondary antibodies were diluted 1:10,000 with blocking solution. The membrane was then probed with diluted secondary anti-IgG antibody for 1 hour at room temperature in the dark. Unbound secondary antibodies were removed by washing the membrane three times with 1 × TBST for 5 minutes with agitation at room temperature in the dark. Immunodetection of proteins was visualized using a Li-COR ODYSEEY infrared imaging system (LI-COR Biosciences). Antibodies and dilutions used are listed in in the appendix.

2.6.4 Coomassie blue staining

After electrophoresis, the gel was submerged in a plastic container containing Coomassie blue stain, which was then sealed. The gel was stained at room temperature for 1 hour with mild agitation. The gel was then transferred to another plastic container containing de-staining solution pre-warmed to 37 - 42°C. The container was tightly sealed, and the gel was destained at 37-42°C in an incubator with agitation. The container was replenished with fresh de-staining solution at regular 15-minute intervals until the protein bands were visible and background coomassie stain had been mostly removed. Gel images were acquired using a Li-COR ODYSEEY infrared imaging system (LI-COR Biosciences).

2.6.5 Concentrating protein by trichloroacetic acid (TCA) precipitation

50g of TCA was initially dissolved in 25ml of HPLC grade water. The final volume was then adjusted to 50ml with HPLC grade water to give a 100% [w/v] working stock. 100% [w/v] TCA was diluted 1:10 to a final concentration of 10% [w/v] into protein samples that were to be precipitated. After the addition of TCA, protein samples were placed on ice for 30 minutes. Protein precipitates were recovered by centrifugation at maximum speed for 15 mins at 4°C in a bench top microcentrifuge. The supernatant was decanted, and the resulting pellets were resuspended and washed in 100% ice cold acetone by vortexing. Proteins were re-pelleted by centrifugation, and the pellets washed with acetone as described above. This was repeated once more. After the 3rd and final centrifugation – acetone wash, protein pellets were allowed to air dry until all the acetone had evaporated. Pellets were then resuspended in an appropriate volume of 1 x Laemmli buffer containing 100mM DTT and boiled at 99°C for 5 minutes ready for analysis by SDS-PAGE.

2.7 Expression and purification of recombinant histidine tagged human FABPs

2.7.1 Inducing the expression of recombinant Hexa-histidine tagged FABPs in bacterial cell cultures

SoluBL21TM *E.coli* bacteria transformed with pET28a (+) plasmid DNA encoding for a recombinant Hexa-Histidine tagged FABP, was streaked out from a bacterial glycerol stock onto a LB Agar antibiotic kanamycin selection plate and grown as in 2.4.2 A single bacterial colony from the agar antibiotic selection plate was inoculated in 5ml of LB Broth containing plasmid selective antibiotic kanamycin as described in 2.4.5. 1ml of the 5ml starter culture was diluted 1:500 in 500ml of LB Broth in a baffled flask and grown with agitation at 250rpm in an orbital shaker at 37°C. The culture was allowed to grow until the cell density reached an OD₆₀₀ of

0.6. At this point, a 1ml fraction of the culture was centrifuged at $13,000 \times g$ for 15 minutes at 4°C , to harvest the uninduced cells (T_0). The cell pellet was then stored at -20°C . Protein expression was then induced by the addition of IPTG at a final concentration of 1mM to the remainder of the culture, which was then incubated for 24 hours in orbital shaker at 250rpm at either 25°C or 37°C . After 24 hours of protein expression, a 1ml fraction of the culture was taken and centrifuged as above to harvest the induced cells ($T_{24\text{h}}$).

2.7.2 Confirmation of recombinant protein expression by SDS-PAGE

The pelleted cells from the T_0 and $T_{24\text{h}}$ fractions were resuspended in $250\mu\text{L}$ of RIPA buffer by gentle pipetting to give homogeneous cloudy cell suspensions. Cell suspensions were subsequently sonicated (pulsed) on ice using a Misonix micro tip ultrasonicator at amplitude 1 for 15 seconds, three times, with 30-second intervals between pulses. The cell lysates were then clarified by centrifugation at $13,000 \times g$ for 15 minutes at 4°C ; the resulting supernatants containing soluble proteins (T_{SOL}) were decanted into a fresh 1.5ml micro centrifuge tube while the remaining pellets containing insoluble proteins (T_{INS}) were resuspended in $250\mu\text{L}$ of RIPA buffer. T_{SOL} and T_{INS} protein samples were diluted with an equal volume of 2x Laemmli loading buffer and denatured by boiling at 99°C for 10 minutes. $40\mu\text{L}$ of samples were then resolved on a 15% SDS-polyacrylamide gel by electrophoresis as in 2.6.2. After electrophoresis proteins were visualized by Coomassie blue staining as described in 2.6.4

2.7.3 Preparation of native cell lysates for protein purification

The remaining overnight cultures were centrifuged in 50ml aliquots in 50ml falcon tubes at $10,000 \times g$ using a fixed angle rotor in an Alegra® X-22R refrigerated centrifuge at 4°C for 15 minutes. Five cell pellets per recombinant protein were used for protein purification. Each pellet was resuspended in 1ml of native lysis

buffer by vigorous vortexing, giving 5 × 1ml cell suspensions, which were then pooled to give a 1 × 5ml cell suspension. Each 5ml cell suspension was sonicated on ice using Misonix micro tip ultrasonicator at amplitude 5 for 15 seconds, 72 times, with 30-second intervals between pulses. The resulting lysate was clarified by centrifugation at 10,000 × *g* at 4°C for 15 minutes. To remove any particulate matter and prepare for metal affinity purification, supernatants were filtered through a 0.45µm Sartorius filter unit using a 5ml syringe.

2.7.4 Purification of Hexa-histidine tagged FABPs by immobilized metal (Ni²⁺) affinity chromatography (IMAC)

A 5ml bio-Scale™ mini profinity™ IMAC cartridge/column (Biorad), pre-charged with nickel (Ni²⁺) ions, was connected to a BioLogic LP system (Bio-Rad) and equilibrated with 5 column volumes (5CV) of native wash buffer 1 at a flow rate of 2ml.min⁻¹. The flow rate was maintained at 2ml.min⁻¹ throughout the entire purification procedure. The absorbance of the column flow through was recorded by the UV-detector continuously at a wavelength of 280nm (*A*₂₈₀). Once the column was equilibrated, a 5ml syringe was used to load 5ml of filtered supernatant onto the BioLogic LP system. The supernatant was passed through the BioLogic LP system and pumped into the IMAC cartridge with native wash buffer 1 until the intensity of the *A*₂₈₀ value returned to baseline. Non specifically bound proteins were eluted from the cartridge by washing with 6 CV native wash buffer 1 followed by 6 CV native wash buffer 2. FABP was eluted from the column by washing with 10 CV of native elution/wash buffer 3. Eluate was collected in 1ml fractions once an *A*₂₈₀ value of ≥ 0.1 was reached. At the end of purification procedure, the 1ml fractions were pooled and stored at 4°C overnight. To confirm the protein purification to near homogeneity, 90µL of the pooled fraction was precipitated with TCA to concentrate specifically eluted protein as described in 2.6.5, ready for analysis by SDS-PAGE – Coomassie blue staining.

2.7.5 De-lipidating purified recombinant FABPs using Lipidex-1000

Preparing methanol free Lipidex-1000: 10g of solid Lipidex-1000 (Fisher Scientific) was weighed into a teared 50ml falcon tube and then resuspended in 10ml of potassium phosphate buffer pH7.4 by *vigorous* vortexing until a cloudy suspension was formed. Lipidex – 1000 was then re-pelleted by centrifugation at $4,000 \times g$ for 10 minutes at 4°C in a swing out bucket rotor.

The supernatant was carefully decanted, and the pelleted lipidex was resuspended in potassium phosphate buffer pH7.4 and centrifuged as above, thrice more. The final 10g lipidex pellet was resuspended by vortexing in 20ml of potassium phosphate buffer pH7.4, to give a 50% [w/v] working stock.

Removal of endogenous bound lipids from purified FABPs: Before use, the 50% [w/v] Lipidex-1000 working stock was vortexed vigorously. 5ml of lipidex suspension was then added in a 1:1 ratio with an equal volume of purified FABP giving a final lipidex concentration of 25% [w/v]. The de-lipidation reaction was incubated at 37°C for 30 minutes with agitation at 250 rpm on an orbital shaker. After completion, the delipidated protein was recovered by centrifugation at $4,000 \times g$ for 10 minutes at 4°C in a swing out bucket rotor. The supernatant containing delipidated protein was then carefully decanted into a fresh 15ml Falcon tube.

2.7.6 Concentrating dilute de-lipidated purified FABPs by ultrafiltration

2ml of dilute de-lipidated purified FABPs were concentrated to a final volume of 200µl using a VivaSpin 2 ultrafiltration spin column device with a 10,000 molecular weight cut off (MWCO) polyethersulfone (PES) membrane (Sartorius, VS0202), according to the manufacturer's instructions.

2.7.7 Determination of protein concentration using the Beer-Lambert law

The absorbance at 280nm (A_{280}) of each concentrated protein sample was determined by measuring absorbance in triplicate using the LVIS plate, as described in 2.5.3. Potassium phosphate buffer pH7.4 served as the 'blank.' The mean A_{280} values for each protein sample were used in the Beer-Lambert equation (equation 2.1) to calculate the concentration of protein in mol.L^{-1} which was then scaled to $\mu\text{mol.L}^{-1}$. Where ϵ is the molar extinction coefficient ($\text{cm}^{-1} \text{M}^{-1}$), C is concentration (mol. L^{-1}), and L is pathlength (cm). The molar extinction coefficient for each FABP was determined by analysing the amino acid sequence of each FABP using ExPASy online software. Extinction coefficients for each FABP are listed in Table 2.2

$$\text{Equation 2.1: Beer Lambert's law: Mean } A_{280} = \epsilon \times C \times L$$

$$C = \text{Mean } A_{280} / \epsilon \times L$$

Table 2.2 – Molar extinction coefficient values for human FABP isoforms 5, 7 and 8.

FABP isotype	Molar extinction coefficient / ϵ ($\text{M}^{-1} \text{cm}^{-1}$)
5	14335
7	14105
8	14105

2.8 *In vitro* fluorescent displacement assays

2.8.1 Generating an FABP – 12 NBD stearate saturation curve

To each well, 12-NBD stearate was added at a final concentration ranging from 0.05 μ M – 2.5 μ M to a fixed concentration of 0.5- 3 μ M of purified FABP in potassium phosphate buffer pH7.4 in a final assay volume of 200 μ L per well. A parallel control plate was run where potassium phosphate buffer pH7.4 was added in place of protein to assess the contribution of free 12-NBD stearate to the recorded fluorescence. Alternatively, 12 – NBD stearate was added at a final concentration of 0.5 μ M to varying concentrations of purified FABP which ranged from 0.05 μ M – 6.0 μ M in a final assay volume of 200 μ L per well. A parallel control plate was run where 12-NBD stearate was replaced with potassium phosphate buffer pH7.4 containing 0.1% [v/v] DMSO, to assess the contribution increasing protein concentration to background fluorescence. Each curve and control or 'blank' were performed in triplicate.

Microwell plates were agitated for 1 minute at ambient temperature. 12-NBD stearate – FABP fluorescent complexes were then allowed to form for 1 minute under dim light at room temperature. Fluorescence was then measured at an excitation: emission wavelength of 484: 520nm at 25°C using an FLUOstar® Omega spectro-fluorometer (BMGLABTECH).

2.8.2 Displacement of bound 12-NBD stearate with AEA and 13 (S) HODE

The ability of ligands to displace bound 12-NBD stearate from FABPs was assessed in a 96 well plate. Each well contained 200 μ L of assay mixture which included 0.5 μ M 12-NBD stearate, 3 μ M FABP and 0.1 - 10 μ M test ligand in potassium phosphate buffer pH7.4 at 25°C. The components of assay mixture were added in a specific order. 12-NBD stearate was added to purified FABP in potassium phosphate buffer pH7.4, followed by agitation of the plate as above to

allow 12-NBD stearate – FABP complexes to form. Potassium phosphate buffer pH7.4 or test ligand was the final component added to the assay mixture.

The microplate was agitated and then incubated in dim light for 1 minute. Each displacement assay was performed in triplicate. To establish the effect that increasing concentration of test ligand had to background fluorescence, a parallel control microplate containing test ligand and potassium phosphate pH7.4 was assembled. The fluorescent signal was then measured at an excitation: emission wavelength of 484: 520nm using an FLUOstar® Omega spectro-fluorometer (BMGLABTECH).

2.9 Primary cell culture methods

2.9.1 Preparation of sterile 10cm coated cell culture dishes

10cm cell culture dishes were coated with 3ml of 500 μ g.ml⁻¹ Poly (DL) ornithine overnight at ambient temperature. The following day, the dishes were rinsed three times with 3ml of sterile HPLC grade water. Dishes were then allowed to dry or further coated with 3ml of 5 μ g.ml⁻¹ laminin for 90 minutes at ambient temperature after which the dishes were washed as above, then dried thoroughly. All coating, washing and drying steps were performed in a cell culture hood with a continuous air flow to maintain sterility.

2.9.2 Primary cell culture: Isolation of rat dorsal root ganglia cell bodies

Adult male Sprague Dawley rats were sacrificed by exposure to CO₂, and the spinal column was removed as described previously by Lindsay et al. (20, 117). DRGs were isolated and washed by gravity with Hanks buffered saline solution containing HEPES, then treated with 2.5mg.ml⁻¹ Collagenase in Neurobasal Media (NBM) supplemented with 10% [v/v] horse serum at 37°C and 5% CO₂ for 90 minutes. Ganglia were then washed with PBS then incubated with PBS containing 2.5mg.ml⁻¹ of porcine trypsin for 10 minutes at 37°C and 5% CO₂. Ganglia were

trituated using a fine tipped pastette. The resulting cell suspension was divided into two equal volumes which were both layered onto 16% [w/v] BSA to create a bilayer. Bilayers were then centrifuged at $500 \times g$ for 6 minutes, and the supernatants were carefully decanted with a 1ml micropipette leaving behind ganglia cell pellets. One ganglia cell pellet was immediately reconstituted in 500 μ l for Tri-Reagent for RNA extraction and cDNA synthesis for RT-PCR as in 2.5.2. The second ganglia cell pellet was reconstituted in 1.5ml of fully supplemented NBM. DRG cell suspension was pipetted onto the centre of a dry 10cm cell culture dish coated with poly (DL) ornithine and laminin. DRG cells were incubated at 37°C and 5% CO₂ for 1 hour at 37°C and 5% CO₂, after which 4.5ml of NBM was added, and the DRG cell preparation was cultured for a further 24 hours as above. After 24 hours in culture, RNA was extracted from the DRG cells for RT-PCR/QRT-PCR experiments as described in 2.5.7.

2.9.3 Isolating DRG neuronal cell bodies from non-neuronal cells

DRGs were isolated from an adult male Sprague Dawley rat as in 2.9.2. Ganglia cell pellets were resuspended initially 1.5ml of NBM supplemented as above; however, the DRG cell suspension was seeded in the centre of a dry 10cm dish coated with just poly (DL) ornithine. After 1 hour in culture, 4.5ml of NBM media was added to DRG cell preparation, which was then cultured for a further 24 hours at 37°C and 5% CO₂ as above. To harvest and enrich in neuronal cells, overnight NBM was removed. The following day, cell debris was removed by gently washing the mixed DRG cell preparation with 4ml of fresh NBM, which was then removed by gentle aspiration. 4ml of fresh NBM was then added to the cells, and the dish was tilted slightly to 'visualise' the cells. NBM was delivered in a 2ml stream directly to the visible cells, using a salinized flame polished Pasteur pipette to dislodge the poorly adherent neuronal cells. This was repeated a total of 15 times. The resulting 'neuronal' cell suspension was harvested by centrifugation at $1,000 \times g$ for 5

minutes at ambient temperature. The supernatant was discarded, and the pelleted neuronal cells were resuspended in 500µl of Tri-Reagent for RNA extraction and qRT-PCR, as were the adherent non-neuronal cells left in the 10cm culture dish.

2.10 Cell line cell culture and transfection of cell lines

2.10.1 Cell Lines

COS-7 (derived from African Green Monkey) and HeLa (human cervical carcinoma) cells were purchased from the American Type Culture Collection (ATCC). Both cell lines were cultured in fully supplemented Dulbecco's Modified Eagles Medium (DMEM). Cells were cultured in a humidified incubator at 37°C and 5% CO₂ in a 75cm² flask.

2.10.2 Resuscitation of cryopreserved cell lines

1ml of cryogenically frozen cells was incubated at 37°C in a water bath until thawed. Cells were immediately transferred to 9ml of pre-warmed supplemented DMEM cell culture medium. The resulting 10ml cell suspension was transferred to a 75cm² flask, and the cells were cultured as above (2.10.1) for 24 hours. The following day, cells were replenished with fresh DMEM cell culture growth medium to remove any dead cells.

2.10.3 Maintenance and sub culturing of cell lines

COS-7 and HeLa cells were grown as a monolayer in 75cm² flasks and subcultured once they had grown to 90% confluency. Exhausted DMEM growth medium was removed from the flask, and the cells were rinsed twice with 10ml of sterile pre-warmed PBS by gentle agitation. Cells were then detached from the surface of the flask by trypsinization with 5ml of trypsin-EDTA (0.25% [w/v] trypsin, 10mM EDTA) for 5 minutes at 37°C and gentle agitation by hand. The trypsin was then inactivated by the addition of a jet stream of 5ml of fresh pre-warmed DMEM

growth medium. To harvest the cells, the resulting cell suspension was transferred to a 50ml falcon tube and centrifuged for 5 minutes at $2,000 \times g$ for 5 minutes at ambient temperature. Pelleted cells were then resuspended in 5ml of fresh DMEM growth medium. The cell suspension was diluted 1:10 with DMEM growth medium into a fresh 75cm^2 flask.

2.10.4 Cell Counting using Cedex-XS cell counting system

Adherent cells were harvested as described in 2.10.3, and $100\mu\text{L}$ of the resulting cell suspension was transferred to an equal volume of Trypan Blue (Sigma) and mixed gently by repeated pipetting. $10\mu\text{L}$ aliquots of the Trypan Blue – cell suspension mixture was transferred to 4 of the eight slots on a Cedex Smart Slide. Cell number (cells.ml^{-1}) was then determined by reading the four loaded slots on the slide using the Cedex-XS cell counting system (Innovatis). A mean cell count was then calculated.

2.10.5 Transiently transfecting adherent cell lines

Cells were seeded in a 12 well plate at a density of $0.7 - 1 \times 10^5 \text{ cells.ml}^{-1}$ in complete DMEM cell growth medium. 1ml of cell suspension was dispensed per well directly onto the surface of a well or a sterilized 19mm circular glass cover slip anchored in the well. Cells were then cultured for 24 hours before transfection with plasmid DNA construct (s). Adherent cells were transfected with up to a total of $2\mu\text{g}$ plasmid DNA per well using X-tremeGENE™ HP (Roche) or Lipofectamine® 2000 (Invitrogen Life Technologies) transfection reagent following manufacturer's instructions. Transfection reagent was used in a '1:1 ratio' with plasmid DNA, i.e. $1\mu\text{l}$ of transfection reagent was used per $1\mu\text{g}$ of plasmid DNA to be transfected. To ensure even distribution of transfection reagent – plasmid DNA complex, cells were gently agitated on an orbital shaker for 5 minutes at 37°C , after which the

cells were maintained for a further 24 hours at 37°C and 5% CO₂ or were maintained for 6 hours at 37°C then 18 hours at 30 °C and 5% CO₂.

2.11 Histology and immunofluorescence

2.11.1 Preparation of DRG tissue sections (performed Dr. J J Burston)

An adult male Sprague Dawley rat weighing 225 grams was sacrificed by overdosing with intraperitoneal (i.p.) injection of sodium pentobarbital 200mg/ml solution. The rat was then perfused with 300 ml physiological saline (0.9% [w/v] NaCl, pH7.4), followed by 300 ml of filtered 4% PFA. The dorsal root ganglion (DRG) were immediately removed and post-fixed overnight in 4% PFA. After which the DRGs were stored in 30% [w/v] sucrose solution in sterile PBS containing 0.01% [w/v] sodium azide for at least one day for cryoprotection. DRGs were then placed in liquid optimal cutting temperature (OCT) compound and frozen into blocks, on dry ice. DRGs were the subsequently sectioned on a Leica cryostat 3050, to give tissue sections 10 µm in thickness. 4-5 sections were collected on a super frost plus glass slide (Thermo-Fisher U.K.).

2.11.2 Cresyl violet staining

Slides were immersed in cresyl violet for 20 minutes at room temperature followed by 2 rinses for 5 minutes in HPLC grade water. Slides were differentiated by immersion in differentiate solution; slides were then immersed for 30 seconds in 90% [v/v] ethanol then 95% [v/v] ethanol. Slides were washed in 100% ethanol for 30 seconds, then transferred to another Coplin jar containing fresh 100% ethanol for 30 seconds. Slides were then immersed in three changes of 100% xylene, and immersed for three mins each time. Slides were then mounted with a rectangular glass cover slide then sealed with DPX mounting media. Microscopy images of cresyl violet stained tissue sections were then acquired with a Zeiss Axioplan microscope at ×10, × 20 and × 40 magnifications.

2.11.3 Immunohistochemistry (IHC)

Fixed Frozen (Fi-Fro) DRG tissue sections were removed from storage at -20°C and allowed to equilibrate to room - ambient temperature for 30 minutes. Tissue sections were then simultaneously permeabilized and blocked with 0.1% [v/v] Triton X-100 and 3% [v/v] serum in Tris-buffered Saline (TTBS) for 1 hour at room temperature with mild agitation. The dual blocking-permeabilization-solution was removed from the sections and replaced with primary antibody/antibodies diluted in TTBS containing 3% [v/v] serum. Sections were incubated with primary antibody/antibodies for 24 hours at 4°C within a closed moist chamber. The following day primary antibody solution was removed, and the sections were rinsed five times with PBS for 10 minutes with agitation in a Coplin jar. This was followed by incubation with anti- IgG Alexa Fluor® 488 or 568, or both (1:500 dilution; Invitrogen) for 2 hours at room temperature in the dark in a closed dry chamber. Cells were then washed with PBS as previously. Immunostained tissue sections were sealed using a rectangular glass cover slide and two drops of Fluoromount™ aqueous mounting medium (Sigma). Images of immunostained tissue sections were acquired using a × 40 objective lens in a Leica fluorescent microscope connected to a CCD QImaging camera. Images were all taken at consistent exposure time. Controls where primary antibody was omitted, and cells were incubated with blocking solution alone, were included to confirm specific immunostaining.

All antibodies are listed in the appendix.

2.11.4 Immunocytochemistry (ICC)

Cells were seeded onto sterile 19mm glass coverslips in a 12 well plate and cultured as described previously. The following day adherent cells were transfected with the appropriate plasmid DNA constructs and cultured for a further 24 hours as described in 2.10.5.

24 hours post transfection, overnight DMEM growth medium was removed the cells followed by three brief washes with PBS. Cells were then fixed with 4% PFA for 5 minutes at room temperature then washed with PBS as described above. Cells were then subsequently permeabilized PBS-Tween 20 (PBST) at room temperature for 10 minutes with agitation followed by three washes with PBS for 5 minutes with gentle agitation. Cells were then incubated with blocking solution for 30 minutes at room temperature with agitation.

Primary antibody was diluted with PBST – 1% [w/v] BSA to the appropriate final concentration. After blocking, cells were incubated for 24 hours with the diluted primary antibody at 4°C with agitation. In order confirm specific immunostaining, 1 well of transfected cells were incubated with PBST-1% [w/v] BSA lacking the primary antibody. The following day, cells were rinsed three times with PBS for 5 minutes at room temperature with agitation followed by incubation with anti- IgG Alexa Fluor® 488 or 568 (1:1000 dilution; Invitrogen) for 1 hour at room temperature with agitation in the dark.

Cells were then washed with three times PBS as described in 2.11.3. Nuclei were subsequently counterstained with DAPI ($1\mu\text{g}\cdot\text{ml}^{-1}$) for 5 minutes at room temperature with agitation then washed with PBS for 10 minutes. Coverslips were mounted then sealed onto super-frost microscopy slide using 2 drops of Fluoromount™ aqueous mounting medium (Sigma). Images of immunostained cells were acquired using a $\times 63$ objective lens and consistent exposure times

using the appropriate fluorescence filters and microscope as described above (2.11.3) All antibodies are listed in the appendix.

2.12 Live cell calcium (Ca²⁺) imaging assays

2.12.1 Preparation of drugs and compounds

Stocks of all drugs, except for carbachol (Sigma), were prepared/dissolved in absolute ethanol. Carbachol was initially dissolved and prepared in autoclaved HPLC grade H₂O. For Ca²⁺ imaging assays, drugs were diluted 1000 – 10,000-fold with Ca²⁺ imaging buffer, with the resulting final ethanol concentration being between 0.01 – 0.1 % [v/v]. Carbachol was diluted in Ca²⁺ free imaging buffer.

2.12.2 Preparation of cells for transfection

COS-7 or HeLa cells were seeded onto 19mm glass coverslips and cultured as described in 2.10.5. If required, cells were transiently transfected with the appropriate plasmid DNA construct(s) and allowed to express the necessary recombinant proteins for 24 hours as described in 2.10.5

2.12.3 Preparing and loading cells with Fura-2AM

Cells maintained on 19mm glass coverslips were removed from culture and immediately transferred to a petri dish flooded with calcium imaging buffer. Cells were then washed a total of 3 times with calcium imaging buffer with gentle agitation by hand at ambient temperature. Cytoplasmic Ca²⁺ indicator Fura-2-acetoxymethyl ester (Fura-2AM) was prepared by diluting a 1mM stock in DMSO with calcium imaging buffer to a final concentration of 5μM. Cells/coverslips were transferred to fresh dry petri dish and immediately loaded with 5μM Fura-2AM, where 300μL of 5μM Fura-2AM was carefully dispensed per coverslip of cells. Cells were then incubated at 37°C for 30 minutes in the dark. Cells were subsequently flooded with fresh Ca²⁺ imaging buffer and incubated at ambient

temperature in the dark. After 15 minutes in fresh Ca^{2+} imaging buffer, cells could be then used for Ca^{2+} imaging assays.

2.12.4 Measuring intracellular Ca^{2+} concentration $[\text{Ca}^{2+}]_i$: Ratiometric imaging

Coverslips were mounted onto a plastic perfusion chamber with Dow® Corning high-vacuum grease, quickly followed by addition of a few drops of Ca^{2+} imaging buffer directly into the chamber to ensure that the cells did not dry out. The chamber was promptly and securely mounted onto the microscope stage and perfused immediately with Ca^{2+} imaging buffer at a flow rate of $2\text{ml}\cdot\text{min}^{-1}$. The flow rate was maintained at $2\text{ml}\cdot\text{min}^{-1}$ for all calcium imaging experiments in this thesis. Before viewing the cells under the microscope, the CCD camera was set to 4×4 binning and the exposure time was fixed at 300 milliseconds. These imaging parameters were consistent with all Ca^{2+} imaging experiments. A live image of the loaded cells was acquired and captured at 380nm. The resulting still image was used to select individual cells or regions of interest (ROI) to measure approximate changes in $[\text{Ca}^{2+}]_i$. $[\text{Ca}^{2+}]_i$ in individual ROI was approximated as the ratios of peak fluorescent emission intensities (measured at $\lambda = 500\text{nm}$) at excitation wavelengths of 340 and 380nm using Andor iQ imaging software and a QImaging Retiga CCD camera. Images/frames were acquired every 5 – 20 seconds.

2.12.5 Measuring changes in $[\text{Ca}^{2+}]_i$ in response to drug

In a typical Ca^{2+} imaging experiment, cells were perfused with Ca^{2+} imaging buffer for 2 to 5 minutes at a flow rate of $2\text{ml}\cdot\text{min}^{-1}$. Cells were then perfused with a drug or vehicle 1 minute followed by a washout period with Ca^{2+} imaging buffer for a pre-determined amount of time, before the addition of a second drug. In most cases, at the end of the experiment cells were perfused with $4\mu\text{M}$ ionomycin for 1

minute after which the experiment was ended. Note that the flow rate of $2\text{ml}\cdot\text{min}^{-1}$ was standardized across all Ca^{2+} imaging experiments.

2.12.6 Ca^{2+} reconstitution experiment after stimulation with carbachol

HeLa cells grown on 19mm glass coverslips were washed, prepared and loaded with $5\mu\text{M}$ Fura-2AM as previously, however Ca^{2+} free imaging buffer was used for washing and diluting Fura-2AM. Coverslips were then mounted onto the perfusion chamber and then microscope stage ready for imaging experiments and selecting ROIs, as above. Cells were then perfused with Ca^{2+} imaging buffer for 5 minutes at a flow rate $2\text{ml}\cdot\text{min}^{-1}$. The flow rate was maintained at $2\text{ml}\cdot\text{min}^{-1}$ throughout the experiment. Cells were then stimulated with $50\mu\text{M}$ CCH for 1 minute. Cells were then rinsed with Ca^{2+} free imaging buffer then reconstituted with imaging buffer containing 2.5mM CaCl_2 (+ Ca^{2+} imaging buffer). Cells were perfused with + Ca^{2+} imaging buffer for 5 minutes, where cells were then exposed to $4\mu\text{M}$ ionomycin for 1 minute after which the experiment was ended. Alternatively, cells were exposed to $0.1\mu\text{M}$ capsaicin for 1 minute, followed by a 5-minute washout period with Ca^{2+} imaging buffer for 5 minutes, then exposed to $4\mu\text{M}$ ionomycin for 1 minute, after which the experiment was ended.

2.13 Quantitative TaqMan® gene expression assays

2.13.1 Primer – probe design for TaqMan® gene expression assays

Primers and probes for TaqMan® gene expression assays were designed against target and reference genes using Primer Express 3.0 software (Applied Biosystems). The reference number of nucleotide template sequences of target and reference genes, used to design primers and probes are listed in the appendix.

All primers and probes were designed to span exon-exon junctions of target and reference genes to avoid amplifying genomic DNA. The specificity of TaqMan® primer – probe oligos to target and reference genes were confirmed *in silico*, by using NCBI BLAST software to align oligonucleotide sequences against the NCBI RNA (cDNA) RefSeq database. Primer and probe synthesis was performed by Eurofins MWG Operon (Germany).

To quantitate the expression levels of target genes, TaqMan® gene expression assays were carried out using oligonucleotide probes labeled with reporter and quencher dyes to give a fluorogenic probe. The reporter dye 6 – carboxyfluorescein or 'FAM' labeled probes at the 5' end, whereas the quencher dye 6-carboxy-tetramethyl rhodamine or 'TAM' labeled probes at their 3' end.

2.13.2 Performing TaqMan® gene expression assays

TaqMan® gene expression assays were performed by using the relative standard curve method. A relative standard curve was generated by diluting cDNA samples 1:2 with HPLC grade water. Diluted cDNA was then pooled to give the first point of the relative standard curve. The first point was referred to as 'NEAT.' From the 'NEAT' sample, a serial 2 or 4-fold, 5-point dilution curve was generated.

The resulting curves had the following points for the 2-fold dilution curve; NEAT, 1:2, 1:4, 1:8 and 1:16. For the 4-fold dilution curve, the points were; NEAT, 1:4,

1:16, 1:64 and 1:256. Remaining NEAT cDNA samples were diluted 1:4 or 1:8 to fall within the range of a 2-fold and 4-fold relative standard curves respectively. A series of separate master mixes each containing specific primers and probes against each specific gene of interest was then assembled (Table 2.3). 10 μ L of master mix was added to 3 μ L cDNA (synthesized from 250-500ng of total RNA) to give a final volume of 13 μ L per well. All samples and standard curves were run in triplicate in a 96 well plate. Relative standard curves were run for each gene of interest for each experimental run. TaqMan[®] gene expression assays were performed using the StepOne[™] Plus thermal cycler (Applied Biosystems). The thermal cycling parameters are summarized in Table 2.4. A relative standard curve was only used to calculate expression levels of a target gene if the correlation coefficient (r^2) value of the curve ≥ 0.99 and the gradient of the slope were -3.2 to -3.6. Mean relative expression levels of each target gene were normalized to expression level of a reference gene.

Table 2.3 - Volume of individual reaction components used per well in TaqMan[®] gene expression assays

Reaction component	Vol (μ l) per well
2 x TaqMan Fast Mix (Applied Biosystems)	6.5
Forward Primer	0.375
Reverse Primer	0.375
Probe	0.25
HPLC grade H ₂ O	2.5
Template cDNA	3

Table 2.4 - Thermal cycling parameters used in TaqMan® gene expression assays

Step/Stage	Temperature (°C)	Duration (secs)	Cycles
1.	95	20	1
2.	90	15	40
3.	60	30	

Chapter 3: The identification of FABP and PPAR isotypes in rat dorsal root ganglia cell cultures

Chapter 3: The identification of FABP and PPAR isotypes in rat dorsal root ganglia cell cultures

3.0 Introduction: *In vitro* rat DRG cell culture model

DRG cell bodies have proved an extremely valuable and useful model when studying the detection of noxious stimuli and the release of modulatory neuropeptides (118). Indeed, it has been shown that the cell bodies express many of the main molecular players to that of the nociceptive nerve terminals (119).

However, DRG cell body preparations from rats or mice produce a heterogeneous cell culture of different sized neuronal cell bodies and their associated non-neuronal cells, the satellite glial cells (SGCs). This presents a significant problem when attempting to detect and confirm the expression of a key gene of interest and its corresponding protein in a specified cell type.

This chapter seeks to resolve this problem by using methods to segregate the neuronal cell bodies from the SGCs in culture. Neuronal cell bodies will be distinguished from the SGCs by using neuronal and non-neuronal cell markers neuronal nuclei (NeuN) and glial fibrillary acid protein (GFAP) respectively. Being able to differentiate between NeuN and GFAP positive cells means it will be possible to elucidate which gene and proteins of interest are expressed in each cell type present in the DRG cell preparations.

3.1 Aim of study

To determine which FABP isoforms and PPAR isotypes are expressed in the DRG neuronal cell bodies/soma.

3.1.1 Summary of specific experimental objectives

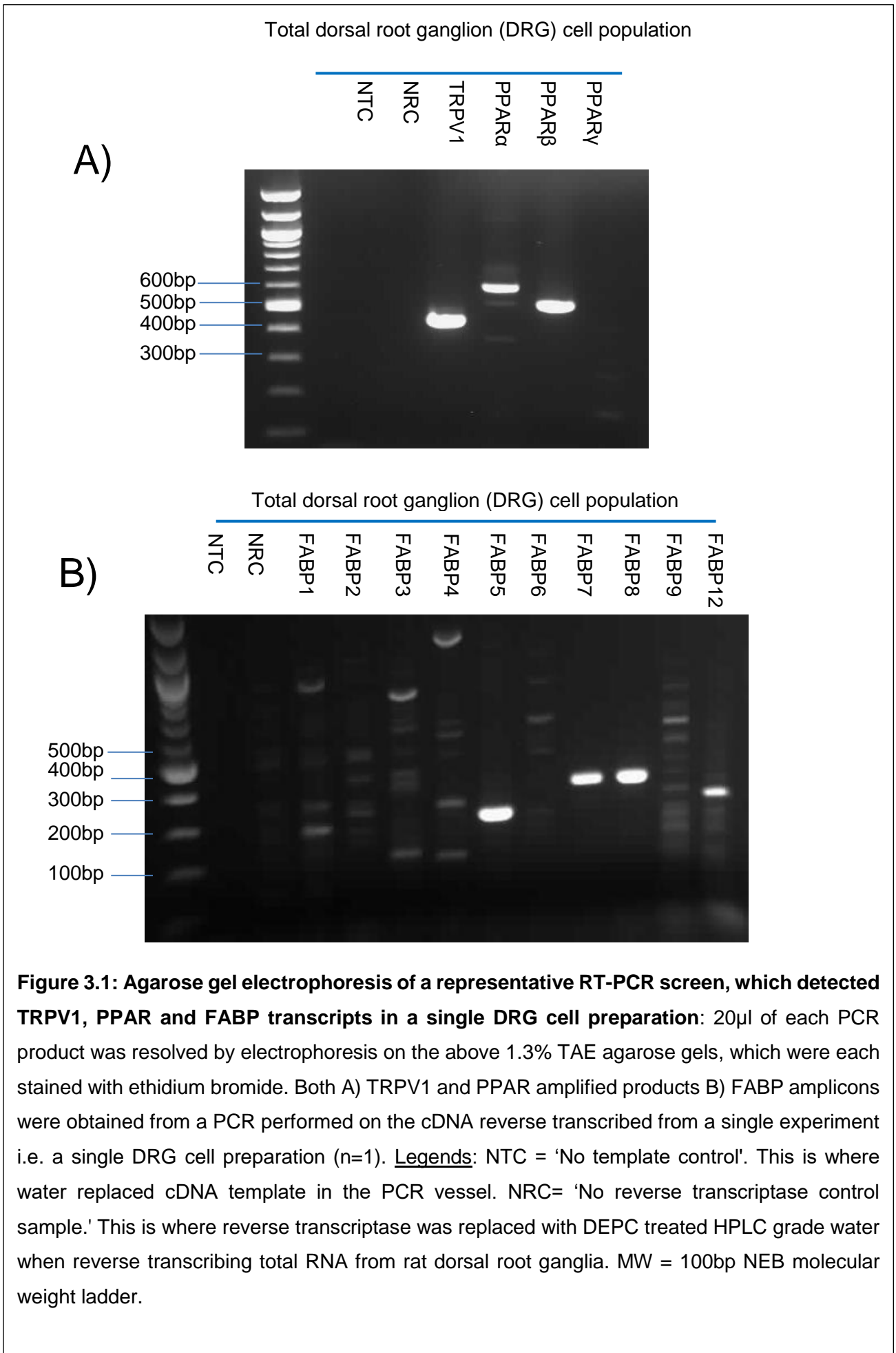
- 1) Identify which FABP and PPAR isoforms are expressed in freshly isolated DRGs by RT-PCR.
- 2) Using QRT-PCR, establish that the FABP and PPAR gene expression profile does not change once the DRG preparation is cultured *in vitro* for 24 hours
- 3) Given the DRG preparation produces a heterogeneous cell population of DRG cell bodies and the associated non-neuronal glial cells, it is necessary to ascertain which cell types express each gene of interest and the corresponding protein. This is assessed by QRT-PCR and by immunofluorescence using the available antibodies.

3.2 Results

3.2.1 Detecting PPAR, FABP and TRPV1 mRNA transcripts in freshly isolated rat DRG cell bodies and the associated cells by RT-PCR

Dorsal root ganglia were freshly isolated from an adult male Sprague Dawley rat giving a DRG cell preparation. Total RNA was isolated from the freshly isolated cell preparation using TriReagent. 500ng of total RNA was then reverse transcribed to cDNA using Agilent multi-temp reverse transcriptase. cDNA was used as template DNA for PCR using Phusion® HF DNA polymerase and the thermocycling parameters listed in chapter 2. At this stage, the purpose of the RT-PCR screen was to establish which of the FABP and PPAR isoforms were expressed at the mRNA level in a freshly isolated rat DRG cell preparation consisting of a mixed population DRG cell bodies and the associated non-neuronal cells.

PCR amplicons were analysed and resolved by agarose gel electrophoresis which revealed single DNA bands migrating at the expected molecular weights for PPAR α and β/δ which were 644 and 555bp respectively (Figure 3.1A). While the PPAR γ 2 transcript was undetectable by RT-PCR in DRG isolations but was present in cultured rat adipocytes (Figure 3.2). As expected, TRPV1 expression was detectable in the DRG cell isolations, given the presence of single band seen migrating at the correct size, 475bp (Figure 3.1A). Whether PPAR γ 1 was expressed at the mRNA level in these cultures remained elusive at this point. Transcripts for FABP isotypes 5, 7, 8 and 12 were also detectable (single DNA bands migrating at 303,386, 251, 312bp respectively, Figure 3.1B). However, the role of FABP12 was not investigated. In contrast, FABP isoforms 1-4 and 6 were not detected in the freshly isolated DRG cell preparations.



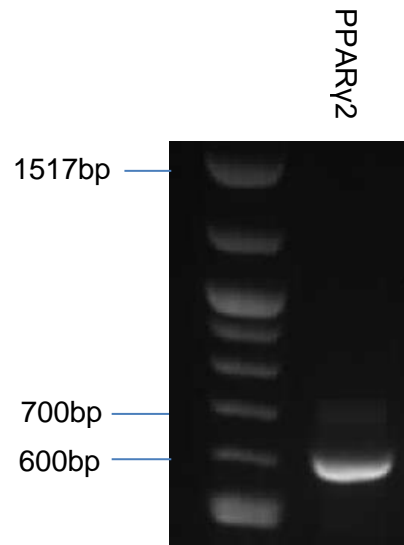


Figure 3.2: Detecting PPAR γ 2 transcript from cultured rat adipocytes: Total RNA from cultured rat adipocyte cells was reverse transcribed to cDNA as in figure 3.1. cDNA was then used as a template for PCR as detailed described in chapter 2. 20 μ l of PCR product was then resolved on the above 1.3% TAE agarose gel.

3.2.2 Comparing FABP, PPAR and TRPV1 expression levels in fresh rat DRG isolations vs. 24-hour static rat DRG cell cultures by QRT-PCR

To ensure that the expression profile of the genes of interest did not change significantly at the mRNA level in cultured DRGs, it was pivotal that the genes identified in 3.2.1 were still expressed when the cells were cultured *in vitro* for 24 hours. Quantitative RT-PCR / TaqMan® gene expression assays were performed to compare the relative expression levels of the PPARs, FABPs, TRPV1 and reference gene GAPDH, between freshly isolated DRGs and the remaining DRG isolations that had been cultured *in vitro*.

There was a small, statistically significant difference in GAPDH gene expression levels when comparing the arbitrary mean value for the freshly isolated DRG cells to that of the DRG cultures. The values +/- SEM were 0.23 ± 0.01 and 0.30 ± 0.01 respectively (Figure 3.3). This corresponds to a 30% higher level of GAPDH expression between the freshly isolated DRG cells in comparison to the cultured DRG cells. However, GAPDH expression was found to be consistent between experiments and the 30% difference in expression was considered when assessing expression of genes of interest.

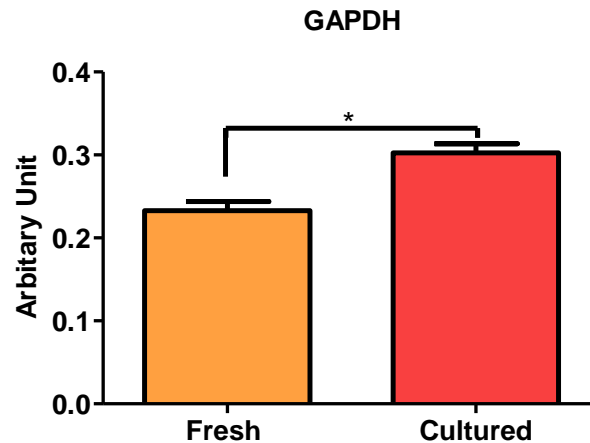
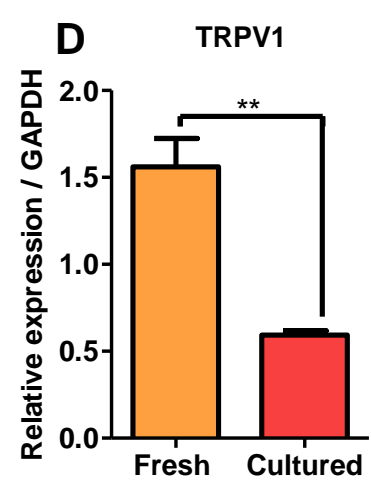
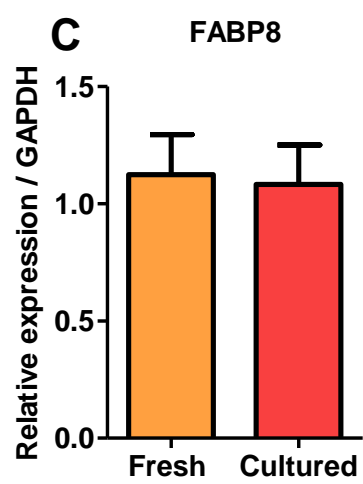
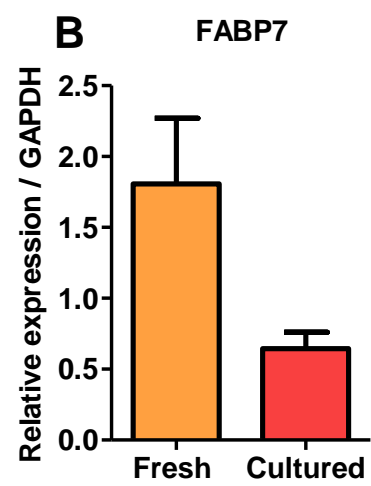
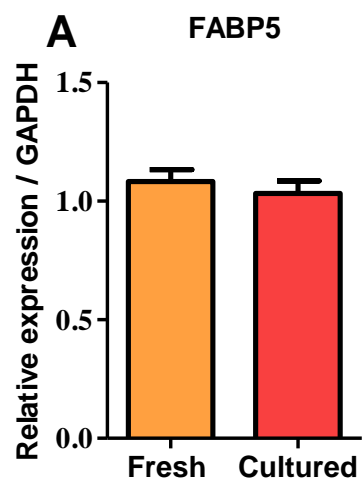


Figure 3.3: A comparison of gene expression levels of the reference gene GAPDH in freshly isolated and cultured Rat DRG cell preparations. Rat dorsal root ganglia were isolated from adult male Sprague Dawley rats as described in chapter 2. Half of the isolation was immediately placed in Tri-Reagent for total RNA isolation and cDNA synthesis, while the other half of the cell preparation – isolation was cultured for 24 hours *in vitro*, which was then followed by RNA isolation and cDNA synthesis. A total amount of 250ng RNA was used for each reverse transcription to generate cDNA for QRT-PCR. Gene expression levels for GAPDH in freshly isolated and cultured DRGs were determined using QRT-PCR TaqMan® gene expression assays. A small but statistically significant difference in GAPDH expression levels was seen between freshly isolated DRG cells when compared to the cultured DRG cells. (n=3 rats/independent DRG cell isolation / DRG cell cultures). Analysis: A unpaired student t-test was used to analyse the difference between fresh and cultured groups. A value of $P < 0.05$ was considered as significant. Data are expressed as a mean \pm SEM.

There were no differences in the expression levels of FABP5 and FABP8 between the freshly isolated and cultured DRG cell preparations (Figure 3.4A & C). There were notably reduced levels of FABP7 expression in the cultured DRG cell preparations compared to the freshly isolated cells, however, when compared directly the difference in expression level was not considered as significant (Figure 3.4C). While TRPV1 expression levels were significantly decreased by 2.6-fold in DRG cells that had been cultured compared to the freshly isolated DRG cells (0.59 ± 0.03 and 1.56 ± 0.16 respectively) (Figure 3.4D).

There were minimal but non-significant differences in the expression levels of PPAR α in the freshly isolated DRG cells and the cultured DRG cells (Figure 3.4E). However, there were statistically significant differences in the relative gene expression levels of PPAR β/δ and PPAR γ 1 between the freshly isolated cells and those cell preparations that had been cultured (Figure 3.4F & G). Both PPAR isotypes were expressed at higher levels in DRG cell cultures to that of the freshly isolated DRG cells. In summary, the mRNA transcripts detected by RT-PCR in freshly isolated DRG cells were still detectable in all 3 independent cell culture preparations.



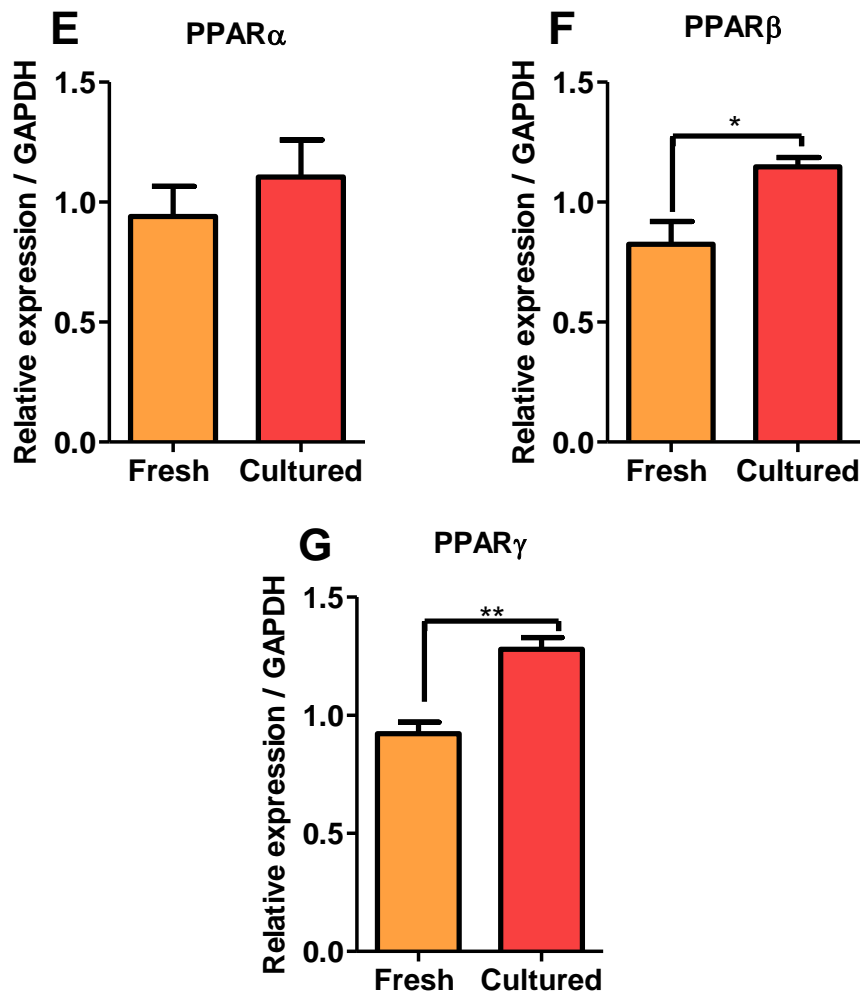


Figure 3.4: QRT-PCR gene expression assays could detect FABP, PPAR and TRPV1 transcripts in both freshly isolated and cultured DRG cell preparations. Fresh and cultured DRG cell preparations were produced from the dorsal root ganglia of three separate adult male Sprague Dawley rats (n=3) as described in figure 3.3. cDNA was then prepared from RNA for TaqMan® gene expression assays as in figure 3.3. After 24 hours in culture the following changes in relative gene expression were determined; **A)** relative FABP5 expression did not change, **B)** FABP7 expression decreased but not significantly, **C)** FABP8 expression did not change, **D)** TRPV1 expression significantly decreased, **E)** PPAR α expression increased but not significantly, **F)** PPAR β/δ expression increased significantly and **G)** PPAR γ expression increased significantly. A value of $P < 0.05$ was considered as significant. A unpaired student t-test was used to analyse the difference between fresh and cultured groups. Data are expressed as a mean \pm SEM.

3.2.3 Isolation of DRG cell bodies from non-neuronal cells in heterogeneous cell culture preparation

Given that the fresh DRG cell isolations and cultures consisted of non-neuronal glial cells associated with the DRGs, it was not possible to deduce whether the genes of interest identified in 3.2.2 were expressed in the associated non-neuronal glial cells or the neuronal DRG cell bodies, or indeed in both cell types. DRG cell bodies in the absence of poly (D) ornithine or poly (D) lysine coated plastic surface fail to adhere to plastic under cell culture conditions. While the non-neuronal glial cells, in the cell isolation, readily attach to the plastic surfaces in cell culture dishes.

The differences in adhesion properties between cell types were exploited to allow for the harvesting of the DRG cell bodies from the adherent non-neuronal glial cells. After 24 hours in culture, the circular DRG cell bodies (highlighted by orange arrows in Figure 3.5A & C) were effectively harvested by rinsing or washing with NBM media leaving behind a population of non-neuronal cells (which are highlighted by green arrows on Figure 3.5B & D).

This gave a cell suspension, which was assumed to contain and be enriched in DRG cell bodies, given that there was a notable absence of any circular DRG cell bodies in the dish, after having washed with NBM (Figures 3.5B and D). In the dish, a population of non-neuronal cells still attached to the plastic cell culture dish remained. The total RNA content of cell suspensions and adherent cells was then isolated ready for cDNA synthesis and downstream TaqMan® gene expression assays.

24 hours in culture / Pre - wash

Post - wash

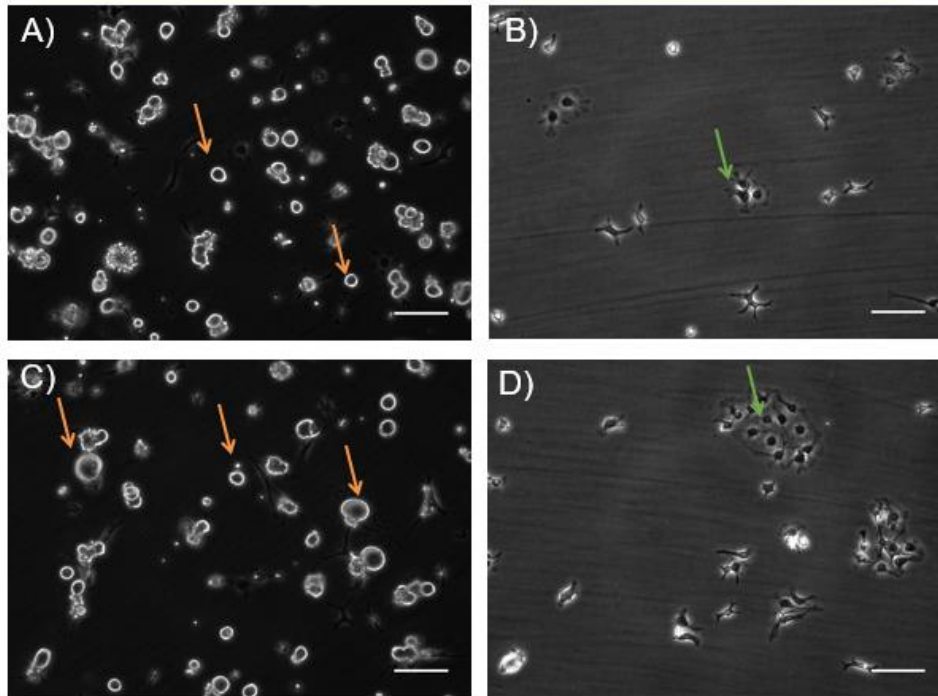


Figure 3.5: Representative light microscopy images illustrating the separation of DRG cell bodies from satellite glial cells (SGCs): DRG mixed cell cultures were prepared from adult male Sprague Dawley rats ($n=3$) and cultured for 24 hours as described. Non-adherent cell bodies (Images A & C) were separated from the adherent satellite glial cells (Images B & D) by washing with a stream of NBM. Orange and green arrows point to DRG cell bodies and non-neuronal cells (satellite glial cells) respectively. Scale bar is $50\mu\text{m}$.

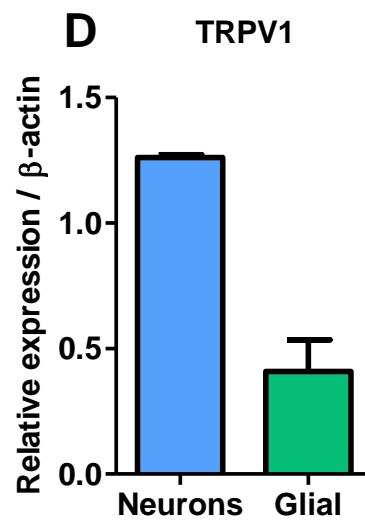
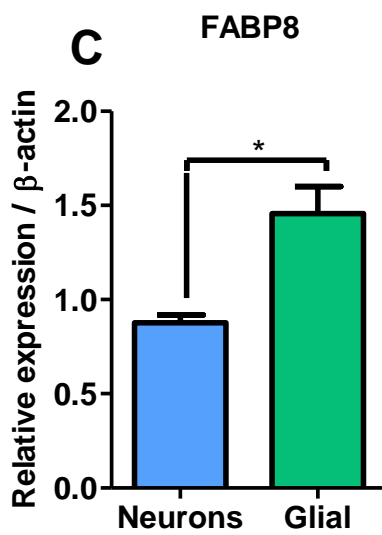
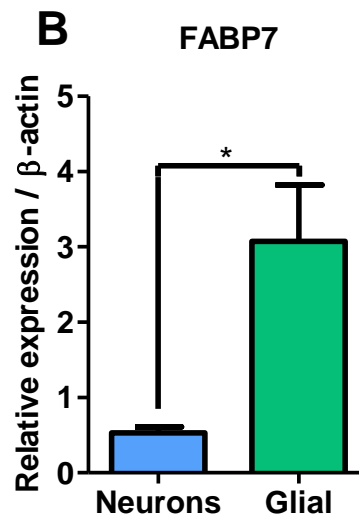
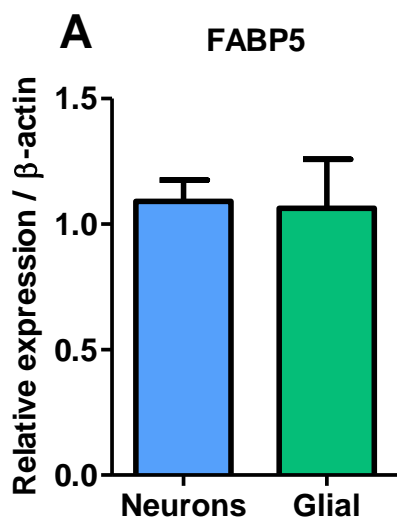
3.2.4 Comparing the gene expression profile of the isolated DRG cell bodies and non-neuronal cells

TaqMan® gene expression assays were performed on cDNA samples generated from the enriched DRG cell body isolations and the non-neuronal glial cells produced in 3.2.3. It was necessary to determine if there were differences in the gene expression profile of the two cell types for the FABPs, PPARs, and TRPV1.

β -actin was found to be expressed at consistent levels when comparing independent DRG cell enrichments/non-neuronal glial cell preparations from separate rats. Therefore, the expression levels for the FABPs, PPARs, TRPV1, NeuN, and GFAP were all normalized to β -actin. Expression levels of β -actin were different when comparing DRG cell bodies and glial cell directly; however, this was expected to be the case when comparing two different cell types.

FABPs: FABP5 was expressed at similar levels in enriched DRG cell preparations and non-neuronal glial cells (Figure 3.6A). However, there were significant differences in FABP7 and FABP8 expression levels when comparing the DRG cell bodies and the non-neuronal glial cells. FABP7 and FABP8 were both expressed at significantly higher levels in the non-neuronal glial cell population compared to that of the neuronal DRG cell bodies (Figure 3.6B and C).

TRPV1 and PPARs: TRPV1 was expression was higher in the enriched DRG cell population compared to that of the non-neuronal glial cell population (Figure 3.6D). PPAR α gene expression levels were higher in the non-neuronal glial cell population compared to the enriched DRG cell population; however, the difference was not considered as significant (Figure 3.6E). Whereas PPAR β/δ and PPAR γ 1 gene expression levels were significantly higher in the enriched DRG cell body population compared to the non-neuronal glial cells (Figure 3.6F and G).



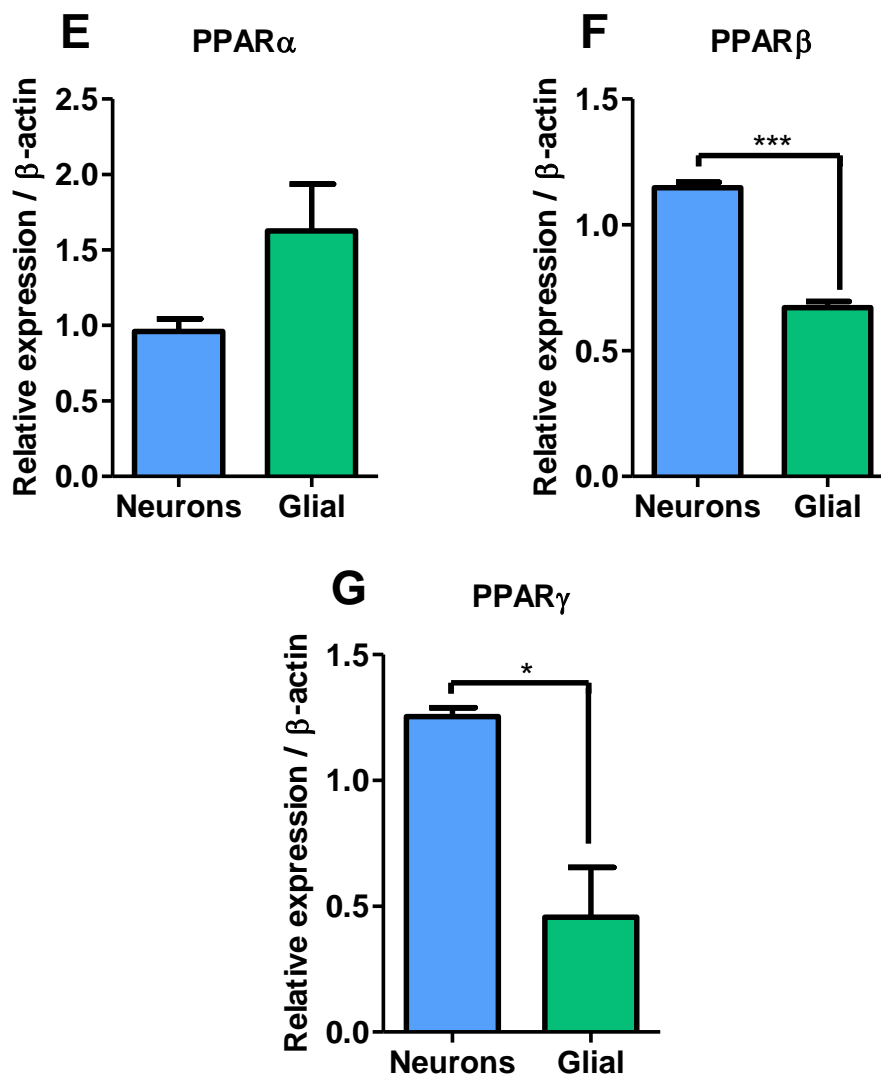


Figure 3.6: QRT-PCR gene expression assays to show differential FABP and PPAR gene expression in recovered DRG cell bodies and satellite glial cells: DRGs were isolated from adult male Sprague Dawley rats then cultured for 24 hours as in 3.2.2, after which DRG cell bodies were separated from the non-neuronal satellite glial cells as in 3.2.3. 250ng of RNA was prepared from both the isolated DRG cell bodies (neurons) and the non-neuronal (glial) cells for reverse transcription to generate cDNA for QRT-PCR. Relative expression levels for FABP5, FABP7, FABP8, PPAR α , PPAR β/δ , PPAR γ and β -actin in DRG cell bodies and satellite glial cells were determined using QRT-PCR TaqMan® gene expression assays. **A)** The relative FABP5 expression levels did not differ between the enriched neuronal cells and glial cells. **B)** FABP7 expression was significantly higher in the fraction enriched in SGCs. **C)** FABP8 expression was significantly greater in the SGC fraction. **D)** TRPV1 expression is higher in the neurons. **E)** PPAR α expression is higher in SGCs than in the neuronal cells **F)** PPAR β and **G)** PPAR γ expression is significantly higher in the neurons. $n = 3$ DRG (neurons) and satellite glial cell (glial) isolations/separations. A value of $P < 0.05$ was considered as significant. A unpaired student t-test was used to analyse the difference between neuronal and glial cells. Data are expressed as a mean \pm SEM. .

The TaqMan® data suggested that the target genes of interest were expressed in both cell types but at varying levels. Therefore, it was necessary to confirm whether the cells harvested by washing with Neurobasal Media (NBM) were solely enriched in DRG bodies or whether there was some contamination of the non-neuronal glial cells and vice versa.

To determine the purity of the DRG isolation and whether the cell preparations had been sufficiently fractionated into neuronal and non-neuronal cell populations, TaqMan® gene expression assays were performed for the neuronal cell marker NeuN / Rbfox3 and the glial cell marker, GFAP. Populations enriched in DRG cell bodies were expected to display high levels of gene expression for NeuN and very low levels of GFAP and vice versa for the glial cells.

NeuN expression levels were significantly higher in the DRG cell population compared to the glial/non-neuronal cell population (Figure 3.7A). Whereas, GFAP expression levels were lower in the DRG cell population compared to that of the glial cells (Figure 3.7B), however, the difference was not significant. Given that NeuN gene expression was detectable in the glial cell population and GFAP expression was detectable in DRG cell population, it was not possible to conclude that the DRG cell bodies and glial cells had completely separated into two distinct cell populations. Therefore, it was not feasible to obtain a definitive gene expression profile for each cell type using this cell culture model.

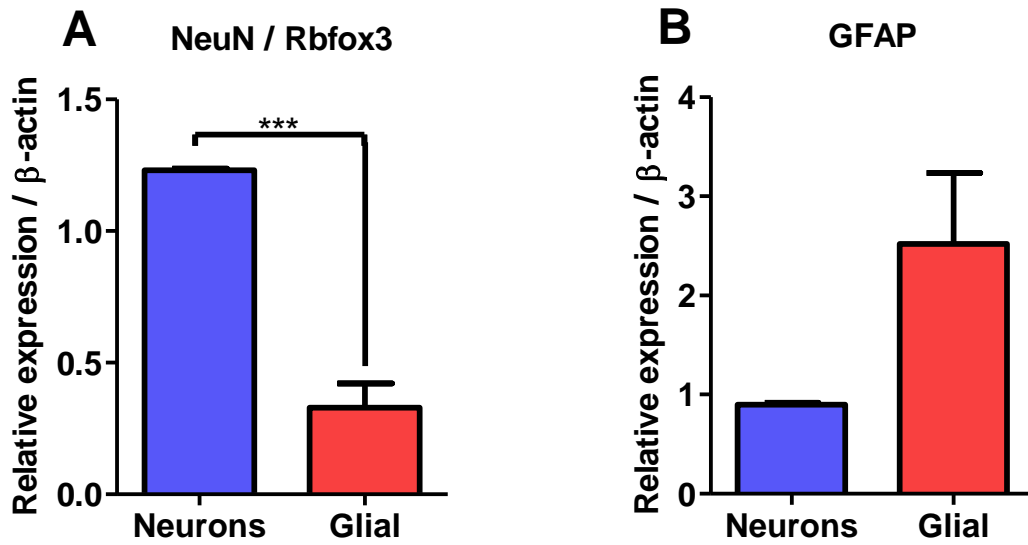


Figure 3.7: TaqMan® gene expression assays for cell specific markers NeuN/Rbfox3 and GFAP: cDNA from the same 3 independent DRG preparations (n=3) used in figure 3.6, was used to confirm the extent to which neuronal and non-neuronal cells had been fractionated into two distinct cell populations and therefore whether the previously identified FABP and PPAR genes were expressed solely in neuronal or non-neuronal cells, or in both cell types. A) NeuN expression is significantly higher in neuronal cells than non-neuronal glial cells B) GFAP expression is higher in non-neuronal cells than neuronal. A value of $P < 0.05$ was considered as significant. A unpaired student t-test was used to analyse the difference in the relative expression levels of NeuN/Rbfox3 and GFAP between neuronal and glial groups.

3.2.5 Immunostaining for FABP5 and FABP7 in DRG tissue sections

Whole intact DRGs dissected from an adult male Sprague Dawley rat, were cut to give tissue sections 10 μ m in thickness which was then stained with cresyl violet. Analysis of cresyl violet stained tissues by microscopy revealed that DRGs had been sectioned to an acceptable standard. This was evident from the prevalence and presence of differentially sized cell bodies with a characteristic circular morphology and different cell diameters, forming a cluster of cells (Figure 3.8). This being an organizational-structural characteristic associated and consistent with the accepted anatomical and histological description of DRGs. In conclusion, the collection of slides with DRG sections were deemed suitable for use in subsequent immunohistochemistry experiments.

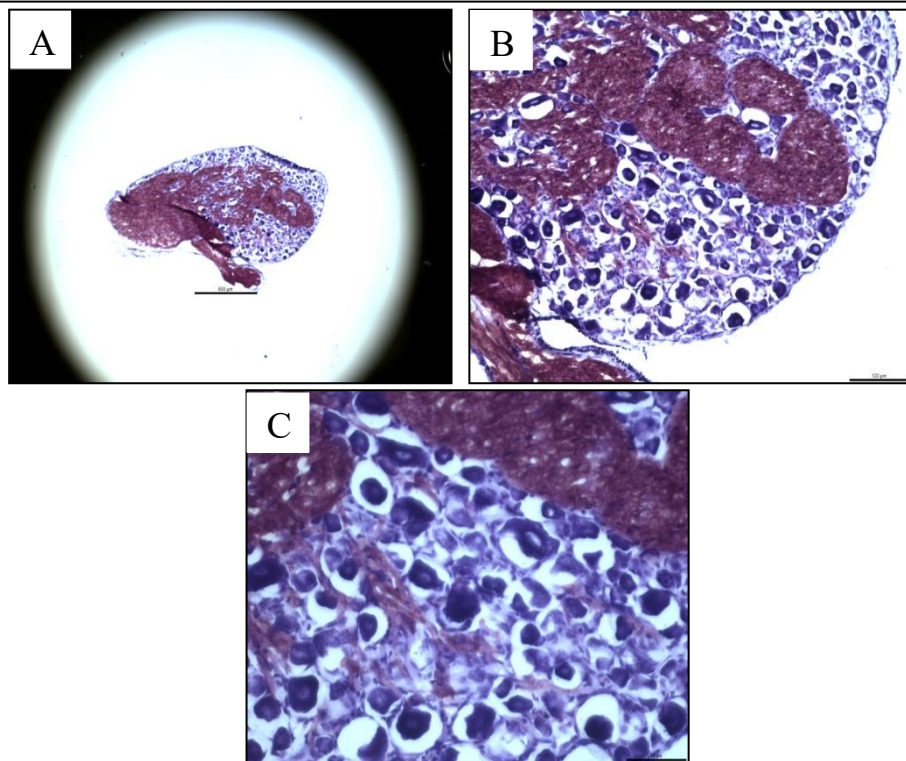


Figure 3.8: Representative images of fixed frozen rat DRG tissue sections stained with cresyl violet: DRGs were isolated from a single PFA perfused adult male Sprague Dawley rat (n=1). DRGs then were embedded in OCT for cutting DRG tissue sections 10 μ m in thickness. Once mounted DRG sections were stained with cresyl violet. Images were acquired at an exposure time of 6.4ms and digital gain of 1 at increasing magnifications A) $\times 10$ B) $\times 20$ C) $\times 40$ magnification using a Zeiss Axioplan light microscope. The respective scale bars are 500, 120 and 50 μ m.

Before immunohistochemistry antibodies for FABP5 and FABP7 were initially validated in house by immunoblotting. Skin (Paw) and brain lysates from rat tissues, known to express FABP5 and 7, were used as controls to show that the antibodies could detect the correct antigen and confirm antibody specificity. Immunoblotting was used opposed to immunohistochemistry to demonstrate that the antigen being detected by the antibodies was of the correct molecular weight (kDa). Immunoblotting with anti-FABP5 and 7 antibodies against control skin and brain tissue lysates gave single protein bands migrating at the expected molecular weights for FABPs 5 and 7 (Figure 3.9)

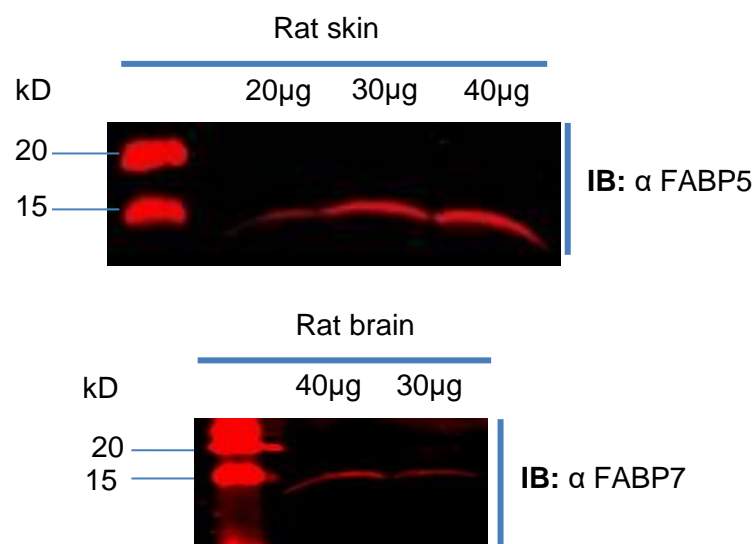


Figure 3.9: Immunoblot (IB) analysis of rat skin and brain tissue lysates to determine the specificity of antibodies for FABP5 and 7: Brain and skin tissues were removed from a single adult male Sprague Dawley rat (n=1) and homogenized in RIPA buffer. Tissue lysates were then centrifuged to give clarified tissue lysates. Clarified cell lysates were boiled in 1× Laemmli loading buffer containing 200mM DTT, then loaded onto 8% or 12% PAGE gel and resolved by electrophoresis. Differing amounts of total protein were loaded onto the gel ranging from 20-40µg. Proteins were transferred to an Amersham™ Hybond™-ECL nitrocellulose membrane. The membrane was probed with rabbit anti-FABP5 or rabbit anti-FABP7 polyclonal antibodies (1:250 dilution) antibodies overnight at 4°C followed by donkey anti-rabbit IgG-IRDYE 660 antibody for 1 hour at room temperature. The membranes were then scanned using a LiCOR Odyssey infrared imager.

The validated antibodies were then used in immunohistochemistry experiments on rat DRG tissue sections. As with 3.2.4, the aim was to determine which of the two cell types, neuronal cell bodies and satellite glial cells, express FABP5 and 7. This was to be achieved by dual or co-staining DRG tissue sections by using an antibody against NeuN/Rbfox3 in tandem with anti-FABP antibodies.

Initially the anti-Neurofilament 200 antibody was used in conjunction with an anti-FABP7 antibody; however, this was replaced with an anti-NeuN/Rbfox3 antibody, as the latter gave stronger and more specific immunostaining and therefore it was easier to distinguish each stained cell body stained from background fluorescence.

Immunostaining for NeuN/Rbfox3 produced a strong fluorescent signal which was detected in the nuclei and cytoplasmic regions of the DRG cell bodies when examined in the TRITC channel (Figure 3.10B). Co staining for FABP5 gave a strong fluorescent signal localized to the cytoplasm of the DRG cell bodies when examined in FITC channel (Figure 3.10C). When images of the cells examined in both FITC and TRITC channels were merged, the immunofluorescence observed in the cytoplasm for FABP5 was detectable in the same DRG cells that had immunostained positive for NeuN (Figure 3.10E).

Furthermore, there were regions where both fluorescent signals detected in the FITC and TRITC channels, appeared to colocalize/merge. This was not surprising as there is some NeuN expression at the protein level, in the cytoplasm. Finally, no immunostaining for FABP5 was observed outside of the DRG cells i.e. in the DAPI stained non-neuronal cells, which were closely associated with or surrounding the individual DRG cell bodies (Figure 3.10D and Figure 3.11).

Immunostaining for FABP7 appeared to produce a fluorescent signal on the periphery of those DRG cell bodies examined by microscopy. When co-stained for NeuN/Rbfox3 or NF200, the fluorescent signal did not co-localise with that of FABP7 (Figures 3.12 and 3.13). However, FABP7 immunofluorescence did co-localise with the peripheral smaller non-neuronal cells that had been stained with DAPI but crucially had not been immunostained positive for NeuN/Rbfox3 (Figure 3.12 – arrows). Together, these observations strongly suggest that FABP7 is mostly expressed in non-neuronal cells.

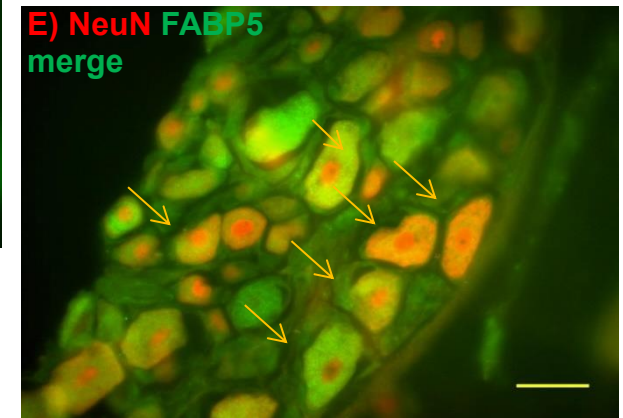
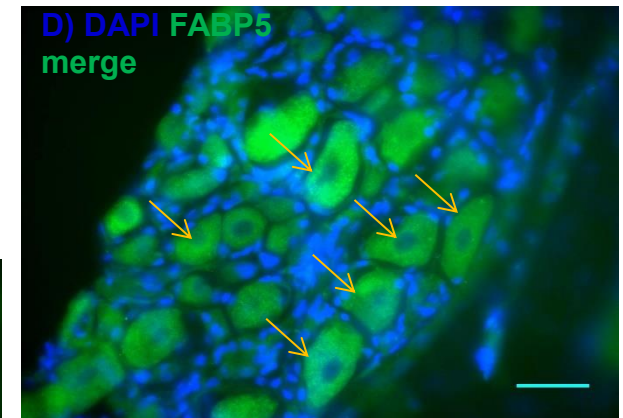
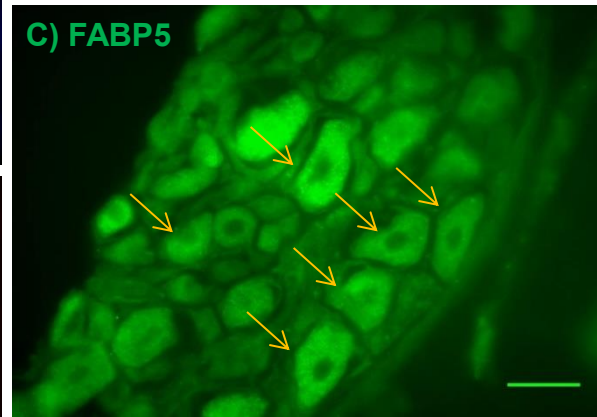
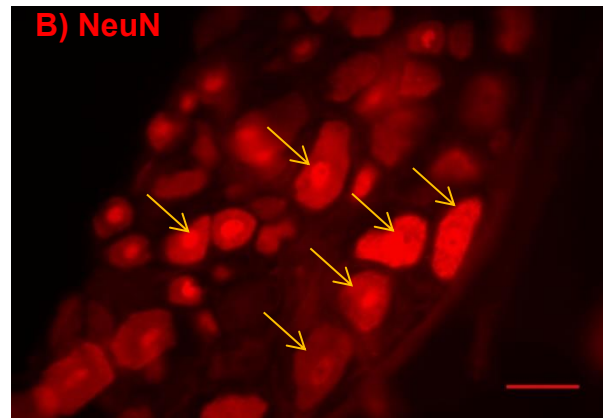
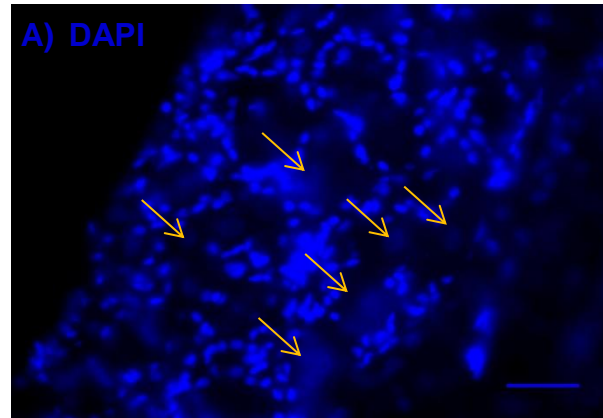


Figure 3.10: Representative images showing co-staining for FABP5 and NeuN/Rbfox3 in DRG tissue sections: Fixed-frozen DRG tissue sections from a single male Sprague Dawley rat (n=1) were dual immunostained with rabbit polyclonal anti-FABP5 and mouse monoclonal anti-NeuN/Rbfox3 antibodies, followed by incubation with goat anti- rabbit IgG Alexa Fluor® 488 and goat-anti mouse IgG Alex Fluor® 568. Images were acquired with a $\times 40$ objective lens. Scale bar is $25\mu\text{m}$. Arrows indicate key regions/cells of interest which are described in section 3.2.5.

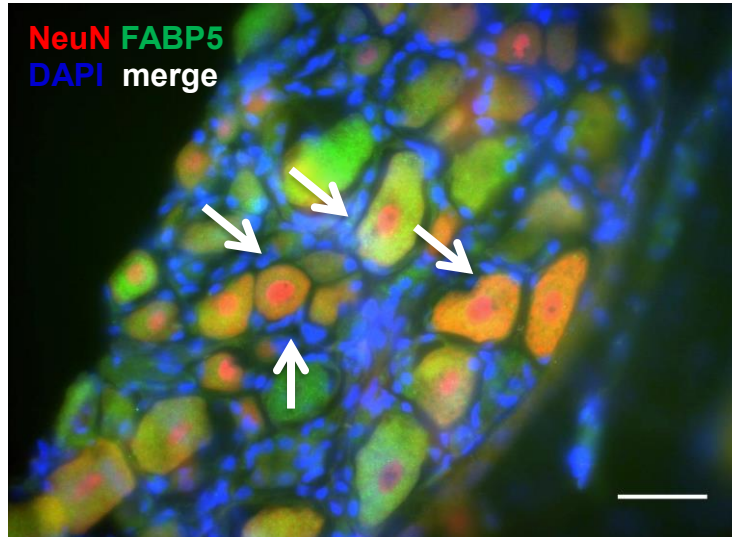


Figure 3.11: Image merge showing DAPI stained nuclei of non-neuronal cells in the same DRG tissue section used for immunofluorescence in figure 3.10. Images of the DAPI stained cells were merged with images acquired in the FITC and TRITC channels examining FABP5 and NeuN immunostaining. White arrows point to those cells who nuclei had stained with DAPI but had not immunostained positive for NeuN. These cells were therefore not considered as neuronal. The absence of any detectable FABP5 immunostaining/immunofluorescence in the FITC channel when the same regions of interest/cells were examined by microscopy, suggests that FABP5 is not expressed in the associated non-neuronal cells.

Scale bar is 25 μ m.

Figure 12

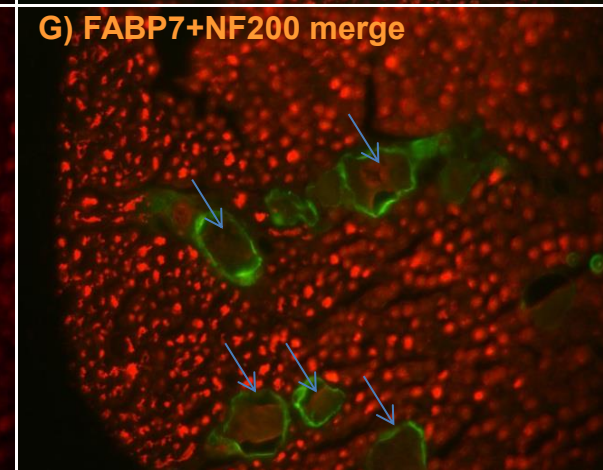
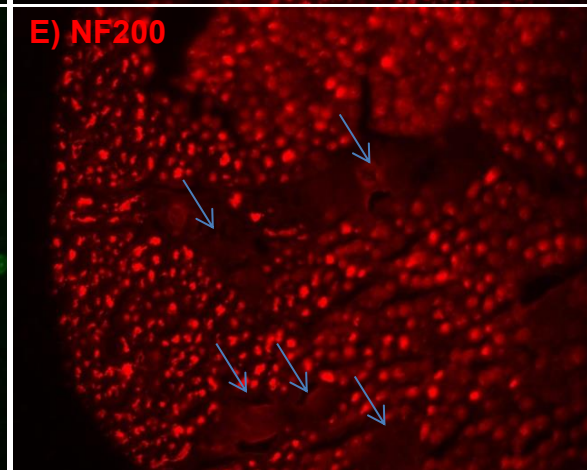
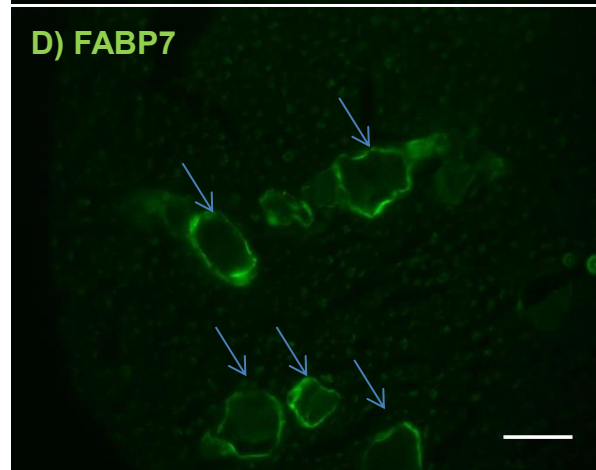
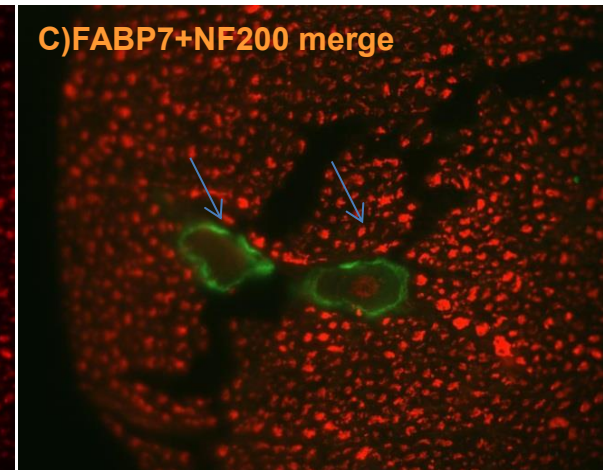
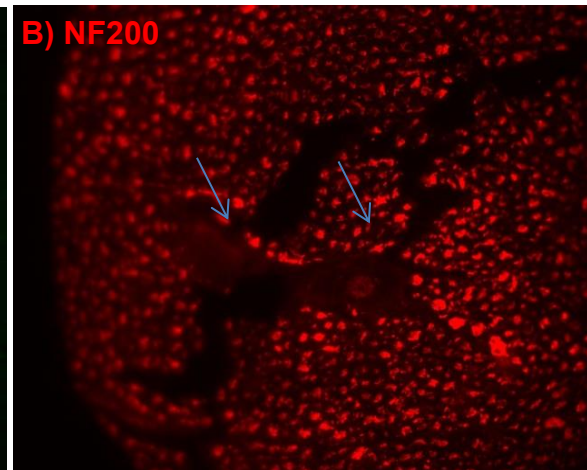
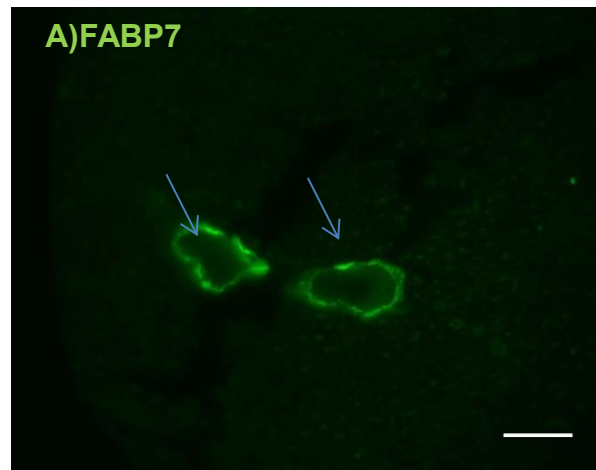


Figure 13

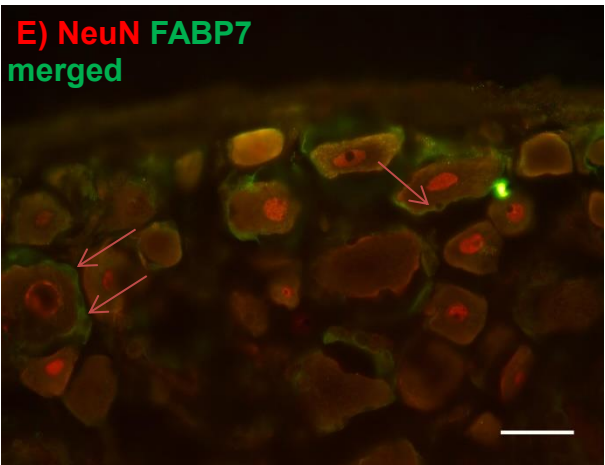
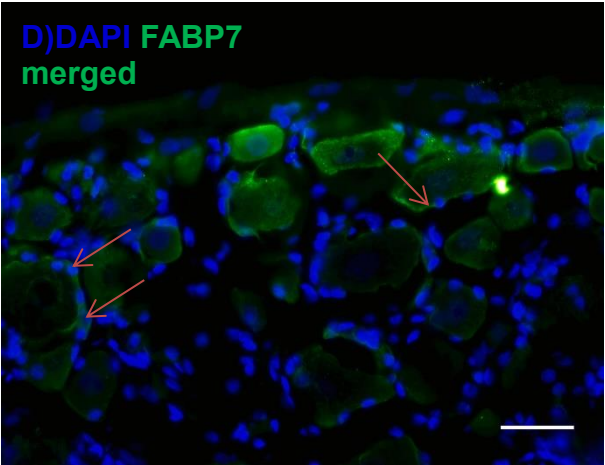
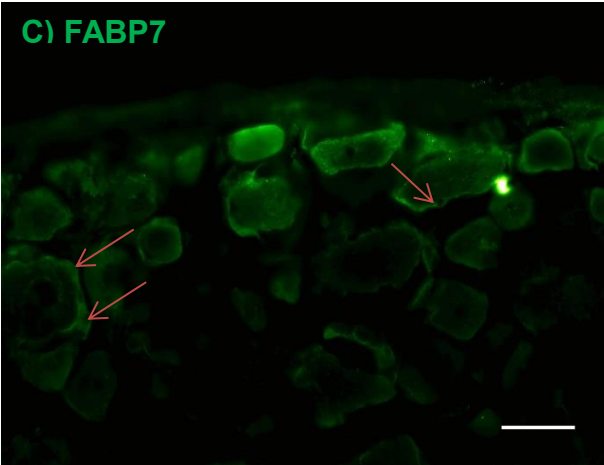
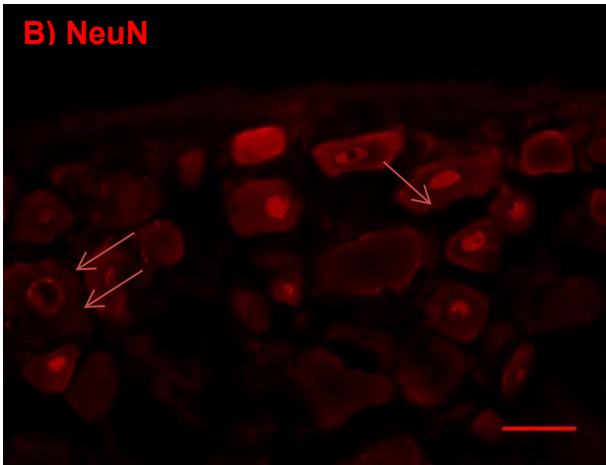
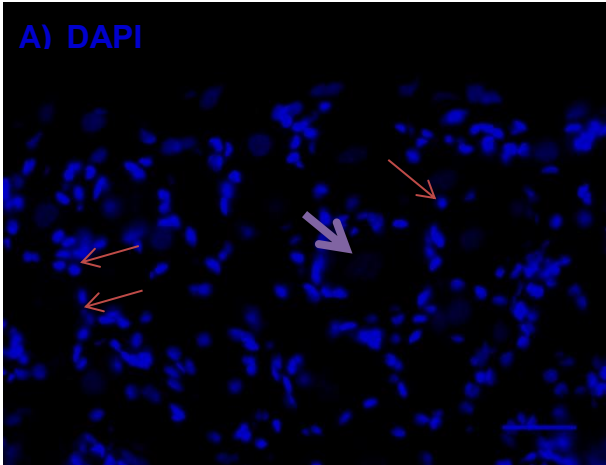
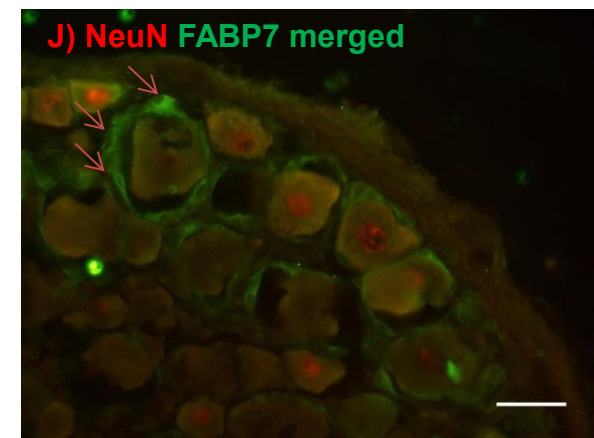
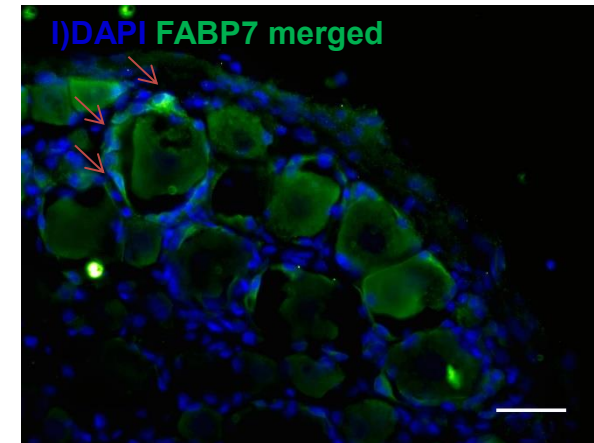
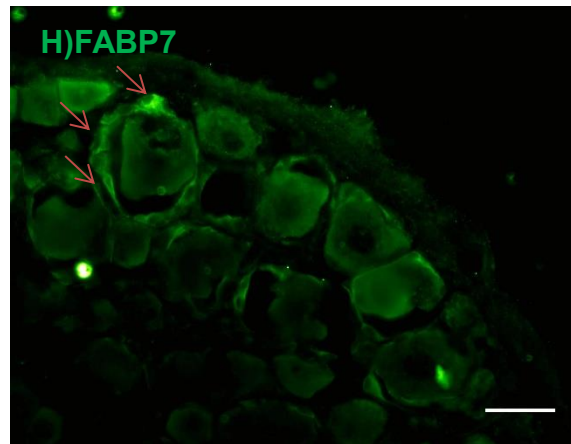
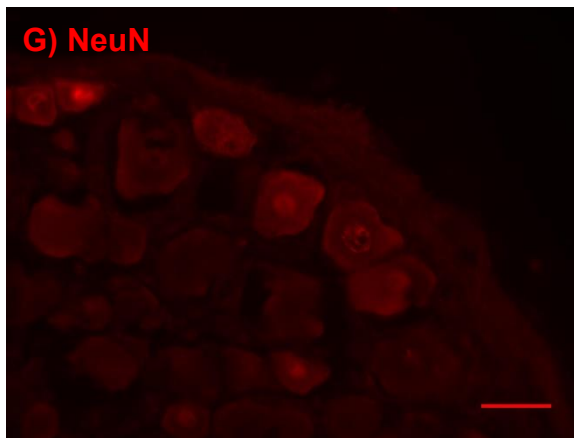
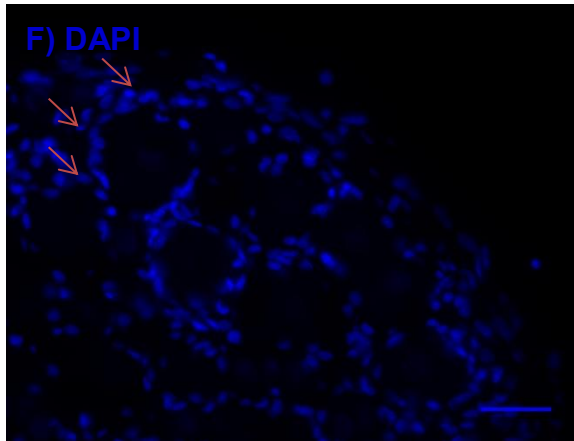


Figure 13



Figures 3.12 & 3.13: FABP7 immunofluorescence in non-neuronal cells: Fixed-frozen DRG tissue sections from a single male Sprague Dawley rat (n=1) were dual immunostained with rabbit polyclonal anti-FABP7 and mouse monoclonal anti- NF200 (Figure 3.12) or rabbit polyclonal anti-FABP7 and polyclonal mouse anti- NeuN/Rbfox3 antibodies (Figure 3.13). In both cases this was followed by incubation with goat anti- rabbit IgG Alexa Fluor® 488 and goat-anti mouse IgG Alex Fluor® 568. Images were acquired with a x 40 objective lens. Scale bar is 25µm. Arrows indicate key regions/cells of interest which are described in section 3.2.5.

3.3 Summary of key findings and results

- TRPV1, FABPs 5, 7, 8 and PPAR isotypes α , β and γ 1 are expressed in a heterogeneous population of DRG cell bodies and non-neuronal cells.
- TRPV1, FABPs 5, 7, 8 and PPAR isotypes α , β and γ 1 transcripts were still detectable in DRG heterogeneous cell cultures after 24 hours. However, when comparing to freshly isolated *ex vivo*, DRGs, relative expression levels of TRPV1 and FABP7 were reduced, whereas levels of PPAR β and PPAR γ 1 were significantly elevated in DRG cell cultures.
- DRG cell cultures were fractionated into neuronal and non-neuronal cell populations-enrichments. Comparative TaqMan® gene expression assays performed on cDNA from neuronal and non-neuronal cells implied the following; FABP5 was expressed in both cell populations, whereas FABP7 and 8 were found to be expressed at significantly higher levels in non-neuronal glial cells.
- PPAR α was expressed at higher levels in non-neuronal glial cell fraction, whereas there were significantly lower levels of relative expression for PPAR β and γ 1 in non- neuronal glial cells compared to neuronal cell fraction. TRPV1 expression levels were also lower in the SGC fraction compared to the neuronal cell enrichment.
- DRG sections immunostained for FABP5 and FABP7. FABP5 appeared to localise to the DRG cell bodies, whereas FABP7 stained non-neuronal cells surrounding and associated the DRG cell bodies. Due to lack of reliable antibodies reactive against FABP8 and the PPARs for immunofluorescence, this limited any further progress.

3.4 Discussion

Despite the extensive knowledge concerning the role and biochemical-cellular function of FABPs and PPARs, little is known or has been investigated concerning their respective roles in nociceptive signalling.

Emerging studies are now beginning to explore the potential role of FABPs in modulating lipid signalling pathways in cell culture experiments and animal (rodent) models of inflammatory hyperalgesia (120, 121). Such studies have explored the consequence of pharmacological inhibition of FABP5 with bespoke chemically synthesized pharmacological inhibitors. However, the downstream consequences of inhibition of FABP5 function are not entirely clear. The exact cellular signalling pathway affected still requires further and extensive characterization.

The aim of this chapter was to identify which FABP and PPAR isoforms were expressed in physiologically relevant cell cultures i.e. dorsal root ganglia cultures. Once identified the role and function of FABPs and PPARs could be explored further. The neuronal cell bodies of the dorsal root ganglion have been routinely isolated from rats and are universally used in lipid signalling and nociception related studies (118, 119). An advantage of DRG cell culture was that they contained the supporting satellite glial cells; therefore, the biological niche was maintained up to a certain point. Conversely, the presence of non-neuronal cells was problematic as discussed later.

For the first time, this study has shown that FABPs 5, 7, 8 and all three PPAR isotypes are expressed in DRG cell culture preparations. Furthermore, transcripts for each of the genes identified were still detectable by TaqMan® gene expression assays even after the cells were cultured *in vitro* for 24 hours.

Relative expression levels did vary for each of the genes when comparing fresh and cultured DRGs. However, for FABP7 and TRPV1, substantial decreases in gene expression levels were observed, but transcripts for both genes were still easily detectable.

SGCs encapsulate cell bodies and are essential for cell body survival in culture. Previous studies have highlighted the ability of DRG cell bodies and SGCs to communicate with each other in a paracrine manner, through the secretion of chemical messengers acting at specific receptors. Coupled with previous findings which have shown that SGCs express nerve growth factor (NGF) (123), a neurotrophin responsible for maintaining and increasing TRPV1 expression levels, it is possible that NGF is secreted from SGCs to their dependent DRG cell body and therefore sustains TRPV1 expression levels.

This loss of close cell-cell contact resulting from the dissociation of the cell preparation may account for the decreased levels of TRPV1 expression in cultured DRGs. But given that TRPV1 is still expressed could be explained by the presence of NGF in the cell culture medium, which may be compensating, but not comparable nor sufficient enough in quantity to have the same effect as in seen *in vivo*. It is tempting to speculate that this could also account for the decrease in FABP7 expression levels observed in cultured DRG cells; however, further investigation is required.

A limitation of the DRG cell culture preparation is that a mixture of DRG cell bodies and non-neuronal cell bodies is produced. This presented a major difficulty when trying to establish which gene was expressed in which cell type. The problem was initially solved by physically separating or fractionating the DRG cell culture into neuronal cell bodies and satellite glial cells.

This was achieved by exploiting the differences in the adherent properties of the two different cell types, as described previously. Once separated into two distinct cell populations it was easy to prepare cDNA for TaqMan® gene expression assays to establish if there was a difference in the gene expression profile of the two cell types.

TaqMan® gene expression data implied that there were some differences in the gene expression profile for FABPs and PPAR present in DRG cell bodies and non-neuronal glial cells. However, genes were found still to be expressed in both cell populations. This may be due in part to the inability to completely fractionate the cell culture preparation into discrete cell types i.e. DRG cell bodies and SGCs. This was exemplified by TaqMan® gene expression assays, which measured the levels of expression for cell specific markers NeuN/Rbfox3 (neuronal cell markers) and GFAP (glial cell marker). NeuN levels were significantly higher than that of GFAP; however, GFAP expression was still detectable; therefore, there were still non-neuronal cells present in the DRG cell body enrichment.

Despite the limitations of these data, preliminary immunohistochemical analysis of DRG tissue sections with anti-FABP and NeuN/Rbfox3 antibodies did indicate that FABP5 was expressed in the DRG cell bodies whereas FABP7 was expressed in glial cells. However, further investigation/confirmation is required using alternative techniques that do not rely on antibodies but still use DRG sections and therefore still allow for the visualization of whole DRG cell bodies and their associated SGC cells.

Chapter 4: Expression and purification of recombinant FABPs for use in fluorescence displacement assays

Chapter 4: Expression and purification of recombinant FABPs for use in fluorescence displacement assays

4.0 Introduction

The lipid binding properties of FABP isoforms; 5,7 & 8, which had been previously identified as being expressed in rat DRG cultures in chapter 3, required investigation. It was necessary to provide experimental evidence to support the notion that FABPs 5, 7 & 8 could physically bind to and act as lipid chaperones for endogenous TRPV1 ligands. It has been previously reported that both 13 (S) HODE and anandamide (AEA) can act as endogenous TRPV1 activators (62, 69). Furthermore, there is already some experimental evidence to suggest that FABP 5 can sequester and transport both AEA and 13(S) HODE (111,112, 124).

It was therefore decided that the affinity and selectivity of FABP 5, 7 & 8 for both endogenous TRPV1 ligands AEA and 13(S) HODE would be assessed in a cell-free assay. In brief, the intention was to optimize a simple non-radioactive assay system that could determine the binding properties of each FABP isoform of interest, for the ligands AEA and 13(S) HODE.

Each FABP was cloned into the inducible expression vector pET28a generating pET28a-FABP plasmids. Using this heterologous inducible expression system, N-terminally Hexa-histidine tagged FABPs (His-tagged FABPs) were overexpressed in SoluBL21™ *E. coli* and then subsequently purified by immobilized Ni²⁺ affinity chromatography.

Hydrophobic probes such as 1,8 -anilinonaphthalene (1,8-ANS) and 12-N-methyl-(7-nitrobenz-2-oxa-1,3-diazo) amino stearic acid (12-NBD stearate) have been widely used in studies exploring the ligand binding properties of FABPs. Both 1, 8-ANS and 12-NBD stearate bind to the hydrophobic binding pockets of FABPs

and iLBPs. When sequestered into hydrophobic binding pockets of the FABPs/iLBPs, there is a marked increase in the measured fluorescence intensity resulting from the newly formed 1,8-ANS or 12-NBD stearate–FABP/iLBP complex (112, 125). This fluorescence is lost when competing ligands displace 1, 8-ANS or 12-NBD stearate from the FABPs/iLBPs. The basic premise of this assay is that loss the of fluorescence intensity can be attributed to a ligand successfully out-competing and displacing bound 1,8-ANS or 12-NBD stearate probe from the FABPs/iLBPs (112, 120, 125), this is depicted in figure 4.1.

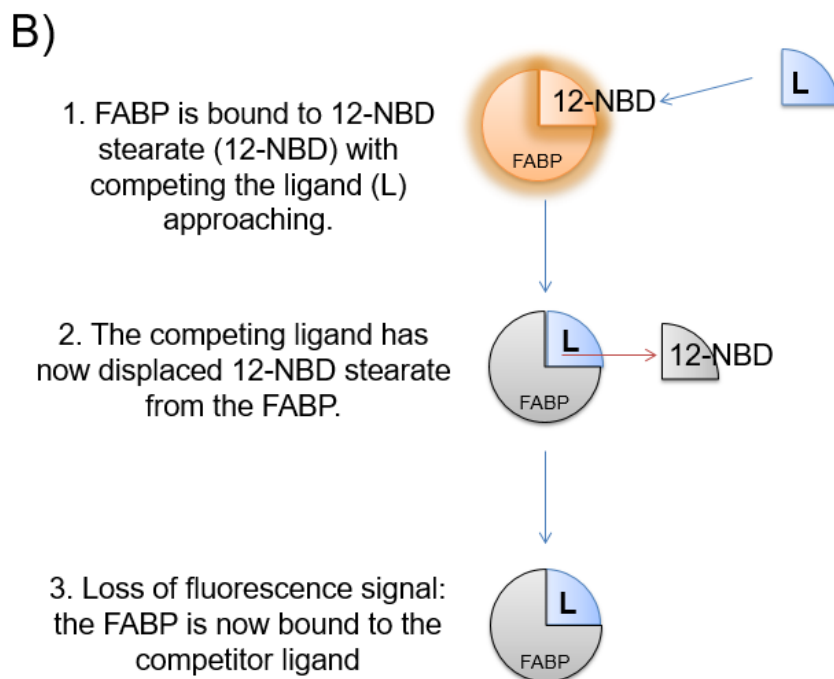
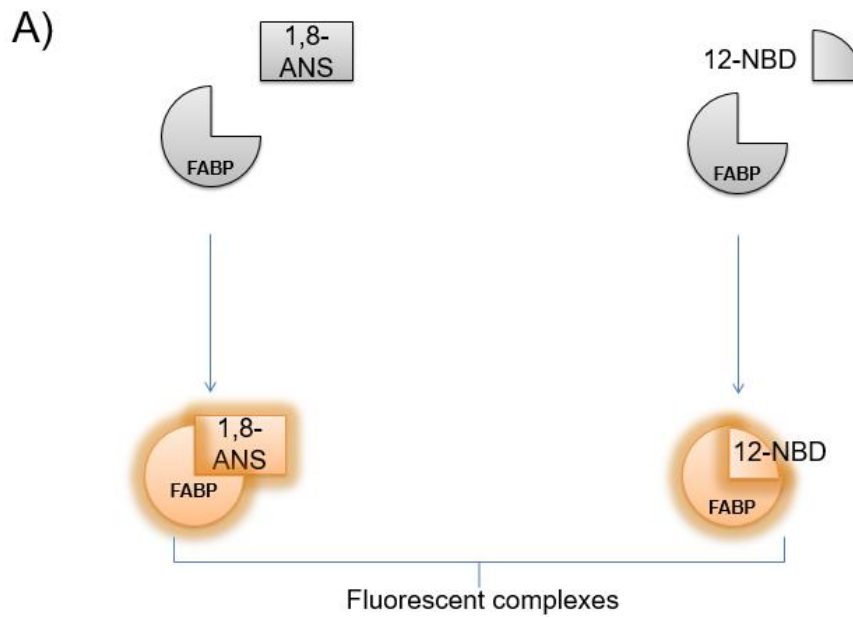
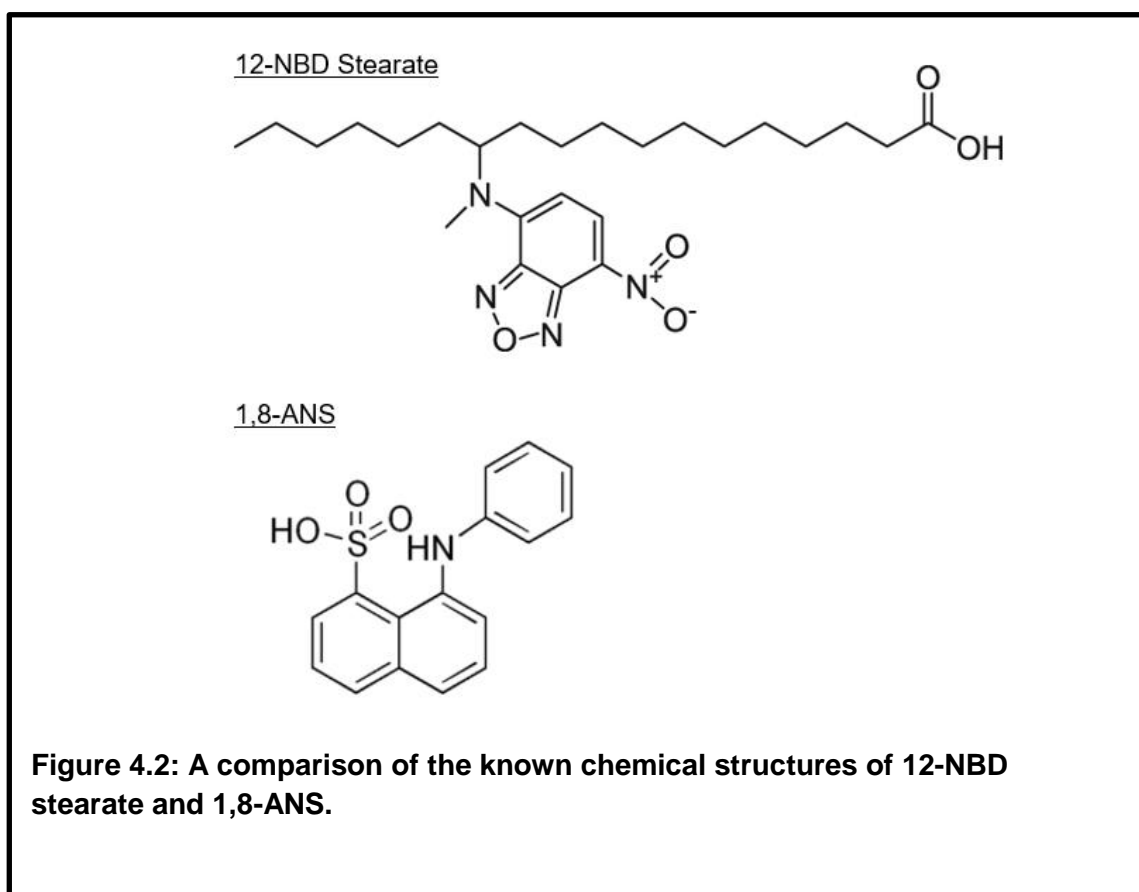


Figure 4.1: Schematic representation of the core principle underpinning the fluorescence displacement assays – A) Fluorescent complexes are formed when non-radioactive probes 1, 8-ANS or 12-NBD stearate interact with purified FABPs *in vitro*. The free probe does not fluoresce when un-sequestered by iLBPs such as the FABPs. **B)** Competing lipophilic ligands (L) that associate with FABPs, are capable of displacing bound probe such as 12-NBD from the FABPs. The result is a loss in fluorescence signal and measured fluorescence intensity. The loss of fluorescence signal is indicative of the lipophilic ligand (L) out-competing 12-NBD stearate for the hydrophobic binding cavity - the pocket of the FABP.

The use of 12-NBD stearate was favoured for this study over 1,8-ANS given that it is more representative of an endogenous FABP ligand. This is particularly relevant when performing displacement assays where one lipid species is competing with another structurally similar lipid species for the same binding cavity of the FABP (Figure 4.2).



4.1 Methods in brief, calculations, and statistics

Protein expression and purification: His-tagged FABP5, 7 & 8 were overexpressed in SoluBL21™ *E.coli* using the pET28a inducible expression system (Novagen). Cultures were grown until the O.D_{600nm} was approximately 0.6. Protein expression was induced with 1mM IPTG for 24 hours at 25 - 37°C after which the cells were pelleted by centrifugation at maximum speed for lysis and sonication in pseudo-native lysis buffer. Cell lysates were clarified by centrifugation, and the FABPs were then purified from the resulting supernatants by Ni²⁺ immobilized metal affinity chromatography.

Fluorescence displacement assays: Fluorescence intensity was measured at an excitation: emission wavelength of 484: 520nm at 25°C using FLUOstar® Omega spectro-fluorometer (BMGLABTECH). In all cases, microwell plates containing the assay mixtures were agitated then allowed to incubate in dim light for 1 minute at 25°C before measuring fluorescence intensity. Fluorescence intensity was measured for increasing concentrations of 12-NBD stearate (0.05 – 2.5µM) in the absence or presence of 3µM purified FABP. The fluorescence intensity was also determined for increasing concentrations of purified FABP (0.05 – 6µM) in the presence or absence of 500nM 12-NBD stearate. The concentration of protein was used/reported as per the protocol reported by Kane et al. (125). 0.5µM – 3µM of purified FABP was complexed with 500nM of 12-NBD stearate in the presence or absence of competitor lipid ligands in potassium phosphate buffer pH7.4. Competitor ligands were added at increasing concentration (0.1 -10µM), and the decay in fluorescence intensity was measured.

Calculations for the determination of Kinetic Parameters K_d and K_i: All analyses and calculations were performed in Prism 5 unless otherwise stated. Fluorescence intensities of each saturation curve were corrected for background fluorescence.

This was calculated by subtracting the measured fluorescence intensities in the absence of FABP or 12-NBD stearate.

Measured fluorescent intensities were reported on a scale ranging from 0.00 to 1.00 relative fluorescence units. Dissociation constants or binding constants (K_d) of 12-NBD stearate for FABPs 5, 7 & 8 were determined from saturating curves by performing a nonlinear regression of the blank corrected data and one site binding analysis. 95% Confidence intervals (CI) were given for each calculated K_d value.

From the processed displacement data IC50 values were calculated by performing a nonlinear regression dose response – inhibition analysis. This was conducted by initially taking the logarithm of each drug concentration tested and plotting log (drug/ligand concentration) vs. scaled fluorescence. Appropriate analyses were then performed as above. Calculated IC50 values were then used to determine the inhibitory constant (K_i) of each competitor ligand tested at each FABP. Calculating the K_i value allowed the binding affinity of lipid ligands for FABPs to be determined. K_i was calculated using the Cheng-Prusoff equation which has been widely used when determining the K_i values of competing for lipid ligands at FABPs/iLBPs (120, 125).

$$K_i = \frac{[IC50]}{(1 + [12\ NBD\ Stearate]/K_d)}$$

Column statistics for grouped data: A unpaired student t- test was used when comparing differences between experimental groups. A p value of <0.05 was considered as significant in all cases.

4.2 Summary of experimental objectives for chapter 4

1. Express and purify soluble and functional His-tagged FABPs for fluorescence – competition displacement assays.
2. Determine the functionality state of purified FABPs by incubation with 12-NBD stearate and subsequent displacement assays with positive control competitor ligand arachidonic acid.
3. Optimization of FABP: 12-NBD stearate molar stoichiometry for the competition assay.
4. Determine the K_d (dissociation – binding constant) of 12-NBD stearate for FABP5, 7 and 8.
5. Assess the affinity and selectivity of purified FABPs for endogenous TRPV1 ligands AEA and 13 (S) HODE by competition for 12-NBD stearate at FABPs 5, 7 & 8 and subsequently determine the kinetic parameter K_i of each screened competitor ligand. Determine K_i values for arachidonic acid, AEA and 13 (S) HODE from using previously calculated K_d values of 12-NBD stearate at each tested FABP and the IC_{50} values for each screened ligand at each tested FABP.

4.3 Results

4.3.1 A fraction of FABP5 and FABP8 is soluble when expressed at 37°C, but FABP7 is not soluble

To confirm that histidine tagged FABPs 5, 7 and 8 had been successfully overexpressed, samples of overnight SoluBL21™ *E.coli* liquid cultures induced with IPTG were compared to un-induced liquid cultures. The samples of liquid culture were then lysed ready for analysis. The resulting supernatants (soluble fraction) from the clarified lysates containing soluble protein and the remaining pelleted cellular debris (insoluble fraction) containing insoluble proteins from both the induced and uninduced liquid cultures were resolved by SDS-PAGE. Proteins bands were then visualized by Coomassie blue staining (Figure 4.3, Gels A – C).

Analysis of the soluble fraction, from the pre induced/un-induced liquid cultures, revealed a series of protein bands corresponding to endogenous *E.coli* protein (Figure 4.3, Gel A). While the insoluble and soluble equivalent fractions obtained from induced cultures gave the same series of protein bands, however, an intense protein band migrating at a molecular weight of 15kDa was detected by Coomassie staining (Figure 4.3 Gel B and C). However, it was only the supernatants (soluble) and cellular debris (insoluble) fractions obtained from induced liquid cultures expressing His tagged FABP5 and 8 that gave these observed 15kDa protein bands in both soluble and insoluble fractions (Figure 4.3 Gels B & C). His tagged FABP7 was only present in the insoluble fraction from the induced culture.

The partitioning and presence of FABP5 and FABP8 into both the soluble and insoluble fractions obtained by cell lysis indicated that not all recombinant FABP5 and 8 expressed, was soluble. However, it was judged that a sufficient quantity of soluble protein was present and that modifying or refining the conditions for protein

expression, to recover more soluble protein, was unnecessary. Whereas for FABP7, no band was detected in the soluble fraction (Figure 4.3 Gel B), but a band was observed in the insoluble fraction (Figure 4.3 Gel C). It was concluded that His tagged FABP7 was insoluble when expressed at 37°C.

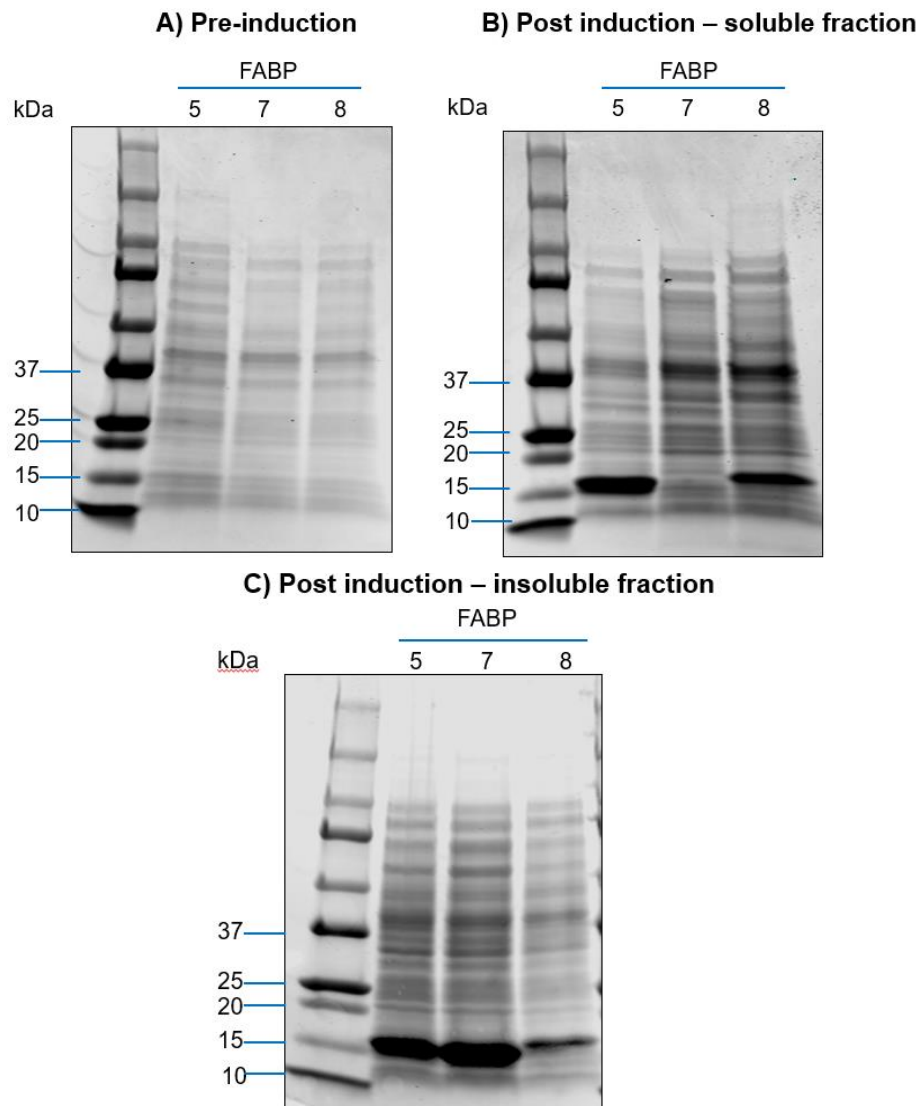


Figure 4.3: Coomassie gel analysis to confirm the expression of recombinant human FABP5, 7 and 8 in SoluBL21TM *E.coli* cultures: 1mM IPTG was used to induce the expression of N-terminally Hexa-histidine tagged FABP isoforms 5, 7 and 8 in SoluBL21TM *E.coli* cultures for 24 hours at 37°C as described chapter 2. Before induction, 1ml aliquots of un-induced liquid culture were retained for centrifugation to harvest the cells for subsequent cell lysis, SDS-PAGE, and Coomassie staining. Gel A) pre-induction, gel B) post induction – soluble fraction, gel C) post induction - insoluble fraction.

4.3.2 Re-expressing FABP7 at lower temperature gives a fraction of soluble protein

Inducing protein expression at a reduced temperature has been widely reported to improve the solubility of recombinant proteins expressed in *E.coli* (126). Lower temperatures favour a reduction in the rate of protein synthesis and therefore the overall cellular – cytosolic protein concentration.

Therefore, FABP7 was re-expressed for 24 hours as previously, but at a reduced temperature of 25°C. Protein bands corresponding to a molecular weight of approximately 15kDa were observed for both soluble and insoluble fractions analysed by SDS-PAGE (Figure 4.4). In conclusion, inducing FABP7 overexpression at 25°C yielded the soluble FABP7 required for subsequent protein purification.

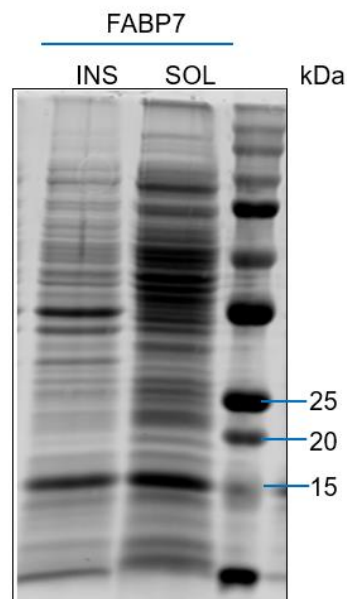


Figure 4.4: Re-expression at 25°C for 24 hours, produces a fraction of soluble N-terminally histidine tagged FABP7: The expression of FABP7 was induced with 1mM IPTG as previously, but at a lower temperature of 25°C for 24 hours. 'INS' denotes insoluble protein/fraction, whereas 'SOL' denotes soluble protein/fraction.

4.3.3 Purification of FABPs by immobilized Ni²⁺ - metal affinity chromatography (IMAC)

Liquid cultures were pelleted then resuspended and lysed with optimized native lysis buffer by sonication. The resulting lysates were clarified, and the supernatants were loaded onto the Ni²⁺ - metal ion affinity columns. Bound proteins were eluted from Ni²⁺ - metal ion affinity columns using a native elution buffer containing a high concentration of imidazole (relative to previous wash buffers). Aliquots of the resulting eluates were concentrated with 10% [w/v] TCA as described previously. Samples of concentrated eluate were analysed by SDS-PAGE and Coomassie blue staining to establish the success of the purification. All three FABPs (5, 7 & 8) were purified to near complete homogeneity in a single purification step, albeit with minimal amounts of contaminating proteins co-purifying with the FABPs (Figure 4.5).

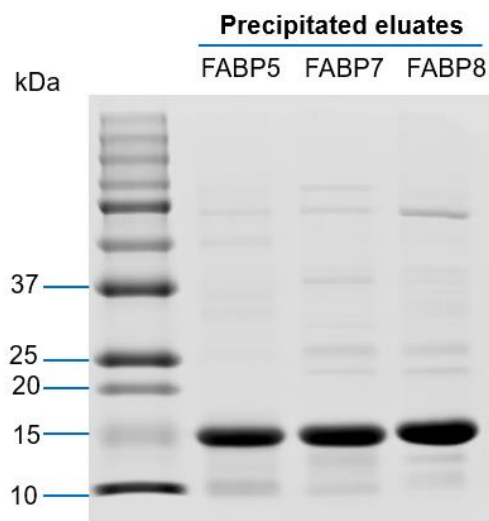


Figure 4.5: Purification of Hexa-histidine tagged FABPs by immobilized metal (Nickel/Ni²⁺) ion affinity chromatography (IMAC) from SoluBL21TM *E.coli* 'native' cell lysates: After 24 hours of protein overexpression, overnight cultures were pelleted by centrifugation and lysed with pseudo-native lysis buffer. His tagged FABPs were purified using a 5ml bio-scaleTM mini profinityTM IMAC Cartridge. Protein samples were resolved by electrophoresis on a 15% polyacrylamide gel and stained with Coomassie blue.

4.3.4 12-NBD stearate binds to purified FABPs 5, 7 & 8

The first aim was to establish that the purified His-tagged FABPs were functional and could, therefore, bind to 12-NBD stearate. Initially, a fixed concentration of 500nM 12-NBD stearate was titrated against increasing concentrations of FABP [μM] in an isothermal binding reaction. Increases in FABP concentration was concomitant with increases in measured fluorescence intensity, for all three FABP isoforms tested. In conclusion, despite the FABPs being fused to a Hexa-histidine tag, it appeared that they had retained their functionality as lipid binding proteins (Figure 4.6). Importantly, such increases in fluorescent signal were undetectable in parallel experiments where 12-NBD stearate had been omitted (Figure 4.6).

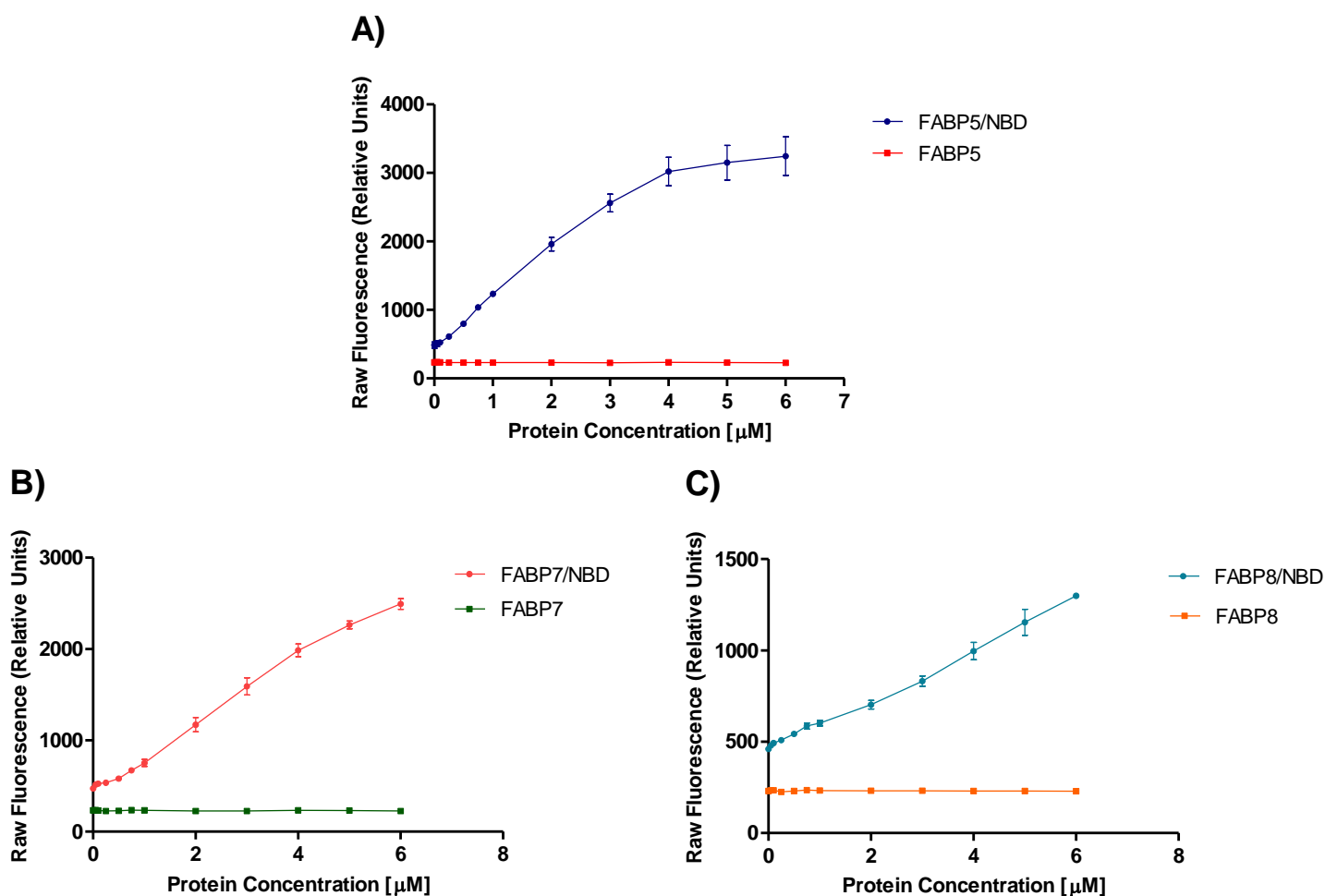


Figure 4.6: Increasing FABP concentration in the presence of a fixed concentration of 12-NBD stearate: 12-NBD stearate was added at a final concentration of 500nM, to increasing concentrations of FABP in 10mM potassium phosphate pH7.4. 12-NBD stearate – FABP complexes were allowed form for 1 minute at ambient temperature in the dark. Fluorescence was then measured at an excitation: emission wavelength of 484:520nm. In a single experiment, the raw fluorescence values for each standard curve were averaged. In all cases, each single assay/experiment was repeated a total of 3 times for each FABP tested, giving a total of three independent experiments for each FABP tested ($n=3$). All graphs are represented as an average \pm SEM. Raw fluorescence values are reported for increasing concentration of FABPs in the presence of 500nM 12-NBD stearate (FABP/NBD) and increasing concentration of FABPs where 12-NBD stearate was absent (FABP). A) FABP5 B) FABP7 C) FABP8.

The precise concentration of protein to be used in the binding assays was then determined by directly comparing the measured fluorescence intensities produced from binding 500nM 12-NBD stearate to either 0.5 μ M or 3 μ M of FABP. Kane et al. (125) had previously used an equimolar ratio of probe: FABP when 1, 8-ANS was used as the probe at a concentration of 500nM. Whereas Kaczocha et al. (112), complexed 3 μ M FABP with 500nM of 12-NBD stearate. To ascertain which approach was the best to emulate concerning which molar ratios of ligand: protein to use, two binding reactions were performed: the first used an equimolar ratio of 500nM 12-NBD stearate to 500nM of FABP, the second used 3 μ M FABP to 500nM 12 –NBD stearate.

When both concentrations of FABP were complexed with 500nM 12-NBD stearate, a significant increase in fluorescent signal was observed when compared directly to 12-NBD/buffer control group. However, it was judged that a better signal: noise/background ratio was observed when using 3 μ M of FABP i.e. the measured fluorescence intensity of the FABP/NBD complexes (signal) to that detected of free or unbound 12-NBD stearate dissolved in buffer solution (noise/background) was superior to that measured when 0.5 μ M of protein was used (Figure 4.7). For this reason, this concentration of protein was used in all subsequent fluorescence displacement assays (Figure 4.7A-C). In conclusion, the molar stoichiometry was finalized for the remaining assays.

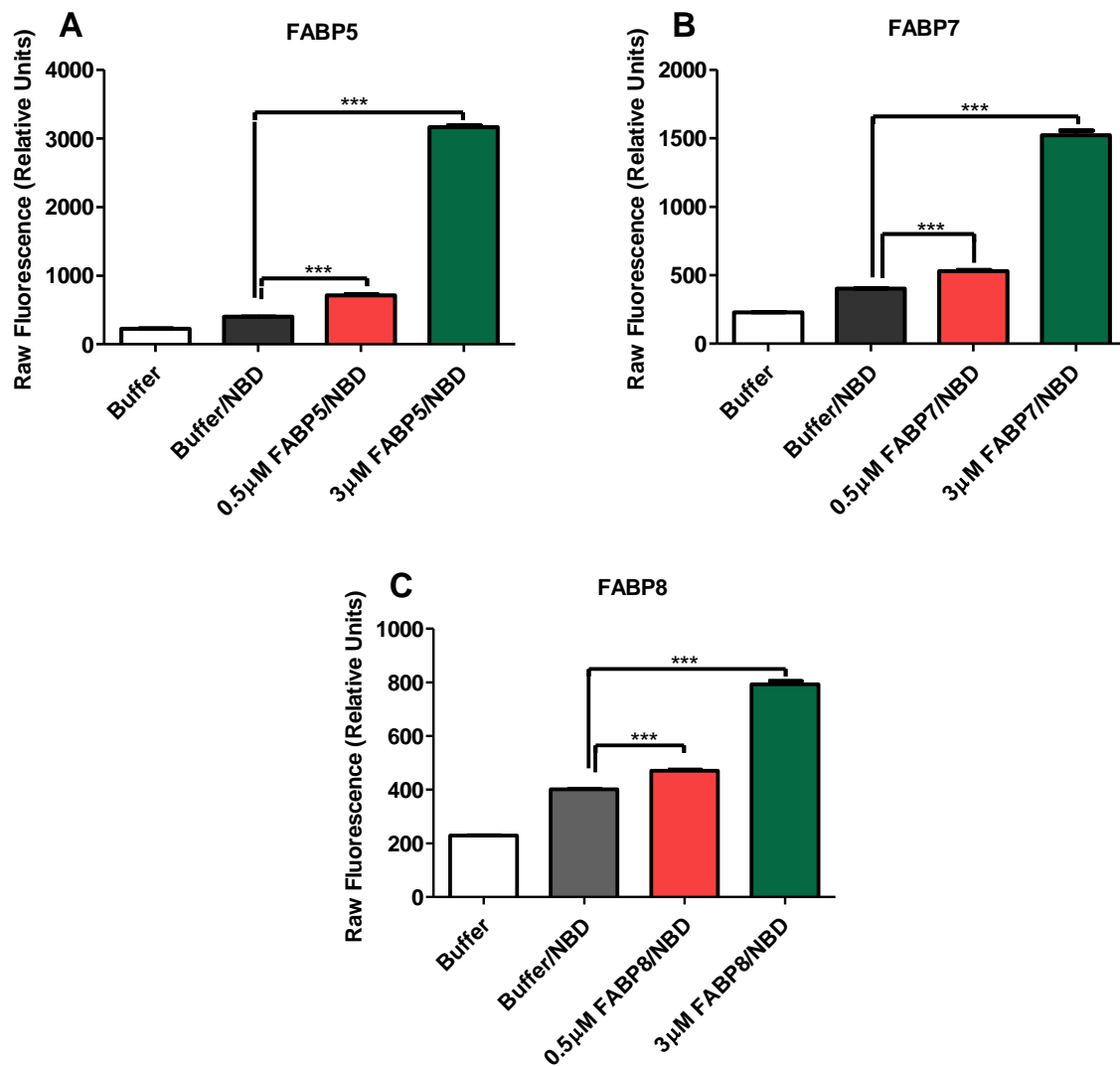


Figure 4.7: Incubation of 500nM 12-NBD stearate with purified FABPs: 12-NBD stearate was added at a final concentration of 500nM, to either 0.5µM or 3µM of purified FABP in 10mM potassium phosphate pH7.4. The raw fluorescence intensity (Fluorescence, Relative Units) of 12-NBD stearate-FABP complexes (FABP/NBD), 500nM 12-NBD stearate (buffer/NBD) and potassium phosphate buffer pH7.4 (buffer) was then measured at excitation: emission wavelengths of 484:520nm at 25°C. A total of 3 independent experiments were performed ($n=3$) and all graphs are represented as an average \pm SEM of raw fluorescence. A unpaired student t-test was used to analyse the differences in raw fluorescence intensities between 0.5µM FABP/NBD and buffer/NBD groups or 3µM FABP/NBD and buffer/NBD groups. A value of $P<0.05$ was considered as significant. ***, $P<0.0001$.

4.3.5 Determining the dissociation constants (K_d) of 12-NBD stearate for FABPs 5, 7 & 8

A fixed concentration of 3 μ M FABP was titrated against increasing concentrations of 12-NBD stearate. Increases in 12-NBD stearate concentration with 3 μ M FABP was accompanied by incremental increases in raw fluorescence intensity (Figure 4.8). In parallel, the fluorescence intensity was determined for a duplicate standard curve where FABP was omitted and replaced with potassium phosphate buffer.

The K_d value for each FABP was calculated from the blank corrected fluorescence intensity data by performing single site binding analysis using nonlinear regression as discussed previously (Table 4.1) The K_d value was then used to calculate binding affinities of the TRPV1 ligands for FABPs 5, 7 & 8. There were differences in the affinity of each of the FABPs for 12-NBD stearate, this is reflected in the calculated K_d values. The calculated K_d values for FABP5, 7 and 8 were 0.39, 0.68 and 0.48 μ M respectively.

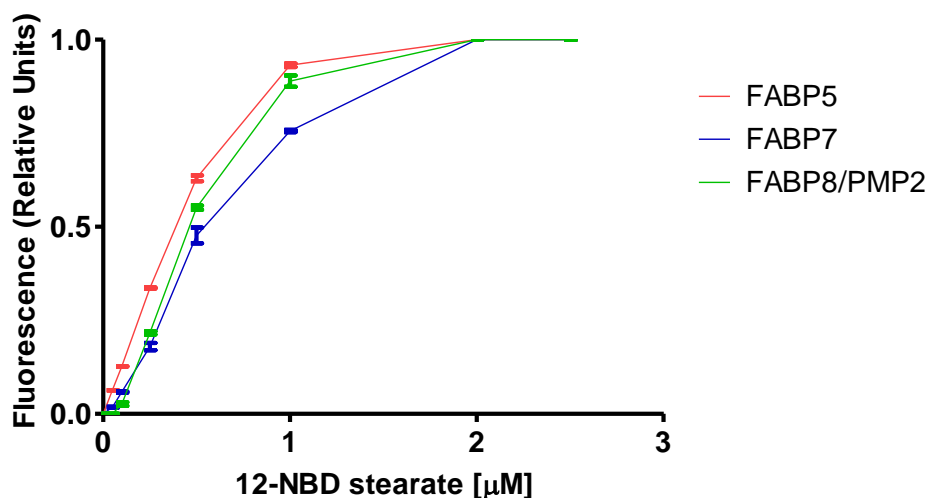


Figure 4.8: Saturation of FABPs with increasing concentrations of 12-NBD stearate: 12-NBD stearate was titrated against a fixed concentration of 3μM FABP. 12-NBD stearate – FABP complexes were allowed to form for 1 minute in potassium phosphate buffer pH7.4. Fluorescence intensity was measured at an excitation: emission wavelength of 484:520nm. Standard curves for each FABP were produced from 3 independent experiments ($n=3$). All graphs are represented as an average \pm SEM.

FABP	Ligand	Binding constant [μM]	95% Conf. Interval
5	12-NBD stearate	0.39 (K_d)	0.36 - 0.42
7	12-NBD stearate	0.63 (K_d)	0.55 - 0.71
8	12-NBD stearate	0.48 (K_d)	0.45 - 0.52

Table 4.1: Calculated dissociation constant (K_d) values of FABPs 5, 7 & 8 for 12-NBD Stearate Binding reactions for each FABP were performed three times. Dissociation constant or binding constants (K_d) of each FABP for 12-NBD stearate were calculated from the mean blank corrected – scaled fluorescence data (Figure 4.8) using one site binding analyses in Prism 5 as per Kaczocha et al. (112). 95% Confidence intervals for each determined K_d is given in Table 4.1.

4.3.6 Determining the binding affinity and specificity of AEA and 13 (S) HODE for FABPs 5, 7 & 8

Displacement assays were implemented to establish both the specificity and affinity of FABP 5,7 & 8 for competing lipid ligands of interest. The IC₅₀ values for each competing ligand were determined then used to determine K_i values as described in 4.1. All IC₅₀ values are reported in Table 4.2a. Competing lipophilic compounds included arachidonic acid (AA) endogenous TRPV1 ligands AEA and 13 (S) HODE.

The long chain fatty acid arachidonic acid (AA) has been widely reported to bind to FABP5 and 7 and displace 12-NBD stearate from FABPs in competition displacement assays (112). Based on this, AA was deemed a good competitor for 12-NBD stearate and was used to demonstrate functional displacement of 12-NBD stearate from the purified FABPs (115, 125).

For all the FABPs complexed with 12-NBD stearate, AA produced a concentration dependent displacement of 12-NBD stearate (Figure 4.9) and displayed K_i values of 0.32, 0.21 & 0.07 μ M for FABPs 5, 7 & 8 respectively (Table 4.2b). The above findings for FABP5 and FABP7 reported in this thesis, are in broad agreement with those of previous studies (112, 125). However, the calculated K_i values for AA at FABP5 and FABP7 in this thesis are ~2.3 and 2.6-fold higher respectively to those determined by Kaczocha et al. (112) who reported that the K_i values for AA were 0.12 μ M at FABP5 and 0.09 μ M at FABP7.

AEA was unable to bring about a robust displacement of 12-NBD stearate from FABP5. The calculated K_i value of AEA for FABP5 was 6.79 μ M, which sharply contrasted with 0.34 and 0.20 μ M AEA required to displace 12-NBD stearate from FABP7 & 8 respectively (Table 4.2b). In short, FABP5 exhibits a low affinity for AEA in comparison to FABP7 and 8, whose calculated K_i values are more than ~20 and ~34-fold lower than that of the K_i of AEA for FABP5.

However, the inability of AEA to physically bind to FABP5 contradicts previously published data which had reported a K_i value of 1.26 μ M for AEA at FABP5 (59). While, the K_i value reported in this thesis for AEA at FABP7, is ~ 2.4-fold lower to that reported by Kaczocha et al. (112).

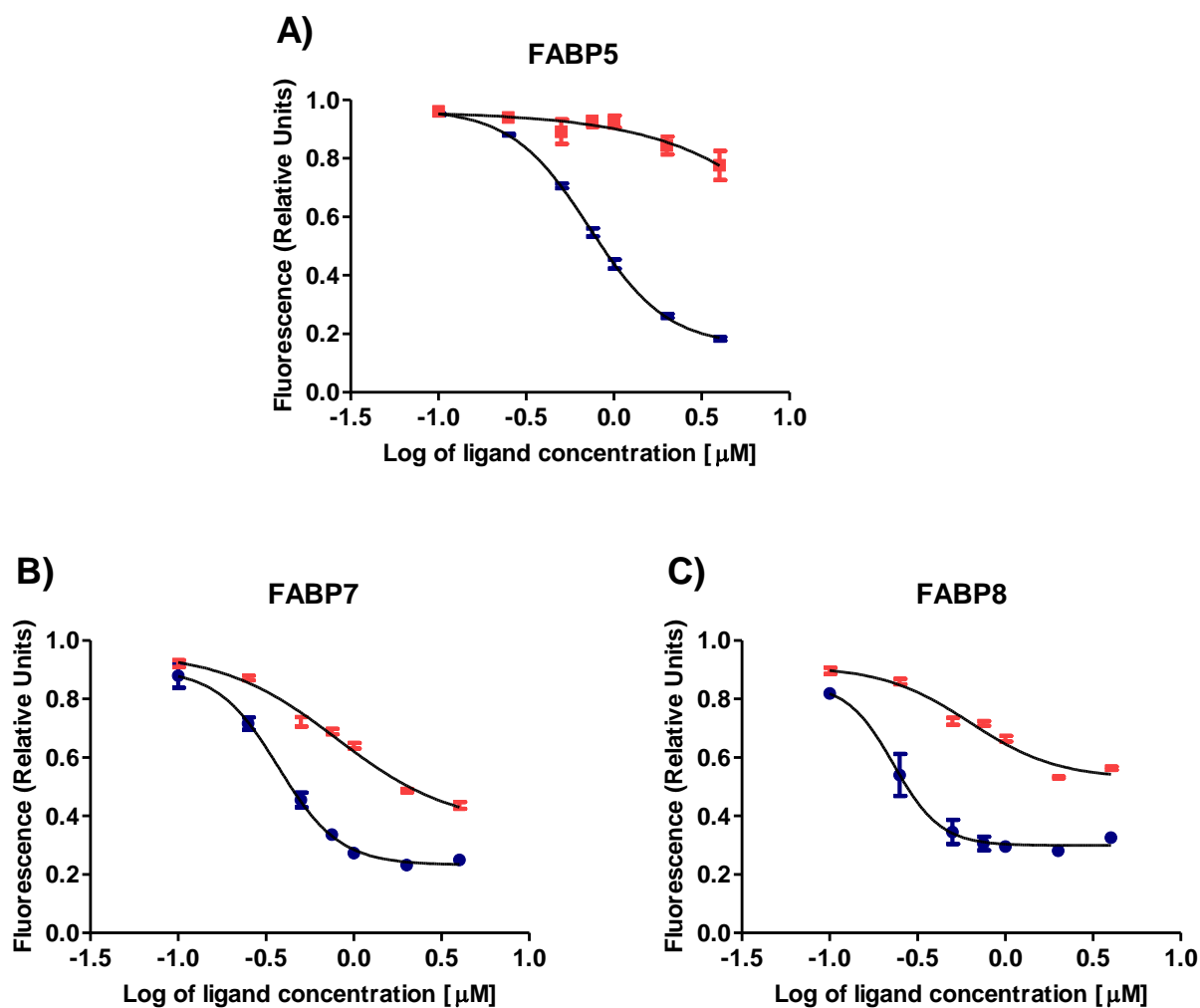


Figure 4.9: Displacement of 12-NBD stearate from FABPs with arachidonic acid and anandamide: 12-NBD stearate – FABP complexes were initially allowed to form for 1 minute in potassium phosphate buffer, pH7.4. Increasing concentrations of competitor ligands [0.1–4 μM], arachidonic acid (blue) and anandamide (red) were titrated against 12-NBD stearate – FABP complexes. The loss of fluorescence intensity was then measured at an excitation: emission wavelength of 484:520nm, then reported on a scale ranging from 0.00 – 1.00 (Fluorescence [Relative Units]). The logarithm of each drug concentration (log of ligand concentration [μM]) was calculated and plotted against scaled fluorescence ('Fluorescence [Relative Units]). Each displacement assay was repeated three times for each concentration of ligand tested; therefore fluorescence (relative units) is reported as an average \pm SEM from 3 independent experiments (n=3) A) FABP5, B) FABP7 C) FABP8.

The ligand binding characteristics of FABP5, 7 & 8 for 13 (S) HODE were then assessed. Initially, the ability of 10 μ M 13(S) HODE to produce a robust displacement of 12 –NBD stearate for all 3 FABPs was evaluated (Figure 4.10). When incubated in the presence of 10 μ M of 13(S)HODE, there was a significant decrease in measured fluorescence intensity for all three FABPs assayed. As with AEA and AA, the concentration of 13 (S) HODE was then titrated to calculate the IC50 value and K_i values of 13(S) HODE at FABPs 5, 7 & 8 (Figure 4.11).

For the first time, it has been shown that 13(S) HODE can displace 12-NBD stearate from FABP5, 7 and 8 in a concentration dependent manner. The calculated K_i values of 13(S) HODE at FABP5, 7 & 8 were 0.93, 0.63 & 0.13 μ M. 13 (S) HODE (Table 4.2b).

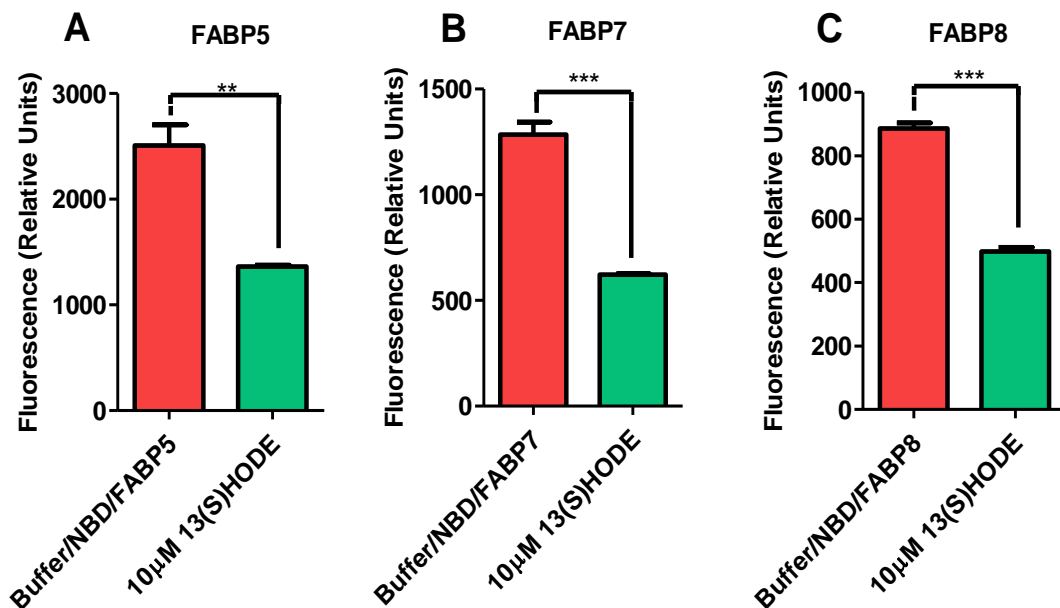


Figure 4.10: 10 μ M 13(S) HODE produces a significant displacement of 12-NBD stearate: 12-NBD stearate – FABP complexes were allowed to form as previously. 10 μ M 13(S)HODE was able to displace 12-NBD stearate from 3 μ M of FABPs 5, 7 and 8 (bar charts A, B, and C respectively) which was concomitant with significant decreases in raw fluorescence intensity. All graphs are presented as an average \pm SEM from four independent displacement experiments. A unpaired student t-test was used to analyse the differences in fluorescence intensities between the buffer/NBD/FABP5 and 10 μ M 13(S) HODE groups. A value of $P < 0.05$ was considered as significant. **, *** is $P < 0.05$, $P < 0.0001$ respectively.

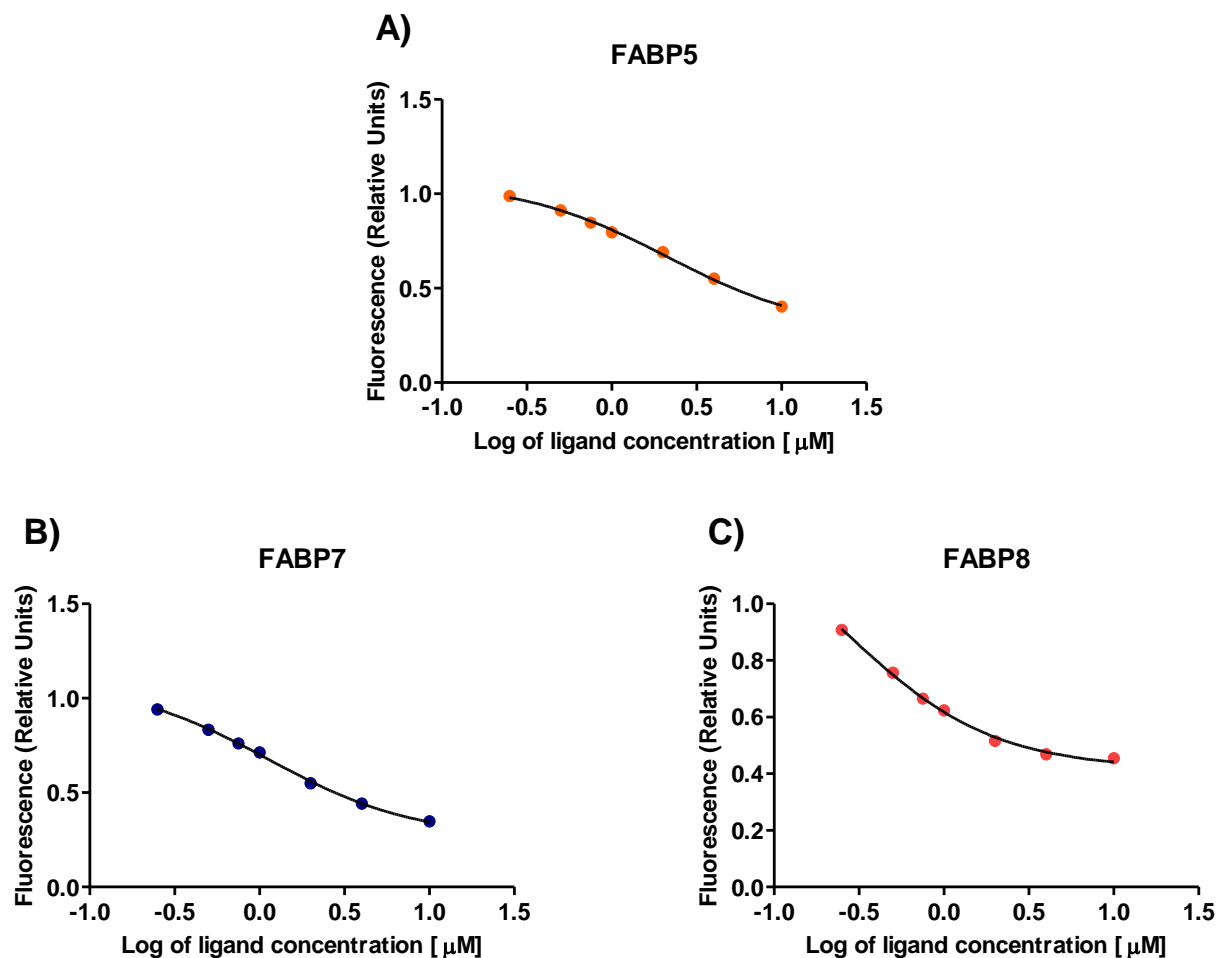


Figure 4.11: 13(S) HODE displaces 12-NBD stearate from FABPs 5, 7, 8: For each displacement assay, 500nM 12-NBD stearate and 3 μM protein were allowed to form fluorescent complexes as previously. Increasing concentrations of competitor ligand [0.25-10 μM] 13 (S) HODE were titrated against 12-NBD stearate – FABP complexes. The loss of fluorescence intensity was determined at an excitation: emission wavelength of 484:520nm, then reported on a scale ranging from 0.00 – 1.00 (Fluorescence [Relative Units]). The logarithm of each concentration of 13 (S) HODE used (log of ligand concentration [μM]) was calculated and plotted against scaled fluorescence ('Fluorescence [Relative Units]). The displacement assay presented is from a single experiment (n=1).

Table 4.2a

Ligand	FABP5		FABP7		FABP8	
	IC50 [μM]	95% Conf. Interval	IC50 [μM]	95% Conf. Interval	IC50 [μM]	95% Conf. Interval
AA	0.72	0.69 to 0.76	0.37	0.32 to 0.43	0.23	0.17 to 0.31
AEA	15.49	0.0096 to 25050	0.80	0.63 to 1.02	0.63	0.49 to 0.82
13(S)HODE	2.12	1.23 to 3.65	1.12	0.78 to 1.62	0.26	0.12 to 0.56

Table 4.2b

Ligand	FABP5	FABP7	FABP8
	K _i [μM]		
AA	0.32	0.21	0.07
AEA	6.79	0.34	0.20
13(S)HODE	0.93	0.63	0.13

Table 4.2: Summary of calculated IC₅₀ and K_i values of competitor ligands screened in fluorescent displacement assays – Fluorescent displacement assays for AEA and AA were performed three times at each tested FABP. 13(S) HODE displacement assay data was collected from a single experiment. The displacement data calculated IC₅₀ values are shown with 95% confidence intervals (Table 4.2a). K_i values of each ligand (Table 2b) were calculated from IC₅₀ (Table 4.2a) and K_d values (Table 4.1) using the equation described in **section 4.1**. AA, Arachidonic Acid, AEA, Anandamide; 13(S) HODE, 13(S)HODE.

4.4 Summary of key findings and results

- Soluble N-terminally His tagged FABP5, 7 & 8 were successfully overexpressed then purified to near homogeneity in a single step by immobilized Ni²⁺ affinity column chromatography.
- All three purified FABPs were functionally active in the established competition assay system. This was demonstrated by the ability of the FABP5, 7 and 8 to not only bind to the lipophilic probe 12-NBD stearate but also allow competitor ligand, arachidonic acid (AA), to displace bound 12-NBD stearate from their respective ligand binding cavities. These avidities were reflected in the calculated K_d values of FABP5, 7 and 8 for 12-NBD stearate were 0.39, 0.63 and 0.48μM respectively. While the calculated K_i values for AA were; 0.32, 0.21 and 0.07μM at FABP5, 7 and 8 respectively.
- AEA was unable to produce a strong displacement of 12-NBD stearate at FABP5 but could at FABP7 and FABP8. K_i values for AEA at FABP5, FABP7 and FABP8 were 6.79, 0.34 and 0.20μM. Whereas 13(S) HODE could effectively out-compete 12-NBD stearate probe from all three FABPs assayed and exhibited K_i values of 0.93, 0.63 and 0.13μM at FABP5, 7 and 8 respectively. In summary, AEA was able to bind to all three FABPs tested, but with variable affinities. The comparatively weak binding and affinity of AEA for FABP5 calls into question its legitimacy as a previously identified intracellular carrier for AEA. Preliminary data from this study also suggests that FABP5, 7 and 8 all bind 13(S)HODE with FABP8 exhibiting the strongest affinity for 13(S) HODE.

4.5 Discussion – FABPs as intracellular shuttles for TRPV1 ligands

The principle aim of this chapter was to optimize an assay system which could determine the specificity and affinity of FABPs for lipid species previously reported to activate TRPV1. More specifically this investigation sought to elucidate whether endogenous TRPV1 activators AEA and 13 (S) HODE were capable of binding to the FABP isoforms previously identified in DRGs by RT-PCR/QRT-PCR experiments in chapter 3. Characterization of TRPV1 ligand – FABP interactions was essential to establish which FABP isoforms may be capable of modulating TRPV1 responses and activity.

Previous studies, which adopted the same assay system as used in this thesis, have already reported on the interaction of AEA with both FABP5 and FABP7 (112). This chapter attempted to corroborate these findings and provide further independent confirmation that FABP5 and 7 can act as intracellular carriers for AEA. However, it was found that FABP5 only exhibited a very weak affinity for AEA while FABP7 could convincingly bind AEA, which was reflected in the marked contrast in the calculated K_i values of AEA at FABP5 and FABP7 reported in this thesis.

The strong affinity of AEA for FABP7 is in broad agreement with the previous findings of Kaczocha et al. (112); however, the reasons as to why AEA did not produce a similarly robust displacement of 12-NBD stearate from FABP5, as previously reported, remains elusive at present. For the first time, the affinity and physical binding of AEA to FABP8 was determined in a cell-free based assay. It was found that AEA could readily bind to FABP8 and this was reflected in a comparatively low K_i value of 0.2 μ M.

Currently, there is limited evidence demonstrating physical binding of 13(S) HODE to iLBPs such as the FABPs. The findings of Ogawa et al. (111) implied FABP5

was capable of sequestering 13(S) HODE as lipid cargo for delivery to intracellular targets i.e. transcription factors, which regulate keratinocyte differentiation. Initially, it was not possible to definitively characterize and categorize FABP5 as a 13(S) HODE transporter in the absence of any physical binding data and calculated kinetic parameters such as K_i .

It was, therefore, necessary to prove that 13(S) HODE – FABP interactions existed using the same fluorescence displacement assay system already used for AEA. It was demonstrated for the first time that 13(S) HODE could physically associate and bind to FABPs 5, 7 & 8. Previous studies have demonstrated that a high concentration (27.5 μ M) of endogenous 13-HODE is required to produce a half maximal response TRPV1 receptors expressed in cultured cell lines (75). It is, therefore, possible that the un-sequestered 13-HODE is unable to evoke TRPV1-mediated Ca^{2+} entry efficiently and necessitates FABP mediated shuttling to TRPV1 receptors.

In conclusion, it is possible that of any of the three FABP isoforms identified in DRG cultures, could act as intracellular lipid chaperones for 13(S) HODE and therefore modulate/regulate the activity of TRPV1.

Chapter 5: The development of an *in vitro* mammalian cell culture system to probe for TRPV1/PPAR – FABP protein-protein interactions

Chapter 5: The development of an *in vitro* mammalian cell culture system to probe for TRPV1/PPAR – FABP protein-protein interactions

5.0 Introduction

5.0.1 Background: Establishing a physical interaction between TRPV1 and FABP isotypes

The aim was to establish that the FABPs act as transporters that solubilize and shuttle endovanilloids to TRPV1 during nociception. It was, therefore, necessary to provide experimental evidence to demonstrate that the FABP isotypes previously identified in the DRG cultures in chapter 3, could physically associate with TRPV1 when bound to pro-nociceptive lipid cargo. Furthermore, it was necessary to determine specifically which of the FABP isotypes, could physically interact with membranous TRPV1 and therefore establish if TRPV1 exhibits selectivity over which FABP it interacts with, or if it is promiscuous in its choice of FABP interaction partner.

A range of techniques are available to investigate putative protein-protein interactions (PPI); however, the selection of method is dependent on the nature of the PPI under investigation. Previous experimental evidence has shown that the FABPs rapidly shuttle between subcellular compartments to deliver their lipid-cargo to the appropriate subcellular structures. The FABPs mediate the delivery of lipid cargo by participating in a rapid, but continuous nucleocytoplasmic shuttling in order mediate the efficient delivery of lipophilic ligands from the cytoplasm to transcription factors – the PPARs - in the nucleus (113). Therefore, there is a body of experimental evidence that suggests, the FABPs associate with their respective protein partners, transiently.

5.1 Bimolecular fluorescence complementation (BiFC)

5.1.1 The principle of the BiFC assay

It was therefore critical that the experimental method adopted in this thesis, could capture the formation of potentially transient protein complexes. It was equally important that the chosen PPI method could also provide direct visualization of TRPV1-FABP protein complexes, to confirm that such complexes were forming in the predicted cellular environment and exhibiting the expected sub-cellular localisation.

The Bimolecular Fluorescence Complementation (BiFC) assay has been shown to be a simplistic but effective means of directly capturing and visualizing transient PPIs and protein complexes in living or chemically fixed cells (135, 136). The BiFC assay is based upon the re-association of the amino (N) and carboxy (C)-terminal non-fluorescent fragments of a fluorescent protein, which results in the formation of a fluorescent protein complex (127-131).

5.1.2 The structure and function of Yellow Fluorescent Protein and its variants

A commonly used fluorophore in BiFC is the yellow fluorescent protein (YFP). Composed of 238 amino acids, YFP is a genetic variant of the Green Fluorescent Protein (GFP) fluorophore, which was originally discovered in the jelly fish *Aequorea victoria* (132). The three-dimensional structure of both GFP and YFP is identical. It is a cylindrical shaped protein composed of 11 antiparallel β -strands connected by loops, forming a β -barrel containing an α -helix inside and several short helical structures at the end of the cylinder (Figure 5.1) (132).

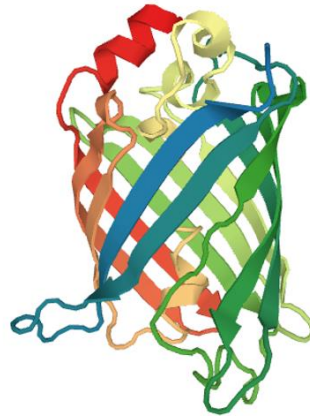


Figure 5.1: The native three-dimensional structure of yellow fluorescent protein – The ribbon cartoon diagram represents the three-dimensional structure of YFP (Protein Data Bank ID: 1MYW taken from the RCSB Data Bank). Secondary structure, the α -helices and β -strands, are represented in rainbow colours using the PV-JavaScript protein viewer

The fluorescent properties of YFP can be attributed to a triad of specific amino acid residues within the α helix located in the β -barrel. In GFP and YFP, these include residues 65,66 and 67 which correspond to Serine (Ser65) or Threonine (Thr65), Tyrosine (Tyr66) and Glycine (Gly67) respectively. After YFP has adopted its native three-dimensional structure, this trio of amino acid residues become critical in the spontaneous formation of the fluorophore/chromogenic centre. Fluorophore formation is initially brought about the cyclization of Ser65/Thr65-Tyr66-Gly67 producing a heterocyclic imidazolinone ring, this is followed by dehydrogenation then finally molecular oxygen-mediated oxidation of the C α - β bond in Tyr66 (132, 134).

Previous research groups were able to manipulate the spectral properties of GFP to create YFP by performing site directed mutagenesis at Thr203 to the aromatic amino acid Tyrosine (T203Y) (133,134). This genetic mutant and a yellow variant of GFP results in a fluorophore with an excitation and emission wavelength approximately 20nm longer to that of wild type GFP.

However, there are issues associated with YFP which include its sensitivity to environmental parameters, such as the effects of acid and the ability of chloride ions to quench YFP fluorescence. For YFP to exhibit stable fluorescence coupled with the desire for brighter fluorescent intensity and improved rates of fluorophore maturation, a further five mutations were introduced into the YFP peptide sequence resulting in a new YFP variant called Venus (127-131).

The resulting amino acid substitutions had the following desired effects; increased the rate of chromophore oxidation, enhanced the folding of YFP into its native 3-D dimensional structure and lastly a reduction in sensitivity when exposed to halide ions and acidosis all of which collectively stabilized YFP fluorescence (134). However, the experiments reported in this thesis used the non-venus form of YFP and its respective N and C-terminal fragments.

5.1.3 Preparing YFP fragments for BiFC

As already partly alluded to, YFP is split into N and C-terminal non-fluorescent fragments (127-131). The fragmentation of YFP is brought about the introduction of splits at specific points in the polypeptide loops that connect the β -strands of the cylindrical β -barrel. YFP can be split at a choice of loops and therefore truncated at different amino acid residues, to produce a range of N and C terminal fragments suitable for BiFC (127-131).

However, it is standard practice for YFP to undergo truncation at amino acid residue 155 located in the loop connecting the 8th and ninth β -strand, this is therefore considered as a canonical split. This produces an N-terminal non-fluorescent (YFP-N 155) fragment that covers amino acid residues 1-154 and a C-terminal fragment covering residues 155-238 (YFP-C 155).

Fragments YFP-N 155 and YFP-C 155 have been reported to manifest high intrinsic levels of fluorescence and high complementation efficiency when fused to a range of different interacting proteins, but importantly produce low-level fluorescence when fused to non-interacting proteins (127-131). These fragments are routinely fused to putative interacting protein partners in BiFC assays. Consequently, in this thesis, these fragments were fused to the proteins of interest.

The structural complementation of the two non-fluorescent fragments of YFP is mediated by and dependent on the interaction between two putative interaction partners, such as FABP and TRPV1. Each separate protein is fused to one of the non-fluorescent constituent fragments of the YFP. Therefore, the interaction of the different proteins is concomitant with the subsequent reconstitution of an intact protein fluorophore, whose fluorescence can be visualized and examined by fluorescence microscopy (135, 136).

The reformation of YFP results in a permanent - irreversible protein complex. This fundamental irreversibility is an essential characteristic of BiFC that makes it an ideally suited technique to capture the transient interactions of FABPs with their putative protein partners i.e. TRPV1 and PPARs, something which would not be possible with other PPI detection methods (Figure 5.2).

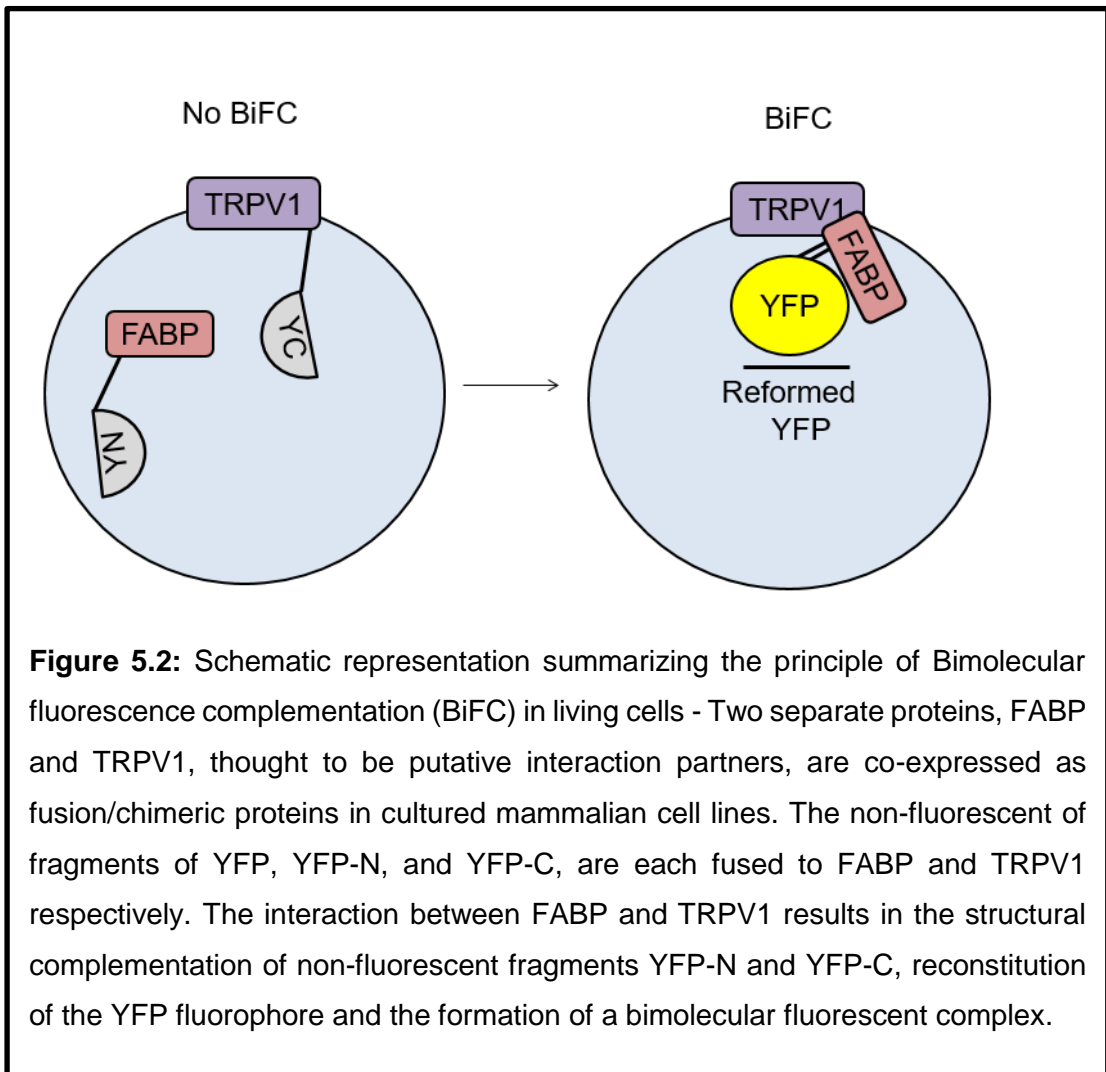


Figure 5.2: Schematic representation summarizing the principle of Bimolecular fluorescence complementation (BiFC) in living cells - Two separate proteins, FABP and TRPV1, thought to be putative interaction partners, are co-expressed as fusion/chimeric proteins in cultured mammalian cell lines. The non-fluorescent fragments of YFP, YFP-N, and YFP-C, are each fused to FABP and TRPV1 respectively. The interaction between FABP and TRPV1 results in the structural complementation of non-fluorescent fragments YFP-N and YFP-C, reconstitution of the YFP fluorophore and the formation of a bimolecular fluorescent complex.

5.1.4 Summary and justification for the use of BiFC in this thesis

In summary, BiFC is a simplistic but useful tool for validating PPIs. It does not necessitate the utilization of the exogenous fluorophores/chromogenic agents that have the potential to perturb cell activity and integrity or undergo uneven distribution when staining (127-131). Instead, BiFC enables molecular cell biologists to directly capture and determine the subcellular localization of interacting proteins in their native cellular environment (127-131). Furthermore, the study of PPI in intact cells circumvents the likelihood of altering protein interactions, which would not be the case in other PPI detection techniques that use cell lysis in their methodology.

5.2 A summary of the experimental aims for chapter 5

1. Generate TRPV1 plasmid DNA constructs to be used for BiFC.
2. Confirm that once transfected into mammalian cell lines, the TRPV1, PPAR, and FABP plasmid DNA constructs express recombinant proteins by immunoblotting and immunocytochemistry.
3. Confirm that C-terminally YFP-C tagged TRPV1 expressed in COS-7 cells retains its functionality by measuring its ability to facilitate calcium influx in response to stimulation with vanilloid agonist capsaicin.
4. Establish then optimize conditions and experimental parameters for BiFC assays. Demonstrate the interaction of YFP- FABP fusion proteins with known associating protein partners, to confirm functionality state of FABP chimeras (Table 5.1).
5. Use BiFC as a tool to illustrate a physical association between TRPV1 and FABP isotypes previously identified in chapter 3 in response to stimulation with 10 μ M AEA. Given that FABP5, 7 and 8 were all identified in DRG cell cultures; these isotypes are predicted to interact with TRPV1

Table 5.1: Summary of known- characterised PPAR-FABP interactions

Interaction	Drug and concentration	Reference for reported PPI
PPAR α and FABP1	WY14, 163 [1 μ M]	138
PPAR α and FABP3	GW7647 [50nM]	Previous experimental data from FRAME
PPAR γ and FABP4	Rosiglitazone [10 μ M]	113
PPAR β and FABP5	GW0742 [100nM]	139
PPAR γ and FABP7	DHA [60 μ M]	114
PPAR β and FABP8	GW0742 [100nM]	Previous experimental data from FRAME

5.3 Results

5.3.1 Generating an expression vector encoding for YFP-C tagged TRPV1: an overview of the cloning strategy

To establish whether a protein-protein interaction exists between TRPV1 and candidate FABPs in cultured mammalian cells, it was necessary to generate a plasmid DNA construct that could encode for functional TRPV1 YFP-C fusion protein. TRPV1 was tagged at its C-terminus with the YFP-C fragment of YFP. TRPV1 and its YFP-C tag were separated by a peptide linker. This was to provide flexibility and independent movement between TRPV1 and its YFP-C tag. Therefore, it was important that the stop codon was removed from TRPV1 cDNA during a PCR using a mutagenic primer. This was to ensure the resulting recombinant DNA sequence encoding for TRPV1 Linker YFP-C fusion protein was translated as one uninterrupted contiguous protein.

5.3.2 Analysis of PCR amplicons by gel electrophoresis

cDNA encoding for the carboxy termini of the non-venus form of YFP, covering amino acid residues 155-238, was cloned into the pcDNA3.1 Zeo (+) vector to generate the first of 3 sequential plasmid DNA constructs. TRPV1 and YFP-C cDNA was successfully amplified by PCR, and the success of the PCR was confirmed by agarose gel analysis. Once resolved by electrophoresis, amplicons migrating at the approximate expected molecular weights for TRPV1 (2.5kb approx.) and YFP-C (255bp) were visualized by staining the gel with ethidium bromide (Figure 5.3).

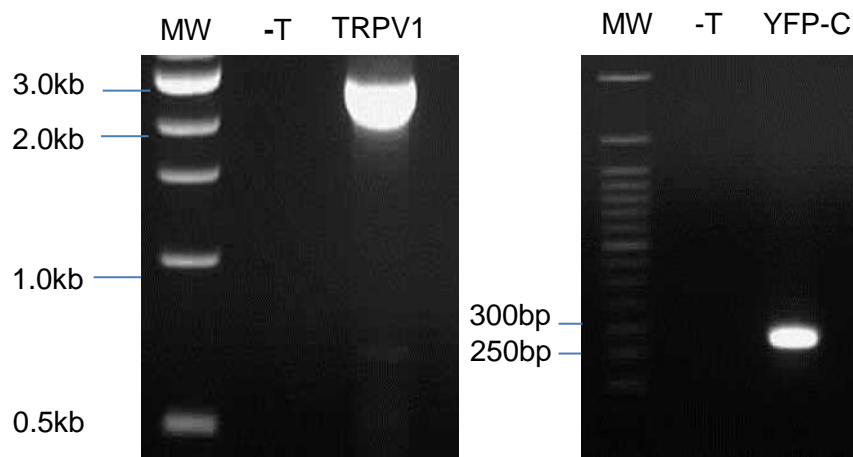


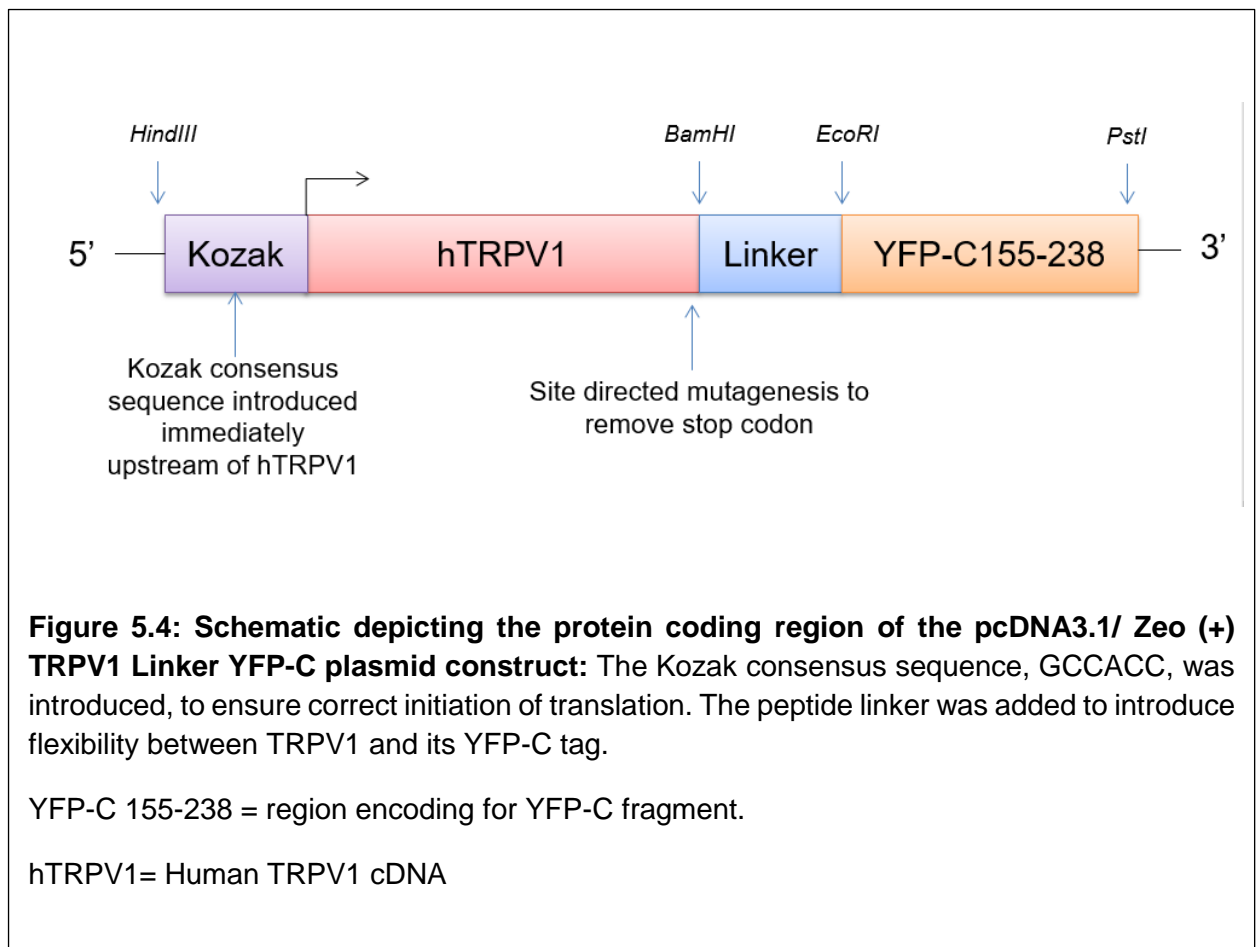
Figure 5.3 Agarose gel analysis to detect PCR amplicons human TRPV1 and YFP-C: 50ng of cDNA template for full-length human TRPV1 and the C-terminal fragment of YFP were amplified by PCR using Phusion High Fidelity DNA polymerase as described in chapter 2.

5 μ L of the reaction was resolved by electrophoresis on a 0.7% (TRPV1) or 1.2% (YFP-C) 1 \times TAE agarose gel. '-T' indicates where cDNA template was replaced with an equivalent volume of autoclaved HPLC grade water in the reaction vessel.

MW = Molecular Weight ladder.

The YFP-C amplicon was then sub-cloned into pcDNA3.1/Zeo (+) to give the first plasmid construct, pcDNA3.1/Zeo (+) YFP-C. This was then followed by the introduction of an oligonucleotide sequence encoding for the peptide linker-spacer. This was cloned immediately upstream of the YFP-C coding region to give the required contiguous protein coding sequence. This gave the second plasmid construct termed pcDNA3.1/Zeo (+) Linker YFP-C or tagging vector.

Full-length human TRPV1cDNA was then sub-cloned into the vector as mentioned earlier, in-frame with the DNA sequence encoding for the peptide linker – YFP-C tag. This gave the final pcDNA3.1/ Zeo (+) TRPV1 Linker YFP-C construct required for the BiFC imaging assay (Figure 5.4). The vector was propagated in *E.coli* and then recovered by alkaline lysis.



5.3.3 Agarose gel analysis of recovered plasmid DNA constructs digested with restriction endonucleases

To confirm the integrity of the recovered pcDNA3.1/ Zeo (+) TRPV1 Linker YFP-C plasmid construct and the successful cloning of human TRPV1 into the tagging vector, a diagnostic restriction digestion reaction was performed. pcDNA3.1/ Zeo (+) TRPV1 Linker YC vector was double digested with restriction endonuclease enzymes HindIII-HF and BamHI-HF and the resulting digested DNA fragments were resolved by agarose gel electrophoresis.

Analysis of the gel revealed a diagnostic banding pattern; a high molecular weight DNA fragment which equated to approximately 5.0kb was observed. This corresponded to linearized plasmid DNA pcDNA3.1/Zeo (+) Linker YFP-C. A second band, which had migrated further and was of a lower molecular weight of approximately 2.5kb, corresponding to the excised TRPV1 cDNA insert was also observed (Figure 5.5).

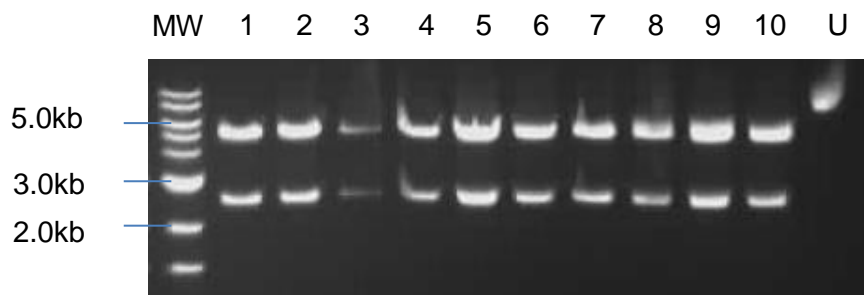


Figure 5.5: Agarose gel analysis of restriction endonuclease digests of pcDNA3.1/Zeo (+) TRPV1-Linker-YFP-C plasmid DNA: Plasmid DNA was recovered

from 11 different bacterial cultures by alkaline lysis as described in chapter 2.

1µg of plasmid DNA was double digested with restriction endonuclease (RE) enzymes HindIII-HF and BamHI-HF for 90 minutes at 37°C. Aliquots of the resulting digests were resolved by electrophoresis on a 0.7% 1×TAE agarose gel. 'U' denotes where the 11th recovered plasmid was not digested with the RE enzymes and therefore the DNA is uncut.

MW = Molecular Weight ladder

Sequencing of the pcDNA3.1/ Zeo (+) TRPV1 Linker YC vector provided final and further confirmation of the successful cloning of YFP-C, linker sequence and TRPV1 as a continuous DNA sequence. It was also confirmed that site directed mutagenesis to remove the stop codon at the end of TRPV1 cDNA sequence, had been successful.

5.3.4 Immunoblot analysis of transfected COS-7 cells

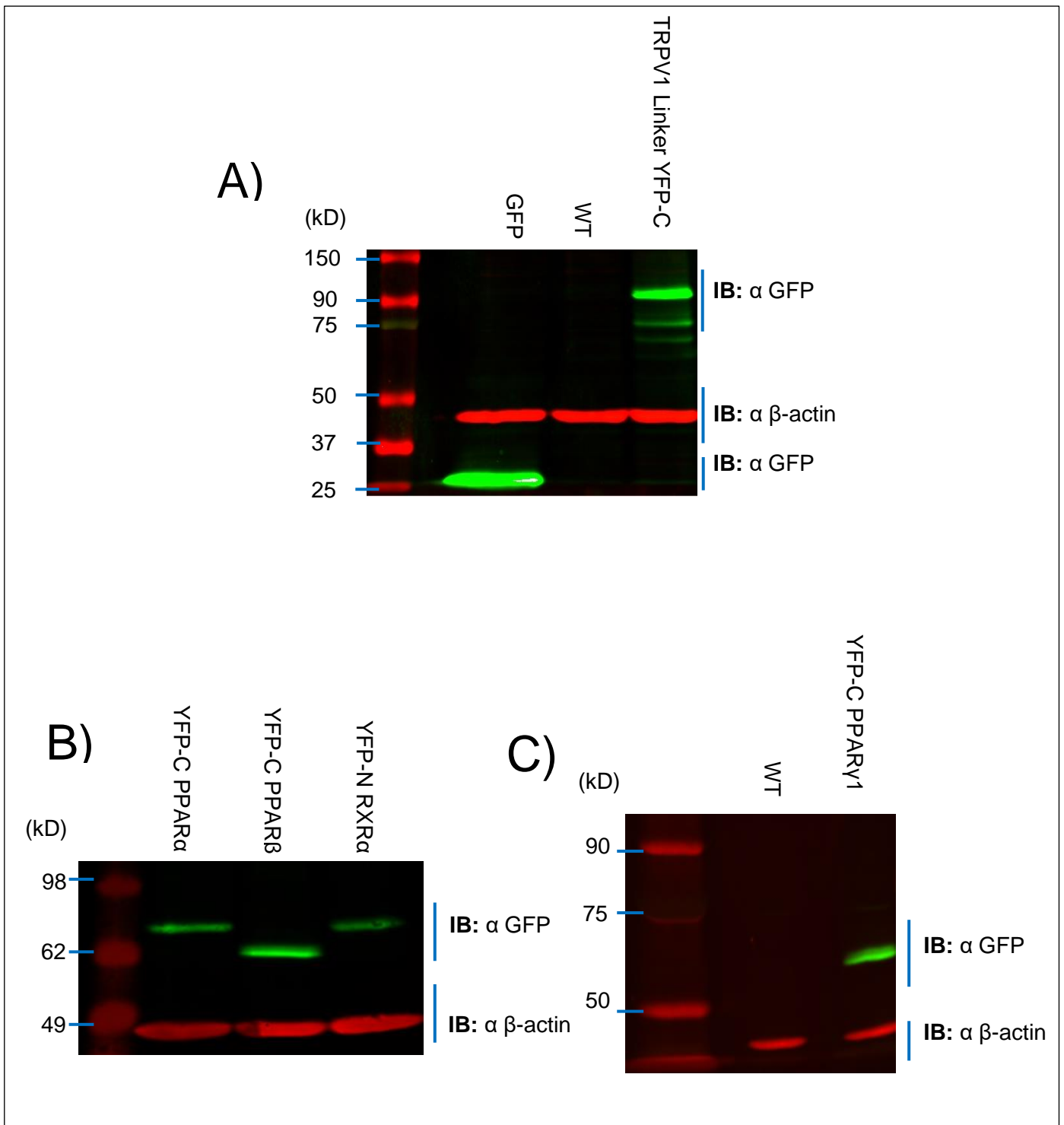
To ensure that the plasmid DNA constructs generated could express the TRPV1-Linker YFP-C, YFP-C PPAR and YFP-N FABP/RXR α fusion proteins, the respective plasmid DNA constructs each encoding the appropriate chimeric proteins, were transiently transfected into the mammalian cell line COS-7. To confirm successful recombinant protein expression of each chimeric protein, transfected COS-7 cells were lysed and prepared for Immunoblotting (IB) analysis using polyclonal anti-GFP antibody. Importantly, this anti-GFP antibody can detect GFP and its variants i.e. YFP and the non-fluorescent fragments of YFP; therefore, it is a particularly useful tool for confirming the expression of the proteins fused to the fragments of YFP.

Validation of the anti-GFP antibody: Initially, it was necessary to ensure that the anti-GFP antibody could detect the correct antigen. Crucially, no protein bands were detectable when analysing the clarified lysates of untransfected (wild type) cells by immunoblotting using the anti-GFP antibody (Figure 5.6A). This confirmed that the antibody does not detect endogenous COS-7 cell proteins and therefore does not engage in non-specific binding to unrelated antigens i.e. those proteins that are not GFP or its variants. The specificity of the antibody was further verified when analysing clarified lysates from COS-7 cells transfected with pcDNA3.1/Zeo (+) GFP. Only a single band corresponding to the molecular weight of GFP (26.9kDa) was detectable by immunoblotting.

Immunoblot analysis of cell lysates from transfected cells: Bands migrating at 100kDa, and approximately 70-kDa corresponding to TRPV1-Linker-YFC and YFP-C PPAR/YFP-N RXR α fusion proteins were all detected by immunoblotting (Figure 5.6A-E). Whereas single bands were migrating at 30kDa corresponding to the expected molecular weight of the YFP- N FABP fusion proteins were also detectable by immunoblotting with the anti-GFP antibody (Figure 5.6D-E).

Together, this confirmed that when transfected into mammalian cell lines, the plasmid DNA vectors that had been constructed could successfully express the recombinant chimeric proteins required for future BiFC assays.

Finally, to show that equal amounts of protein were loaded from each cell lysate, from both transfected and wild type cells, blots were also probed with an antibody immunoreactive against human β -actin. In all immunoblotted cell lysates, single bands migrating at the approximate molecular weight for β -actin were detected.



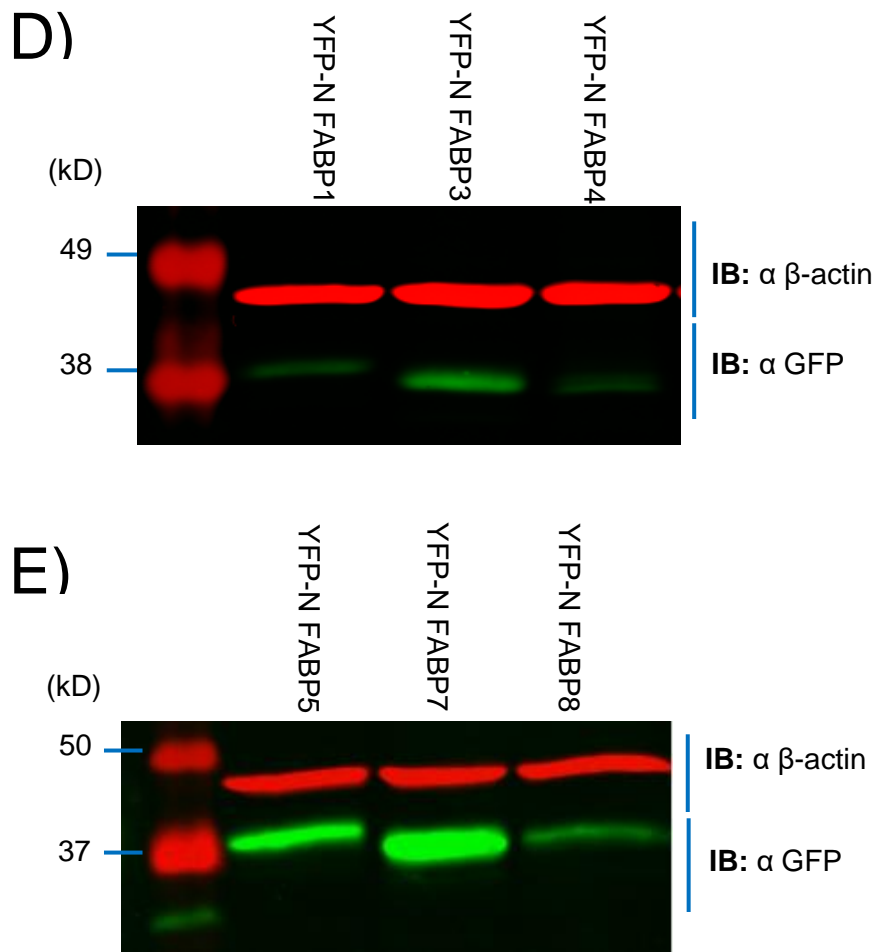


Figure 5.6: Immunoblot (IB) analysis confirming the expression of recombinant TRPV1-YFP-C, YPF-C PPAR, YFP-N FABP and RXR α chimeric proteins in transiently transfected COS-7 cells: COS-7 cells were seeded at a density of $0.7 \text{ cells.ml}^{-1}$ wells in a 12 well plate and cultured for 24 hours to reach 70-90% confluency. Adherent COS-7 cells were then transiently transfected with $1\mu\text{g}$ of plasmid DNA construct per well using X-treme geneTM HP transfection reagent. Cells were maintained for 6 hours at 37°C then 18 hours at 30°C . Transfected COS-7 cells were then prepared for immunoblotting. Transfected and wild type (WT) cells were harvested and lysed with RIPA buffer. Cell lysates were sonicated then centrifuged to give clarified cell lysates. Clarified cell lysates were boiled in $1\times$ Laemmli loading buffer containing 200mM DTT, then loaded onto 8% or 12% PAGE gel and resolved by electrophoresis. Proteins were transferred to an AmershamTM HybondTM-ECL nitrocellulose membrane. The membrane was probed with anti GFP rabbit polyclonal (1:500 dilution) and mouse anti-human- β -actin monoclonal (1:2000 dilution) antibodies overnight at 4°C (IB: α GFP/ IB: - β -actin respectively) followed by donkey anti-rabbit IgG- IRDYE 800 and goat anti-mouse IgG-IRDYE 680 LI-COR[®] antibodies for 1 hour at room temperature. The membranes were then scanned using an LI-COR[®] Odyssey infrared imager.

5.3.5 Immunostaining and immunolocalization of chimeric proteins in transfected COS-7 cells

A parallel set of transfections were performed as described in 5.3.4, this was for the same purposes of confirming recombinant protein expression and but also to establish that the expressed fusion proteins adopt the same subcellular localization to that of their untagged native counterparts.

Using the same polyclonal anti-GFP antibody and secondary antibody, anti-IgG Alexa Fluor® 488, those COS-7 cells that had been transfected were successfully immunostained for either TRPV1-Linker YFP-C, YFP-CC PPAR/YFP-N RXR or YFP- N FABP chimeric proteins. In all cases, the examination of cells in the FITC channel by fluorescence microscopy showed that a significant proportion of cells exhibited intense immunofluorescence, which was indicative of a successful set of transfections (Figure 5.7).

However, as expected, no immunostaining was observed for those COS-7 cells that been cultured *in vitro* but not subjected to transient transfection with plasmid DNA construct. In summary, this confirmed that successful transfections had taken place and that the key fusion proteins of interest had been expressed, both of which complement and corroborate the results of IB analyses of the clarified lysates from transfected cells, in which it was also clearly demonstrated the chimeric proteins were expressed and were the predicted molecular weights. Furthermore, immunostaining provided some qualitative information concerning the subcellular localization of the expressed chimeric proteins.

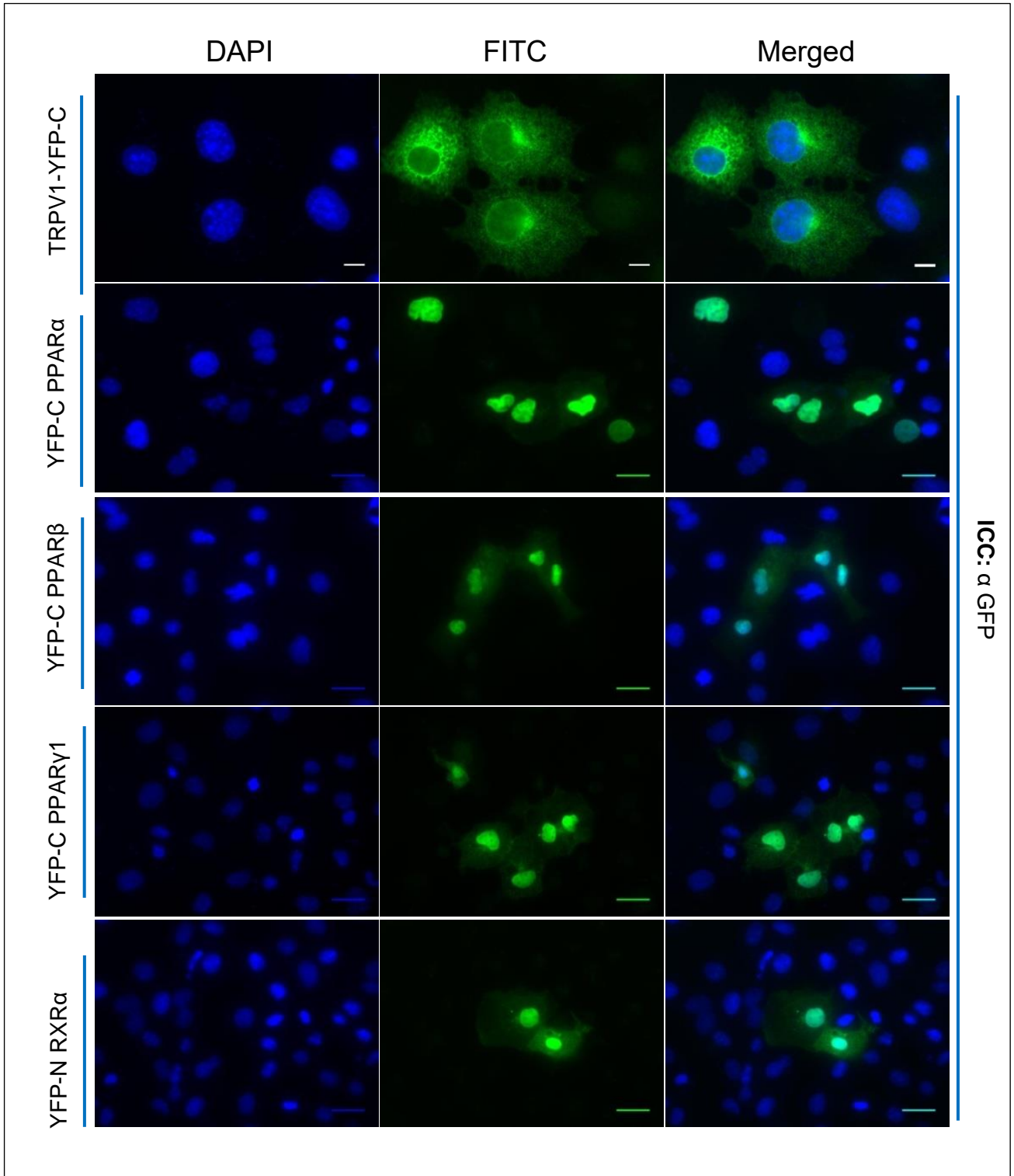
Receptors: Channels and Nuclear receptors chimeras – It appeared that some of the over-expressed TRPV1 Linker YFP-C protein was localized to the endoplasmic reticulum (ER) in COS-7 cells. (Figure 5.7: TRPV1 YFP-C).

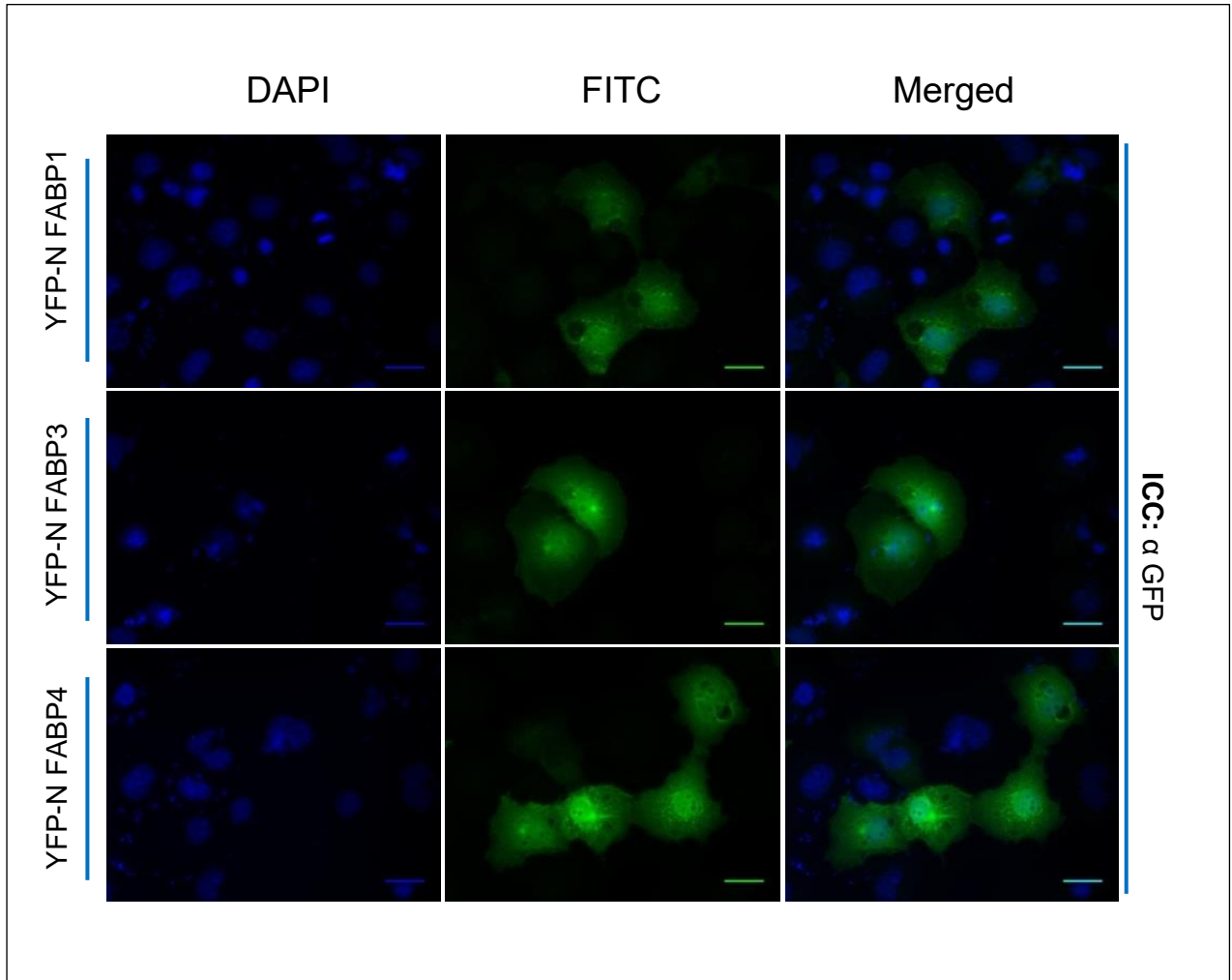
However, the degree of TRPV1-YC ER localization was variable when directly comparing each of the three cells. In short, not all expressed TRPV1 linker YFP-C fusion protein is localized to the ER and a good majority of the cytosolic regions

in the individual cells immunostained positive for the TRPV1-YC fusion protein with little immuno-fluorescence emitted from the nuclei of cells. In conclusion, the localization of TRPV1-YC is not restricted to any one subcellular structure. However, further confirmation is required, and it is recommended that TRPV1 expressing COS-7 cells are subjected to subcellular fractionation to determine the proportion of TRPV1 linker YFP-C expressed in each cellular compartment.

Immunostaining showed that the PPAR/RXR chimeric proteins were mostly localized to the nucleus (Figure 5.7: PPAR – YFP-C). There was some comparatively faint immunostaining observed in the cytosol of cells analysed by microscopy, but it was markedly less when it was compared directly to the intensity of immunofluorescence exhibited by the nuclei. Furthermore, there was substantial co-localization with DAPI stained nuclei. It is therefore clear that most of the expressed tagged nuclear receptor proteins were predominately localized to the nucleus (Figure 5.7). In conclusion, this was a clear indication that the fusion of a YFP-C or YFP-N tag at the N-terminus of PPAR or RXR α does not govern and bring about any changes in their subcellular localization.

iLBPs – transporters: FABPs – Immunostaining of cells showed that when expressed, the tagged FABPs in all cases, exhibited no distinct subcellular localization. Immunofluorescence was detected in both the cytosol and nucleus. This is consistent with the role of FABPs as lipid transporters for example studies have shown that FABPs transiently shuttle between cellular compartments such as the nucleus and cytoplasm in response to binding lipophilic cargo (106, 113).





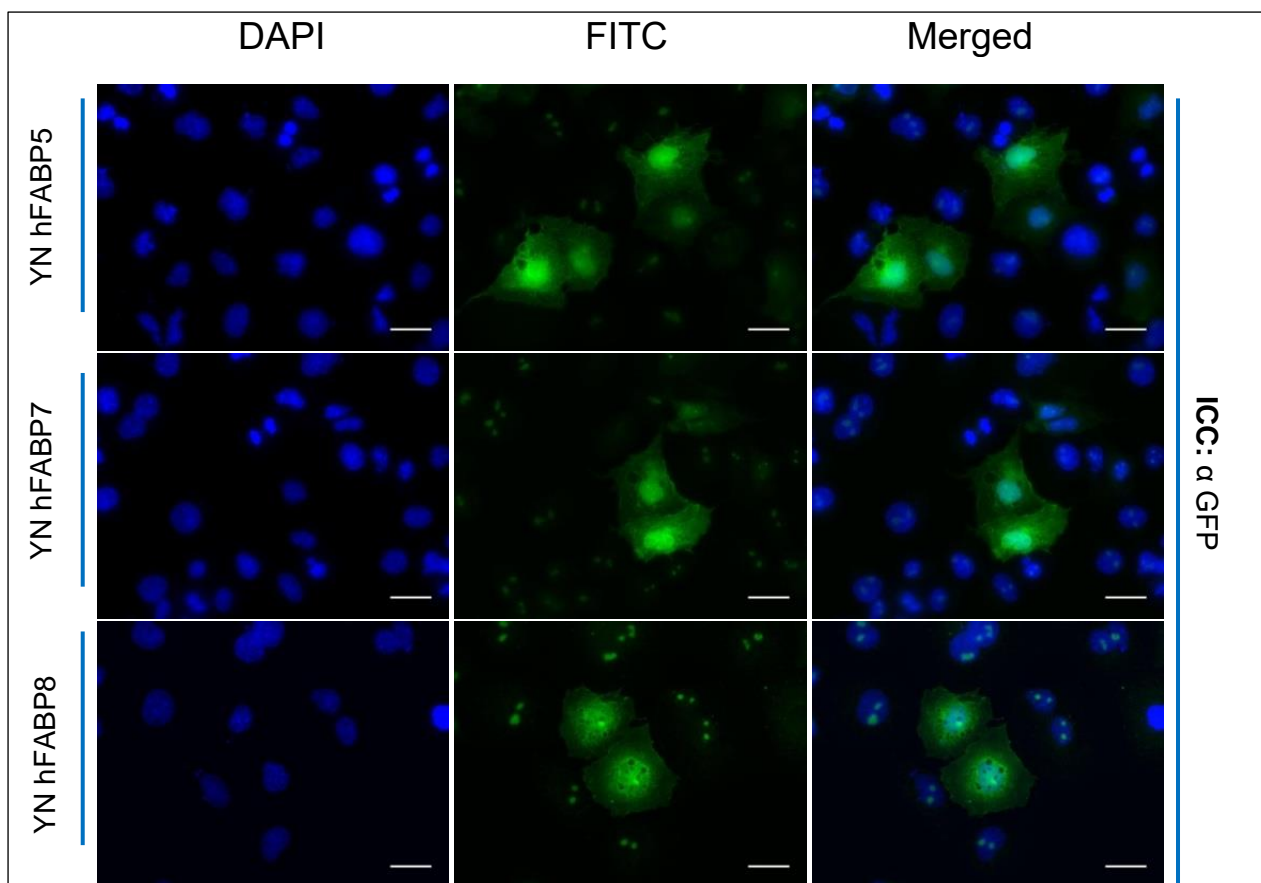


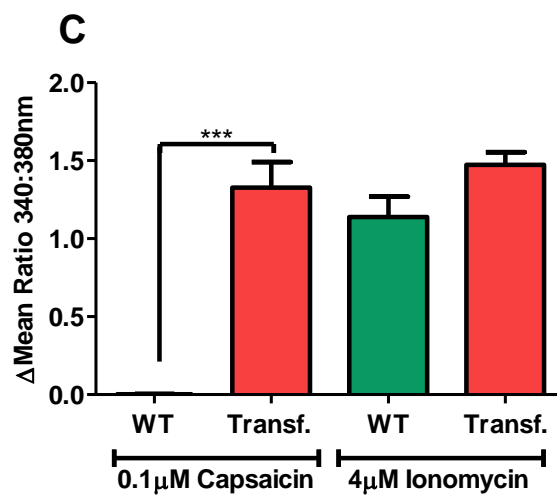
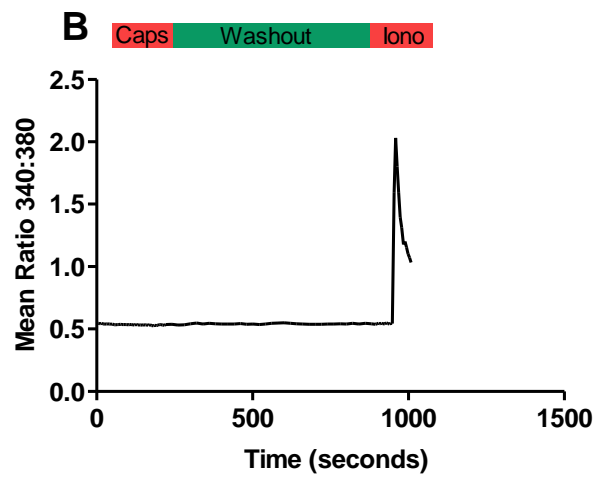
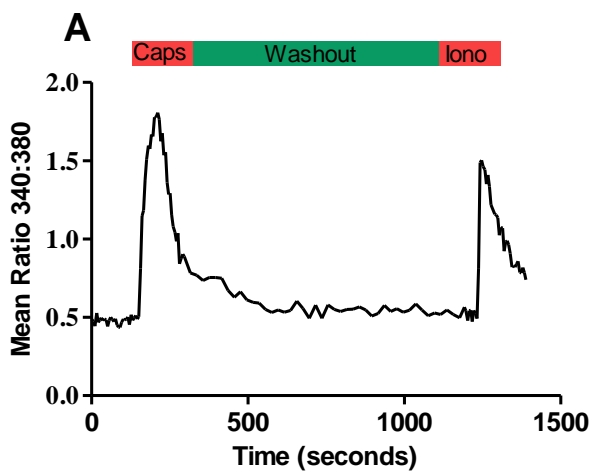
Figure 5.7: Confirmation of the expression of recombinant TRPV1-YFP-C, YPF-C PPAR isotypes, YFP-N FABP isoform and RXR α chimeric proteins in transiently transfected COS-7 cells by immunocytochemistry: COS-7 cells were seeded then transiently transfected with plasmid DNA construct then allowed to express chimeric protein exactly as described in figure 5.6. The following day, cells were with fixed in 4% PFA then subsequently immunostained with anti-GFP rabbit polyclonal antibody (1:500 dilution) overnight at 4°C with agitation (**ICC: α GFP**), this was followed by incubation with goat anti-rabbit IgG Alexa Fluor® 488 (1:500 dilution) for 2 hours at room temperature. Cells were then counterstained with DAPI (1 μ g.ml⁻¹). Images were taken with a \times 63 objective lens with a Leica DMRB fluorescent microscope. Scale bar for TRPV1-YFP-C is 11 μ m and 16 μ m for all other images.

5.3.6 Does TRPV1 retain its functionality as a tagged protein when expressed in COS-7 cells?

Before pursuing any future PPI studies, it was important to ensure that when TRPV1 is expressed as a tagged protein, it retains its ability to give functional responses when stimulated with vanilloid and endovanilloid receptor agonists, in a manner broadly comparable to that of its untagged equivalent.

An initial comparison of the two representative traces of two separate imaging experiments on transfected and WT COS-7 cells illustrates that COS-7 cells expressing recombinant TRPV1 Linker YFP-C fusion proteins gate Ca^{2+} in response to a 1-minute treatment with $0.1\mu\text{M}$ capsaicin (Figure 5.8A). This response was absent in wild type-untransfected COS-7 cells exposed to the same concentration of capsaicin (Figure 5.8B), this is evident when making a direct comparison of the calculated Δ Mean Ratio 340:380 values for the capsaicin response in transfected cells to that of the wild type – untransfected cells (Figure 5.8C).

This confirmed that COS-7 cells do not express endogenous functional TRPV1 and therefore the calcium influx-response observed in response to perfusion with capsaicin in the transfected COS-7 cells can be entirely attributed to the cells that have been successfully transfected and expressing functional TRPV1 Linker YFP-C fusion protein. Furthermore, only a subpopulation of selected cells from the transfection group gave a response to the capsaicin treatment; only 30% (20/65) of the cells or regions of interest (ROI) gated calcium upon stimulation with capsaicin.



D

High cytosolic
[Ca²⁺]

Low cytosolic
[Ca²⁺]

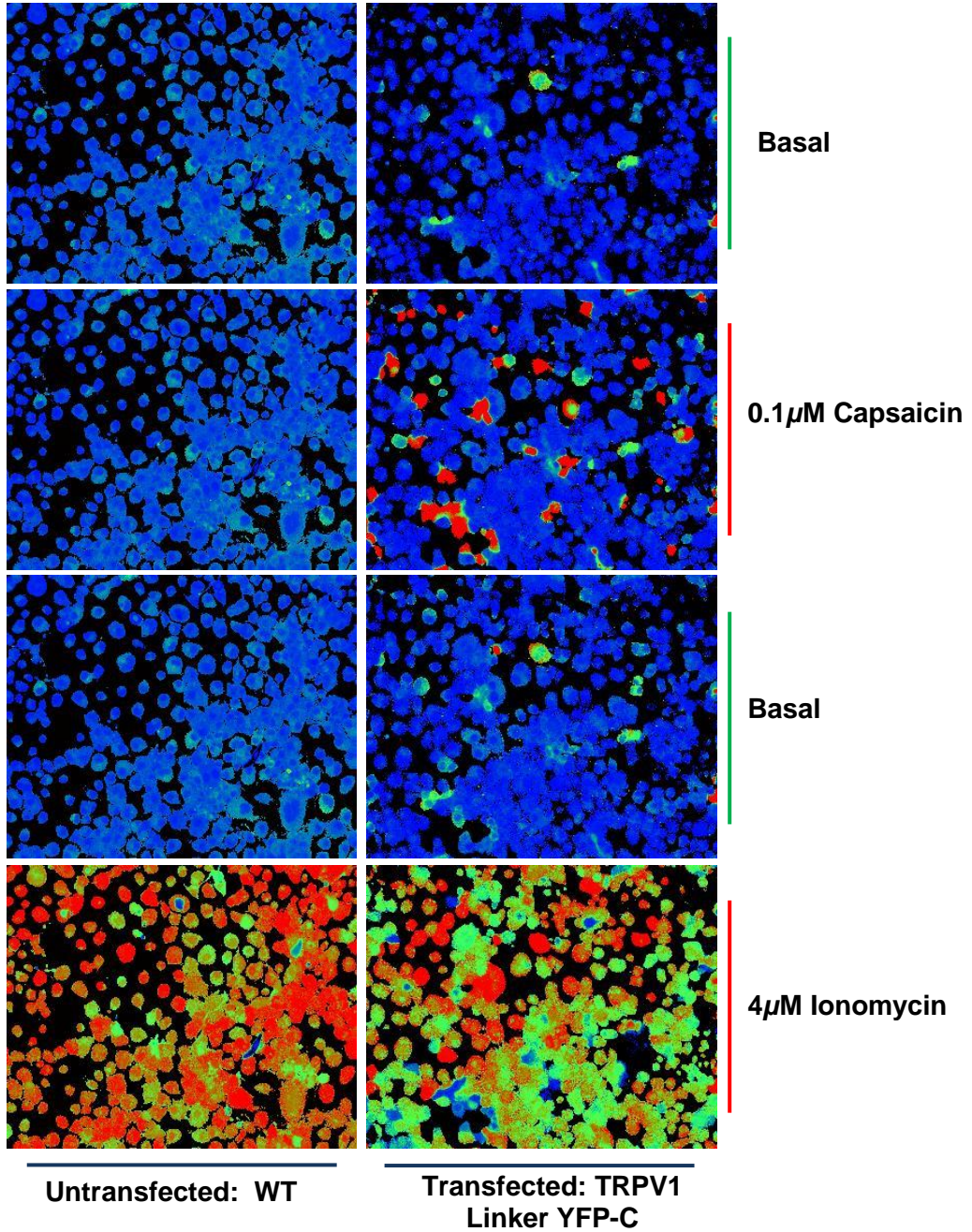


Figure 5.8: The effect of capsaicin on transfected and wild type COS-7 cells to confirm functionality of recombinant TRPV1 linker YFP-C: COS-7 cells were transiently transfected with 1µg of plasmid DNA construct encoding for YFP-C tagged TRPV1. Chimeric protein was expressed as described in figure 5.6. Before calcium imaging, COS-7 cells were pre-loaded with calcium indicator dye Fura-2AM [5µM] for 30 minutes in the dark at 37°C. Representative traces illustrating the effect of 0.1µM capsaicin on intracellular calcium concentration (Mean 340:380nm ratios) in **A)** COS-7 cells transfected with 1µg of pcDNA3.1/Zeo(+) TRPV1 YFP-C plasmid DNA construct or **B)** untransfected - wild type (WT) COS-7 cells. Both transfected and wild type cells were then exposed to capsaicin [0.1µM, red rectangle] for 1 minute, followed by calcium imaging buffer then ionomycin [4µM, red rectangle] after which the experiment was ended.

C) 340:380nm ratios reported as the difference in values between the mean 340:380nm stimulus ratio values and the mean basal ratio values for capsaicin and ionomycin (Δ Mean Ratio 340:380) for both wild type (green) and transfected cells (red). Δ Mean Ratio 340:380 values are reported as a SEM. The Δ Mean Ratio 340:380 value for capsaicin response in TRPV1 expressing cells was a SEM of 1.33 (\pm 0.16) which was significantly higher compared to the 0.003 (\pm 0.001) Δ Mean Ratio 340:380 value for the WT-untransfected cells, also exposed to capsaicin. For both transfected and transfected-wild type cells, a total of 20 ROIs or cells were tested across three independent experiments (n=3). Analysis: A unpaired student t-test was used to analyse and compare the differences in Δ Mean Ratio 340:380 values between the wild type-untransfected and transfected group. A P value of <0.05 was considered as significant. ***, < 0.0001. **D)** Representative high-intensity ratiometric images of WT and TRPV1 YFP-C expressing COS-7 cells.

5.3.7 Validation of the BiFC method with positive controls

Initially, it was necessary to confirm that the BiFC assay was a viable technique for detecting protein-protein interactions in cultured mammalian cell lines. To achieve this, COS-7 cells were co-transfected with plasmid DNA constructs encoding two different proteins known and widely reported to strongly interact when co-expressed as recombinant proteins in cultured cells. These proteins were; bFos and bJun, these two proteins strongly dimerize to form the activator-protein-1 (AP-1) transcription factor. Consequently, they are well established protein-protein interaction partners and have been widely used as positive controls for the BiFC assay (136).

Plasmid DNA constructs encoding bFos fused to the amino portion of YFP (YFP-N) and Jun tagged to the carboxy fragment of YFP (YFP-C) were co-transfected and then co-expressed in cultured COS-7 cells. This was performed in conjunction with a parallel transfection, in which the plasmid encoding for the native form bFos was substituted for one encoding for a mutant form of the Fos protein. The bFosMut form of the protein lacked the crucial basic Leucine Zipper (bZIP) protein-protein interaction domain required for interaction with Jun.

As expected COS-7 cells co-expressing Fos-YFP-N and Jun-YFP-C exhibited a strong fluorescent signal localized to the nucleus (Figure 5.9 C, F& I). Equally as important was the apparent absence of fluorescent signal in those COS-7 cells co-transfected with the plasmid DNA constructs encoding for FosMut-YFP-N and Jun-YFP-C (Figure 5.9J-L). This indicated that there was no interaction between FosMut-YFP-N and Jun-YFP-C. From this, it is possible to infer that there was a genuine interaction between Fos-YFP-N and Jun-YFP-C, and the observed BiFC signal was not just a consequence of the YFP-C and YFP-N fragments re-associating independently of Fos and Jun.

It was, therefore, noted that the re-association of these YPF-C and YFP-N non-fluorescent fragments was dependent on PPI between two separate proteins interacting and mediating the reconstitution of the YFP fluorophore. Furthermore, given that strong fluorescent signal is attributed only to a select population of co-transfected COS-7 cells and is not exhibited by all the cells in any one field of view, it is possible to rule out auto-fluorescence as the cause of the signal seen for the co-transfected cells.

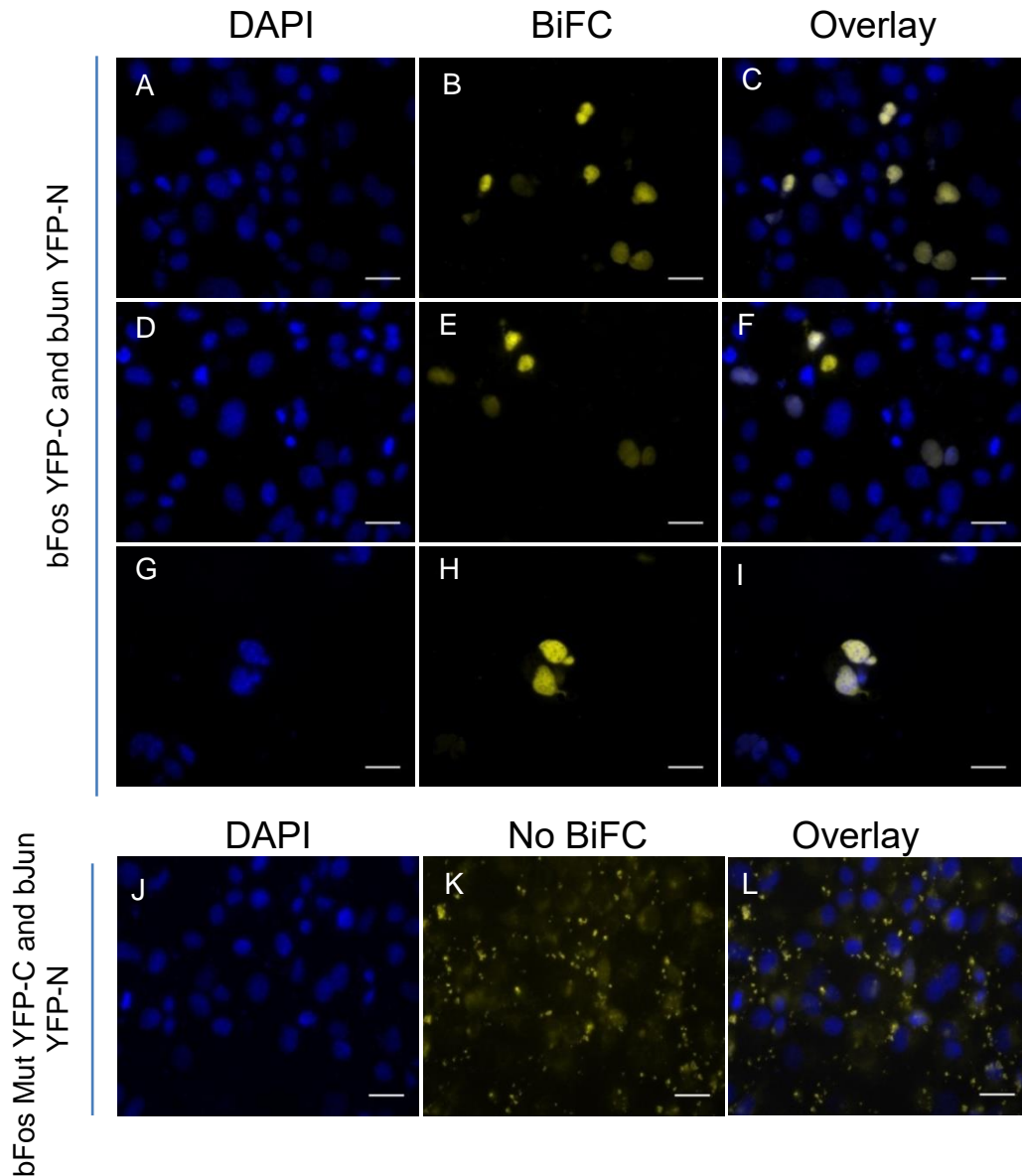


Figure 5.9: Detecting the reformation of the Activator Protein (AP1) transcription factor by BiFC in fixed COS-7 cells - COS-7 cells were maintained then transiently co-transfected plasmid DNA construct, then further cultured as described in figure 5.8. Each plasmid construct encoded for the individual subunits which constitute AP1 transcription factor. These subunits are bFos and bJun and were each tagged with tagged YFP-C or YFP-N. In a parallel transfection, a plasmid construct encoding for an inactive bFos mutant (YFP-C bFos Mut) replaced the vector encoding for WT bFos YFP-C. The absence or presence of BiFC signal in cells co-expressing bFos YFP-C / bJun YFP-N (Images B-H) and bFos Mut YFP-C / bJun YFP-N (Image K) was confirmed by the examination of fixed cells in FITC channel by fluorescence microscopy. BiFC signal localized to nuclei was diagnostic of YFP –C bFos-YFP-N bJun interactions, mediating the reformation of YFP (Images B-H). Meanwhile BiFC signal was absent in a parallel transfection where bJun YFP-N was co-expressed as the inactive mutant form of bFosMut YFP-N, confirming that independent re-association of YFP-C and YFP-N fragments had not occurred. Each transfection was performed in triplicate, and a representative image of each replicate is shown for the bFos YFP-C / bJun YFP-N co-transfection. Scale bar is 16 μ m

5.3.8 BiFC: Establishing a functional PPAR – RXR α dimerization in COS-7 cells

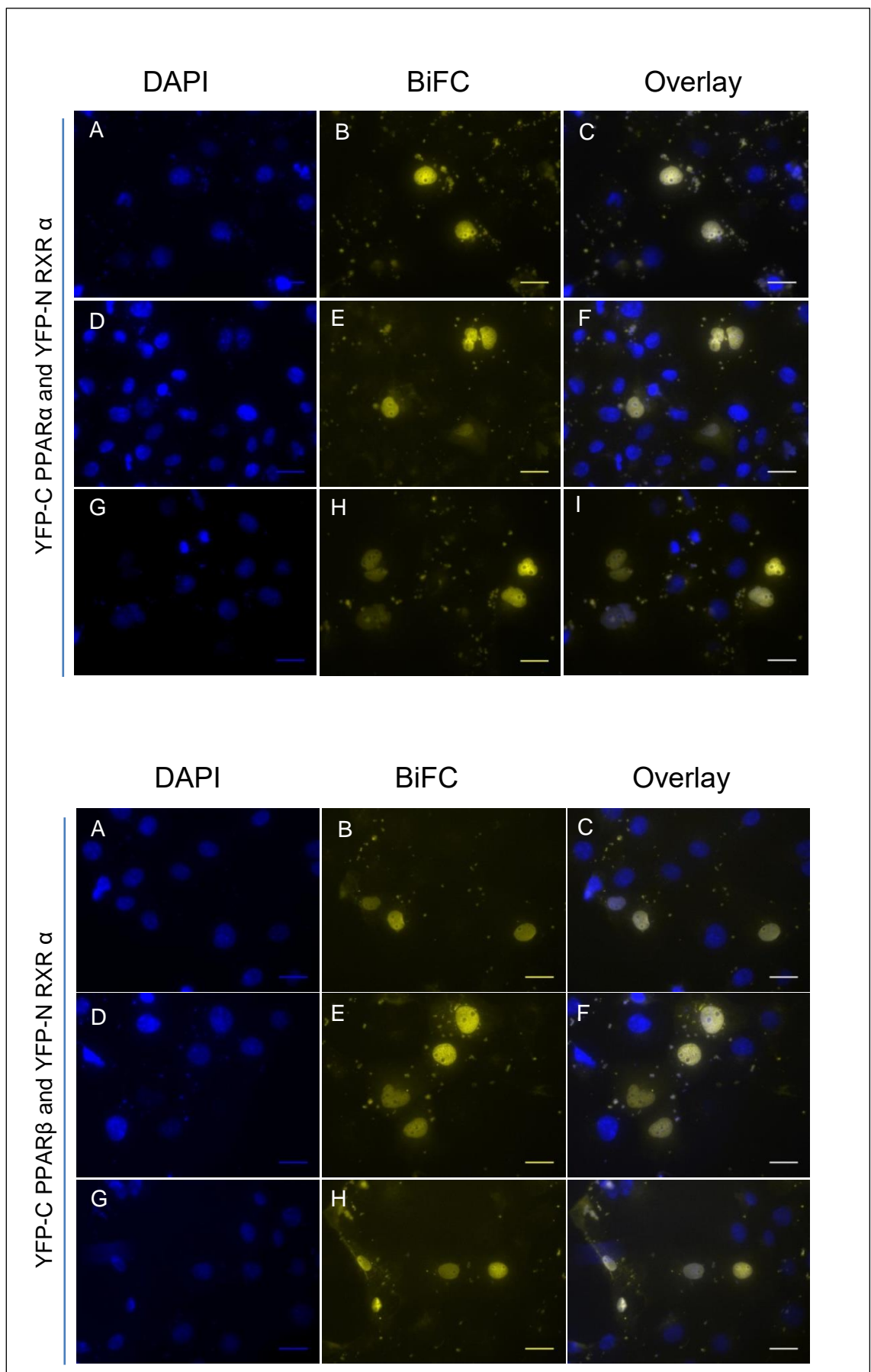
It is well recognized that PPARs form obligate functional heterodimers with the Retinoid X Receptor α (RXR α). PPAR-RXR α heterodimers serve as part of an operational protein complex that regulates the expression of PPAR target genes. This PPI was selected to demonstrate that YFP-C tagged PPARs were still able to functionally associate with known and well-characterized protein interaction partners such as RXR α . The verification of PPAR functionality was particularly important if the YFP-C PPAR fusion proteins were to be used in PPI studies with YFP-N tagged FABPs. Demonstrating known YFP-C PPAR – YFP-N FABP interactions in cultured cells was also performed to provide indirect evidence that FABPs tagged with YFP-N were also functional when expressed as chimeric proteins.

When examined by microscopy, COS-7 cells co-expressing YFP-C PPAR α and YFP-N RXR α exhibited a strong fluorescent signal that was predominantly localized to the nucleus (Figure 5.10: YFP-C PPAR α and YFP-N RXR, Images C, F & I). The same was observed for COS-7 cells co-expressing YFP-C PPAR β in place of PPAR α (Figure 5.10: YFP-C PPAR β and YFP-N RXR, Images C, F & I). The emitted fluorescence signal was indicative of an interaction between PPAR α/β and RXR α .

COS-7 cells co-expressing YFP-C PPAR γ 1 and YFP-N RXR α also emitted strong fluorescence signal indicative of PPAR γ 1 and RXR α interaction. However, the subcellular localization of the fluorescence signal was more varied compared to the BiFC signal detected in PPAR α/β and YFP-N RXR α co-expressing cells.

The representative images in Figure 5.10 of YFP-C PPAR γ 1 / YFP-N RXR α co-expressing cells (Figure 5.10: YFP-C PPAR γ 1 and YFP-N RXR, Images C, F & I), illustrate that there is still strong fluorescent signal localized to the nucleus, but it is also accompanied by some visible fluorescence in the cytoplasm. Other cells examined in Figure 5.10 (YFP-C PPAR γ 1 and YFP-N RXR, Images C, F & I), showed nuclei devoid of any observable BiFC signal but did exhibit detectable fluorescence localized to the cytoplasm.

This can be explained by the fact that the PPARs are not constitutively localized to the nucleus. Previous studies have shown that GFP tagged PPAR γ mostly localized to the nucleus in COS-7 cells however it is possible for PPAR γ to move between the nucleus and cytoplasm in a phenomenon known as nucleocytoplasmic shuttling (108). This may account for the variety of cytoplasmic and nuclear fluorescence observed in those cells co-expressing YFP-C PPAR γ 1 and YFP-N RXR (Figure 5.10). It was concluded that all three YFP-C tagged PPAR isotypes could form functional dimers with YFP-N RXR α when co-expressed in COS-7 cells.



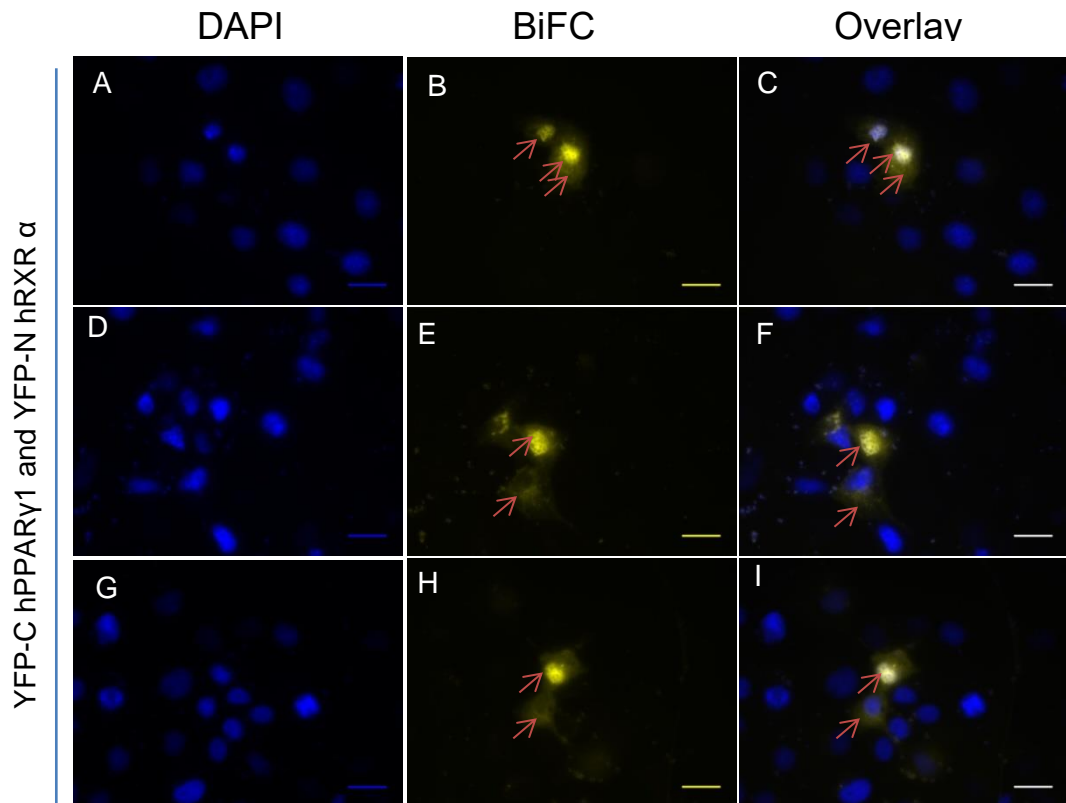


Figure 5.10: Visualizing the heterodimerization of YFP-C PPAR isotypes with YFP-N RXR α in fixed COS-7 cells by BiFC – COS-7 cells were maintained then transiently co-transfected plasmid DNA construct, then cultured further to allow the cells to co-express YFP-C PPAR and YFP-N RXR α chimeric proteins. When examined under the FITC channel by fluorescence microscopy, COS-7 cells co-expressing YFP-C PPAR α/β and YFP-N RXR α gave a strong fluorescent signal mostly localized to the nucleus, except for PPAR γ 1 and RXR α , where both cytoplasmic and nuclear fluorescence was detected. In all cases, the fluorescence observed in the FITC channel was indicative of YFP reconstitution caused by successful PPAR-RXR α heterodimerization. Each transfection was performed in triplicate. A single representative image the from DAPI (A, D & G) and FITC/BiFC (B, E & H) channels were taken for each replicate. Images C, F & I (Overlay) co-localises the fluorescence observed in both channels. Scale bar is 16 μ m.

5.3.9 BiFC: Probing for a physical association between YFP-N FABPs and TRPV1 linker YFP-C

It was imperative that when expressed as YFP-N tagged chimeric proteins, the FABPs retained their functionality as lipid chaperones, especially if they were to be used in BiFC studies. It has been widely reported that specific FABP isotypes functionally interact with distinct PPAR isoforms in a ligand dependent manner. In summary, the functional state of YFP-N FABPs was determined based on whether they could successfully interact with YFP-C PPARs, by measuring BiFC signal emitted from co-transfected COS-7 cells.

Aside from determining the functionality state of YFP-N FABPs chimeras another aim was to demonstrate that they interacted with known protein partners. This was to show that any absence of apparent interaction with other tested YFP-C chimeric proteins was not due to non-functional YFP-N FABP chimeras but a consequence of genuine non-interaction. To ascertain if this was the case COS-7 cells were co-expressed with a particular combination of PPAR isoforms and FABP isotypes in the presence or absence of specific ligand as positive controls. The combinations of tested PPARs and FABPs, plus the ligand used are listed in Table 5.1.

Three of the 8 PPAR-FABP interactions were captured by BiFC: These included YFP-N FABP1 and YFP-C PPAR α (Figure 5.11), YFP-N FABP5 and YFP-C PPAR β and YFP-N FABP8 and YFP-C PPAR β (Figure 5.12). The interaction of PPAR β and FABP8 had been previously demonstrated via the firefly luciferase gene reporter based system in previous unpublished work carried out in the FRAME laboratory.

It was noted that in the most cases the cells that had been treated for 18 hours with PPAR superligand appeared to exhibit a comparably higher intensity of nuclear fluorescence to those cells treated with 0.1% DMSO vehicle. Given that a baseline level of fluorescence was observed in cells that had not been treated

with a ligand suggested that endogenously generated cytosolic lipid ligands may be driving some of the PPAR-FABP associations observed. This seems plausible given that the COS-7 cell had been cultured in DMEM growth supplemented with lipid free serum throughout the entire experiment. However, COS-7 co-expressing YFP-C PPAR α and YFP-N FABP1 appeared to exhibit the same level of fluorescence irrespective of ligand/vehicle treatment. In summary, it was not possible to determine the functionality of all the YFP-N FABP chimeras.

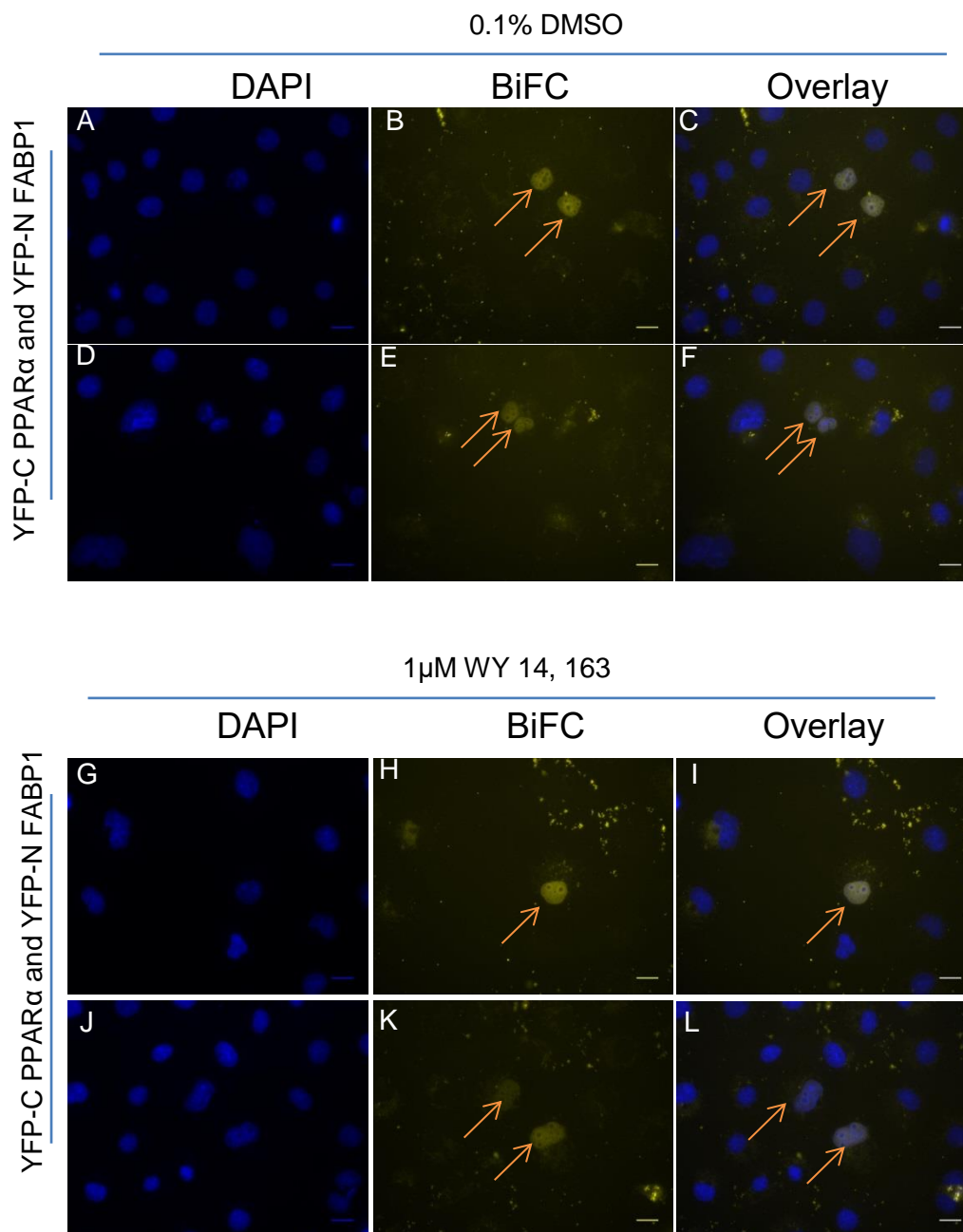
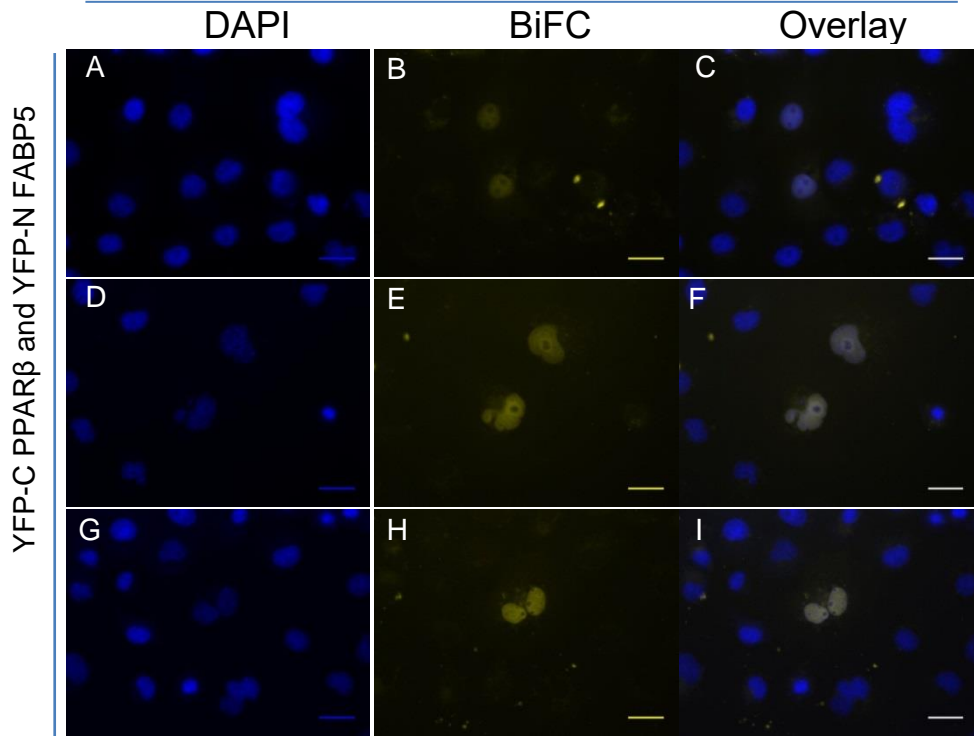
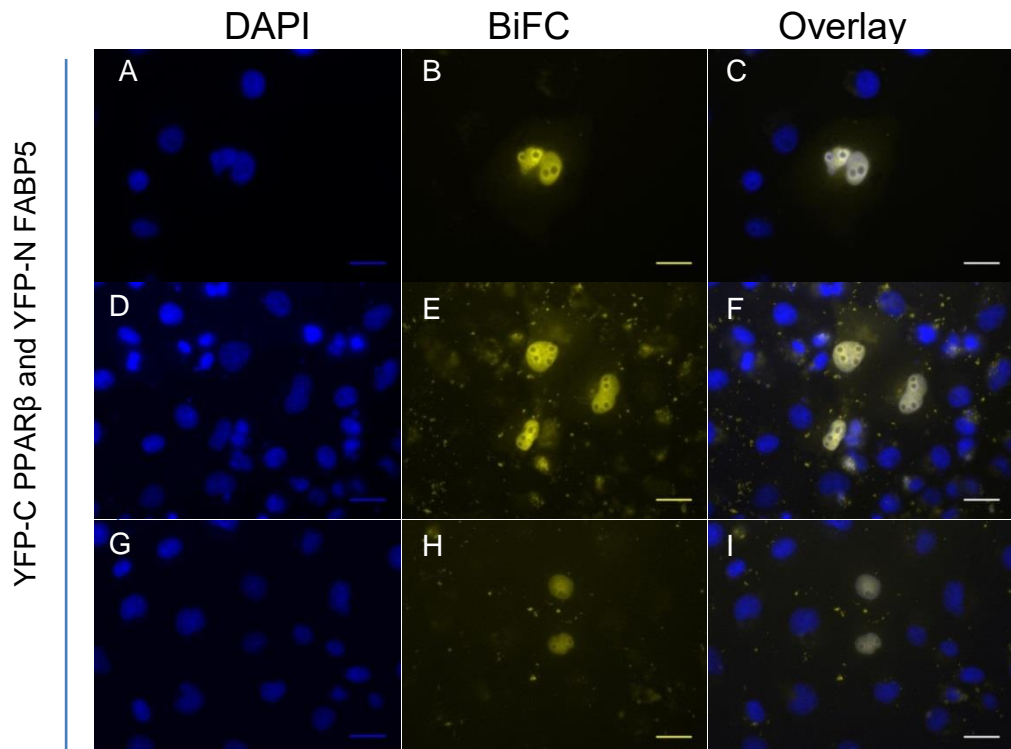


Figure 5.11: Interaction of YFP-C PPAR α and YFP-N FABP1 in COS-7 cells - COS-7 cells were co-transfected with the appropriate plasmids and allowed to express recombinant proteins YFP-C PPAR α and YFP-N FABP1 as with previous BiFC assays in this chapter. After which cells were replenished with fresh fully supplemented DMEM growth medium containing either 0.1% DMSO/vehicle or 1 μ M WY14, 163. Cells were then incubated at 30°C for a further 18 hours. After a total of 24 hours, cells were prepared for fluorescent microscopy. When examined in the FITC channel fluorescence was observed in a subpopulation of cell nuclei which was indicative YFP-N FABP1 and YFP-C PPAR α interaction (green arrows). The nuclei from cells treated with WY14, 163 (Image B & E) or DMSO (Images H & K) exhibited similar fluorescence intensities when examined by fluorescence microscopy at the same exposure times and digital gain. Scale bar is 16 μ m.

+ 0.1 % (v/v) DMSO in lipid free FBS



+ GW0472 [100nM]



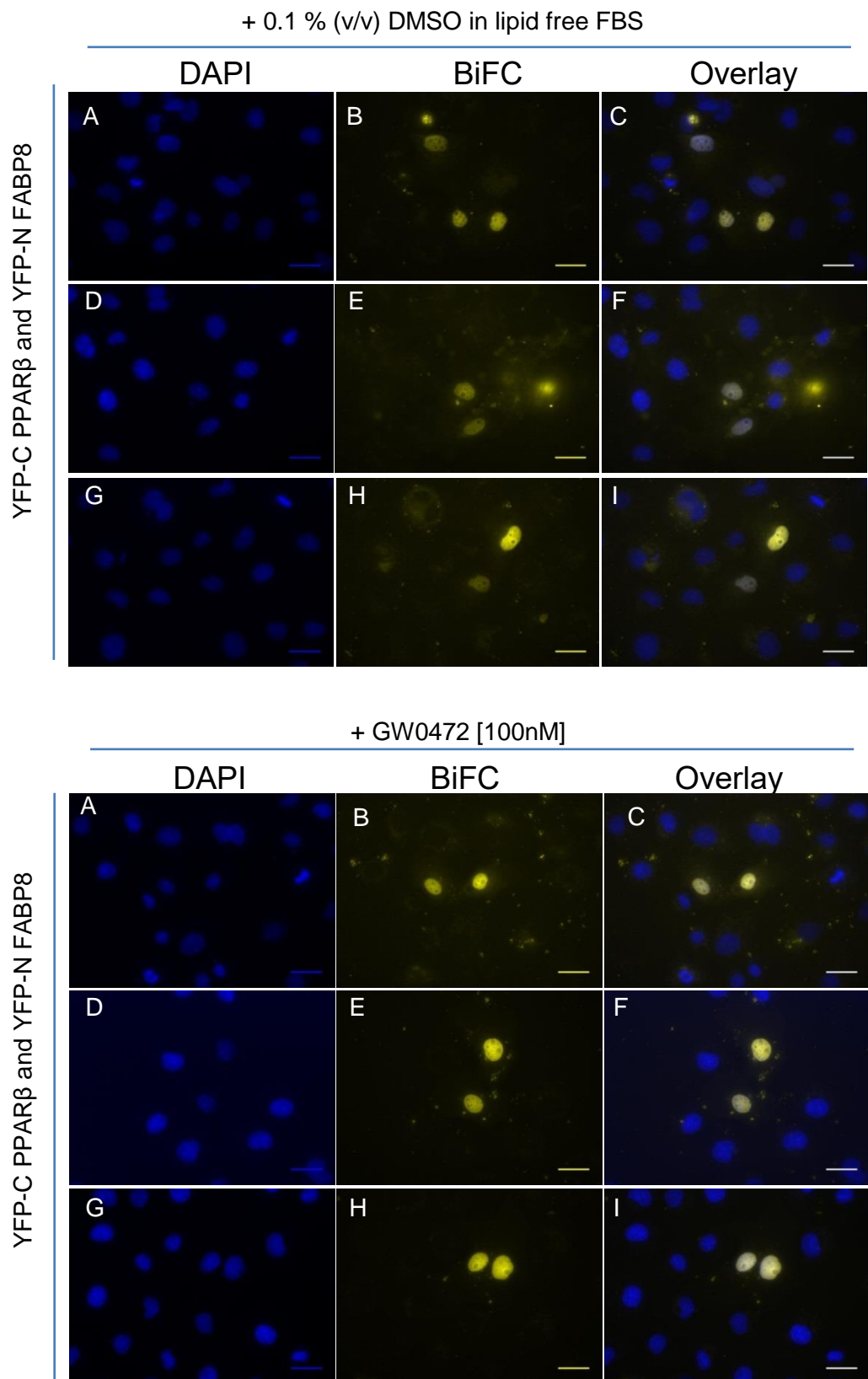
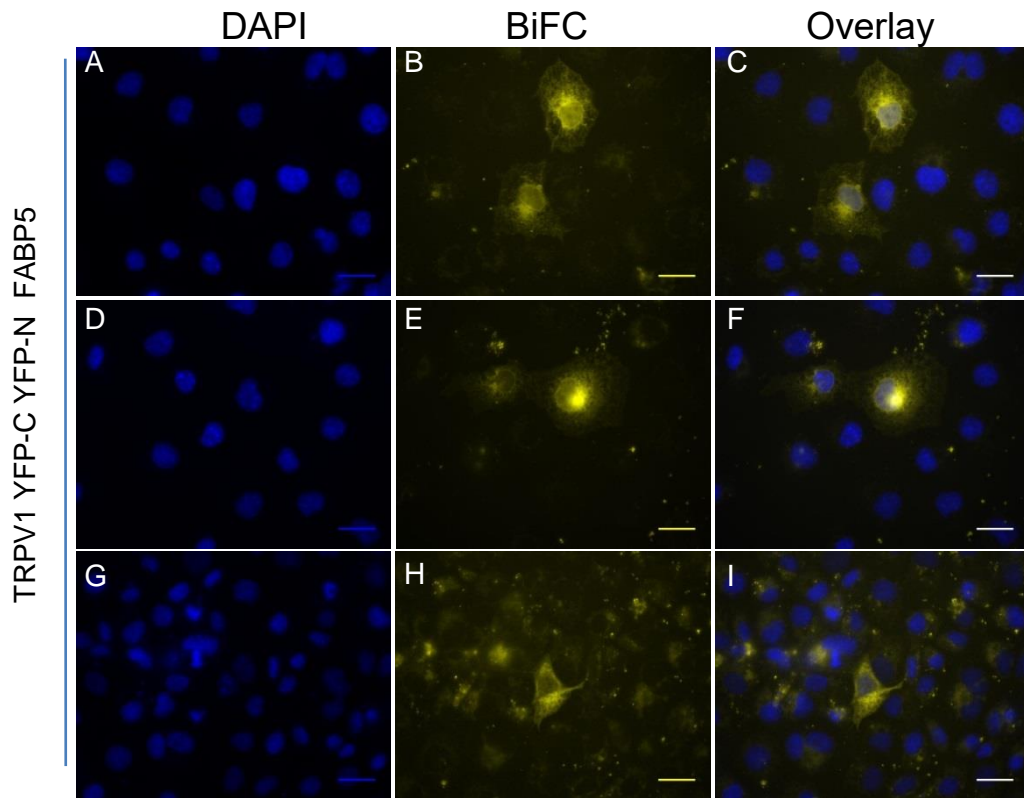


Figure 5.12: Interaction of YPF-C PPAR β with YFP-N FABP5 or FABP8 in COS-7 cells - COS-7 were co-transfected and allowed to co-express recombinant YFP-C PPAR β and YFP-N FABP5 or FABP8 at 37°C. After 6 hours, transfected cell cultures were replenished with fresh fully supplemented DMEM growth medium containing either 0.1% DMSO/vehicle or 100nM GW0472. Cells were incubated for a further 18 hours at 30°C after which the cells were fixed and then examined by fluorescence microscopy. As seen previously, cells cultures exposed to PPAR agonist gave a subpopulation of nuclei exhibiting intense fluorescence compared those nuclei from cultures treated with 0.1% DMSO. Scale bar is 16 μ m

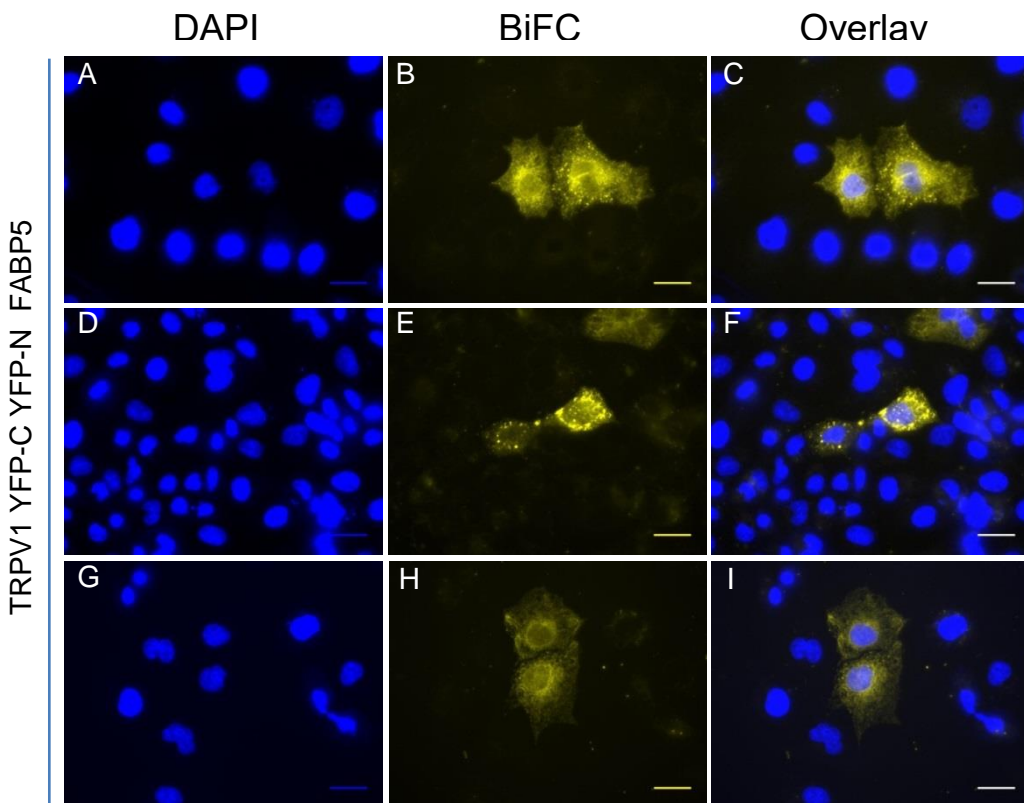
In summary, the BiFC interaction assays in Figure 5.11& 5.12 demonstrated that YFP-N FABP1, FABP5, and FABP8 appeared to have retained their functionality as chimeric proteins given their ability to interact with PPAR α or β in what seems to be a partly ligand dependent interaction for PPAR β .

While the absence of any supporting BiFC interaction data for YFP-N FABP 3, 4 and 7 with YFP-C PPAR receptors meant that was not possible to deduce that these YFP-N FABP fusion proteins were functionally active under the conditions used. The intention was to try to show that TRPV1 interacts with FABPs, previously identified in DRG cultures in chapter 3. It was hypothesized that the FABPs would interact only with TRPV1, in a ligand dependent manner i.e. when they are bound to lipid cargo such as the neuromodulatory lipid AEA. BiFC data reported in figure 5.13 implied that FABP5, 7 and 8 could all physically interact with TRPV1. However, attempts to replicate these findings proved unsuccessful.

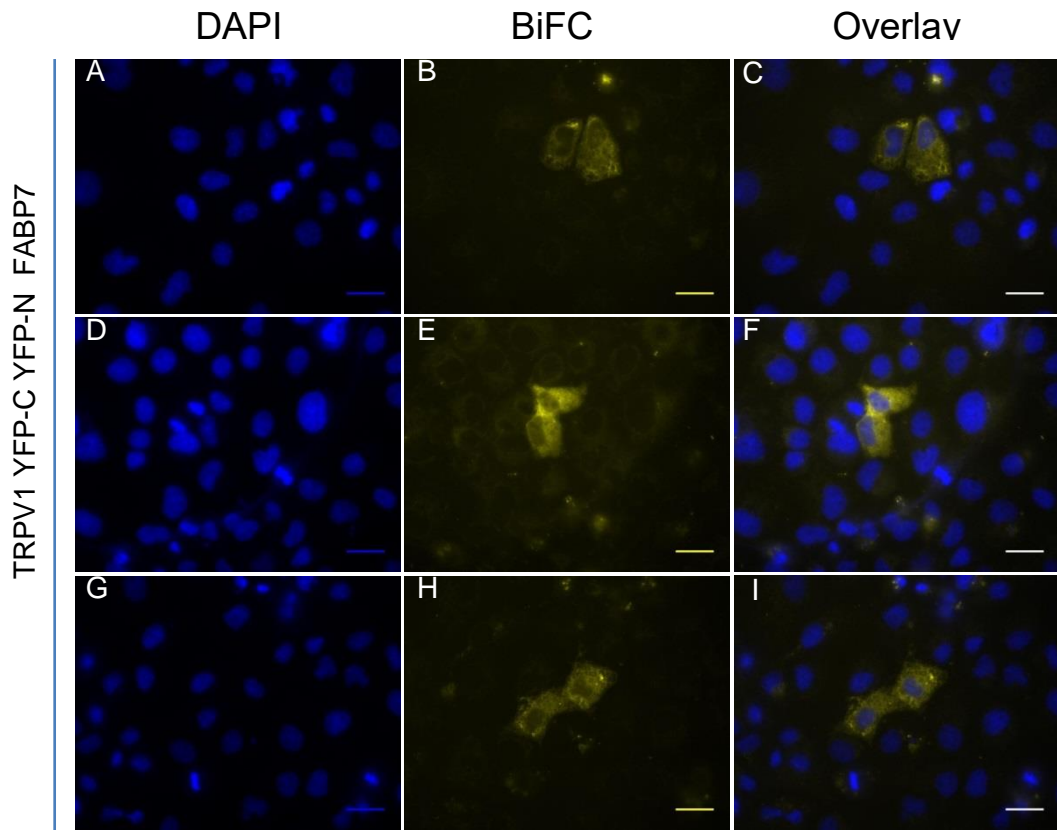
+ 0.1% EtOH in lipid free FBS



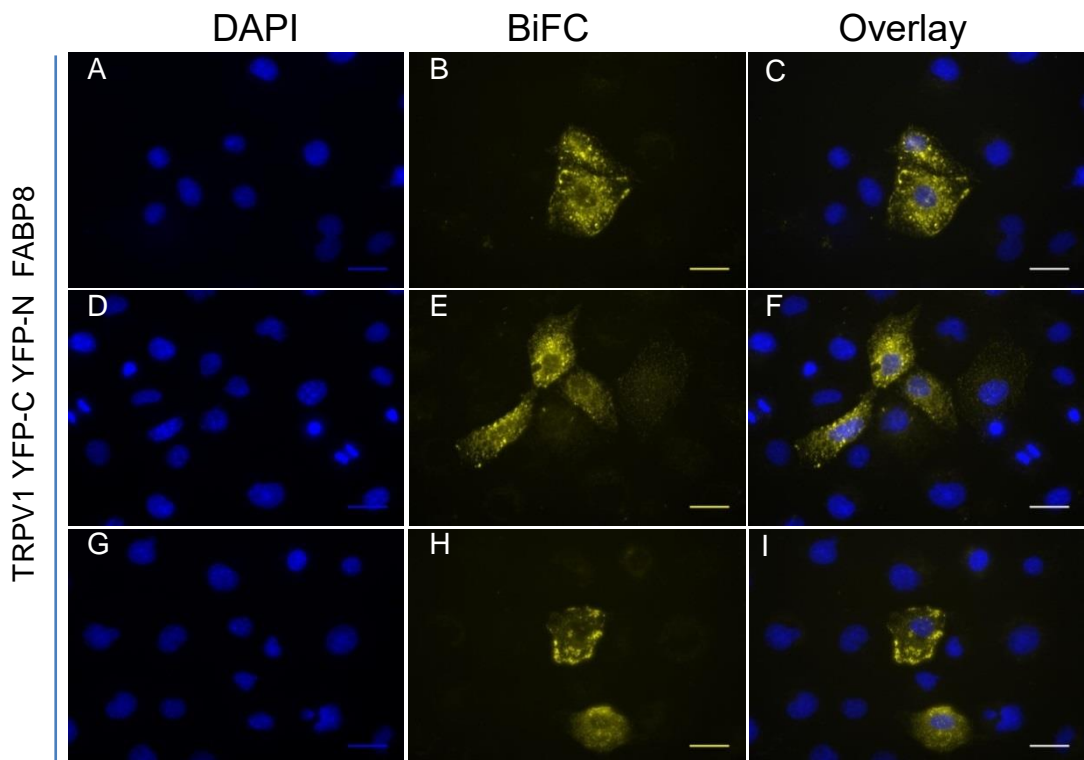
+ 10 μ M AEA in lipid free FBS



+ 10 μ M AEA in lipid free FBS



+ 0.1% EtOH in lipid free FBS



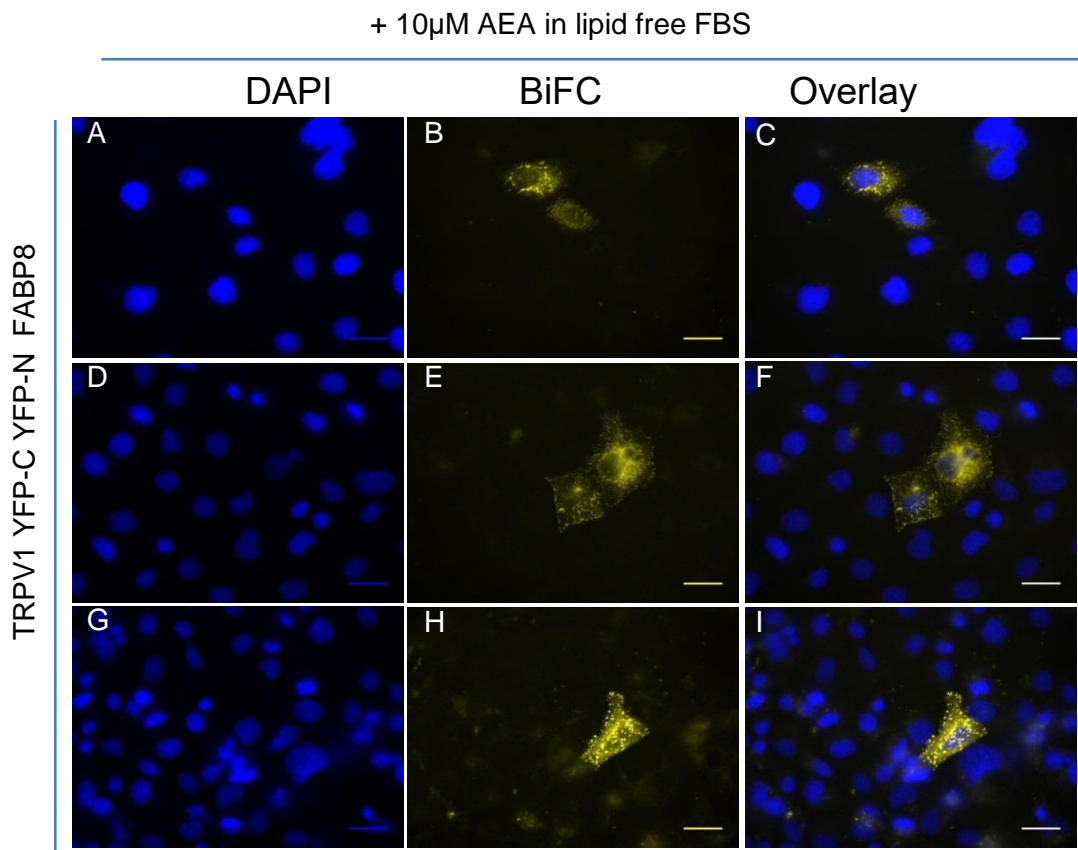


Figure 5.13: Co-expression of YFP-N FABPs and TRPV1 YFP-C produces apparent BiFC in COS-7 cells - COS-7 cells were co-transfected with the appropriate plasmids and expressed recombinant proteins TRPV1 YFP-C and YFP-N FABPs. The FABP isotype co-expressed with TRPV1YFP-C is indicated in the figure i.e. TRPV1 YFP-C YFP-N FABP5. After 6 hours of protein expression at 37°C, cells were replenished with growth medium containing either 0.1% ethanol/vehicle or exogenous 10 μ M AEA. Cells were incubated for a further 18 hours at 30°C. Except for cells co-expressing TRPV1 YPF-C and YFP-N FABP7, BiFC was detected in cells treated either 0.1 % ethanol or 10 μ M AEA. The fluorescence observed in all cases seem to be punctate and localized to the cytosol or the ER. Scale bar is 16 μ m.

5.4 Discussion

The overall aim of this chapter was to establish if FABPs 5,7 and 8 when loaded with or without pro-nociceptive lipid cargo, would physically interact with TRPV1 in transiently transfected cultured mammalian cell lines. The plasmid DNA constructs used/generated were shown to successfully express the chimeric proteins of interest in this chapter. Both immunoblotting and immunofluorescence revealed that YFP-C and YFP-N tagged TRPV1/PPARs and FABPs were all expressed when COS-7 cells were transfected and maintained under the specific conditions required for successful BiFC. In summary, there were no issues associated with a lack of or impaired protein expression.

Critically, when tagged with YFP-C or YFP-N fragments of YFP and expressed at 30°C, the chimeric proteins remained functional in COS-7 cells. YFP-C tagged TRPV1 was shown to have retained its functionality as a Ca²⁺ channel when exposed to the agonist capsaicin. While the PPAR isotypes, each tagged with YFP-C, were still able to functionally interact and form obligate heterodimers with YFP-N tagged RXR α when co-expressed in COS-7 cells. Furthermore, the cells co-expressing PPAR and RXR α , which were each tagged with the same non-fluorescent fragments of YFP as their TRPV1 and FABP counterparts, exhibited high levels of detectable fluorescence (BiFC) signal. Therefore, it was also concluded that the choice of non-fluorescent fragments of YFP and the temperature at which the cells were incubated, were both appropriate for successful BiFC assays.

Under the same conditions, BiFC captured YFP-N tagged FABP1, FABP5, FABP8 interacting with their previously reported PPAR interaction partners, however, this was not observed for YFP-N FABP3, 4 and 7. It is possible that under the conditions used, these FABP isotypes, when tagged with YFP-N, do not interact

with the PPARs in the same manner to that of their untagged equivalents. However, initial BiFC data did show that YPF-N FABP7 could interact with TRPV1 YFP-C, as could YPF-N FABP5 and 8. Interestingly, despite using the same experimental conditions, FABP-TRPV1 interactions, were not detected by BiFC in replicate experiments, this was despite FABP5 and FABP8 still appearing to functionally interact with PPAR β in parallel replicate BiFC assays.

In conclusion, an alternative approach to capturing PPIs is required and should be considered as a means of verifying that the proteins discussed do or do not interact when co-expressed in mammalian cell lines under the same experimental conditions to those used previously. Techniques such as fluorescence resonance energy transfer (FRET) allow for the direct visualization of protein complexes *in situ*, which, as discussed in 5.0 and 5.1, is of particular importance given that interaction of FABPs with other proteins is transient and not easy to detect/capture with other PPI methods.

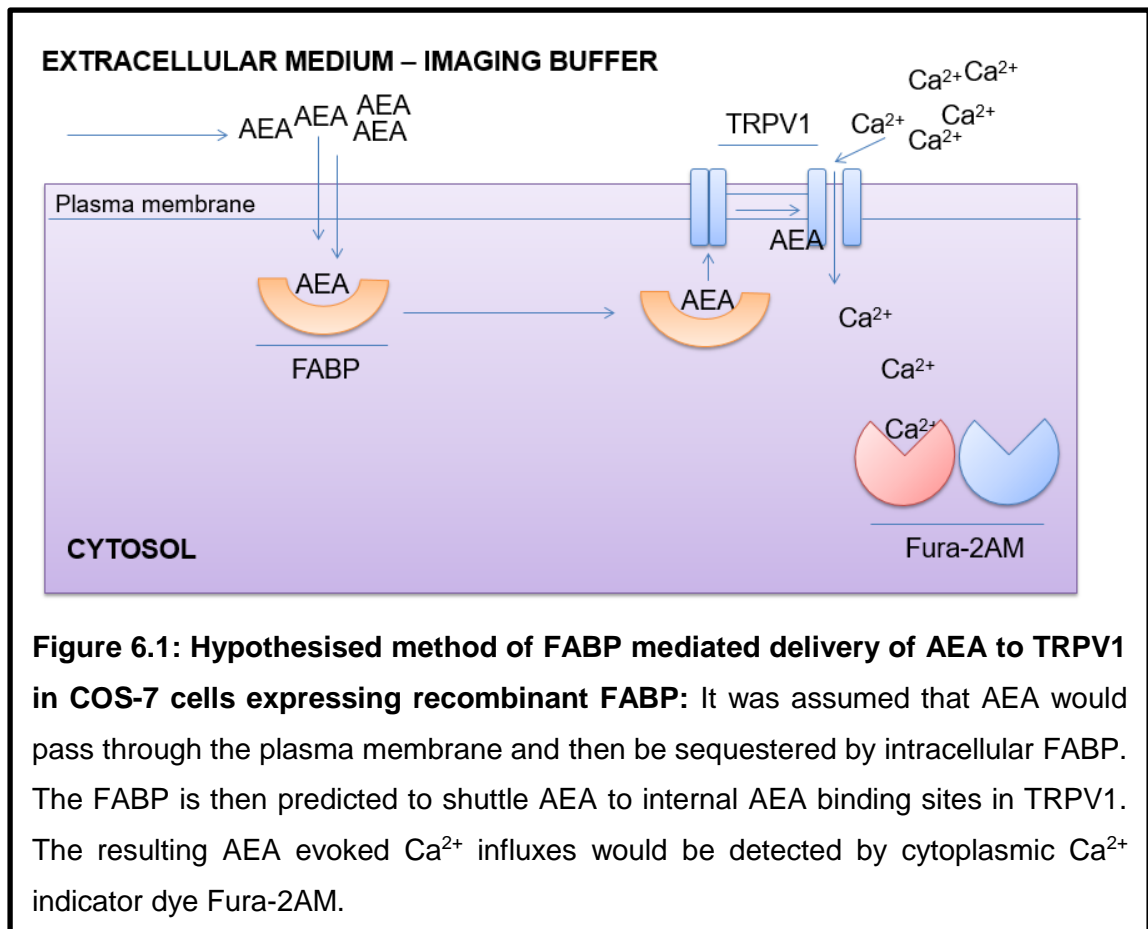
Chapter 6: Developing Fura-2AM based fluorescent Ca^{2+} imaging assays to demonstrate a functional association between TRPV1 and FABPs

Chapter 6: Developing Fura-2AM based fluorescent Ca²⁺ imaging assays to demonstrate a functional association between TRPV1 and FABPs

6.0 Introduction

The aim of this chapter was to develop an alternative methodology to demonstrate the hypothesized role of FABPs as modulators of TRPV1 activity, i.e. do FABP isoforms actively shuttle endovanilloids such as AEA to TRPV1 and regulate its activity. This was to be achieved in a non-native cell based fluorescence *in vitro* Ca²⁺ imaging assay system. Due to its limited availability, the role of 13 (S) HODE was not investigated. Two experimental approaches were adopted and are summarized below.

Approach I – the effects of co-expressing FABPs with TRPV1: The first experimental approach took a similar means of assessing the role of FABPs as enhancers of endogenous ligands to those used for luciferase gene reporter assays when examining functional PPAR-FABP interactions (112, 113). In summary, the first approach seeks to establish whether the application of exogenous AEA and its stimulation of TRPV1 mediated Ca²⁺ entry is functionally influenced i.e. is it enhanced or suppressed in COS-7 co-expressing members of the FABP family. This approach assumes that when AEA is exogenously applied to the cells, it passes through the plane of the membrane and is then sequestered by overexpressed cytosolic FABP to become endogenous AEA. This approach presumes that FABP bound AEA is subsequently shuttled to internal AEA binding sites in TRPV1, as opposed to diffusing towards TRPV1. This theory and hypothesis are summarized in Figure 6.1.



The concentration of AEA that gives the half maximal response (EC₅₀) at TRPV1 receptors has been reported to range from 0.7 μM to 5 μM in cell lines overexpressing TRPV1 (62). Therefore, it was decided that a sensible starting point would be 1 μM AEA. In summary, the first approach seeks to establish whether AEA evoked Ca²⁺ entry was functionally influenced in COS-7 co-expressing TRPV1 and members of the FABP family, i.e. did overexpressed FABP enhance or reduce the effects of 1 μM AEA.

Approach II - The synthesis of endogenous Anandamide (AEA) in cultured cell lines: The general principles underpinning the 2nd alternative approach/assay system are based on the previous work of Van der Stelt et al. (65). They demonstrated that it was possible to induce the synthesis of the TRPV1 ligand anandamide (AEA) via the N-acyl ethanol phosphatidylethanolamine (NAPE) –

specific phospholipase D (PLD) enzyme in WT HEK293 and HEK293 cells stably expressing recombinant TRPV1 (hTRPV1-HEK293). The underlying mechanism of AEA synthesis in HEK293 cells is as follows; stimulation of the metabotropic muscarinic G_q coupled receptors (mACh-R) with receptor agonist carbachol (CCH), leads to the activation of phospholipase-C (PLC). PLC mediated cleavage of plasma membrane phosphatidyl-4, 5-bisphosphate (PIP_2) releases inositol-1, 4, 5-triphosphate (IP_3). IP_3 diffuses through the cytoplasm and acts at IP_3 receptors (IP_3R) at the ER membrane of the ER- Ca^{2+} stores, which evokes a transient increase in cytosolic Ca^{2+} concentration. The resulting Ca^{2+} transients are sufficient to drive NAPE-PLD mediated biosynthesis of endogenous AEA and transiently increase its levels. The functional consequence of elevated AEA levels was then exemplified by its ability to amplify Ca^{2+} influxes via acting at TRPV1 receptors (Figure 6.2).

The facility of being able to induce the biosynthesis of AEA on demand produced an opportunity for this investigation in which AEA evoked - TRPV1 mediated Ca^{2+} influxes could be measured in a fluorescence based assay using the Ca^{2+} sensitive dye Fura-2AM in which Fura-2AM acts a cytoplasmic indicator of intracellular Ca^{2+} concentration. This 2nd method also presented the possibility of being able to determine the effect of modulating the activity of endogenous AEA on TRPV1 activity measurably and empirically.

As previously discussed, the intracellular lipid binding proteins (iLBPs), the FABPs sequester and transport lipophilic – hydrophobic ligands such as AEA. This chapter and thesis hypothesizes that member(s) of the FABP family may mediate the delivery of AEA to TRPV1. If true, pharmacological or genetic inhibition of endogenous FABP function in CCH treated hTRPV1 expressing cell lines, would negatively influence TRPV1 activity by reducing the level of activating AEA ligand being delivered at TRPV1 receptors. The functional consequence of this would be

a measurable reduction in intracellular Ca^{2+} concentration indicative of reduced TRPV1 activity.

HeLa vs. HEK293 cell lines: The transient transfection procedure produces a heterogeneous population of untransfected and transfected HeLa cells because the transfection procedure is always less than (<) 100% efficient. Therefore, it is important that populations of cells that have been transfected not be lost during the Ca^{2+} imaging assay-procedure. Using HeLa cell lines which have superior adhesion properties compared to HEK293 cells, eliminates this problem. Fortunately, HeLa cells also express functional mACh-R and have been reported to express AEA transporter FABP5. Overall, based on these reasons, HeLa cells were judged to be a suitable substitute for HEK293 cells and were selected for this study. However, a characterisation of the HeLa cells was still deemed necessary i.e. confirming the expression of FABP5 and NAPE-PLD. In summary, the overall aim of the chapter was to establish and use the same assay system described by Van der Stelt et al. (65) but to probe for a functional TRPV1-FABP relationship in HeLa cell lines expressing human TRPV1.

6.1 Methods in brief

N.B.: Note that only selected or appropriate methods have been summarized, i.e. those methods where details necessitate highlighting-clarification or are specific to the experiments discussed in the context of this chapter and are not mentioned in the general methods (chapter 2).

Molecular Biology I- Cloning human TRPV1 and FABP7: cDNA encoding for full-length human TRPV1 and FABP7 were separately cloned into pcDNA3.1/Zeo (+) to give pcDNA3.1/Zeo (+) TRPV1 and FABP7 expression vectors. The ATG initiation codon for TRPV1 and FABP7 was immediately flanked by a Kozak consensus sequence of GCCACC to ensure initiation of translation.

Cell culture and transient transfection: 1ml of cell suspension containing HeLa/COS-7 cells at a density of $0.7 \text{ cells.ml}^{-1}$ were dispensed per well onto a sterile 19mm glass coverslip, in a 12 well plate. Cells were cultured for 24 hours at $37^{\circ}\text{C}/5\% \text{ CO}_2$ so that they could reach 70-90% confluency on the day of transfection. Co-transfection of COS-7 cells: The following day cells were transiently co-transfected with $1\mu\text{g}$ of pcDNA3.1/Zeo (+) TRPV1 and $1\mu\text{g}$ of pcDNA3.1/Zeo (+) / FABP7/8 or pcDNA3.1/Zeo (+) using Lipofectamine 2000 transfection reagent according to the manufacturer's instructions. Cells were then allowed to co-express recombinant proteins for a further 24 hours at $37^{\circ}\text{C}/5\% \text{ CO}_2$. HeLa cells were transfected with $1\mu\text{g}$ of pcDNA3.1/Zeo (+) TRPV1 and allowed to express recombinant proteins as above. Transfected and wild type cells were then prepared for RT-PCR/TaqMan® gene expression assays, immunoblotting (see chapter 2), immunofluorescence (see chapter 2), and Ca^{2+} imaging assays.

Molecular Biology II – 500ng of total RNA from WT and transfected HeLa cells was reverse transcribed to cDNA for semi-quantitative/end point detection RT-PCR

and TaqMan® gene expression assays to detect endogenous FABP isotypes 1-9, NAPE-PLD and TRPV1.

Ca²⁺ imaging assays: WT and transfected HeLa/COS-7 cells were washed with Ca²⁺ imaging buffer then loaded with 5µM cytoplasmic Ca²⁺ indicator dye Fura-2AM as in chapter 2. After loading, cells were washed with Ca²⁺ imaging buffer for 5 minutes to stabilize the cells.

Exposure of capsaicin to transfected COS-7/HeLa cells: Cells were exposed to vehicle or drug for 1 minute. A 45-minute washout with regular Ca²⁺ imaging buffer followed which was then followed by the next drug-ligand exposure.

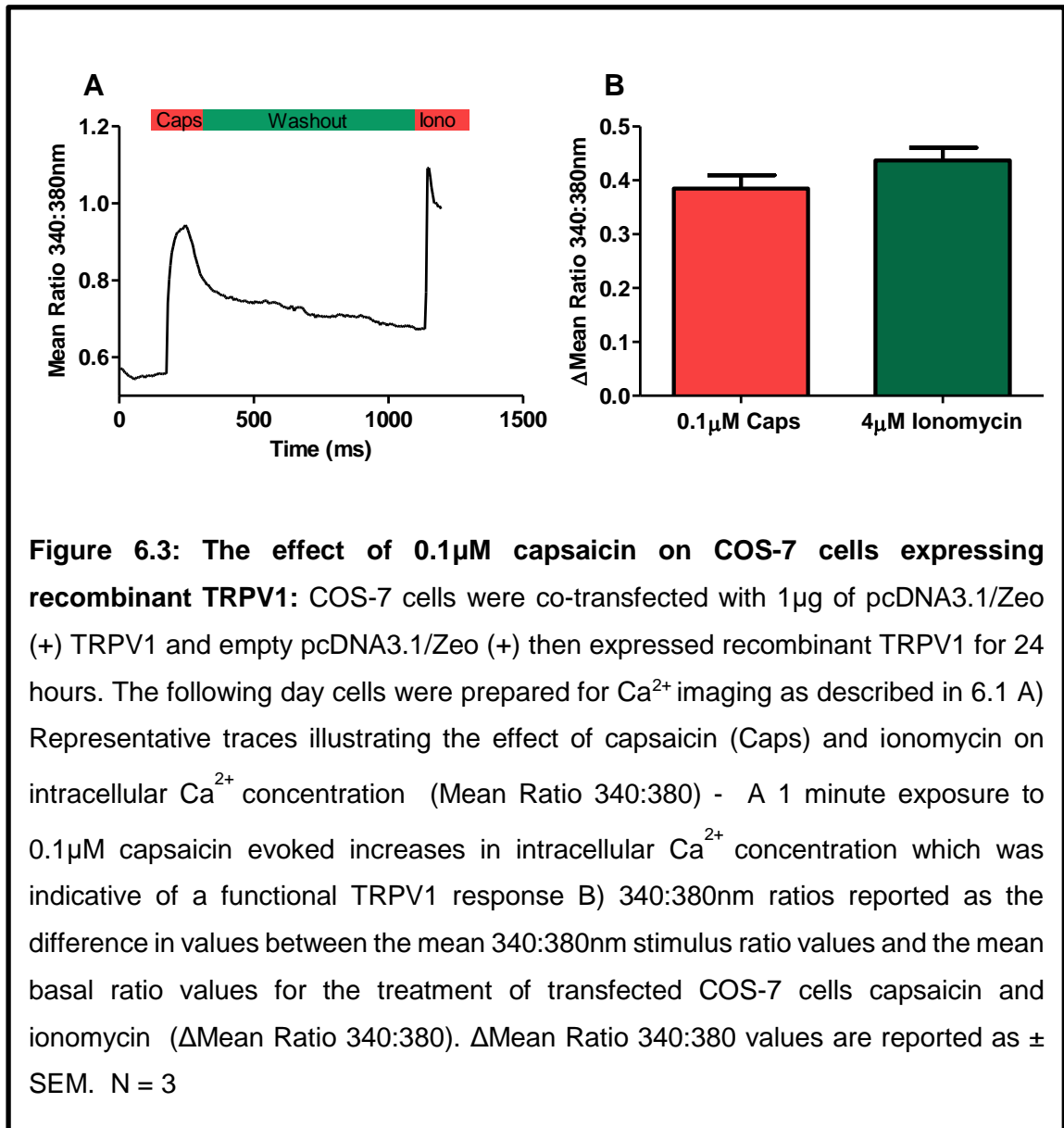
Ca²⁺ reconstitution protocol for WT/Transfected HeLa cells: Cells were perfused with Ca²⁺ imaging buffer at a continuous flow rate of 2ml.min⁻¹ for 5 minutes, this was then switched to Ca²⁺ free imaging buffer for a further 5 minutes to allow cells to stabilize. Cells were then exposed to store depleting agent carbachol (CCH) or vehicle for 1 minute, followed by a 5-minute washout with Ca²⁺ free imaging buffer. Cells were subsequently reconstituted in Ca²⁺ buffer containing 2.5mM CaCl₂. Transfected cells were then subjected to an approximate 5-minute washout period with regular imaging buffer followed by 1-minute exposures to 0.1µM capsaicin (Caps) and then 4µM ionomycin (Iono). For wild type cells, there was a washout as above, followed by a 4µM ionomycin exposure.

6.2 A summary of the experimental aims for chapter 6

1. Establish whether the effects of AEA are enhanced at TRPV1 in COS-7 cell co-expressing recombinant FABP isotypes previously identified as intracellular NAE carriers.
2. Emulate and modify the approach of Van der Stelt et al. (65) to address the central hypothesis of this thesis, i.e. do the FABPs mediate delivery of endogenous ligands to TRPV1?

6.3 Approach I – Confirmation of TRPV1 functionality in transfected COS-7 cells

Initially, it was necessary to confirm that when expressed as a recombinant protein in COS-7 cells, TRPV1 could give functional responses to both capsaicin and AEA.



Capsaicin could evoke functional responses from recombinant TRPV1 receptors expressed in transfected COS-7 cells (Figure 6.3A and B). Previously, ethanol has been shown to activate TRPV1 receptors, therefore, it was important to verify that AEA and not 0.1% ethanol was responsible for evoking TRPV1 – mediated Ca^{2+} entry (44). Exposure of transfected COS-7 cells to 0.1% ethanol did not evoke a change in intracellular Ca^{2+} ; however, a later exposure of capsaicin to the same selection of cells did evoke a change in intracellular Ca^{2+} concentration (Figure 6.4A). This is reflected in the $\Delta\text{Mean Ratio}$ value for the capsaicin response which was significantly higher compared to that of the negligible response for the 0.1% ethanol group (Figure 6.4B). Exposing the same selection of cells to capsaicin showed that these cells were expressing functional TRPV1 receptors. It indicated that TRPV1 expressing cells had been selected in the imaging assay and that the failure of 0.1% ethanol to evoke a response at TRPV1 receptors was genuine and not a consequence of measuring changes in untransfected-WT cells.

A subsequent experiment showed that $1\mu\text{M}$ AEA could evoke robust changes in intracellular Ca^{2+} response in a fraction of the selected cell population of which 33/56 cells were responsive to AEA (Figure 6.4C). The same regions of interest (ROIs) or cells and number of cells were also responsive to capsaicin.

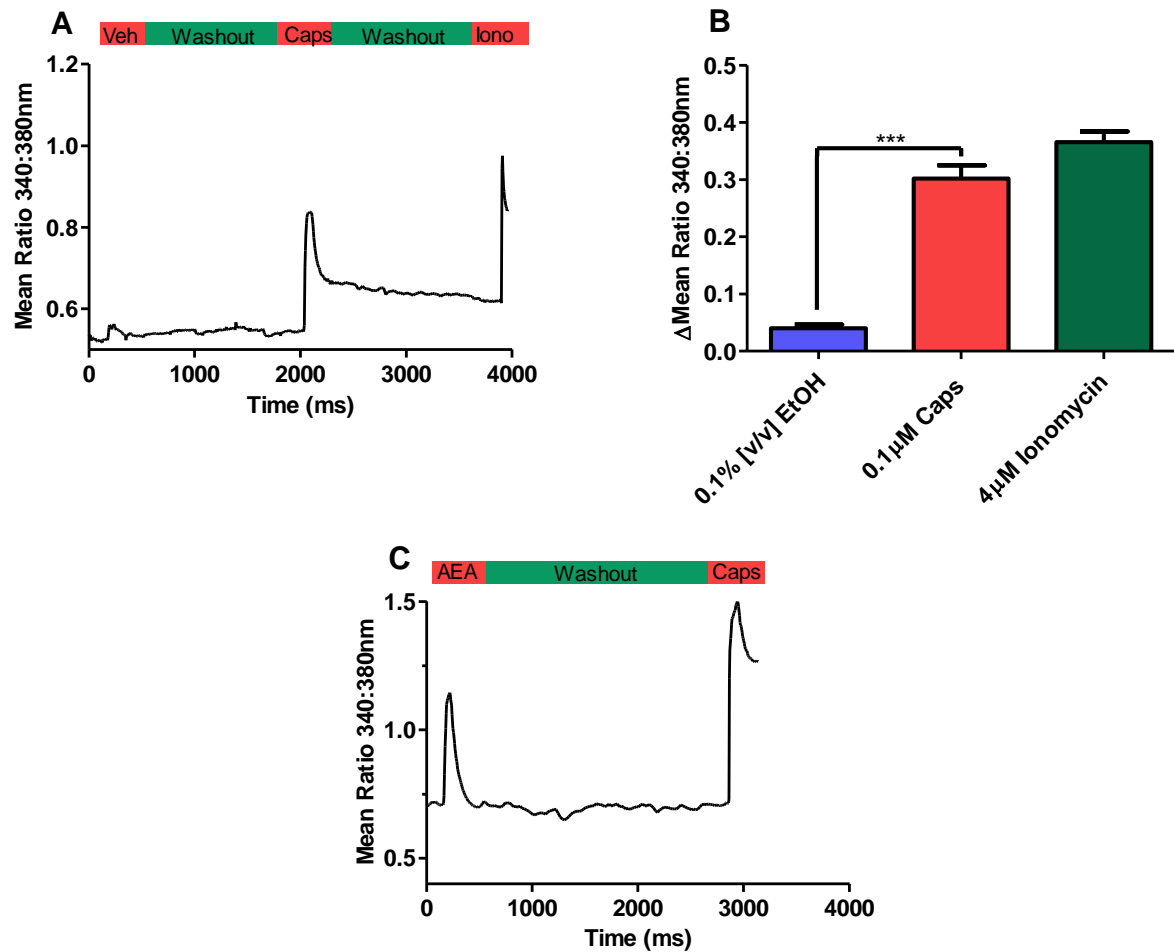


Figure 6.4: The effect of 0.1% [v/v] ethanol and 1 μM anandamide on COS-7 cells expressing recombinant TRPV1: COS-7 cells were co-transfected and prepared for Ca^{2+} imaging as described previously. A) Representative traces illustrating the effect of 0.1% ethanol - solvent (Veh/EtOH), capsaicin (Caps) and ionomycin (Iono) on intracellular Ca^{2+} concentration (Mean Ratio 340:380) / $[\text{Ca}^{2+}]_i$. 1-minute exposures of transfected cells to 0.1% ethanol did not evoke increases $[\text{Ca}^{2+}]_i$, which indicated that the vehicle was insufficient to produce functional TRPV1 responses. Cells were then perfused with imaging buffer (Washout) for 45 minutes. This was followed by a 1-minute exposure to 0.1 μM capsaicin to show that the selected cells used for Ca^{2+} imaging express functional TRPV1 and the failure of 0.1% ethanol to evoke a change in $[\text{Ca}^{2+}]_i$ was not attributable to having selected un-transfected cells for analysis. This point is further reinforced in B) when directly comparing the Δ Mean Ratio 340:380 value for the 0.1 μM capsaicin group to that of the 0.1% EtOH [v/v] group using unpaired student t-test. The Δ Mean Ratio 340:380 value for 0.1 μM capsaicin group was significantly higher than the Δ Mean Ratio 340:380 values for 0.1% EtOH [v/v]. Δ Mean Ratio 340:380 values are reported as \pm SEM. A $p < 0.05$ was considered as significant. ***, < 0.0001 . $n = 89$ ROIs or cells. C) Representative trace illustrates that 1 μM anandamide prepared in 0.1% [v/v] ethanol (AEA) was able to evoke a change in $[\text{Ca}^{2+}]_i$ (Mean Ratio 340:380). A total of 298 ROIs or cells tested across 3 independent experiments ($n=3$).

6.4 Approach I – Does co-expressing FABP7 or FABP8 enhance the effect of AEA at TRPV1 receptors

To ascertain whether and how FABP7 and FABP8 could play a functional role in regulating the activity of AEA at TRPV1, TRPV1 receptors were co-expressed with FABP7 or FABP8 in COS-7 cells. More specifically, how would FABP7 and 8 as overexpressed proteins acting as intracellular lipid binding proteins, influence the pool of available AEA for TRPV1 and therefore influence its potency as a TRPV1 ligand? It was hypothesized that two situations were possible: the first was that FABP7 or 8 could sequester then deliver AEA to TRPV1, and therefore play a role in activating TRPV1. The second being where FABP7 and FABP8 sequester the available AEA away from TRPV1, preventing AEA acting as a TRPV1 ligand. To address this question, the effect of 1 μ M AEA on TRPV1 – mediated Ca²⁺ entry was assessed in COS-7 cells expressing TRPV1 or cells co-expressing TRPV1 and FABP isotypes. It was found that there were no significant differences when directly comparing AEA evoked – TRPV1 mediated Ca²⁺ entry in COS-7 cells expressing just TRPV1 or TRPV1 and FABP7 or 8 (Figure 6.5).

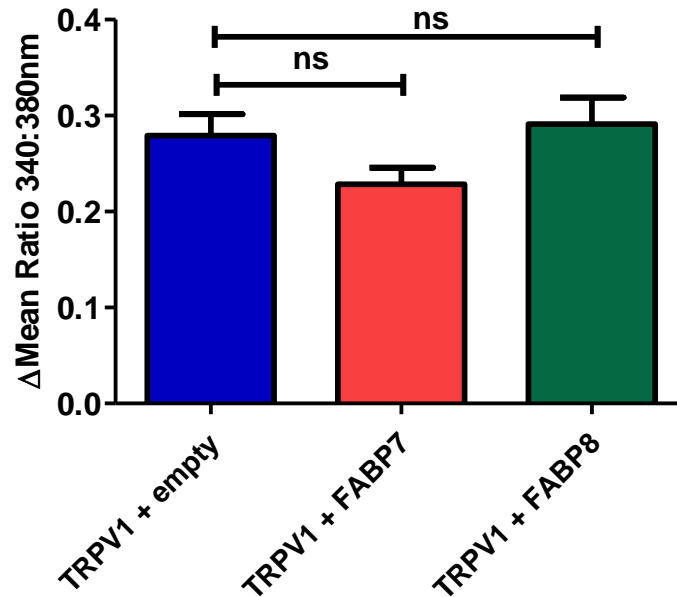


Figure 6.5: Co-expressing FABP isotypes 7 or 8 in TRPV1 expressing COS-7 cells does not influence AEA mediated functional TRPV1 responses - COS-7 cells were either co-transfected with 1 μ g of pcDNA3.1/Zeo (+) TRPV1 and pcDNA3.1/Zeo (+) or pcDNA3.1/Zeo (+) TRPV1 (TRPV1+empty) and pcDNA3.1/Zeo (+) FABP7/8 (TRPV1 + FABP7/8) and allowed to express recombinant proteins as described previously. No significant differences (ns) were observed when directly comparing the Δ Mean Ratio 340:380 value for the TRPV1 + empty group to that of the TRPV1 + FABP7 or TRPV1 + FABP8 group using unpaired student t-test. Δ Mean Ratio 340:380 values are given as \pm SEM. A total of 39 cells or ROIs across 3 independent experiments (n=3) were analysed for each group.

6.5 Approach II - Characterization of HeLa cell lines I: Detection of FABP and NAPE –PLD mRNA transcripts by RT-PCR, TaqMan® gene expression assays and immunoblotting

Before performing any functional Ca^{2+} imaging studies, it was necessary to corroborate previous experimental data which had shown that FABP5 was the single FABP isotype expressed in HeLa cells.

Simple end point detection – semi quantitative RT-PCR was used to screen for the expression of the different FABP isotypes in cultured HeLa cells. PCR amplicons were resolved and analysed by agarose gel electrophoresis. Faint single bands corresponding to the expected molecular weights for FABP3 (412 bp) and FABP5 (348 bp) were observed. Meanwhile, the transcripts for FABP1, 2, 4 and 7 -9 were undetectable by RT-PCR. To verify that the inability of the RT-PCR to detect the aforementioned FABP isotype transcripts did not lie with non-functional PCR primer pairs, cDNA was prepared from RNA extracted from available control tissues known to express the particular FABP isotype transcripts. RT-PCR on control tissues using the same pairs for FABPs1, 4, 7 and 8 was performed (Figure 6.6). Analysis of PCR amplicons by electrophoresis was implemented as previously. Single bands were migrating at the expected molecular weights for the FABPs mentioned above, were detected.

The expression levels of endogenous FABP3 and FABP5 in cultured HeLa cells were then quantified by TaqMan® gene expression assays or QRT-PCR. Expression levels of FABP3 and FABP5 were normalized to β -actin. β - Actin was selected as a house keeper gene given that it had been shown in this study and previous- other studies to be a constitutively expressed gene in HeLa cells. Relative expression levels of FABP3 (1.03 ± 0.04) and FABP5 (0.96 ± 0.02) were not significantly different when directly compared, therefore both isotypes were expressed at similar levels (Figure 6.7A).

As already discussed NAPE-PLD is a critical player in the biosynthesis of endogenous TRPV1 ligand anandamide (AEA). To verify the expression of NAPE-PLD in cultured HeLa cells, NAPE-PLD transcripts were detected and quantified by TaqMan® gene expression assays. In parallel, TaqMan® gene expression assays were performed on cDNA from human brain tissue as a positive control. (Figure 6.7B) As expected, relative NAPE-PLD expression levels were significantly higher in brain tissue (3.04 ± 0.08) compared to cultured HeLa cells (0.121 ± 0.001). Furthermore, normalized expression levels of NAPE-PLD were comparably low to that of the identified FABPs, but it was concluded that NAPE-PLD was still detectable at sufficient levels to suggest that functional NAPE-PLD enzyme may be expressed in HeLa cells.

Ideally, reliable antibodies immunoreactive against FABP3, FABP5, and NAPE-PLD would be used to demonstrate the genes mentioned above were expressed at the protein level in cultured HeLa cells. However, this was only possible for FABP5. Anti-FABP5 antibody was used in immunoblotting to detect the expression of endogenous FABP5 from wild type HeLa cell lysates. Total protein (10-20 μ g) was titrated in the immunoblotting procedure to determine the optimum amount of total protein required. A single band migrating at 15kDa which corresponds to the expected molecular weight of FABP5 was detected (Figure 6.8).

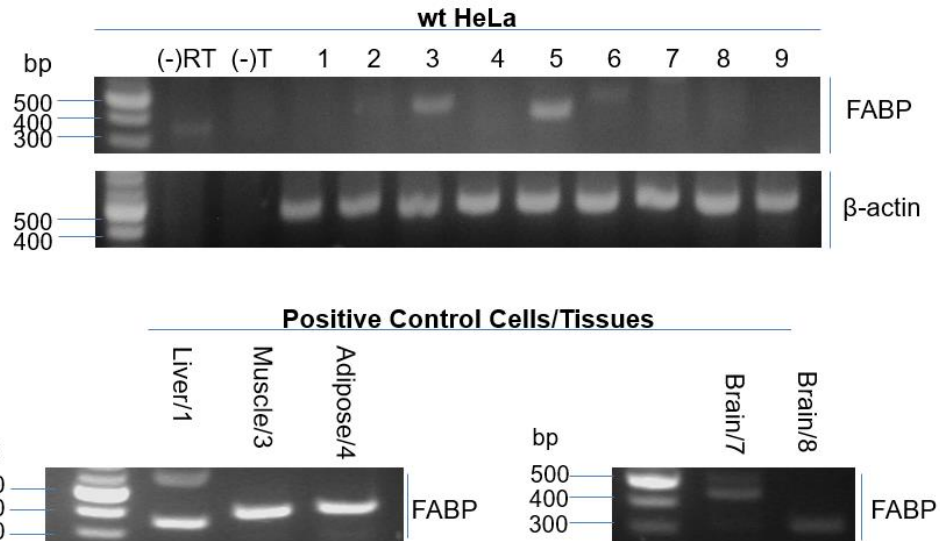


Figure 6.6: RT-PCR screen for the different FABP isotypes in cultured HeLa cells and control tissues: cDNA was prepared as described above and used as template DNA for PCR using Phusion High Fidelity DNA polymerase. 20 μ L of PCR amplicon was resolved on the above 1 \times TAE – 1.5% Agarose gels. NTC = 'No template control,' denotes where water replaced cDNA template in the PCR vessel. NRC= 'No reverse transcriptase control sample' this is where reverse transcriptase was replaced with water when reverse transcribing total RNA. MW = 100bp NEB molecular weight ladder.

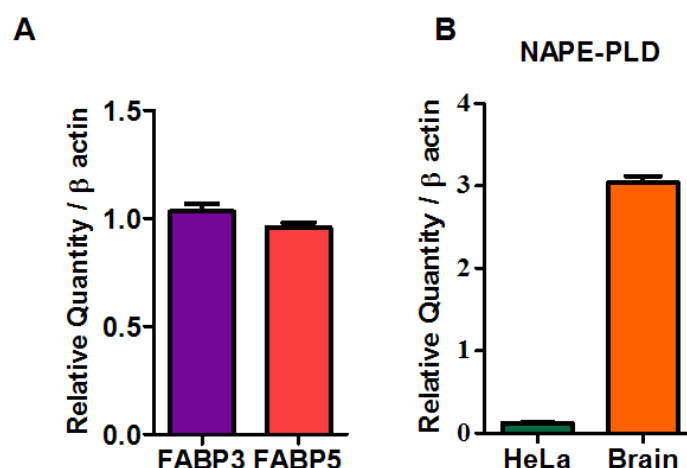


Figure 6.7: TaqMan® Gene expression assays to detect endogenous FABP3, FABP5 and NAPE-PLD in cultured HeLa cells: The relative expression levels of the previously identified FABPs and NAPE-PLD were determined using TaqMan® gene expression assays on cDNA samples obtained from the RT of RNA isolated from cultured HeLa cells and human brain tissue. Expression levels of FABP3 and FABP5 (A) in HeLa cells and NAPE-PLD (B) in HeLa cells and human brain tissue were all normalized to β -actin. All graphs – relative expression levels are reported as \pm SEM of a sextuplet set of measurements from a single experiment (n=1).

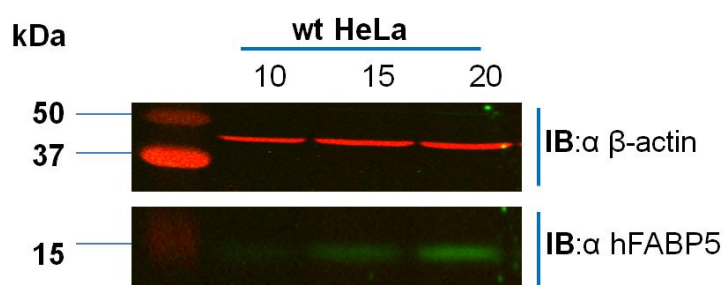


Figure 6.8: Immunodetection of endogenous of FABP5 from the lysates of cultured wild type HeLa cells: From a duplicate 12 well plate the total protein content of the HeLa cells was harvested with RIPA buffer. 10, 15 and 20 μ g aliquots of total protein were resolved by SDS-PAGE. Proteins were then transferred to an Amersham™ Hybond™-ECL nitrocellulose membrane. Blots were probed with 5% [w/v] milk TBST containing rabbit polyclonal anti-FABP5 (1:1000 dilution) and mouse monoclonal anti – β – actin (1:2000) overnight at 4°C. This was followed by washing the membrane/blot as described and then probing with a LiCOR® secondary antibodies goat anti-mouse IgG IRDYE 680 and goat anti-rabbit IgG IRDYE 800 in 3% [w/v] milk TBST (1:10,000 dilution) for 1 hour at room temperature in the dark. The membranes were then scanned using an LI-COR® Odyssey infrared imager.

6.6 Confirmation of TRPV1 expression by TaqMan® gene expression assays, immunofluorescence and functional Ca²⁺ imaging

It was necessary to confirm that the plasmid DNA vector pcDNA3.1/Zeo (+) human TRPV1 successfully encoded for fully functional human TRPV1 when transiently transfected into cultured mammalian cells.

TaqMan® gene quantification: β -actin expression levels did not vary when directly comparing wild type and transfected HeLa cells. Therefore, TRPV1 expression levels from wild type and transfected HeLa cells were normalized to β -actin. TRPV1 expression was detected by QRT-PCR in HeLa cells transiently transfected with pcDNA3.1/ Zeo (+) TRPV1 but was undetectable in wild type – untransfected cells (Figure 6.9A).

Immunostaining: Both transfected and wild type-untransfected HeLa cells were subject to immunostaining using TRPV1 with a pre-validated anti-TRPV1 antibody. Transfected HeLa cells immunostained positive for TRPV1 while untransfected-wild type cells did not show any detectable immunofluorescence when examined by microscopy (Figure 6.9B). It can be concluded that wild type HeLa cells do not express TRPV1.

Ca²⁺ imaging: Finally, it was necessary to show when expressed in HeLa cells as a recombinant protein, TRPV1 forms a functional ion channel. Transfected HeLa cells were exposed to 0.1 μ M capsaicin, which increased intracellular Ca²⁺ concentration (Figure 6.10). In summary, this response indicated the successful expression of functional TRPV1 receptors.

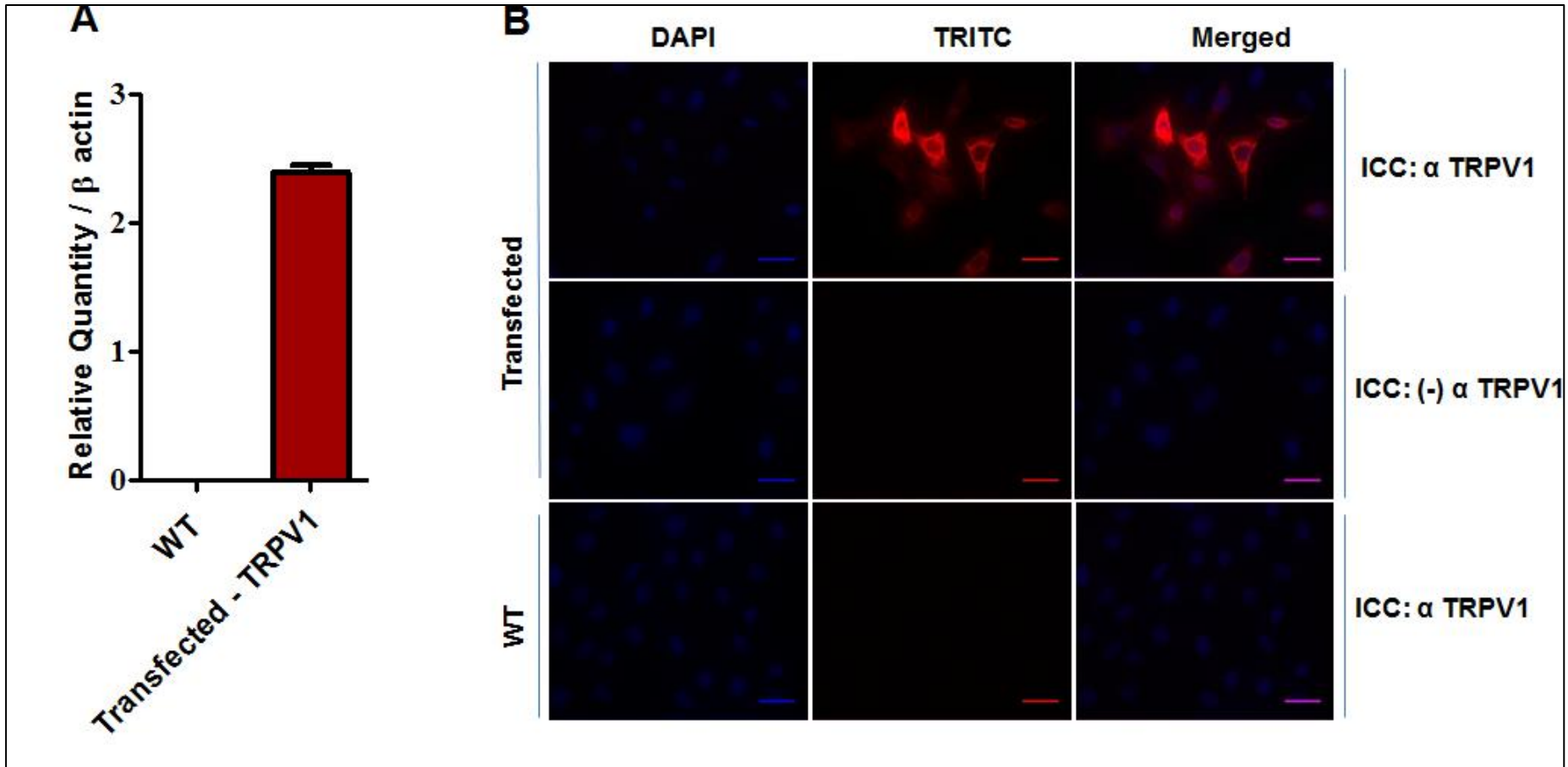


Figure 6.9: Determining the expression of human TRPV1 in wild type and transiently transfected HeLa cells. HeLa cells were seeded at a density of $0.7 \text{ cells.ml}^{-1}$ /well in a 12 well plate and cultured for 24 hours to reach 70-90% confluency. Adherent HeLa cells were then transiently transfected with $1 \mu\text{g}$ of pcDNA3.1/Zeo (+) TRPV1 per well using Lipofectamine 2000. A duplicate 12 well plate was left un-transfected to give wild type HeLa cells (WT). WT and transfected cells were incubated for a further 24 hours after which cells were prepared for quantitative RT-PCR, immunocytochemistry or calcium imaging.

- A) **TaqMan® gene expression assays for TRPV1 and β -actin in wild type and transfected HeLa cells:** cDNA was prepared from wild type and transfected HeLa cells for TaqMan® gene expression assays as in chapter 2. Expression levels of TRPV1 in wild type and transfected cells were normalized to β -actin. A direct comparison of the relative expression levels of TRPV1 for wild type and transfected cells showed that TRPV1 expression was only detectable when the HeLa cells were transfected with pcDNA3.1/Zeo(+) TRPV1. Relative expression levels are reported as \pm SEM from a single experiment ($n=1$). Relative expression level of TRPV1 for transfected HeLa cells was 2.40 ± 0.06 .
- B) **Representative fluorescent microscopy images illustrating immunocytochemical (ICC) evidence for the expression of recombinant human TRPV1 in transiently transfected HeLa cells:** Transfected and WT cells maintained on 19mm glass coverslips were fixed with 4% PFA, permeabilized with 0.25% [v/v] Tween-20 then blocked with 10% (v/v) donkey serum. Cells were then immunostained with $0.4 \mu\text{g.ml}^{-1}$ goat polyclonal α TRPV1 antibody for 18 hours at 4°C followed by $2 \mu\text{g.ml}^{-1}$ donkey anti goat IgG Alexa Fluor® 568 for 1 hour at RT in the dark (ICC: α TRPV1). 'ICC (-) α TRPV1' denotes that the TRPV1 primary antibody was omitted from the staining mentioned above. Cells were counterstained with $1 \mu\text{g.ml}^{-1}$ DAPI for 5 minutes. Glass coverslips were mounted onto glass microscopy slides. Images were acquired from a single experiment ($n=1$) using a DMRB fluorescent microscope using the appropriate filter set at a $\times 63$ magnification. Images acquired in TRITC channel were all taken at an exposure time of 250ms and a digital gain of 2. Scale bar is $16 \mu\text{m}$.

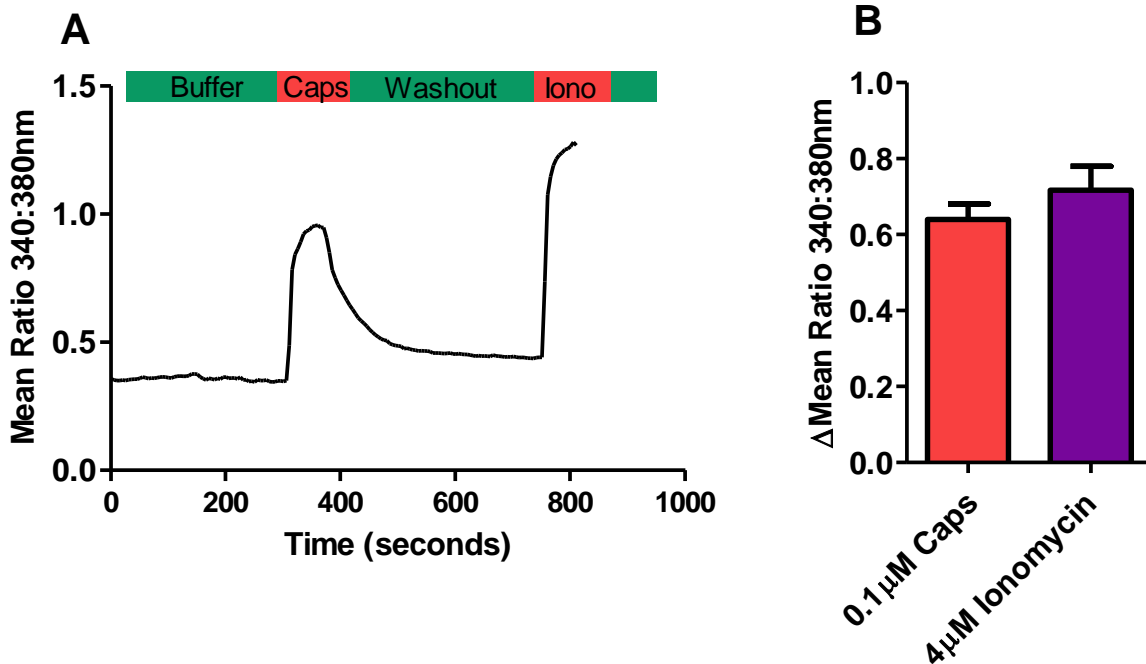


Figure 6.10: Transfected HeLa cells expressing recombinant TRPV1 give functional responses when exposed to 0.1 μM capsaicin: After expressing recombinant TRPV1 for 24 hours, transfected HeLa cells were prepared for Ca^{2+} imaging by loading with 5 μM Fura-2AM as in previous Ca^{2+} imaging experiments A) The representative traces illustrates the changes in intracellular Ca^{2+} concentration (Mean Ratio 340:380nm) in HeLa cells expressing recombinant TRPV1 in response to a 1 minute stimulation with 0.1 μM capsaicin (Red rectangle). After treatment with capsaicin, cells were perfused with Ca^{2+} imaging for 5 minutes (Washout) then exposed to 4 μM ionomycin after which the experiment was ended. B) 340:380nm ratios reported as the difference in values between the mean 340:380nm stimulus ratio values and the mean basal ratio values for capsaicin and ionomycin (Δ Mean Ratio 340:380) for transfected HeLa cell Δ Mean Ratio 340:380 value was reported as \pm SEM. Δ Mean Ratio 340:380 value for capsaicin was 0.6400 ± 0.04033 . A total of 60 ROIs or capsaicin sensitive cells, across 3 independent experiments (n=3) were analysed.

6.6 WT HeLa cells express functional muscarinic receptors that are responsive to stimulation with carbachol (CCH)

Carbachol (CCH) induced elevations in intracellular - cytosolic Ca^{2+} concentration has been shown to induce the synthesis of endogenous Anandamide in HEK293 cells (65). For this investigation, the same Ca^{2+} dependent driven synthesis of internal AEA was to be replicated in HeLa cells. In 6.5, HeLa cells had already been shown to express NAPE-PLD, and previous studies had shown that HeLa cells express functional metabotropic muscarinic (CCH) receptors. Furthermore, HeLa cells do not express functional fatty acid amide hydrolase (FAAH), the enzyme responsible for the degradation – turnover of AEA to ethanolamine and arachidonic acid (77, 116). Therefore, endogenously synthesized AEA will be not degraded as would normally be the case for lipophilic-hydrophobic intracellular messengers such as AEA. Therefore, HeLa cells were selected as a suitable cell line to be used for this investigation. However, it was still necessary to confirm that the batch of HeLa cells used in this study was responsive to exposures with CCH and exhibited elevations in intracellular Ca^{2+} concentration under conditions comparable to those used by Van der Stelt et al. (65).

HeLa cells were initially perfused with imaging buffer (extracellular media) containing 2.5mM CaCl_2 , after 5 minutes this was replaced with imaging buffer absent of any CaCl_2 . Cells were perfused for a further 5 minutes in Ca^{2+} free imaging buffer to allow the cells to adjust to the extracellular media devoid of any Ca^{2+} . This was followed by exposure of the HeLa cells to 50 μM CCH prepared in Ca^{2+} free imaging buffer; this was sufficient to empty internal ER- Ca^{2+} stores which were concomitant with increases in cytosolic Ca^{2+} concentration ($\Delta\text{Mean Ratio}$ 340:380: 0.64 ± 0.01) (Figure 6.11A and B). Normally, the depletion of internal ER- Ca^{2+} stores via the PLC/ IP_3 will result in Ca^{2+} re-entry from the extracellular environment via the gating of Ca^{2+} release activated channels (CRAC) to replenish

and recharge the depleted internal ER Ca²⁺ stores. However, there was no Ca²⁺ re-entry into the cytosol when the WT-HeLa cells were reconstituted in extracellular medium containing 2.5mM CaCl₂ (Δ Mean Ratio 340:380: 0.039 \pm 0.001) (Figure 6.11B). This was attributed to the inherent non-excitability of the WT HeLa cells, which is also reflected to some extent in previous findings in 6.5 where both TRPV1 transcripts and protein was undetectable.

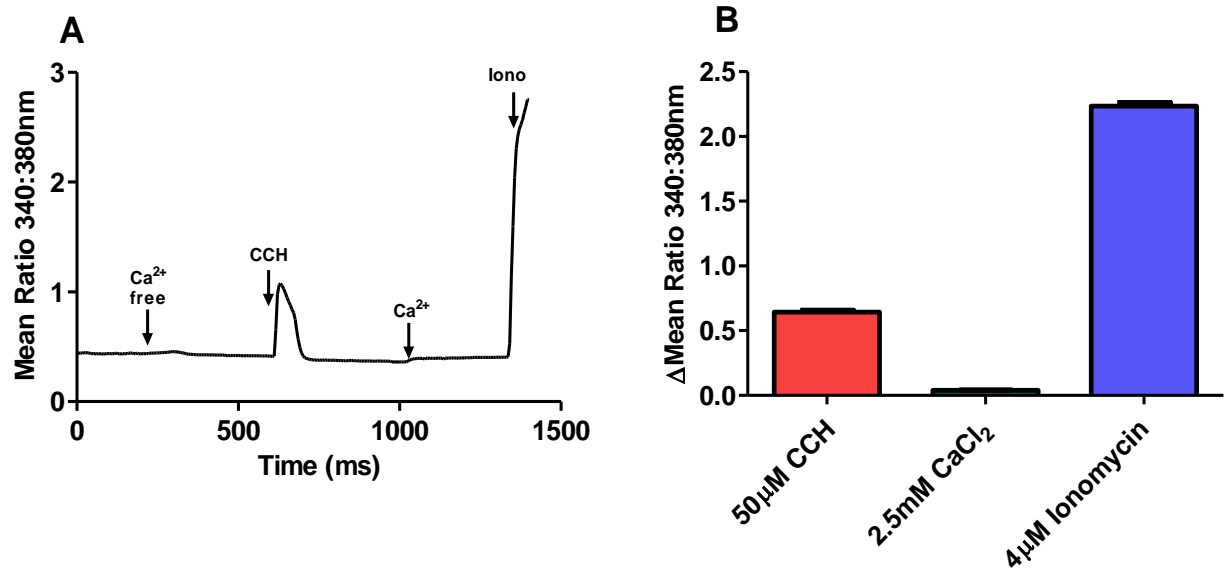


Figure 6.11: Carbachol evoked mobilization of intracellular Ca²⁺ from internal ER Ca²⁺ stores in wild type HeLa cells - HeLa cells were seeded at a density of 0.7×10^5 cells.ml⁻¹ onto 19mm glass coverslips and cultured for 24 hours. The following day cells were prepared for imaging as previously A) Representative trace illustrating the mean changes in intracellular calcium concentration [Ca²⁺]_i (Mean Ratio 340:380) in wild type HeLa cells in response to treatment with carbachol (CCH), CaCl₂ (Ca²⁺) reconstitution and ionomycin (Iono). Arrows indicate time points at which the HeLa cells were exposed to drug/buffer. Wild type HeLa cells were perfused with calcium imaging buffer for 5 minutes followed by calcium free calcium imaging buffer for 5 minutes. Internal ER-calcium stores were then depleted by exposure to carbachol [CCH, 50 μM] for 1 minute and followed by a washout with calcium free calcium imaging buffer. Cells were then reconstituted with CaCl₂ / calcium imaging buffer [Ca²⁺, 2.5 mM] for 5 minutes followed by the addition of ionomycin [Iono, 4 μM] for 1 minute. B) 340:380nm ratios reported as the difference in values between the mean 340:380nm stimulus ratio values and the mean basal ratio values for CCH, Ca²⁺ reconstitution and ionomycin treatments - exposures (ΔMean Ratio 340:380). The ΔMean Ratio 340:380 values for each treatment are reported as a SEM. 300 ROIs or cells were tested across 3 separate experiments (n=3)

6.7 TRPV1 expressing HeLa cells reconstituted in CaCl_2 allow Ca^{2+} re-entry into the cytosol independent of CCH stimulation

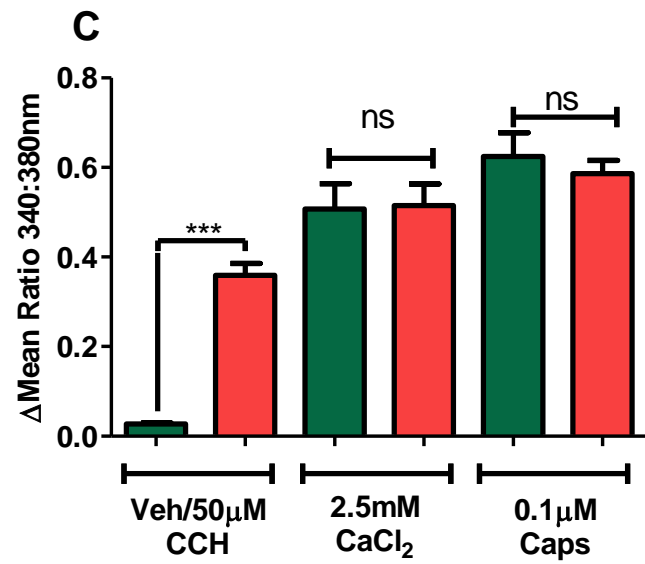
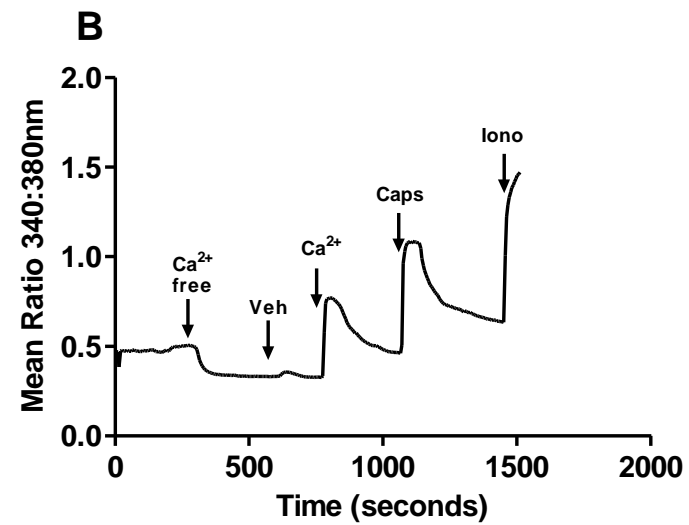
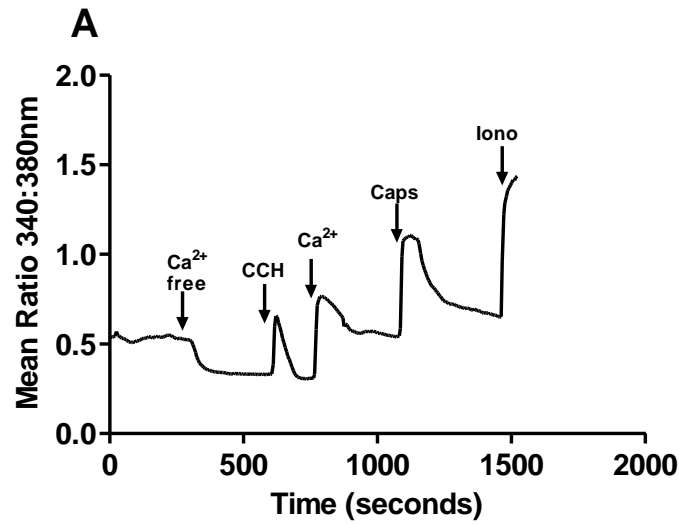
The effects of CCH evoked Ca^{2+} transients on TRPV1 functionality in transfected HeLa cells (hTRPV1-HeLa) were investigated. Metabotropic muscarinic receptors in hTRPV1-HeLa cells were exposed to 50 μM CCH or vehicle. Stimulation with 50 μM CCH resulted in the release of Ca^{2+} from internal ER stores resulting in a transient increase in cytosolic Ca^{2+} concentration (Figure 6.12A & D). Ca^{2+} transients were absent when hTRPV1-HeLa cells were exposed to the vehicle in place of CCH (Figure 6.12B & D).

When reconstituted in 2.5mM CaCl_2 , both CCH and vehicle treated hTRPV1-HeLa cells gave comparable increases in intracellular – cytosolic Ca^{2+} concentration (Figure 6.12A and B). A direct comparison of the $\Delta\text{Mean Ratio 340:380}$ values for the Ca^{2+} reconstitution response of CCH (0.51 ± 0.06) and vehicle (0.52 ± 0.05) treated hTRPV1-HeLa cells showed that there were no statistical differences between the two values (Figure 6.12C).

hTRPV1-HeLa cells responsive to Ca^{2+} reconstitution were then exposed to capsaicin to show that the same population of selected cells was expressing functional TRPV1 receptors. It was found that the magnitude of Ca^{2+} influxes evoked by capsaicin was similar; the $\Delta\text{Mean Ratio 340:380}$ values for capsaicin evoked Ca^{2+} entry in hTRPV1-HeLa cells pre-treated with CCH (0.62 ± 0.05) or vehicle (0.59 ± 0.03) were not significantly different (Figure 6.12C).

In summary, it was clear that TRPV1 was mediating Ca^{2+} re-entry in response to CaCl_2 reconstitution independent of CCH treatment. Therefore, it could not be concluded that CCH evoked Ca^{2+} transients indirectly activate TRPV1 via the synthesis of endogenous AEA. Furthermore, TRPV1 mediated Ca^{2+} re-entry was not a direct response to replenish depleted internal ER- Ca^{2+} stores given that Ca^{2+} influxes were observed in hTRPV1-HeLa cells treated with either vehicle or CCH.

It was apparent that Ca^{2+} re-entry, in response to Ca^{2+} reconstitution, was mostly if not entirely TRPV1 mediated given that increases in intracellular-cytosolic Ca^{2+} concentration were only observed for hTRPV1-HeLa cells and not WT HeLa cells. Figure 6.13 shows a direct comparison of the $\Delta\text{Mean Ratio 340:380}$ values of WT and hTRPV1-HeLa cells for the Ca^{2+} reconstitution response. The $\Delta\text{Mean Ratio 340:380}$ value of the reconstitution response for hTRPV1-HeLa cells (0.52 ± 0.05) was significantly higher compared to that of the WT cells (0.039 ± 0.003).



D

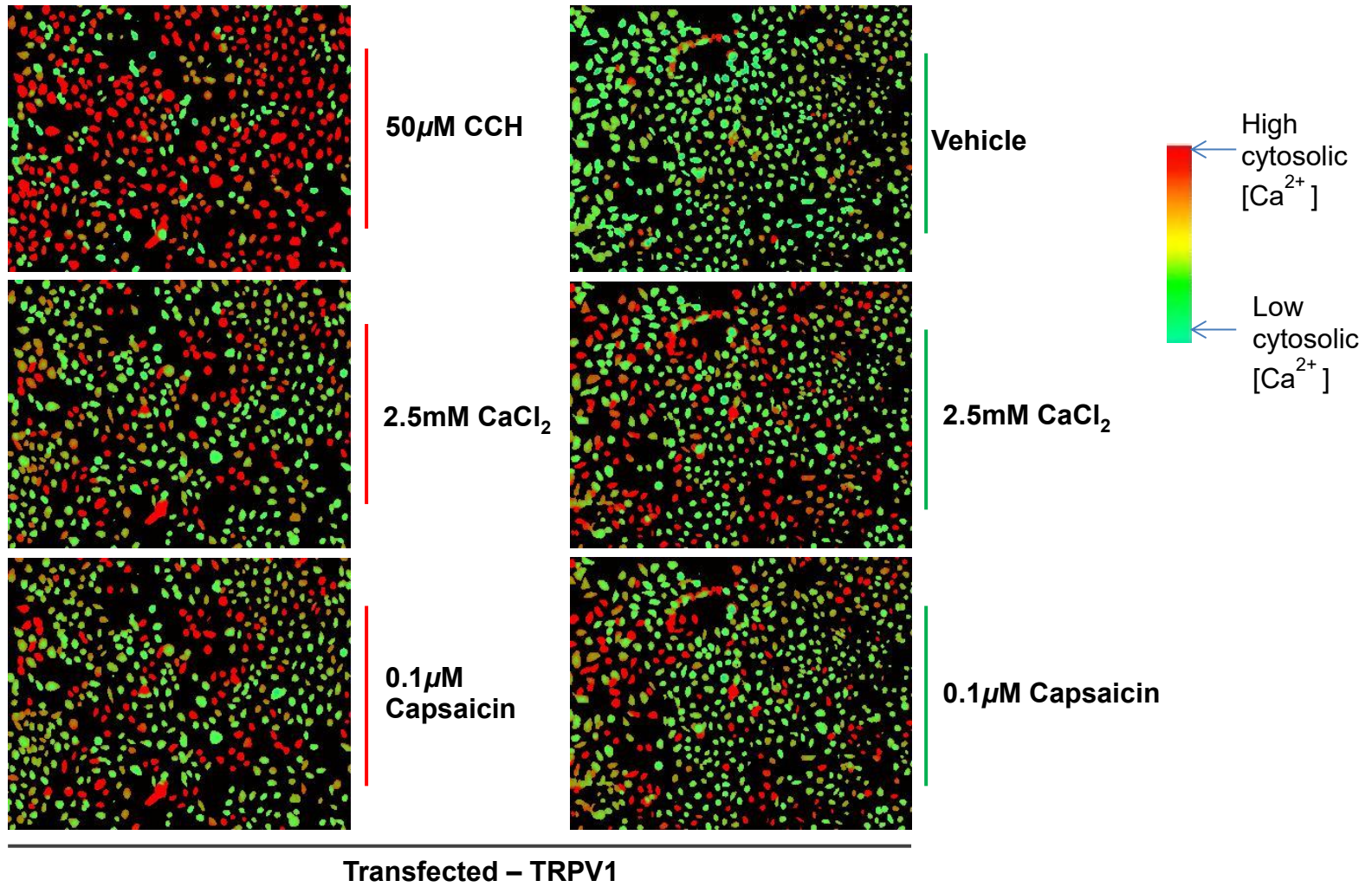


Figure 6.12: Influxes of extracellular Ca^{2+} into the cytosol is independent of CCH treatment in TRPV1 expressing HeLa cells: HeLa cells were seeded then transiently transfected with 1 μg pcDNA3.1/Zeo (+) TRPV1. Cells were then allowed to express recombinant TRPV1 for 24 hours and prepared for Ca^{2+} imaging as in Figure 6.10. **A) and B)** Representative traces of calcium reconstitution experiments illustrating mean changes in intracellular calcium concentration (Mean Ratio 340:380) in HeLa cells transfected with pcDNA3.1/Zeo (+) TRPV1. Cells were perfused with calcium imaging buffer for 5 minutes, then perfused with calcium free calcium imaging buffer for a further 5 minutes before the addition of vehicle (Veh) or carbachol (CCH, 50 μM) for 1 minute. Cells were then reconstituted with CaCl_2 / calcium imaging buffer (Ca^{2+} , 2.5mM) for 5 minutes. Cells were then exposed to capsaicin for 1 minute then treated with ionomycin (Iono, 4 μM). Irrespective of whether cells were treated with 50 μM CCH, increases in intracellular Ca^{2+} concentration were observed in transfected HeLa cells in response to reconstitution in 2.5mM CaCl_2 . **C)** Directly comparing the $\Delta\text{Mean Ratio 340:380}$ values for Ca^{2+} reconstitution responses of transfected HeLa cells that had been exposed to vehicle (green) or 50 μM CCH (red) in an unpaired student t-test. No differences were seen between the $\Delta\text{Mean Ratio 340:380}$ for the vehicle and CCH groups. The $\Delta\text{Mean Ratio 340:380}$ values for each treatment are reported as a \pm SEM. A total 39 ROIs or cells tested across 3 independent experiments (n=3). **D)** Representative high-intensity ratiometric images comparing TRPV1 expressing HeLa cells pre-treated with vehicle or CCH in response to reconstitution with 2.5mM CaCl_2 and 0.1 μM capsaicin

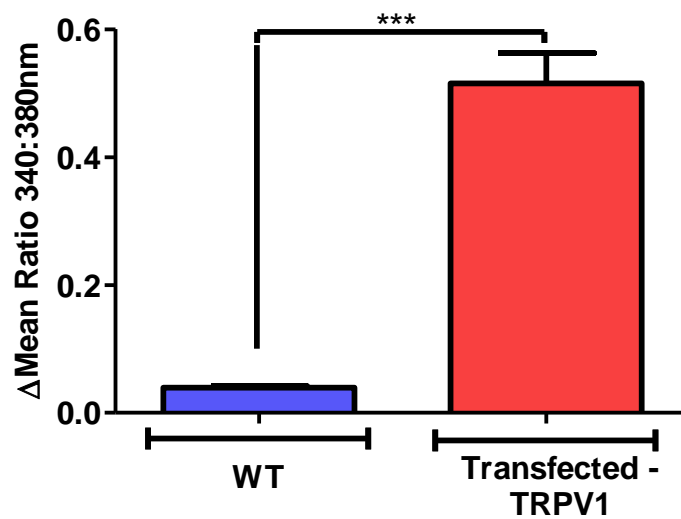


Figure 6.13: Comparing changes in $[Ca^{2+}]_i$ between wild type HeLa and HeLa cells transfected with pcDNA3.1/Zeo(+)TRPV1** construct, in response to reconstitution in 2.5mM $CaCl_2$** - Directly comparing the Δ Mean Ratio 340:380 values for both untransfected (WT) HeLa cells and capsaicin responsive HeLa cells (Transfected - TRPV1) illustrates that the increases in intracellular Ca^{2+} concentration in transfected cells must be pre-dominantly driven or attributed to the expression of recombinant TRPV1. The Δ Mean Ratio 340:380 values are given as \pm SEM from 3 independent experiments (n=3). A student unpaired t test was used to directly compare the Δ Mean Ratio 340:380 values from the WT and Transfected – TRPV1 group. A $P < 0.05$ was considered as significant. ***, < 0.0001 . Δ Mean Ratio 340:380 values < 0.1 were considered as noise.

6.8 Summary of key findings and results

Approach I

- hTRPV1 COS-7 cell exposed to 1 μ M AEA evoked a TRPV1 mediated increase in [Ca²⁺]_i. hTRPV1 COS-7 cells also expressing FABP7 or 8 did not enhance or reduce the potency of AEA at TRPV1 receptors.

Approach II

- CCH could deplete internal ER-Ca²⁺ stores in WT HeLa cells maintained under Ca²⁺ free extracellular media-imaging buffer. When reconstituted in media containing 2.5mM CaCl₂ imaging buffer there were no observable increases in intracellular Ca²⁺ concentration.
- hTRPV1-HeLa cells reconstituted in 2.5mM CaCl₂ resulted in Ca²⁺ re-entry into the cytosol. This re-entry was absent in WT cells implying the Ca²⁺ entry was TRPV1 mediated. Furthermore, the observed TRPV1 Ca²⁺ mediated re-entry was comparable and not significantly different in hTRPV1-HeLa cells pre-treated with CCH or Vehicle. This suggested TRPV1 Ca²⁺ entry was unaffected by CCH treatment.

6.9 Discussion

The main aim of this chapter was to develop a non-native cell line based assay system to probe for a functional relationship between TRPV1 and candidate FABPs. Two approaches were taken, one of which was performed in COS-7 cells. Approach I: Stimulation of TRPV1 with AEA was predicted to be enhanced in cells co-expressing FABP7 or FABP8. This hypothesis was tested by measuring and comparing AEA evoked TRPV1 mediated Ca^{2+} influxes in COS-7 cells expressing TRPV1 alone or co-expressing TRPV1 and FABP7/8. It was found that the levels of AEA evoked TRPV1- Ca^{2+} entry were not enhanced nor reduced in COS-7 cells expressing TRPV1 and FABP7 or 8 and were broadly comparable to those cells only expressing TRPV1.

One of the key reasons for why this was the case could be attributed to the concentration of AEA used to evoke a TRPV1 response. It is possible that using $1\mu\text{M}$ AEA could have been excessive to what was required i.e. this concentration of AEA was sufficient to activate TRPV1, and therefore AEA did not require FABP mediated shuttling to TRPV1 to exert its effect. A future study should titrate the concentration of AEA to establish whether the concentration needs to be reduced further to capture the shuttling capacity/effect of the FABPs evoking or modulating TRPV1-mediated Ca^{2+} entry.

The second reason could lie with a major assumption that was made in this approach. It is assumed that AEA will pass through the plasma membrane into the cytosol where it is sequestered and shuttled by cytosolic FABP to the AEA binding sites in TRPV1. Given that AEA was initially applied exogenously and not generated internally i.e. in the cytosol via NAPE-PLD mediated de novo biosynthesis meant that the applied AEA could have simply moved within the plane of the hydrophobic plasma membrane to the TRPV1 receptors. The membrane

can solubilise what effectively is a hydrophobic-lipophilic entity, making the cytosolic overexpressed FABPs ready to shuttle AEA irrelevant.

Approach II: The previous works of Van der Stelt et al. (65) show that is possible to induce *de novo* synthesis of AEA in HEK293 cells overexpressing recombinant TRPV1 in response to stimulation with muscarinic receptor agonist and Ca^{2+} store depleting agent carbachol (CCH). As already discussed, AEA activates TRPV1 channels and potentiates further increases intracellular Ca^{2+} concentration. It was hypothesized that endogenous FABP5 might mediate the delivery of AEA to TRPV1 and therefore inhibition of FABP5 would reduce AEA evoked TRPV1- Ca^{2+} entry which could be measured using the aforementioned Fura-2AM Ca^{2+} imaging assay system.

Before investigating the effect of FABP5 inhibition on TRPV1 activity, it was necessary to establish that the assay system employed by Van der Stelt et al. (65) could be replicated in HeLa cells. TRPV1 expressing HeLa cells were pre-treated with either vehicle or CCH then reconstituted in imaging buffer containing 2.5mM CaCl_2 however it was found that the magnitude of Ca^{2+} re-entry for the vehicle and CCH treated HeLa cells were similar. This implied that the gating of TRPV1 was entirely independent of CCH treatment and it was, therefore, possible that AEA was not synthesized. Furthermore, the comparable/similar levels of Ca^{2+} entry observed in both the vehicle and CCH treated HeLa cells cannot be attributed to 'leaky cells' given that HeLa cells are non-excitabile. Especially given there were no measurable levels of Ca^{2+} re-entry in response to Ca^{2+} reconstitution when using WT/untransfected cells also treated with CCH. It was therefore concluded that the Ca^{2+} entry observed was mediated by TRPV1.

One reason for the Ca^{2+} influxes observed in both the vehicle and CCH pre-treated TRPV1-HeLa cells could be attributed to the overexpressed TRPV1 channels

already being open. The opening state of TRPV1 could have been influenced by unaccounted for endogenous factors in the HeLa cells; this, however, requires further investigation. In summary, the fundamental problem was the underlying design of the assay system. The ramifications of this meant that little progress was made and the effects of FABP5 inhibition were not explored.

Chapter 7: General discussion

Chapter 7: General discussion

7.1 An alternative approach to TRPV1 antagonism

Antagonism of the TRPV1 receptor has become a key focus in the treatment of pain during the last 10-15 years (5, 39). Despite attempts, there are no synthetic or naturally occurring TRPV1 antagonists, able to both reduce pain and not cause unwanted side effects (5,8). However, in recent years extensive work has established the many ways TRPV1 can be activated or how its activity can be modulated during nociception (5, 3, 39). This thesis hypothesized that it was possible to disrupt one of the many nociceptive specific signalling pathways which regulate TRPV1 activity, as opposed to direct antagonism of the receptor thus avoiding the widespread disruption of other normal physiological processes where TRPV1 is essential i.e. thermoregulation.

A considerable body of research over the last decade has revealed the existence of many endogenous TRPV1 agonists/endovanilloids (67,74). Two of the most well-known examples include 13(S) HODE and the endocannabinoid anandamide (AEA) (62, 72, 74). The aqueous environment of the cytosol dictates that hydrophobic lipid species such as AEA and 13(S) HODE necessitate sequestration in the form of intracellular lipid binding proteins (iLBPs), examples of such iLBPs include members of the fatty acid binding protein family (FABP). The FABPs are cytosolic proteins with a principal role of sequestering free fatty acids and their derivatives from the plasma or nuclear membrane in the cell (104).

The overall aim of this thesis was to define and characterize the FABPs as intracellular carriers for the endovanilloids. It was hypothesized that the FABPs could, therefore, modulate TRPV1 activity by controlling the pool of available endovanilloids during nociception. However, it was essential to establish which FABP isoforms, in physiologically relevant cells or tissues, could be implicated in

endovanilloid trafficking to TRPV1. This would determine which FABP isoforms could be targeted genetically or pharmacologically, as a means indirectly inhibiting TRPV1-mediated Ca^{2+} entry and reducing nociceptor excitability during nociception. In summary, disrupting the transport of pro-algesic lipid cargo could represent an alternative approach to analgesia which would avoid direct TRPV1 antagonism and its associated side effects.

7.2 Proof of concept: Identifying distinct FABP isoforms as intracellular endovanilloid carriers

The expression of the FABPs was assessed in the cells of the DRG isolated from rats. The cell preparation which produced a heterogeneous culture of neuronal cell bodies and their associated satellite glial cells (SGCs) served as a cell model representative of a population of primary sensory neurons. Novel data presented in this thesis shows that FABP 5, 7 and 8 and all 3 PPAR isoforms were expressed in DRG cell cultures at the mRNA level. Importantly these findings were consistent-reproducible between independent DRG cell culture preparations. In summary, the DRG cell preparations-isolations were found to be a suitable cell model.

However, the heterogeneity of DRG cells and non-neuronal satellite glial cells (SGCs) presented a problem. The presence of non-neuronal SGCs meant that it was not possible to definitively conclude whether the identified FABPs and PPAR transcripts were expressed in exclusively neuronal cells or SGCs, or even in both cell types.

Therefore, the method of preparing DRG cell cultures was adapted to allow the separation of the two cell types as described in chapter 2 and 3, to give discrete populations of cells. Gene expression assays performed on the two cell populations showed some differences in the gene expression profile for the FABPs and PPARs. FABP5 and 8 were detectable in both cell populations, while FABP7

was expressed at significantly higher levels in the glial cell population. This was not surprising given that FABP7 has been used a key molecular marker for glial-like cells (16,114,123). All 3 PPAR isoforms were detectable in both cell cultures but at variable levels. However, it emerged that the method used to separate two cell populations did not produce the two distinct cell populations required.

Instead, immunohistochemistry was performed on DRG tissue sections with the available antibodies. IHC also suggested that FABP5 was expressed in neuronal cells (cell bodies) while FABP7 immunostaining appeared to be non-neuronal; however, further investigation is required. Nonetheless, for the first time, the FABPs have been potentially identified in DRG neurons, and the potential of these FABP isoforms to transport endovanilloid was successfully investigated (see section 7.3). The role of PPARs in signalling nociceptive pain processing was not explored further due to time constraints; however, suggestions for future investigation are discussed later in this chapter (see subsection 7.4.3).

7.3 Proof of concept: Characterisation of the identified FABPs as intracellular AEA and 13(S)HODE carriers

It was necessary to establish that the FABPs detected in DRG cultures could physically associate with endogenous TRPV1 ligands (endovanilloids). There is a growing list of emerging endogenous TRPV1 ligands, however, due to time constraints, the two most well-established ligands; AEA and 13(S) HODE were tested (67,74). It has been widely reported that both FABP5 and FABP7 act as intracellular shuttles for AEA (116,120,121) where they mediate the uptake of AEA and other N-acylethanolamines for catabolism to FAAH (76-79). Furthermore, cell-free based competition displacement assays have shown that AEA can physically associate with FABP5 and FABP7, findings which were partly supported by the data reported in chapter 4 (112, 124). In this thesis, it was found that AEA could

bind to FABP7 robustly and for the first time, it was demonstrated that AEA associated with FABP8.

However, unlike the findings of Kaczocha et al. (112), AEA was shown to very weakly associate with FABP5. The inability of FABP5 to associate with AEA was thought to be a consequence of non-functional recombinant FABP5. However, it was found that arachidonic acid could affect a robust displacement of 12-NBD stearate from FABP5 in the competition assay. It was therefore concluded that the inability of FABP5 to bind to AEA did not lie with a loss of its functionality when expressed as N-terminally His tagged protein. In summary, the underlying reasons as to why there was negligible AEA binding at FABP5 require further investigation as to ascertain why the findings of this thesis conflict with previously published data.

13(S) HODE was the second endogenous TRPV1 ligand to be investigated. It has been widely reported that 13(S) HODE is synthesized in response to thermal injury in neuronal tissues (68-70). As discussed in chapter 1 in section 1.7.3, previous work investigating the role of 13(S)HODE in the differentiation of keratinocytes, alluded to the possibility that FABP5 could be potentially implicated in the transportation of 13(S) HODE to lipid sensitive transcription factors (111). It was therefore plausible that FABP5 could bind and shuttle 13(S) HODE cargo to TRPV1 during noxious thermal stimulation.

Given that there was no previous or established experimental evidence reporting on the binding affinities of FABPs 5, 7 and 8 for 13(S) HODE, the binding properties of the three FABPs for 13(S) HODE were all investigated. This thesis for the first time provided evidence to show that 13(S) HODE could physically bind not only to FABP5 but also FABP7 and FABP8. In conclusion, these data suggested that any of the three FABPs identified in the DRG cultures could

sequester then shuttle 13(S)HODE to TRPV1 and evoke TRPV1-mediated Ca²⁺ entry.

7.4 Future work

7.4.1 In situ hybridization (ISH)

It has been shown that a specific repertoire of FABPs is expressed in a heterogeneous cell culture of DRG cells and SGCs. Future work now needs to definitively establish which cell type expresses each identified FABP. Given the limited availability of commercially available antibodies for immunohistochemistry (IHC), alternative methods not reliant on antibodies, such as *in situ* hybridization (ISH) are required. Understanding the distribution or partitioning of FABP expression between DRGs and SGCs is now critical to ascertain exactly which FABP isoform could be implicated in AEA or 13(S) HODE delivery to TRPV1.

7.4.2 Developing alternative approaches to investigating TRPV1/PPAR-FABP interactions in cultured cells

As discussed in chapter 5, despite producing plasmid constructs that encoded for mostly functional YFP-C or YFP-N tagged chimeric proteins, inconsistencies in the absence/presence fluorescence between experimental repeats signified that BiFC was not a viable method for detecting PPIs. For example, initial BiFC data indicated that a physical association existed between TRPV1 and FABPs 5, 7 and 8, however, attempts to replicate this finding were unsuccessful. Furthermore, several positive controls using pairs of proteins widely reported to interact, failed to do so when expressed in COS-7 cells in BiFC assays. This suggested that under the conditions utilized in the assay, these proteins do not interact. Therefore, as briefly alluded to in chapter 5, future work needs to focus on using other fluorescence based techniques such as fluorescence resonance energy transfer (FRET), which are as sensitive as BiFC to capturing transient PPIs, such as those

involving FABPs, but also allow for the direct visualisation of PPIs in their native cellular environment. FRET is widely used in PPI studies and has been successful capturing many interactions, a particularly relevant example includes detecting the interaction and co-localization of FABP4 with the enzyme hormone-sensitive lipase (115).

Alternative PPI techniques that do not rely on the expression of recombinant proteins in non-native cultured cell lines for use in fluorescence based techniques or Ca^{2+} imaging also need to be developed. Instead, isolated DRG cells which already express TRPV1, the FABPs, the enzymes that synthesize endogenous TRPV1 ligands and the metabotropic muscarinic receptor, could be used as a viable alternative to demonstrate TRPV1-FABP interactions under physiologically relevant conditions. Once it is known which FABPs are expressed in the DRG cell bodies, the effects of FABP inhibition on TRPV1 activity could be definitively investigated.

As briefly discussed in chapter 1, previous studies have shown that TRPV1 activation in response to tissue acidosis can upregulate the expression and secretion of the neuropeptide CGRP from DRG cells (40). Therefore, using TaqMan® gene expression assays, immunoblotting or enzyme-linked immunosorbent assays (ELISA), it is possible to investigate/quantify how CGRP expression levels are influenced in response to TRPV1 activation. Despite the findings in chapter 6, previous work by Van der Stelt et al. (65) showed stimulation of the muscarinic receptor with carbachol in DRG cells could successfully induce the de novo synthesis of AEA. The newly synthesized AEA was then able to gate TRPV1 receptors. Therefore, this provides an opportunity to investigate if AEA evoked Ca^{2+} entry in DRG cells influences the expression and secretion of CGRP. If AEA did have an influence and given that AEA is shuttled by the FABPs, assessing the effects of FABP inhibition with pharmacological agents on TRPV1-

mediated increases in CGRP expression, would be a plausible alternative to demonstrate that the FABPs modulate TRPV1 activity.

7.4.3 Investigating the role of PPAR signalling in the DRGs and their possible interactions with the FABPs

The role of PPAR signalling nociceptive pain processing was not explored further due to time constraints. However future work should also focus on establishing the influence of identified FABPs on PPAR activity. Interestingly emerging data from other research groups have also suggested that pharmacological inhibition of FABPs has an anti-nociceptive effect. However, the underlying mechanism involved differs to that hypothesized in this thesis. Inhibition of FABP5 function produces an analgesic effect by reducing the levels of AEA being transported to FAAH for degradation (120). This results in the accumulation of AEA that is then free to activate anti-nociceptive CB receptors. The same mechanism has been observed in the regions of the brain that are associated with cognitive development, where CB receptor activation leads to impaired learning (101). FABP5, therefore, promotes the hydrolysis and inactivation of AEA.

A similar mechanism could be applicable regarding the role of PPAR α . Both OEA and PEA are PPAR α ligands produced at high levels in unstimulated or resting nociceptors. Consequently, PPAR α is constitutively active and therefore able to suppress inflammatory gene expression but also inhibit key ion channels that govern neuronal excitability (95,98).

Given OEA and PEA are both subject to amidase mediated turnover by N-acylethanolamines-hydrolysing enzyme (NAAA) and that FABP5 has been previously shown to bind OEA, it is possible that FABP5 could shuttle OEA to NAAA for degradation under conditions such as inflammatory hyperalgesia, the result of which would be a loss in PPAR α activity and the activation of nociceptive afferents. Therefore, in instances of inflammatory pain, pharmacological

intervention with compounds that inhibit FABP5 function could indirectly maintain PPAR α activity and return the nociceptors to a normal resting state, by preventing the degradation and turnover of ligands such as OEA (92, 95, 98). Conversely, FABP5 has been shown to shuttle OEA to PPAR α in non-native cell lines, therefore could play the opposite role, where disruption of its function could cause pain (112).

Chapter 8: References

Chapter 8: References

1. Caterina, M. J., Schumacher, M. A., Tominaga, M., Rosen, T. A., Levine, J. D., and Julius, D. (1997) The capsaicin receptor: a heat-activated ion channel in the pain pathway. *Nature* **389**, 816-824
2. Tominaga, M., Caterina, M. J., Malmberg, A. B., Rosen, T. A., Gilbert, H., Skinner, K., Raumann, B. E., Basbaum, A. I., and Julius, D. (1998) The cloned capsaicin receptor integrates multiple pain-producing stimuli. *Neuron* **21**, 531-543
3. Brain, S. D., and Annals, N. Y. A. S. (2011) TRPV1 and TRPA1 channels in inflammatory pain: elucidating mechanisms. *Animal Models: Their Value in Predicting Drug Efficacy and Toxicity* **1245**, 36-37
4. Brederson, J.-D., Kym, P. R., and Szallasi, A. (2013) Targeting TRP channels for pain relief. *European Journal of Pharmacology* **716**, 61-76
5. Holzer, P. (2008) The pharmacological challenge to tame the transient receptor potential vanilloid-1 (TRPV1) nociceptor. *British Journal of Pharmacology* **155**, 1145-1162
6. Wong, G. Y., and Gavva, N. R. (2009) Therapeutic potential of vanilloid receptor TRPV1 agonists and antagonists as analgesics: Recent advances and setbacks. *Brain Research Reviews* **60**, 267-277
7. Premkumar, L. S., and Abooj, M. (2013) TRP channels and analgesia. *Life Sciences* **92**, 415-424
8. Szallasi, A., and Sheta, M. (2012) Targeting TRPV1 for pain relief: limits, losers and laurels. *Expert Opinion on Investigational Drugs* **21**, 1351-1369
9. Ghilardi, J. R., Rohrich, H., Lindsay, T. H., Sevcik, M. A., Schwei, M. J., Kubota, K., Halvorson, K. G., Poblete, J., Chaplan, S. R., Dubin, A. E., Carruthers, N. I., Swanson, D., Kuskowski, M., Flores, C. M., Julius, D., and Mantyh, P. W. (2005) Selective blockade of the capsaicin receptor TRPV1 attenuates bone cancer pain. *Journal of Neuroscience* **25**, 3126-3131
10. Gavva, N. R., Bannon, A. W., Surapaneni, S., Hovland, D. N., Jr., Lehto, S. G., Gore, A., Juan, T., Deng, H., Han, B., Klionsky, L., Kuang, R., Le, A., Tamir, R., Wang, J., Youngblood, B., Zhu, D., Norman, M. H., Magal, E., Treanor, J. J. S., and Louis, J.-C. (2007) The vanilloid receptor TRPV1 is tonically activated in vivo and involved in body temperature regulation. *Journal of Neuroscience* **27**, 3366-3374
11. Basbaum, A. I., Bautista, D. M., Scherrer, G., and Julius, D. (2009) Cellular and Molecular Mechanisms of Pain. *Cell* **139**, 267-284

12. Julius, D. (2013) TRP Channels and Pain. *Annual Review of Cell and Developmental Biology*, Vol 29 **29**, 355-384
13. Julius, D., and Basbaum, A. I. (2001) Molecular mechanisms of nociception. *Nature* **413**, 203-210
14. Patapoutian, A., Tate, S., and Woolf, C. J. (2009) Transient receptor potential channels: targeting pain at the source. *Nature Reviews Drug Discovery* **8**, 55-68
15. Woolf, C. J., and Ma, Q. F. (2007) Nociceptors-noxious stimulus detectors. *Neuron* **55**, 353-364
16. Hanani, M. (2005) Satellite glial cells in sensory ganglia: from form to function. *Brain Research Reviews* **48**, 457-476
17. Huang, J., Zhang, X., and McNaughton, P. A. (2006) Inflammatory pain: The cellular basis of heat hyperalgesia. *Current Neuropharmacology* **4**, 197-206
18. Lawson, S. N. (2002) Phenotype and function of somatic primary afferent nociceptive neurones with C-, A delta- or A alpha/beta-fibres. *Experimental Physiology* **87**, 239-244
19. Lawson, S. N., McCarthy, P. W., and Prabhakar, E. (1996) Electrophysiological properties of neurones with CGRP-like immunoreactivity in rat dorsal root ganglia. *Journal of Comparative Neurology* **365**, 355-366
20. Lindsay, R. M. (1988) NERVE GROWTH-FACTORS (NGF, BDNF) ENHANCE AXONAL REGENERATION BUT ARE NOT REQUIRED FOR SURVIVAL OF ADULT SENSORY NEURONS. *Journal of Neuroscience* **8**, 2394-2405
21. Todd, A. J. (2010) Neuronal circuitry for pain processing in the dorsal horn. *Nature Reviews Neuroscience* **11**, 823-836
22. Mathie, A. (2010) Ion channels as novel therapeutic targets in the treatment of pain. *Journal of Pharmacy and Pharmacology* **62**, 1089-1095
23. Hucho, T., and Levine, J. D. (2007) Signaling pathways in sensitization: Toward a nociceptor cell biology. *Neuron* **55**, 365-376
24. Venkatachalam, K., and Montell, C. (2007) TRP channels. in *Annual Review of Biochemistry*, Annual Reviews, Palo Alto. pp 387-417
25. Masuyama, R., Voets, T., Karashima, Y., Torrekens, S., Moermans, K., Bosch, A. V., Bouillon, R., Nilius, B., and Carmeliet, G. (2008) TRPV4-mediated calcium influx regulates terminal differentiation of osteoclasts. *Bone* **42**, S39-S39
26. Masuyama, R., Vriens, J., Voets, T., Karashima, Y., Owsianik, G., Vennekens, R., Lieben, L., Torrekens, S., Moermans, K., Bosch, A. V., Bouillon, R., Nilius, B., and Carmeliet, G. (2008) TRPV4-mediated calcium influx regulates terminal differentiation of Osteoclasts. *Cell Metabolism* **8**, 257-265

27. Shim, W. S., Tak, M. H., Lee, M. H., Kim, M., Koo, J. Y., Lee, C. H., and Oh, U. (2007) TRPV1 mediates histamine-induced itching via the activation of phospholipase A(2) and 12-lipoxygenase. *Journal of Neuroscience* **27**, 2331-2337
28. Engler, A., Aeschlimann, A., Simmen, B. R., Michel, B. A., Gay, R. E., Gay, S., and Sprott, H. (2007) Expression of transient receptor potential vanilloid 1 (TRPV1) in synovial fibroblasts from patients with osteoarthritis and rheumatoid arthritis. *Biochemical and Biophysical Research Communications* **359**, 884-888
29. Idris, A. I., Landao-Bassonga, E., and Ralston, S. H. (2010) The TRPV1 ion channel antagonist capsazepine inhibits osteoclast and osteoblast differentiation in vitro and ovariectomy induced bone loss in vivo. *Bone* **46**, 1089-1099
30. Asagiri, M., and Takayanagi, H. (2007) The molecular understanding of osteoclast differentiation. *Bone* **40**, 251-264
31. Jules, J., Shi, Z. Q., Liu, J. Z., Xu, D. R., Wang, S. Q., and Feng, X. (2010) Receptor Activator of NF-kappa B (RANK) Cytoplasmic IVVY535-538 Motif Plays an Essential Role in Tumor Necrosis Factor-alpha (TNF)-mediated Osteoclastogenesis. *Journal of Biological Chemistry* **285**, 37427-37435
32. Hayami, T., Pickarski, M., Wesolowski, G. A., McLane, J., Bone, A., Destefano, J., Rodan, G. A., and Duong, L. T. (2004) The role of subchondral bone remodeling in osteoarthritis - Reduction of cartilage degeneration and prevention of osteophyte formation by alendronate in the rat anterior cruciate ligament transection model. *Arthritis and Rheumatism* **50**, 1193-1206
33. Wada, T., Nakashima, T., Hiroshi, N., and Penninger, J. M. (2006) RANKL-RANK signaling in osteoclastogenesis and bone disease. *Trends in Molecular Medicine* **12**, 17-25
34. Boyce, B. F., and Xing, L. (2007) Biology of RANK, RANKL, and osteoprotegerin. *Arthritis Research & Therapy* **9**
35. Weilbaecher, K. N., Motyckova, G., Huber, W. E., Takemoto, C. M., Hemesath, T. J., Xu, Y., Hershey, C. L., Dowland, N. R., Wells, A. G., and Fisher, D. E. (2001) Linkage of M-CSF signaling to Mitf, TFE3, and the osteoclast defect in Mitf(mi/mi) mice. *Molecular Cell* **8**, 749-758
36. Hellwig, N., Albrecht, N., Harteneck, C., Schultz, G., and Schaefer, M. (2005) Homo- and heteromeric assembly of TRPV channel subunits. *Journal of Cell Science* **118**, 917-928
37. Szolcsanyi, J. (2014) Capsaicin and Sensory Neurones: A Historical Perspective. *Capsaicin as a Therapeutic Molecule* **68**, 1-37
38. Leffler, A., Moenter, B., Caterina, M. J., Julius, D., and Koltzenburg, M. (2000) Disruption of the vanilloid receptor 1 gene impairs the responses of sensory

neurons to protons. *Society for Neuroscience Abstracts* **26**, Abstract No.-632.631

39. Szallasi, A., Cortright, D. N., Blum, C. A., and Eid, S. R. (2007) The vanilloid receptor TRPV1: 10 years from channel cloning to antagonist proof-of-concept (vol 6, pg 357, 2007). *Nature Reviews Drug Discovery* **6**
40. Nakanishi, M., Hata, K., Nagayama, T., Sakurai, T., Nishisho, T., Wakabayashi, H., Hiraga, T., Ebisu, S., and Yoneda, T. (2010) Acid Activation of Trpv1 Leads to an Up-Regulation of Calcitonin Gene-related Peptide Expression in Dorsal Root Ganglion Neurons via the CaMK-CREB Cascade: A Potential Mechanism of Inflammatory Pain. *Molecular Biology of the Cell* **21**, 2568-2577
41. Kaszas, K., Keller, J. M., Coddou, C., Mishra, S. K., Hoon, M. A., Stojilkovic, S., Jacobson, K. A., and Iadarola, M. J. (2012) Small Molecule Positive Allosteric Modulation of TRPV1 Activation by Vanilloids and Acidic pH. *Journal of Pharmacology and Experimental Therapeutics* **340**, 152-160
42. Yoneda, T., Nakanishi, M., Nishisho, T., Wakabayashi, H., and Hata, K. (2011) Involvement of acidic microenvironment in bone pain associated with cancer colonization. *Bone* **48**, S11-S11
43. Yoneda, T., Hata, K., Nakanishi, M., Nagae, M., Nagayama, T., Wakabayashi, H., Nishisho, T., Sakurai, T., and Hiraga, T. (2011) Involvement of acidic microenvironment in the pathophysiology of cancer-associated bone pain. *Bone* **48**, 100-105
44. Trevisani, M., Smart, D., Gunthorpe, M. J., Tognetto, M., Barbieri, M., Campi, B., Amadesi, S., Gray, J., Jerman, J. C., Brough, S. J., Owen, D., Smith, G. D., Randall, A. D., Harrison, S., Bianchi, A., Davis, J. B., and Geppetti, P. (2002) Ethanol elicits and potentiates nociceptor responses via the vanilloid receptor-1. *Nature Neuroscience* **5**, 546-551
45. Schaible, H. G., Ebersberger, A., and Natura, G. (2011) Update on peripheral mechanisms of pain: beyond prostaglandins and cytokines. *Arthritis Research & Therapy* **13**
46. Spicarova, D., and Palecek, J. (2010) Tumor necrosis factor alpha sensitizes spinal cord TRPV1 receptors to the endogenous agonist N-oleoyldopamine. *Journal of Neuroinflammation* **7**, 7
47. Devesa, I., Planells-Cases, R., Fernandez-Ballester, G., Gonzalez-Ros, J. M., Ferrer-Montiel, A., and Fernandez-Carvajal, A. (2011) Role of the transient receptor potential vanilloid 1 in inflammation and sepsis. *Journal of inflammation research* **4**, 67-81
48. Zhang, X. M., Huang, J. H., and McNaughton, P. A. (2005) NGF rapidly increases membrane expression of TRPV1 heat-gated ion channels. *Embo Journal* **24**, 4211-4223
49. Huang, J. J., Zhang, X. M., and McNaughton, P. A. (2006) Modulation of

- temperature-sensitive TRP channels. *Seminars in Cell & Developmental Biology* **17**, 638-645
50. Zhuang, Z. Y., Xu, H. X., Clapham, D. E., and Ji, R. R. (2004) Phosphatidylinositol 3-kinase activates ERK in primary sensory neurons and mediates inflammatory heat hyperalgesia through TRPV1 sensitization. *Journal of Neuroscience* **24**, 8300-8309
 51. Moriyama, T., Higashi, T., Togashi, K., Iida, T., Segi, E., Sugimoto, Y., Tominaga, T., Narumiya, S., and Tominaga, M. (2005) Sensitization of TRPV1 by EP1 and IP reveals peripheral nociceptive mechanism of prostaglandins. *Molecular Pain* **1**
 52. Mu, Z. Z., and Pan, H. L. (2007) Role of TRPV1 and intracellular Ca²⁺ in excitation of cardiac sensory neurons by bradykinin. *American Journal of Physiology-Regulatory Integrative and Comparative Physiology* **293**, R276-R283
 53. Shin, J., Cho, H., Hwang, S. W., Jung, J., Shin, C. Y., Lee, S. Y., Kim, S. H., Lee, M. G., Choi, Y. H., Kim, J., Haber, N. A., Reichling, D. B., Khasar, S., Levine, J. D., and Oh, U. (2002) Bradykinin-12-lipoxygenase-VR1 signaling pathway for inflammatory hyperalgesia. *Proceedings of the National Academy of Sciences of the United States of America* **99**, 10150-10155
 54. Chuang, H. H., Prescott, E. D., Kong, H. Y., Shields, S., Jordt, S. E., Basbaum, A. I., Chao, M. V., and Julius, D. (2001) Bradykinin and nerve growth factor release the capsaicin receptor from PtdIns(4,5)P₂-mediated inhibition. *Nature* **411**, 957-962
 55. Ricciotti, E., and FitzGerald, G. A. (2011) Prostaglandins and Inflammation. *Arteriosclerosis Thrombosis and Vascular Biology* **31**, 986-1000
 56. Vellani, V., Mapplebeck, S., Moriondo, A., Davis, J. B., and McNaughton, P. A. (2001) Protein kinase C activation potentiates gating of the vanilloid receptor VR1 by capsaicin, protons, heat and anandamide. *Journal of Physiology-London* **534**, 813-825
 57. Van der Stelt, M., and Di Marzo, V. (2004) Endovanilloids - Putative endogenous ligands of transient receptor potential vanilloid 1 channels. *European Journal of Biochemistry* **271**, 1827-1834
 58. Morales-Lazaro, S. L., Simon, S. A., and Rosenbaum, T. (2013) The role of endogenous molecules in modulating pain through transient receptor potential vanilloid 1 (TRPV1). *Journal of Physiology-London* **591**, 3109-3121
 59. Huang, S. M., Bisogno, T., Trevisani, M., Al-Hayani, A., De Petrocellis, L., Fezza, F., Tognetto, M., Petros, T. J., Krey, J. F., Chu, C. J., Miller, J. D., Davies, S. N., Geppetti, P., Walker, J. M., and Di Marzo, V. (2002) An endogenous capsaicin-like substance with high potency at recombinant and native vanilloid VR1 receptors. *Proceedings of the National Academy of Sciences of the United States*

60. Hwang, S. W., Cho, H., Shin, J. S., Cho, S. H., Lee, S. Y., Kang, C. J., Kwak, J. Y., Wang, M. H., Suh, Y. G., and Oh, U. (1999) Direct activation of capsaicin receptors by products of lipoxygenases: Endogenous capsaicin-like substances. *Society for Neuroscience Abstracts* **25**, 2256
61. Chu, C. J., Huang, S. M., De Petrocellis, L., Bisogno, T., Ewing, S. A., Miller, J. D., Zipkin, R. E., Daddario, N., Appendino, G., Di Marzo, V., and Walker, J. M. (2003) N-oleoyldopamine, a novel endogenous capsaicin-like lipid that produces hyperalgesia. *Journal of Biological Chemistry* **278**, 13633-13639
62. Ross, R. A. (2003) Anandamide and vanilloid TRPV1 receptors. *British Journal of Pharmacology* **140**, 790-801
63. Zygmunt, P. M., Julius, D., Di Marzo, V., and Hogestatt, E. D. (2000) Anandamide - the other side of the coin. *Trends in Pharmacological Sciences* **21**, 43-44
64. Di Marzo, V., and De Petrocellis, L. (2010) Endocannabinoids as Regulators of Transient Receptor Potential (TRP) Channels: a Further Opportunity to Develop New Endocannabinoid-Based Therapeutic Drugs. *Current Medicinal Chemistry* **17**, 1430-1449
65. Van der Stelt, M., Trevisani, M., Vellani, V., De Petrocellis, L., Moriello, A. S., Campi, B., McNaughton, P., Geppetti, P., and Di Marzo, V. (2005) Anandamide acts as an intracellular messenger amplifying Ca²⁺ influx via TRPV1 channels. *Embo Journal* **24**, 3026-3037
66. Zygmunt, P. M., Petersson, J., Andersson, D. A., Chuang, H. H., Sorgard, M., Di Marzo, V., Julius, D., and Hogestatt, E. D. (1999) Vanilloid receptors on sensory nerves mediate the vasodilator action of anandamide. *Nature* **400**, 452-457
67. Starowicz, K., Nigam, S., and Di Marzo, V. (2007) Biochemistry and pharmacology of endovanilloids. *Pharmacology & Therapeutics* **114**, 13-33
68. Patwardhan, A. M., Akopian, A. N., Ruparel, N. B., Diogenes, A., Weintraub, S. T., Uhlson, C., Murphy, R. C., and Hargreaves, K. M. (2010) Heat generates oxidized linoleic acid metabolites that activate TRPV1 and produce pain in rodents. *Journal of Clinical Investigation* **120**, 1617-1626
69. Patwardhan, A. M., Scotland, P. E., Akopian, A. N., and Hargreaves, K. M. (2009) Activation of TRPV1 in the spinal cord by oxidized linoleic acid metabolites contributes to inflammatory hyperalgesia. *Proceedings of the National Academy of Sciences of the United States of America* **106**, 18820-18824
70. Ruparel, S., Green, D., Chen, P., and Hargreaves, K. M. (2012) The cytochrome P450 inhibitor, ketoconazole, inhibits oxidized linoleic acid metabolite-mediated peripheral inflammatory pain. *Molecular Pain* **8**, 9
71. Ruparel, S., Henry, M. A., Akopian, A., Patil, M., Zeldin, D. C., Roman, L., and

- Hargreaves, K. M. (2012) Plasticity of cytochrome P450 isozyme expression in rat trigeminal ganglia neurons during inflammation. *Pain* **153**, 2031-2039
72. Jarvis, M. F. (2012) Cytochrome P450 mediated linoleic acid metabolism in peripheral inflammatory nociception. *Pain* **153**, 1987-1988
73. Green, D. P., Ruparel, S., Roman, L., Henry, M. A., and Hargreaves, K. M. (2013) Role of endogenous TRPV1 agonists in a postburn pain model of partial-thickness injury. *Pain* **154**, 2512-2520
74. Alsalem, M., Wong, A., Millns, P., Arya, P. H., Chan, M. S. L., Bennett, A., Barrett, D. A., Chapman, V., and Kendall, D. A. (2013) The contribution of the endogenous TRPV1 ligands 9-HODE and 13-HODE to nociceptive processing and their role in peripheral inflammatory pain mechanisms. *British Journal of Pharmacology* **168**, 1961-1974
75. De Petrocellis, L., Moriello, A. S., Imperatore, R., Cristino, L., Starowicz, K., and Di Marzo, V. (2012) A re-evaluation of 9-HODE activity at TRPV1 channels in comparison with anandamide: enantioselectivity and effects at other TRP channels and in sensory neurons. *British Journal of Pharmacology* **167**, 1643-1651
76. Cravatt, B. F., Giang, D. K., Mayfield, S. P., Boger, D. L., Lerner, R. A., and Gilula, N. B. (1996) Molecular characterization of an enzyme that degrades neuromodulatory fatty-acid amides. *Nature* **384**, 83-87
77. Day, T. A., Rakhshan, F., Deutsch, D. G., and Barker, E. L. (2001) Role of fatty acid amide hydrolase in the transport of the endogenous cannabinoid anandamide. *Molecular Pharmacology* **59**, 1369-1375
78. Kaczocha, M., Hermann, A., Glaser, S. T., Bojesen, I. N., and Deutsch, D. G. (2006) Anandamide uptake is consistent with rate-limited diffusion and is regulated by the degree of its hydrolysis by fatty acid amide hydrolase. *Journal of Biological Chemistry* **281**, 9066-9075
79. Glaser, S. T., Kaczocha, M., and Deutsch, D. G. (2005) Anandamide transport: A critical review. *Life Sciences* **77**, 1584-1604
80. Ricote, M., and Glass, C. K. (2007) PPARs and molecular mechanisms of transrepression. *Biochimica Et Biophysica Acta-Molecular and Cell Biology of Lipids* **1771**, 926-935
81. Berger, J., and Moller, D. E. (2002) The mechanisms of action of PPARs. *Annual Review of Medicine* **53**, 409-435
82. Itoh, T., Fairall, L., Amin, K., Inaba, Y., Szanto, A., Balint, B. L., Nagy, L., Yamamoto, K., and Schwabe, J. W. R. (2008) Structural basis for the activation of PPAR gamma by oxidized fatty acids. *Nature Structural & Molecular Biology* **15**, 924-931

83. Berger, J., and Wagner, J. A. (2002) Physiological and therapeutic roles of peroxisome proliferator-activated receptors. *Diabetes technology & therapeutics* **4**, 163-174
84. Yu, S. L., Levi, L., Siegel, R., and Noy, N. (2012) Retinoic Acid Induces Neurogenesis by Activating Both Retinoic Acid Receptors (RARs) and Peroxisome Proliferator-activated Receptor beta/delta (PPAR beta/delta). *Journal of Biological Chemistry* **287**, 42195-42205
85. Varga, T., Czimmerer, Z., and Nagy, L. (2011) PPARs are a unique set of fatty acid regulated transcription factors controlling both lipid metabolism and inflammation. *Biochimica Et Biophysica Acta-Molecular Basis of Disease* **1812**, 1007-1022
86. Waku, T., Shiraki, T., Oyama, T., Fujimoto, Y., Maehara, K., Kamiya, N., Jingami, H., and Morikawa, K. (2009) Structural Insight into PPAR gamma Activation Through Covalent Modification with Endogenous Fatty Acids. *Journal of Molecular Biology* **385**, 188-199
87. Wang, Y., Li, B., and Li, Y. (2011) Research progression of PPARgamma to bone remodeling. *Sheng wu yi xue gong cheng xue za zhi = Journal of biomedical engineering = Shengwu yixue gongchengxue zazhi* **28**, 213-216
88. Wei, W., Wang, X. D., Yang, M., Smith, L. C., Dechow, P. C., and Wian, Y. H. (2010) PGC1 beta Mediates PPAR gamma Activation of Osteoclastogenesis and Rosiglitazone-Induced Bone Loss. *Cell Metabolism* **11**, 503-516
89. Wei, W., and Wan, Y. (2011) Thiazolidinediones on PPAR gamma: The Roles in Bone Remodeling. *Ppar Research*
90. Maeda, T., and Kishioka, S. (2009) PPAR AND PAIN. *Advances in Neuropharmacology* **85**, 165-177
91. Lin, Q. O., Ruuska, S. E., Shaw, N. S., Dong, D., and Noy, N. (1999) Ligand selectivity of the peroxisome proliferator-activated receptor alpha. *Biochemistry* **38**, 185-190
92. LoVerme, J., Russo, R., La Rana, G., Fu, J., Farthing, J., Mattace-Raso, G., Meli, R., Hohmann, A., Calignano, A., and Piomelli, D. (2006) Rapid broad-spectrum analgesia through activation of peroxisome proliferator-activated receptor-alpha. *Journal of Pharmacology and Experimental Therapeutics* **319**, 1051-1061
93. Costa, B., Comelli, F., Bettoni, I., Colleoni, M., and Giagnoni, G. (2008) The endogenous fatty acid amide, palmitoylethanolamide, has anti-allodynic and anti-hyperalgesic effects in a murine model of neuropathic pain: involvement of CB1, TRPV1 and PPAR gamma receptors and neurotrophic factors. *Pain* **139**, 541-550

94. Ambrosino, P., Soldovieri, M. V., Russo, C., and Tagliatela, M. (2013) Activation and desensitization of TRPV1 channels in sensory neurons by the PPAR alpha agonist palmitoylethanolamide. *British Journal of Pharmacology* **168**, 1430-1444
95. D'Agostino, G., La Rana, G., Russo, R., Sasso, O., Iacono, A., Esposito, E., Raso, G. M., Cuzzocrea, S., Lo Verme, J., Piomelli, D., Meli, R., and Calignano, A. (2007) Acute intracerebroventricular administration of palmitoylethanolamide, an endogenous peroxisome proliferator-activated receptor-alpha agonist, modulates carrageenan-induced paw edema in mice. *Journal of Pharmacology and Experimental Therapeutics* **322**, 1137-1143
96. Jhaveri, M. D., Richardson, D., Robinson, I., Garle, M. J., Patel, A., Sun, Y., Sagar, D. R., Bennett, A. J., Alexander, S. P. H., Kendall, D. A., Barrett, D. A., and Chapman, V. (2008) Inhibition of fatty acid amide hydrolase and cyclooxygenase-2 increases levels of endocannabinoid related molecules and produces analgesia via peroxisome proliferator-activated receptor-alpha in a model of inflammatory pain. *Neuropharmacology* **55**, 85-93
97. Di Cesare Mannelli, L., D'Agostino, G., Pacini, A., Russo, R., Zanardelli, M., Ghelardini, C., and Calignano, A. (2013) Palmitoylethanolamide is a disease-modifying agent in peripheral neuropathy: pain relief and neuroprotection share a PPAR-alpha-mediated mechanism. *Mediators of Inflammation* **2013**, 328797
98. Khasabova, I. A., Xiong, Y., Coicou, L. G., Piomelli, D., and Seybold, V. (2012) Peroxisome Proliferator-Activated Receptor alpha Mediates Acute Effects of Palmitoylethanolamide on Sensory Neurons. *Journal of Neuroscience* **32**, 12735-12743
99. Hughes, M. L. R., Liu, B., Halls, M. L., Wagstaff, K. M., Patil, R., Velkov, T., Jans, D. A., Bunnett, N. W., Scanlon, M. J., and Porter, C. J. H. (2015) Fatty Acid-binding Proteins 1 and 2 Differentially Modulate the Activation of Peroxisome Proliferator-activated Receptor alpha in a Ligand-selective Manner. *Journal of Biological Chemistry* **290**, 13895-13906
100. Morgan, E., Kannan-Thulasiraman, P., and Noy, N. (2010) Involvement of Fatty Acid Binding Protein 5 and PPARbeta/delta in Prostate Cancer Cell Growth. *PPAR research* **2010**
101. Yu, S., Levi, L., Casadesus, G., Kunos, G., and Noy, N. (2014) Fatty Acid-binding Protein 5 (FABP5) Regulates Cognitive Function Both by Decreasing Anandamide Levels and by Activating the Nuclear Receptor Peroxisome Proliferator activated Receptor beta/delta (PPAR beta/delta) in the Brain. *Journal of Biological Chemistry* **289**, 12748-12758
102. Kannan-Thulasiraman, P., Seachrist, D. D., Mahabeleshwar, G. H., Jain, M. K., and Noy, N. (2011) Fatty acid-binding protein 5 and PPAR beta/delta are critical mediators of epidermal growth factor receptor-induced carcinoma cell growth (vol 285, pg 19106, 2010). *Journal of Biological Chemistry* **286**, 36161-36161

103. Furuhashi, M., and Hotamisligil, G. S. (2008) Fatty acid-binding proteins: role in metabolic diseases and potential as drug targets. *Nature Reviews Drug Discovery* **7**, 489-503
104. Storch, J., and McDermott, L. (2009) Structural and functional analysis of fatty acid-binding proteins. *Journal of Lipid Research* **50**, S126-S131
105. Storch, J., and Thumser, A. E. (2010) Tissue-specific Functions in the Fatty Acid-binding Protein Family. *Journal of Biological Chemistry* **285**, 32679-32683
106. Tan, N. S., Shaw, N. S., Vinckenbosch, N., Liu, P., Yasmin, R., Desvergne, B., Wahli, W., and Noy, N. (2002) Selective cooperation between fatty acid binding proteins and peroxisome proliferator-activated receptors in regulating transcription (vol 22, pg 5119, 2002). *Molecular and Cellular Biology* **22**, 6318-6318
107. Helledie, T., Antonius, M., Sorensen, R. V., Hertzog, A. V., Bernlohr, D. A., Kolvraa, S., Kristiansen, K., and Mandrup, S. (2000) Lipid-binding proteins modulate ligand-dependent trans-activation by peroxisome proliferator-activated receptors and localize to the nucleus as well as the cytoplasm. *Journal of Lipid Research* **41**, 1740-1751
108. Umemoto, T., and Fujiki, Y. (2012) Ligand-dependent nucleo-cytoplasmic shuttling of peroxisome proliferator-activated receptors, PPAR alpha and PPAR gamma. *Genes to Cells* **17**, 576-596
109. Doud, M. K., Noy, N., and Tochtrop, G. P. (2014) Inhibition of fatty acid binding protein 5 suppresses mammary carcinoma cell growth in a retinoic acid dependent manner. *Abstracts of Papers of the American Chemical Society* **248**
110. Armstrong, E. H., Goswami, D., Griffin, P. R., Noy, N., and Ortlund, E. A. (2014) Structural Basis for Ligand Regulation of the Fatty Acid-binding Protein 5, Peroxisome Proliferator-activated Receptor beta/delta (FABP5-PPAR beta/delta) Signaling Pathway. *Journal of Biological Chemistry* **289**, 14941-14954
111. Ogawa, E., Owada, Y., Ikawa, S., Adachi, Y., Egawa, T., Nemoto, K., Suzuki, K., Hishinuma, T., Kawashima, H., Kondo, H., Muto, M., Aiba, S., and Okuyama, R. (2011) Epidermal FABP (FABP5) Regulates Keratinocyte Differentiation by 13(S)-HODE-Mediated Activation of the NF-kappa B Signaling Pathway. *Journal of Investigative Dermatology* **131**, 604-612
112. Kaczocha, M., Vivieca, S., Sun, J., Glaser, S. T., and Deutsch, D. G. (2012) Fatty Acid-binding Proteins Transport N-Acylethanolamines to Nuclear Receptors and Are Targets of Endocannabinoid Transport Inhibitors. *Journal of Biological Chemistry* **287**, 3415-3424
113. Ayers, S. D., Nedrow, K. L., Gillilan, R. E., and Noy, N. (2007) Continuous nucleocytoplasmic shuttling underlies transcriptional activation of PPAR gamma

by FABP4. *Biochemistry* **46**, 6744-6752

114. De Rosa, A., Pellegatta, S., Rossi, M., Tunici, P., Magnoni, L., Speranza, M. C., Malusa, F., Miragliotta, V., Mori, E., Finocchiaro, G., and Bakker, A. (2012) A Radial Glia Gene Marker, Fatty Acid Binding Protein 7 (FABP7), Is Involved in Proliferation and Invasion of Glioblastoma Cells. *Plos One* **7**
115. Mita, R., Beaulieu, M. J., Field, C., and Godbout, R. (2010) Brain Fatty Acid-binding Protein and omega-3/omega-6 Fatty Acids MECHANISTIC INSIGHT INTO MALIGNANT GLIOMA CELL MIGRATION. *Journal of Biological Chemistry* **285**, 37005-37015
116. Kaczocha, M., Glaser, S. T., and Deutsch, D. G. (2009) Identification of intracellular carriers for the endocannabinoid anandamide. *Proceedings of the National Academy of Sciences of the United States of America* **106**, 6375-6380
117. Winter, J., Forbes, C. A., Sternberg, J., and Lindsay, R. M. (1988) NERVE GROWTH-FACTOR (NGF) REGULATES ADULT-RAT CULTURED DORSAL-ROOT GANGLION NEURON RESPONSES TO THE EXCITOTOXIN CAPSAICIN. *Neuron* **1**, 973-981
118. Cummins, T. R., Rush, A. M., Estacion, M., Dib-Hajj, S. D., and Waxman, S. G. (2009) Voltage-clamp and current-clamp recordings from mammalian DRG neurons. *Nature Protocols* **4**, 1103-1112
119. Malin, S. A., Davis, B. M., and Molliver, D. C. (2007) Production of dissociated sensory neuron cultures and considerations for their use in studying neuronal function and plasticity. *Nature Protocols* **2**, 152-160
120. Berger, W. T., Ralph, B. P., Kaczocha, M., Sun, J., Balius, T. E., Rizzo, R. C., Haj-Dahmane, S., Ojima, I., and Deutsch, D. G. (2012) Targeting Fatty Acid Binding Protein (FABP) Anandamide Transporters - A Novel Strategy for Development of Anti-Inflammatory and Anti-Nociceptive Drugs. *Plos One* **7**, 12
121. Kaczocha, M., Rebecchi, M. J., Ralph, B. P., Teng, Y.-H. G., Berger, W. T., Galbavy, W., Elmes, M. W., Glaser, S. T., Wang, L., Rizzo, R. C., Deutsch, D. G., and Ojima, I. (2014) Inhibition of Fatty Acid Binding Proteins Elevates Brain Anandamide Levels and Produces Analgesia. *Plos One* **9**
122. Kaczocha, M., Glaser, S. T., Maher, T., Clavin, B., Hamilton, J., O'Rourke, J., Rebecchi, M., Puopolo, M., Owada, Y., and Thanos, P. K. (2015) Fatty acid binding protein deletion suppresses inflammatory pain through endocannabinoid/N-acylethanolamine-dependent mechanisms. *Molecular Pain* **11**
123. Kurata, S., Goto, T., Gunjigake, K. K., Kataoka, S., Kuroishi, K. N., Ono, K., Toyono, T., Kobayashi, S., and Yamaguchi, K. (2013) Nerve Growth Factor Involves Mutual Interaction between Neurons and Satellite Glial Cells in the Rat Trigeminal Ganglion. *Acta Histochemica Et Cytochemica* **46**, 65-73

124. Sanson, B., Wang, T., Sun, J., Wang, L., Kaczocha, M., Ojima, I., Deutsch, D., and Li, H. (2014) Crystallographic study of FABP5 as an intracellular endocannabinoid transporter. *Acta Crystallographica Section D-Biological Crystallography* **70**, 290-298
125. Kane, C. D., and Bernlohr, D. A. (1996) A simple assay for intracellular lipid-binding proteins using displacement of 1-anilinonaphthalene 8-sulfonic acid. *Analytical Biochemistry* **233**, 197-204
126. Rosano, G. L., and Ceccarelli, E. A. (2014) Recombinant protein expression in *Escherichia coli*: advances and challenges. *Frontiers in Microbiology* **5**
127. Kerppola, T. K. (2006) Visualization of molecular interactions by fluorescence complementation. *Nature Reviews Molecular Cell Biology* **7**, 449-456
128. Kerppola, T. K. (2008) Bimolecular fluorescence complementation: Visualization of molecular interactions in living cells. in *Fluorescent Proteins, Second Edition* (Sullivan, K. F. ed.). pp 431-+
129. Kerppola, T. K. (2008) Biomolecular fluorescence complementation (BiFC) analysis as a probe of protein interactions in living cells. in *Annual Review of Biophysics*. pp 465-487
130. Kerppola, T. K. (2009) Visualization of molecular interactions using bimolecular fluorescence complementation analysis: Characteristics of protein fragment complementation. *Chemical Society Reviews* **38**, 2876-2886
131. Kerppola, T. K. (2006) Design and implementation of bimolecular fluorescence complementation (BiFC) assays for the visualization of protein interactions in living cells. *Nature Protocols* **1**, 1278-1286
132. Tsien, R. Y. (1998) The green fluorescent protein. *Annual Review of Biochemistry* **67**, 509-544
133. Wachter, R. M., Elsliger, M. A., Kallio, K., Hanson, G. T., and Remington, S. J. (1998) Structural basis of spectral shifts in the yellow-emission variants of green fluorescent protein. *Structure with Folding & Design* **6**, 1267-1277
134. Griesbeck, O., Baird, G. S., Campbell, R. E., Zacharias, D. A., and Tsien, R. Y. (2001) Reducing the environmental sensitivity of yellow fluorescent protein - Mechanism and applications. *Journal of Biological Chemistry* **276**, 29188-29194
135. Grinberg, A. V., Hu, C. D., and Kerppola, T. K. (2004) Visualization of Myc/Max/Mad family dimers and the competition for dimerization in living cells. *Molecular and Cellular Biology* **24**, 4294-4308
136. Hu, C. D., Chinenov, Y., and Kerppola, T. K. (2002) Visualization of interactions among bZip and Rel family proteins in living cells using bimolecular fluorescence complementation. *Molecular Cell* **9**, 789-798

137. Robida, A. M., and Kerppola, T. K. (2009) Bimolecular Fluorescence Complementation Analysis of Inducible Protein Interactions: Effects of Factors Affecting Protein Folding on Fluorescent Protein Fragment Association. *Journal of Molecular Biology* **394**, 391-409
138. Hostetler, H. A., McIntosh, A. L., Atshaves, B. P., Storey, S. M., Payne, H. R., Kier, A. B., and Schroeder, F. (2009) L-FABP directly interacts with PPAR alpha in cultured primary hepatocytes. *Journal of Lipid Research* **50**, 1663-1675
139. Kannan-Thulasiraman, P., Seachrist, D. D., Mahabeleshwar, G. H., Jain, M. K., and Noy, N. (2010) Fatty Acid-binding Protein 5 and PPAR beta/delta Are Critical Mediators of Epidermal Growth Factor Receptor-induced Carcinoma Cell Growth. *Journal of Biological Chemistry* **285**, 19106-19115
140. Hertzler, A. V., Hellberg, K., Reynolds, J. M., Kruse, A. C., Juhlmann, B. E., Smith, A. J., Sanders, M. A., Ohlendorf, D. H., Suttles, J., and Bernlohr, D. A. (2009) Identification and Characterization of a Small Molecule Inhibitor of Fatty Acid Binding Proteins. *Journal of Medicinal Chemistry* **52**, 6024-6031
141. Smith, A., Sanders, M., Londos, C., and Bernlohr, D. (2004) Co-localization of hormone-sensitive lipase and adipocyte fatty acid binding protein using fluorescence resonance energy transfer. *Faseb Journal* **18**, C263-C263

Chapter 9: Appendices

Chapter 9: Appendices

9.1 PCR cloning primers and the corresponding plasmid DNA vectors constructed.

Primer pairs used for cloning into pBluescript SK- to give pBluescript vectors

- Primer Sequences are reported 5' > 3'
- Gene – vector generated listed
- cDNA template used in PCR is listed
- 'cDNA template used to amplify...' refers to the nucleotide sequence used from NCBI nucleotide when designing PCR primer pairs.

Primer pairs for cloning to give pcDNA3.1/Zeo (+) Expression vectors for BiFC

- Sequences are reported 5' > 3'
- Kozak consensus sequence in **Red**
- Gene – vector generated listed

Gene: YFP-C – Vector: pcDNA3.1/Zeo (+) YFP-C Version 1

This vector was used for C-terminally tagged proteins with YFP-C

Forward Primer with an *EcoRI* restriction site

CACACAGAATTCGACAAGCAGAAGAACGGCATC

Reverse Primer with a *PstI* restriction site (purple TCA is a stop codon)

CACACACTGCAGTCACTTGTACAGCTCGTCCATGCC

Gene: YFP-C – Vector: pcDNA3.1/Zeo (+) YFP-C Version 2

This vector was used for N-terminally tagged proteins with YFP-C

Forward Primer with a *BamHI* restriction site

CACACAGGATCCGCCACCATGGACAAGCAG

Reverse Primer with an *EcoRI* restriction site (purple TCA is a stop codon)

CACACAGAATTCCTTGTACAGCTCGTCCATGC

cDNA template used to amplify YPF-C:

cDNA for YPF-C and the encodes Residues 156-239 of YFP (the C-terminus) or YFP-C

```
1   gacaagcagaagaacggcatcaaggtgaacttcaagatccgc
    D K Q K N G I K V N F K I R
46  cacaacatcgaggacggcagcgtgcagctcgccgaccactaccag
    H N I E D G S V Q L A D H Y Q
91  cagaacacccccatcggcgacggccccgtgctgctgcccgacaac
    Q N T P I G D G P V L L P D N
136 cactacctgagctaccagtccgccctgagcaaagacccaacgag
    H Y L S Y Q S A L S K D P N E
181 aagcgcgatcacatggtcctgctggagttcgtgaccgccgccggg
    K R D H M V L L E F V T A A G
226 atcactcttggcatggacgagctgtacaag 255
    I T L G M D E L Y K
```

Gene: Human TRPV1 – Vector: pcDNA3.1/Zeo (+) TRPV1 Linker YFP-C

Full length TRPV1 cDNA amplified from this primer pair

Forward Primer with a *HindIII* restriction site

CACACAAAGCTT**GCCACC**ATGAAGAAATGGAGCAGACA GACTTGG

Reverse Primer with a *BamHI* restriction site

CACACAGGATCCTC**C**CTTCTCCCCGGAAGCGGC

*cDNA template used to amplify human TRPV1: NCBI Reference
Sequence: NM_080706.3*

Gene: Human PPAR γ 1 – Vector: pcDNA3.1/Zeo (+) YPF-C PPAR γ 1

Full length PPAR γ 1 cDNA amplified from this primer pair

Forward Primer with NO restriction site

CTATGACCATGGTTGACACAGAG

Reverse Primer with NO restriction site

TCAGTACAAGTCCTTGTAGATCTCCT

*cDNA template used to amplify PPAR γ 1 NCBI Reference Sequence:
NM_005037.5*

Oligonucleotide strands encoding for peptide linker connecting to YFP-C to TRPV1

5'-3' strand 57mer

5'GATCCAGGCCCGCCTGCAAGATCCCCAACGACTTGAAGCAGAAGGTGAT
GAACCACG 3'

3'-5' strand (complement of the above 5'-3' strand) 57mer

5'AATTCGTGGTTCATCACCTTCTGCTTCAAGTCGTTGGGGATCTTGCAGGC
GGGCCTG 3'

The encoded flexible peptide linker sequence: RPACKIPNDLKQKVMNH

Primer pairs for cloning into full length human TRPV1 and FABP7 into pcDNA3.1 Zeo (+) to give pcDNA3.1/Zeo (+) Expression vectors

- Sequences are reported 5' > 3'
- Restriction sites underlined
- Kozak consensus sequence in Red
- Gene – vector generated listed

Gene: Human TRPV1 – Vector: pcDNA3.1/Zeo (+) TRPV1

Full length TRPV1 cDNA amplified from this primer pair

Forward Primer with a *HindIII* restriction site

CACACAAAGCTTGCCACC ATGAAGAAATGGAGCAGCACA

Reverse Primer with a *BamHI* restriction site

CACACAGGATCCTCACTTCTCCCCGGAAGC

cDNA template used to amplify human TRPV1: NCBI Reference
Sequence: NM_080706.3

Gene: Human FABP7-Vector: pcDNA3.1/Zeo (+) FABP7

Full length FABP7 cDNA amplified from this primer pair

Forward Primer with a *HindIII* restriction site

CACACAAAGCTTGCCACCATGGTGGAGGCTTTCTGTG

Reverse Primer with a *BamHI* restriction site

CACACAGGATCCTTATGCCTTCTCATAGTGGCG

cDNA template used to amplify human FABP7: NCBI Reference Sequence: NM_001446

9.2 Sequence verified Plasmid DNA constructs supplied by others

Table 9.1 Sequence verified Plasmid DNA vectors sourced or constructed by fellow academic colleagues. Each plasmid encodes for the full length cDNA of each gene.

Vector	Supplier/Location
pET28a(+) FABP5 (Human)	Dr Simon Dawson, Uni of Nottingham, UK
pET28a(+) FABP7 (Human)	Dr Simon Dawson, Uni of Nottingham, UK
pET28a(+) FABP8 (Human)	Dr Simon Dawson, Uni of Nottingham, UK
pCDNA3.1/Zeo(+) FABP8 (Human)	Nisha Kurian, Uni of Nottingham, UK
pCMVTag2b- YPF-N FABP1 (Human)	Yan Sun, Uni of Nottingham, UK
pCMVTag2b- YPF-N FABP3 (Human)	Yan Sun, Uni of Nottingham, UK
pCMVTag2b- YPF-N FABP4 (Human)	Yan Sun, Uni of Nottingham, UK
pCMVTag2b- YPF-N FABP5 (Human)	Dr Simon Dawson, Uni of Nottingham, UK
pCMVTag2b- YPF-N FABP7 (Human)	Yan Sun, Uni of Nottingham, UK
pCMVTag2b- YPF-N FABP8 (Human)	Dr Simon Dawson, Uni of Nottingham, UK
pCMVTag2b- YPF-N FABP7 (Human)	Yan Sun, Uni of Nottingham, UK
pCMVTag2b- YPF-N FABP8 (Human)	Yan Sun, Uni of Nottingham, UK
pFLAG-CMV2 Fos-YFP-N (Human)	Yan Sun, Uni of Nottingham, UK
pHA-CMV Jun-YFP-C (Human)	Yan Sun, Uni of Nottingham, UK
pFLAG-CMV2 Fos (mut)-YFP-N (Human)	Yan Sun, Uni of Nottingham, UK

9.3 PCR primers pairs used in RT-PCR

Table 9.2: Primers used in RT-PCR on cDNA from rat DRGs and tissues

Rat Gene	Forward Primer 5'>3' Reverse Primer 5'>3'	Tm (°C)/ GC (%)	Product Length (bp)
PPAR α	GAGGCGAGCCAAGACTGAAG TGCATTGTGTGACATCCCGA	61/60 60/50	644
PPAR β/δ	GCTCCTGCTCACTGACAGAT CCAAAGCGGATAGCGTTGTG	59/55 60/55	555
PPAR γ	GGAGATCCTCCTGTTGACCC ACCTGATGGCATTGTGAGACA	59/60 60/48	613
TRPV1	AGTGAGACCCCTAACCGTCA TCTGCTGGAATCCTCGGGTA	60/55 60/55	475
FABP1	ACCAAGTGCAGAGCCAAGAG GTAGACGATGTCACCCAGTGT	60/55 59/52	341
FABP2	TGGCATTGATGGCACTTGG AAGTCGACGCCGAGTTCAAA	59/50 60/50	205
FABP3	ACCGACATCGACCTCCTTTC GTAAGCGTAGTCTCCTGCCC	59/55 59/60	347
FABP4	TCGTCATCCGGTCAGAGAGT ACACATTCCACCACCAGCTT	60/55 59/50	208
FABP5	AACTAGGAGTAGGGCTGGCT TGGCATTGTTGATGACGCAC	59/55 59/50	303
FABP6	TATGGCCTTCACCGGCAAAT AGCCACCCTCTTGCTTACAC	60/50 59/55	385
FABP7	GGGCAAGGATGGTAGATGCT ACGACATCCCCAAAGGTGAG	59/55 59/55	379
FABP8/Pmp2	GCTCCTTGAAGCAAGTGCAG TGTCACTCTGCAACGGTGAT	59/55 59/50	386
FABP9	TGCAGACAACCGGAAAGTGA ACTGTCCCTGGAGCTGAGTT	59/50 60/55	251
FABP12	TCAATGAGACGCGATGGTGG CTTTGCCATCCCAGTCCTGA	60/55 59/55	317

Table 9.3 Primers used in RT-PCR on HeLa cells and positive control tissues

Human Gene	Forward Primer 5'>3' Reverse Primer 5'>3'	Tm (°C))/ GC (%)	Product Length (bp)
FABP1	CGCAGGTCAGTCGTGAAGAGGGA CGCCGTTGAGTTCGGTCACAGAC	60/60 60/60	356
FABP2	TCTCGCCCAAGGACAGACCTGA TGGACTGTGCGCCAAGAATAATGCT	60/60 60/48	480
FABP3	TGCACGCCTGCTCTCTTGTAGC TGCCGTGGGTGAGTGTGAGGATGA	59/61 59/58	412
FABP4	GCACCCTCCTGAAAAGTGCAGCT ACGCCTTTCATGACGCATTCCACC	59/60 56/54	431
FABP5	TCTCTGCACGCCAGCCCG TGTGCTTTCCTTCCCATCCCACT	59/55 59/57	348
FABP6	AGGAAAGCCTCCCAGCAGCA GCCTGGCTGCTTAGGCCAGT	57/59 60/65	416
FABP7	CATGAAGGCTCTAGGCGTGGGC TTCCACCTCCACACCAAGGATAACC	59/58 63/52	463
FABP8/Pmp2	GAAAGCTCTGGGTGTGGGGTTAGC AGATTCTGGTGCACACCACGC	59/57 58/57	323
FABP9	GGTTGAGCCCTTCTTGGGAACCTG TGCCATGTTCCGGGCTGCGAA	59/61 58/62	100

9.4 Primers and Probes used in TaqMan®/QRT-PCR gene expression assays

Table 9.4 DNA sequences of primers and probes used in QRT-PCR gene expression assays on Rat DRG cell cultures

Rat Gene	Sequence
PPAR α	Fwd: TGGAGTCCACGCATGTGAAG Rev: TGTTCCGGTTCTTTTTCTGAATCT Probe: CTTCTTTTCGGCGAACTATTCGGCTAAAGC
PPAR γ	Fwd: TGCCAAAATATCCCTGGTTTC Rev: TGAATCCTTGCCCTCTGATATGA Probe: AGATCATCTACACCATGCTGGCCTCCC
TRPV1	Fwd: TCAAAGACCCAGAGACAGGAAAG Rev: CTGTCTTCCGGGCAACGT Probe:AAAAGCCATGCTCAATCTGCACAATGG
NeuN/Rbfox3	Fwd:TCCAAGGGTTTTGGGTTTGTA Rev:ACGATCGTCCCATTGAGCTT Probe:TAGCTCAGATGCTGACCGAGCCCG
GFAP	Fwd:GAGAGAGATTCGCACTCAGTACGA Rev:TCTGCAAACCTGGACCGATACC Probe:CAGTGGCCACCAGTAACATGCAAGAAACA
FABP4	Fwd:CTTCAAACCTGGGCGTGGAA Rev:CCAGGGTTATGATGCTCTTCACT Probe:TCGATGAAATCACCCCAGATGACAGGA
FABP5	Fwd:TGAGGACTACATGAAGGAACTAGGAGTAG Rev:TTTTGACGGTGAGGTTGTTGTT Probe:CCAAACCAGACTGCATCATTACCCTCGA
FABP7	Fwd:CTCTGGGCGTGGGCTTT Rev:CAAACCTTTCTCCCAGCTGGAA Probe:TGGTGATCCGGACACAATGCACATTC
FABP8	Fwd:GGGAAAATGGTAGTGGAATGTATAATG Rev:CAACGATTTTCTCAGACCTTCTCA Probe:AGGGTGTGGTCTGCAC
GAPDH	Fwd:TCTGCTCCTCCCTGTTCTAGAGA Rev:CGACCTTACCATCTTGTCTATGA Probe:ATCTTCTTGTGCAGTGCCAGCCTCGT
β -actin	Fwd:GTGAAAAGATGACCCAGATCATGT Rev:CACAGCCTGGATGGCTACGT Probe:TGAGACCTTCAACACCCCAGCCATG

Table 9.5 DNA sequences of primers and probes used in QRT-PCR quantitative gene expression assays on HeLa cell lines

Human Gene	Sequence
FABP3	Fwd: CGGGAGCTAATTGATGGAAAAC Rev: CTCATAAGTGCGAGTGCAAACCTG Probe: CATCCTGACACTCACCCACGGCAC
FABP5	Fwd: CCCTGGGAGAAGTTTGAAGA Rev: AATGCACCATCTGTAAAGTTGCA Probe: ACCACAGCTGATGGCAGAAAAACTCAGAC
β -actin	Fwd:CCTGGCACCCAGCACAAT Rev:GCCGATCCACACCACGGAGTACT Probe:ATCAAGATCATTGCTCCTCCTGAGCGC

9.5 Primary and secondary antibodies used in this thesis

Table 9.6: Primary antibodies

Primary antibody and manufacturer	Dilution, application and related experiments
Rabbit polyclonal anti-GFP (Abcam UK, cat.no ab290)	<ul style="list-style-type: none"> • 1:500, overnight at 4°C. • Used in ICC and IB • Chapter 5: Figures 5.6 and 5.7
Mouse anti-human β actin (Sigma, cat no. A5441)	<ul style="list-style-type: none"> • 1:2000, overnight at 4°C • Used in IB • Chapter 5: Figure 5.6
Rabbit polyclonal anti –rat FABP5 (Protein tech, cat.no 12348-1-AP)	<ul style="list-style-type: none"> • 1:100, overnight at 4°C • Used in IHC and IB • Chapter 3: Figure 3.9 and 3.10
Rabbit polyclonal anti human-FABP5 (Abcam UK, cat no. ab37267)	<ul style="list-style-type: none"> • 1:1000, overnight at 4°C • Used in ICC and IB • Chapter 6: Figure 6.8
Rabbit polyclonal anti rat FABP7 (Abcam UK cat no. ab32423)	<ul style="list-style-type: none"> • 1:100-250, overnight at 4°C • Used in IHC and IB • Chapter 3: Figure 3.12 and 3.13
Goat polyclonal anti-human TRPV1 (Santa Cruz, cat no. P-19)	<ul style="list-style-type: none"> • 1:500, overnight at 4°C. • Used in ICC • Chapter 6: Figure 6.9
Mouse monoclonal anti-rat NF200 (Merck Millipore, cat.no MAB5266)	<ul style="list-style-type: none"> • 1:100, overnight at 4°C • Used in IHC • Chapter 3: Figure 3.12
Mouse polyclonal anti-rat NeuN/Rbfox3 (Merck Millipore, cat.no MAB377)	<ul style="list-style-type: none"> • 1:100, overnight at 4°C • Used in IHC • Chapter 3: Figures 3.10 and 3.13

Table 9.10: Secondary antibodies

Secondary antibody and manufacture	Dilution, application and related experiments
anti-IgG AlexaFluor® 488 or 568 from Invitrogen	<ul style="list-style-type: none"> • 1:500, for 2 hours at ambient temperature • Used in ICC and IHC in the dark
Anti-IgG IRDYE 600/800 from LI-COR®	<ul style="list-style-type: none"> • 1:10,000, for 1 hour at ambient temperature • Used in IB/WB